

**Experimental and numerical investigations of implant infection-  
associated bacterial biofilms in dynamic bioreactor systems**

**Von der Naturwissenschaftlichen Fakultät der  
Gottfried Wilhelm Leibniz Universität Hannover  
zur Erlangung des Grades**

Doktorin der Naturwissenschaften

Dr. rer. nat.

**genehmigte Dissertation**

**von**

**Henryke Rath, M. Sc.**

geboren am 07.06.1987 in Hannover

2017

**Referent:** Prof. Dr. Peter Behrens

**Korreferent:** Prof. Dr. Franz Renz

**Tag der Promotion:** 01.12.2016

*Für meine Familie*

*Das Ganze ist mehr als die Summe seiner Teile – Aristoteles*



## Danksagung

Ich danke Frau Prof. Meike Stiesch für das interessante, vielseitige und interdisziplinäre Dissertationsthema und die Möglichkeit, an der Zahnärztlichen zu promovieren. Ich bedanke mich für die gute fachliche Betreuung und die Durchsicht aller Manuskripte.

Ich bedanke mich auch bei Herrn Prof. Peter Behrens für die Betreuung meiner Promotion, die positive Unterstützung und insbesondere für die Mitgestaltung dieser Dissertation.

Ich möchte mich außerdem bei meinem Korreferenten Herrn Prof. Ralf Renz für die Beurteilung dieser Arbeit und der Teilnahme an meiner Disputation bedanken. Herrn Prof. Thomas Scheper danke ich für die Übernahme des Vorsitzes meiner Disputation.

Ich danke dem Promotionsprogramm MARIO der Leibniz Universität Hannover für die Finanzierung meines Forschungsprojektes.

Herrn Dr. Nico Stumpp danke ich für seine fachliche Unterstützung, seine Diskussionsbereitschaft und Kreativität, sein handwerkliches Geschick und die Durchsicht meiner Manuskripte und der Dissertation.

Ich bedanke mich bei Herrn Dr. Andreas Winkel für die Ideen, Gedanken und die nie abbreißende Diskussionsbereitschaft.

Herrn Dr. Sebastian Grade danke ich für die Hilfe am Mikroskop. Außerdem danke ich ihm für die hilfreichen Diskussionen, die Motivation und die positive Unterstützung.

Ich danke meinen Kollegen, die meine Arbeit durch viele Diskussionen und Ideen bereicherten und stets für eine freundschaftliche Arbeitsatmosphäre sorgten: Eva Bettenhausen, Carina Brickwedde, PhD Philipp Dillschneider, Dr. Andreas Greuling, Henning Hartwig, Claudius Moritz Lehr, Sylvia Müller, Annike Rand, Nina Robens, Jörn Schaeske, Leana Subh, Dr. Jürgen Stempel, Karlotta Struckmann, und Richard Werth.

Bei einigen Kollegen möchte ich mich besonders bedanken: Marly Dalton für die technische Unterstützung im Labor und am Mikroskop, für alle projektbezogenen Diskussionen und die Motivation in allen Phasen meiner Promotion. Außerdem danke ich Ihr für Ihre nie endende Freude, ihre Eigenschaft als stetiger Fels in der Brandung und für den Geheimaffen. Nadine Kommerein danke ich für unser Nizza-Projekt, die Motivation, die Ideen bezüglich aller fachlichen und persönlichen Fragestellungen, unsere Kaffeerunden und die ewigwährende gute Laune. Katharina Doll danke ich für die vielen fachlichen Diskussionen, Ihre Kreativität und die Hilfe bei jeglichen Fragestellungen. Außerdem danke ich ihr für die Übernahme und

Betreuung unseres „Babys“. Ich danke Alexandra Ingendoh-Tsakmakidis für Ihre fröhliche und erdende Art, ihre Motivation, die vielen fachlichen Gespräche und für die schönen Erinnerungen. Svenja Kosin danke ich für ihre Motivation, die immerwährende Freude und die positive Unterstützung bei technischen Fragen. Rainer Schreeb danke ich für seine erfrischende Art, Dinge mit Leichtigkeit zu betrachten, die man sonst nur selten findet. Außerdem danke ich ihm für die Hilfe bei technischen Fragen, die gute Zuarbeit und die vielen musikalischen Intermezzi. Dr. Szymon Szafranski danke ich für die Ideen bei technischen und fachlichen Problemen und seinen Optimismus. Ich danke Karin Burgwitz für die gemeinsame Zeit im Büro und die motivierenden und ehrlichen Worte. Ich danke Frau Dr. Chirstina Tiede für die letzten 3 Monate als Büronachbarin und die schöne Zeit.

Ich danke Bastian Dreyer und seinen Betreuern Herrn Prof. Sindelar und Herrn Prof. Franz Renz für die produktive Zusammenarbeit. Bastian Dreyer danke ich zusätzlich noch für die Unterstützung bei der Finanzplanung, Stockholm und unsere Kaffeemeetings.

Ich danke Dianlei Feng und seinen Betreuern Frau Prof. Insa Neuweiler und Herrn Prof. Nackenhorst für die Bereitschaft, die Grenzen verschiedener „Welten“ zu öffnen. Dianlei Feng möchte ich insbesondere für die super Atmosphäre während der Publikationsphase danken.

Zusätzlich bedanke ich mich bei Meisam Soleimani und Herrn Prof. Peter Wriggers für die ertragreiche Zusammenarbeit.

Ich danke Frau Alena Rosenberger für jegliche Hilfestellung und Frau Dorit Schulte für die Betreuung während des Stipendiums.

Ich danke Herrn Prof. Nick Cogan für die inspirierende Kooperation über viele tausende Kilometer hinweg und die vielen Diskussionen.

Ein ganz großer Dank gilt meiner Familie für die Unterstützung, die stete Motivation, die vielen Anregungen, den liebevollen Rückhalt und den Optimismus, der meine Persönlichkeit sehr geprägt hat.

Ich bedanke mich bei Jan Reidenbach und Gordon Lax für die Unterstützung und Motivation in den letzten drei Jahren. Gordon danke ich sehr für das Korrekturlesen dieser Dissertation.

Ich danke meinem Partner Matthias Grünberg von ganzem Herzen für seine Motivation, Unterstützung, Geduld, die Korrekturen an dieser Dissertation und die Liebe über viele Kilometer hinweg.

## Abstract

The present demographical change leads to an aging society. This shift entails new demands to the health sector and financial challenges to ensure an adequate health care system for all age groups. Special attention is drawn on the implantology, because the requirements for the replacement of body parts increase continuously. Especially dental prostheses are in the focus. In Germany, about one million dental prostheses are implanted annually. Unfortunately, these replacements are often associated with bacterial inflammations of the oral cavity, resulting in severe secondary diseases, such as endocarditis. The prevalence of dental implant infection was 20% in 2012.<sup>1-3</sup> These infections are accompanied by tissue and bone loss, reoperation, implant failure and dramatic costs for the health care system. Researchers and clinicians are devoted to the development of non-invasive treatment strategies, personalized implants, cell compatible implant surfaces and the prevention of bacterial infections. The bacterial inflammations are typically induced by the bacterial colonization of the abiotic implant surfaces. The adherent can form sessile synergistic bacterial communities called biofilm, in which the bacteria are embedded in a self-produced extracellular polymeric substance (EPS). This tenacious matrix shields the bacteria from external hazards and builds a diffusion barrier for antibiotics, preventing the successful bacterial eradication. Furthermore, it repels the immune response of the host. Even though the research efforts have tremendously increase during the last thirty years, there is still a great request for a new generation of innovative biofilm repelling implants.

This thesis is part of the doctoral program Multifunctional Active and Reactive Interfaces and Surfaces (MARIO) of the Leibniz University Hannover (LUH) in cooperation with the Hannover Medical School and the University of Applied Sciences and Arts in Hannover. The main aim of this program is the development of methods for the mechanical-thermo-chemo interactions at contact surfaces and interfaces.

In this study, two different thematic objectives with three cooperation partners were examined. The first project included the calibration and validation of numerical simulations of the *Streptococcus gordonii* biofilm formation with respect to the influences of flow velocity and different nutrient concentrations on the biofilm growth behavior. Moreover, the spatial distribution of the live and dead bacterial portion in the biofilm was determined to validate the numerical model. The second numerical simulation dealt with the modeling of the *Staphylococcus aureus* biofilm formation under different flow rates. For the experimental establishment, two different flow chamber systems under physiological fluid conditions were evaluated.

As an affiliated project to the numerical simulation of the MARIO program, a cooperation project with the University of Florida was initiated. Here, a numerically developed disinfection protocol was validated by biological experiments of *S. aureus*. Three different regimes of antibiotic treatment were investigated to eliminate so called persister cells that are assumed to be the main reason for chronic infections. One antibiotic regime was successfully as predicted by the numerical model.

The aim of the second MARIO project was the determination of electrical stimulation parameters for successfully inhibition of bacterial adhesion in the oral cavity. To define clinical accurate parameters for the patients, the stimulation was performed on biocompatible piezoelectric polyvinylidene fluoride (PVDF) membranes manufactured by a MARIO cooperation partner. Two electrical devices were successfully evaluated and the inhibition parameters for three bacterial species were determined. Furthermore, the alterations in the genetic expression patterns of the stimulated bacterium *S. gordonii* were analyzed compared to unstimulated samples.

**Keywords:** dental implant-associated infection • bacterial biofilm • flow chamber system • numerical biofilm modeling • time-dependent antibiotic treatment • electrical stimulation parameter

## Kurzzusammenfassung

Der gegenwärtige demographische Wandel führt zu einer immer älter werdenden Gesellschaft. Diese Verschiebung ist mit neuen Anforderungen an den Gesundheitssektor und finanziellen Herausforderungen verbunden, um eine angemessene Versorgung aller Altersschichten zu gewährleisten. Besondere Aufmerksamkeit wird dabei der Implantologie gewidmet, da der Bedarf an spezifischen Prothesen stets zunimmt. Nennenswert sind darunter vor allem Zahnimplantate. Alleine in Deutschland werden jährlich etwa eine Million Dentalimplantate eingesetzt. Leider ist eine solche Behandlung oft mit bakteriellen Entzündungen der Mundhöhle verbunden, die ihrerseits zu schweren Folgeerkrankungen, etwa Herzinnenhautentzündungen, führen können. Studien aus dem Jahr 2012 konnten zeigen, dass die Prävalenz eines Zahnimplantates aufgrund bakterieller Infektionen, der sogenannten „Peri-Implantitis“, bei 20% liegt.<sup>1-3</sup> Diese Entzündungen gehen meist einher mit Gewebeschwund, körperlich fordernden Reoperationen und lebensbedrohlichen oder sogar tödlichen Folgeerkrankungen, die neben den tragischen Einzelschicksalen auch dramatische Kosten für unser Gesundheitssystem verursachen. Aus diesen Gründen widmen sich Kliniker und Forscher der Entwicklung präziserer, nicht-invasiver Behandlungsmethoden, personalisierter Implantate, dem Design Zell-kompatibler Implantatoberflächen und der Prävention bakterieller Infektionen. Die Hauptursache bakterieller Entzündungen ist der sogenannte Biofilm. Dieser besteht aus einer sessilen bakteriellen Lebensgemeinschaft, die von einer selbstproduzierten extrazellulären polymeren Substanz umgeben ist. Die so vor äußeren Einflüssen geschützten Bakterien können nur schwer mit üblichen Behandlungsmethoden bekämpft werden. Obwohl die Forschung in den letzten dreißig Jahren stark zugenommen hat, wurde bisher noch keine zufriedenstellende Lösung erarbeitet. Ein grundlegendes Verständnis der im bakteriellen Biofilm ablaufenden Prozesse ist daher unumgänglich, um die gezielte Entwicklung neuartiger Therapieansätze zu beschleunigen.

Diese Arbeit ist ein Teilprojekt des MARIO der LUH in Zusammenarbeit mit der Medizinischen Hochschule Hannover und der Hochschule Hannover. Der Hauptfokus dieses Programmes liegt auf der Entwicklung von mechano-, thermo-, chemischen Wechselwirkungen an Kontakt- und Grenzflächen. In dieser Arbeit wurden zwei verschiedene Themenblöcke mit drei Kooperationspartnern untersucht. Das erste Projekt umfasste die Kalibrierung und Validierung einer numerischen Simulation zur Biofilmentwicklung von *S. gordonii* bezüglich des Einflusses verschiedener Flussgeschwindigkeiten und Nährstoffkonzentrationen. Zudem wurde die räumliche Verteilung lebender und toter Bakterien im Biofilm für die Validierung des numerischen Systems evaluiert. Die zweite numerische Simulation befasste sich mit der Modellierung der Biofilmbildung des partikelförmigen *S. aureus*. Hier wurde die Biofilmbildung auf den Einfluss verschiedenen Strömungsgeschwindigkeit hin analysiert. Für die experimentellen Untersuchungen, wurden zwei verschiedene Flusskammersysteme entwickelt, welche die Biofilmentstehung unter physiologischen Bedingungen im Mund nachstellte.

Als weiteres Projekt zur numerischen Simulation wurde ein numerisches Desinfektionsprotokoll für *S. aureus* Persister in Zusammenarbeit mit der University of Florida entwickelt. Drei verschiedene antibiotische Kultivierungsbedingungen wurden simuliert und experimentell untersucht, wobei nur ein Antibiotikumregime erfolgreich war, wie es mit der Simulation vorhergesagt worden ist.

Das Ziel des zweiten MARIO Projekts war die Ermittlung von elektrischen Inhibierungsparametern für dental relevante Bakterien. Um realistische Parameter für den Patienten zu definieren, erfolgte die Stimulation auf biokompatiblen piezoelektrischen PVDF Membranen, welche von einem der Kooperationspartner hergestellt worden sind. Zwei elektrische Stimulationsgeräte wurden entwickelt und erfolgreich evaluiert. Zudem wurden die Inhibierungsparameter für drei Bakterienspezies erfolgreich ermittelt. Darüber hinaus wurde der Einfluss der elektrischen Stimulation auf die Veränderungen der Genexpressionsmuster von *S. gordonii* hin analysiert.

**Stichworte:** Zahnimplantat-assoziierte Infektion · bakterielle Biofilmbildung · Flusskammersystem · numerische Biofilm-Modelle · zeitabhängige Antibiotika-Behandlung · elektrische Stimulationsparameter



## Table of Contents

<b>List of Figures</b>	<b>I</b>
<b>List of Tables</b>	<b>III</b>
<b>List of Abbreviations</b>	<b>IV</b>
<b>1. Introduction and Objectives</b> .....	<b>7</b>
<b>2. Fundamentals</b> .....	<b>11</b>
2.1 The tooth and dental implants .....	11
2.1.1 Tooth disease and implant-associated infections .....	11
2.1.1.1 Periodontitis and peri-implantitis .....	11
2.1.1.2 Tooth decay and pulpitis .....	13
2.2 Biofilm .....	13
2.2.1 Definition and composition .....	13
2.2.2 Appearance .....	15
2.2.3 Biofilm formation and communication .....	15
2.2.4 Biofilm in the human oral cavity .....	16
2.2.4.1 <i>Streptococcus gordonii</i> .....	18
2.2.4.2 <i>Streptococcus oralis</i> .....	18
2.2.4.3 <i>Streptococcus salivarius</i> .....	19
2.2.4.4 <i>Porphyromonas gingivalis</i> .....	19
2.2.4.5 <i>Aggregatibacter actinomycetemcomitans</i> .....	19
2.2.4.6 <i>Staphylococcus aureus</i> .....	20
2.3 Interaction of bacterial infections and the host immune response .....	20
2.4 Flow chamber systems .....	22
2.5 Persistence in the biofilm .....	23
2.6 Electrical stimulation .....	23
2.6.1 Piezoelectricity .....	26
2.6.2 Polyvinylidene fluoride as piezoelectric material .....	28
2.7 Biofilm modeling .....	28
<b>3. Materials and Methods</b> .....	<b>31</b>
3.1 Nutrient broth, buffer, chemicals, enzymes, kits, devices and laboratory equipment .....	31
3.1.1 Nutrient broth and buffer .....	31
3.1.2 Chemicals and enzymes .....	32

---

3.1.3	Molecular biology kits .....	33
3.1.4	Experimental devices and laboratory equipment .....	34
3.2	Bacterial strains .....	35
3.3	Culture conditions .....	35
3.4	Biofilm experiments .....	36
3.4.1	Aerobic biofilm cultivation .....	36
3.4.2	Anaerobic biofilm cultivation .....	36
3.5	Determination of colony-forming units.....	36
3.6	Microscopic investigations.....	37
3.6.1	Scanning electron microscopy.....	37
3.6.2	Staining protocol .....	37
3.6.3	Confocal laser scanning microscopy.....	37
3.6.4	Calculation of biofilm height .....	38
3.7	Flow chamber experiments .....	38
3.8	Electrical stimulation.....	39
3.8.1	Production of PVDF membranes .....	39
3.8.2	Determination of pH values .....	40
3.8.3	Determination of chlorine and hydrogen peroxide content.....	40
3.8.4	Agar plates.....	40
3.8.5	Viability test on agar plates .....	41
3.9	Molecular investigations .....	41
3.9.1	Isolation of DNA.....	41
3.9.2	Isolation of RNA .....	41
3.9.3	Propidium monoazide assay .....	42
3.9.4	Quantitative real-time PCR .....	43
3.9.5	Microarray analysis .....	43
3.10	Antibiotic treatment of <i>S. aureus</i> .....	45
3.11	Statistical analyses.....	45
3.12	Numerical simulation .....	45
<b>4.</b>	<b>Results and Discussion.....</b>	<b>47</b>
4.1	Development of a flow chamber system for the reproducible <i>in vitro</i> analysis of biofilm formation on implant materials.....	47
4.1.1	Abstract .....	48
4.1.2	Introduction .....	48
4.1.3	Materials and methods .....	51
4.1.3.1	Bacterial strains .....	51

## Table of Contents

---

4.1.3.2	Bacterial cultivation and biofilm formation .....	51
4.1.3.3	Flow chamber system .....	52
4.1.3.4	Biofilm imaging and analysis .....	52
4.1.3.5	Statistical analysis .....	52
4.1.4	Results .....	53
4.1.4.1	The flow chamber system .....	53
4.1.4.2	Micro- and macroscopic evaluation of biofilm formation .....	53
4.1.4.3	Calculation of mean biofilm height.....	54
4.1.5	Discussion .....	55
4.2	Biofilm formation by the oral pioneer colonizer <i>Streptococcus gordonii</i> an experimental and numerical study .....	59
4.2.1	Abstract .....	60
4.2.2	Introduction .....	61
4.2.3	Material and methods .....	62
4.2.3.1	Bacterial strain.....	62
4.2.3.2	Bacterial cultivation and biofilm formation .....	62
4.2.3.3	Open flow chamber system .....	62
4.2.3.4	Biofilm imaging and analysis.....	63
4.2.4	Biofilm formation modeling.....	64
4.2.4.1	Selection of a mathematical model .....	64
4.2.4.2	Mathematical model .....	67
4.2.4.3	Numerical methods .....	69
4.2.5	Results and discussion.....	69
4.2.5.1	The influence of the medium concentration on the biofilm height .....	69
4.2.5.2	Time dependent spatial distribution of active / inactive biomass within a biofilm .....	73
4.2.6	Conclusion.....	75
4.3	Numerical simulation and experimental validation of biofilm in a multi-physics framework using an SPH based method.....	77
4.3.1	Results .....	94
4.3.2	Discussion .....	95
4.4	Theoretical and experimental evidence of the effects of varying disinfection timing .....	97
4.5	Definition of electrical stimulation parameters for the inhibition of bacterial growth on PVDF membranes .....	105
4.5.1	Abstract .....	106
4.5.2	Introduction .....	106

---

4.5.3	Materials and methods .....	108
4.5.3.1	PVDF film preparation.....	108
4.5.3.2	Bacterial strains .....	108
4.5.3.3	Bacterial cultivation .....	108
4.5.3.4	Electrical stimulation set-up and parameters.....	109
4.5.3.5	pH control and viability testing.....	110
4.5.3.6	Biofilm imaging and analysis.....	110
4.5.3.7	Determination of chlorine and hydrogen peroxide content.....	111
4.5.3.8	Propidium monoazide assay and DNA isolation.....	111
4.5.3.9	Quantitative real-time PCR .....	112
4.5.4	Results .....	112
4.5.4.1	Stimulation parameters.....	112
4.5.4.2	pH measurement before and after electrical stimulation.....	113
4.5.4.3	Measurements of the chlorine and hydrogen peroxide content.....	115
4.5.4.4	Average biofilm heights of stimulated bacteria under static and dynamic cultivation on PVDF membranes .....	115
4.5.4.5	Biofilm morphology of stimulated and unstimulated bacteria on PVDF membranes .....	116
4.5.4.6	Viability control of the bacteria in stimulated and unstimulated supernatants.....	118
4.5.4.7	PMA treatment and quantitative real-time PCR .....	118
4.5.5	Discussion .....	120
4.5.5.1	Stimulation parameter .....	120
4.5.5.2	Vitality test of the stimulated and unstimulated bacteria of the supernatant on agar plates and quantitative real- time PCR.....	121
4.5.5.3	Influence of the pH on the bacterial growth behavior.....	122
4.5.5.4	Measurements of the chlorine and hydrogen peroxide content.....	123
4.6	Gene expression profiles of electrically stimulated and unstimulated dental-relevant bacterium <i>S. gordonii</i> .....	125
4.6.1	Results .....	125
4.6.1.1	RNA and microarray quality .....	125
4.6.1.2	Up- and down-regulated genes in stimulated supernatant .....	126
4.6.1.3	Up- and down-regulated genes in stimulated biofilm .....	127
4.6.2	Discussion .....	128
4.6.2.1	RNA and microarray quality .....	128
4.6.2.2	Gene expression patterns of the stimulated bacteria in the supernatant .....	128
4.6.2.3	Genetic expression patterns of the stimulated bacteria in the biofilm ..	129

<b>5. Conclusion and Outlook .....</b>	<b>133</b>
<b>6. Literature .....</b>	<b>135</b>
<b>7. Supplementary Information .....</b>	<b>175</b>
<b>8. Curriculum Vitae .....</b>	<b>211</b>
<b>9. Publications .....</b>	<b>213</b>



## List of Figures

<b>Figure 1:</b> Biofilm formation cycle on a surface. ....	16
<b>Figure 2:</b> Complex classification of oral bacteria. ....	18
<b>Figure 3:</b> Potential mechanisms of electrical stimulation. ....	24
<b>Figure 4:</b> The piezoelectric effect. A-C direct-, and D-F inverse effect .....	27
<b>Figure 5:</b> Structural formula of polyvinylidene fluoride.....	28
<b>Figure 6:</b> Example of a PVDF film. ....	40
<b>Figure 7:</b> Flow chart of the sample preparation for a microarray assay.....	44
<b>Figure 8:</b> Sketch of the flow chamber and flow chamber system. ....	53
<b>Figure 9:</b> 3D reconstruction of biofilms in side view. ....	54
<b>Figure 10:</b> Biofilm heights on titanium substrata in the flow chamber system. ....	55
<b>Figure 11:</b> Schematic description of an open flow chamber system. ....	63
<b>Figure 12:</b> The biofilm is imaged at different focal planes by gradual scanning across the sample.....	64
<b>Figure 13:</b> Mean height of <i>S. gordonii</i> biofilms after 24 h of cultivation at flow velocities between 100-400 $\mu\text{L}/\text{min}$ . ....	66
<b>Figure 14:</b> Two dimensional illustration of the computational domains. ....	67
<b>Figure 15:</b> Illustration of the objective function values with different parameters sets. ....	71
<b>Figure 16:</b> The biofilm height of <i>S. gordonii</i> after 24 h with increasing nutrient concentrations.....	73
<b>Figure 17:</b> Height of <i>S. gordonii</i> biofilm in a time dependent open flow chamber experiment. ....	75
<b>Figure 18:</b> Biofilm formation of <i>S. aureus</i> under different velocities in a flow chamber system.....	94
<b>Figure 24:</b> Stimulation devices.....	110
<b>Figure 25:</b> Biofilm height of stimulated and unstimulated bacteria.....	116
<b>Figure 26:</b> 3 D-biofilm reconstruction of CLSM stacks. ....	117
<b>Figure 27:</b> SEM images of bacterial biofilms. ....	117
<b>Figure 28:</b> Representative viability test results of the stimulated bacterial SNS, SNNS and the respective growth medium. ....	118
<b>Figure 29:</b> qRT-PCR results of the total and viable distribution of bacteria under stimulated and unstimulated conditions after 24 h. ....	119
<b>Figure 30:</b> Fluorescence signal intensities of the microarray assay. ....	126
<b>Figure 31:</b> Up- and down-regulated genes of the stimulated bacteria in the supernatant. ....	126
<b>Figure 32:</b> Up- and down-regulated genes of stimulated biofilm bacteria.....	127
<b>Figure S 1:</b> Two-dimensional illustration of the computational domain. ....	177
<b>Figure S 2:</b> Comparison of experimental results and numerical simulation results of the biofilm height at different concentrations of medium after 24 h growth. ....	181
<b>Figure S 3:</b> Influence of the maximum biofilm growth rate $\mu$ on the active biofilm height, inactive biofilm height and inactivation fraction over different input TSB medium concentrations.....	183

<b>Figure S 4:</b> Influence of the Monod half-rate constant $k_s$ on the active biofilm height, inactive biofilm height and inactivation fraction over different input TSB medium concentrations. ....	<b>184</b>
<b>Figure S 5:</b> Influence of the inactivation rate $k_i$ on the active biofilm height, inactive biofilm height and inactivation fraction over different input TSB medium concentrations. ....	<b>185</b>
<b>Figure S 6:</b> Influence of the biofilm yield $Y$ on the active biofilm height, inactive biofilm height and inactivation fraction (from top to bottom) over different input TSB medium concentrations.....	<b>187</b>
<b>Figure S 7:</b> Influence of the biofilm yield $Y$ on the active biofilm height over time with input TSB medium concentrations of 0.05 x (left) and 1 x (right).....	<b>188</b>
<b>Figure S 8:</b> Ofloxacin susceptibility test for the identification of antibiotic resistance of <i>S. aureus</i> . ....	<b>193</b>
<b>Figure S 9:</b> Bacterial viability testing via CFUs determination for regime I at time point 0 (start point). ....	<b>193</b>
<b>Figure S 10:</b> Bacterial viability testing via CFUs determination for regime I after 24 h.....	<b>194</b>
<b>Figure S 11:</b> Bacterial viability testing via CFUs determination for regime I after 28 h. ....	<b>194</b>
<b>Figure S 12:</b> Bacterial viability testing via CFUs determination for regime I after 48 h.....	<b>194</b>
<b>Figure S 13:</b> Bacterial viability testing via CFUs determination for regime I after 52 h.....	<b>195</b>
<b>Figure S 14:</b> Bacterial viability testing via CFUs determination for regime I after 72 h.....	<b>195</b>
<b>Figure S 15:</b> Bacterial viability testing via CFUs determination for regime I after 76 h. ....	<b>195</b>
<b>Figure S 16:</b> Bacterial viability testing via CFUs determination for regime I after 96 h. ....	<b>196</b>
<b>Figure S 17:</b> Bacterial viability testing via CFUs determination for regime I after 100 h....	<b>196</b>
<b>Figure S 18:</b> Bacterial viability testing via CFUs determination for regime I after 120 h. ..	<b>196</b>
<b>Figure S 19:</b> Bacterial viability testing via CFUs determination for regime I after 124 h....	<b>197</b>
<b>Figure S 20:</b> Electrical stimulation initial trials on polysterol for the evaluation of the growth inhibiting parameter. ....	<b>201</b>



## List of Tables

<b>Table 1:</b> Nutrient broth and buffer supply. ....	<b>31</b>
<b>Table 2:</b> Chemicals and enzymes supply. ....	<b>32</b>
<b>Table 3:</b> The supplier and manufacture of the kits. ....	<b>33</b>
<b>Table 4:</b> Experimental devices and laboratory equipment. ....	<b>34</b>
<b>Table 5:</b> The origin of the respective bacterial strains. ....	<b>35</b>
<b>Table 6:</b> Primer for real- time PCR of <i>S. gordonii</i> , <i>S. salivarius</i> , and <i>P. gingivalis</i> . ....	<b>43</b>
<b>Table 7:</b> Parameters for the numerical simulation. ....	<b>72</b>
<b>Table 9:</b> Primer for real- time PCR of <i>S. gordonii</i> , <i>S. salivarius</i> , and <i>P. gingivalis</i> . ....	<b>112</b>
<b>Table 10:</b> Parameter of the electrical stimulation on PVDF membranes. ....	<b>113</b>
<b>Table 11:</b> pH values of the bacterial solution and the respective medium before electrical stimulation in triplicates. ....	<b>114</b>
<b>Table 12:</b> The pH values of the bacterial supernatant and the respective medium after electrical stimulation in triplicates. ....	<b>115</b>
<b>Table 13:</b> RNA concentration and quality of the stimulated and unstimulated <i>S. gordonii</i> supernatant and biofilm. ....	<b>125</b>
<b>Table S 1:</b> Parameters used for the simulation. ....	<b>180</b>
<b>Table S 2:</b> Sensitivity of the biofilm heights $h_1$ , $h_2$ and inactivation fraction $f$ to the parameters $\mu$ , $k_s$ , $k_i$ and $Y$ . ....	<b>189</b>
<b>Table S 3:</b> Determination of electrical effective parameter on polystyrene for the static stimulation. ....	<b>199</b>
<b>Table S 4:</b> The organisms, the genome size, calculated genome weight and the corresponding reference for the qRT-PCR. ....	<b>202</b>
<b>Table S 5:</b> Up- and downregulated genes and their function of stimulated supernatant samples of <i>S. gordonii</i> . ....	<b>203</b>
<b>Table S 6:</b> Up- and down-regulated genes and their function of stimulated bacteria in the biofilm of <i>S. gordonii</i> . ....	<b>205</b>

## List of Abbreviations

<i>A. actinomycetemcomitans</i>	<i>Aggregatibacter actinomycetemcomitans</i>
AC	alternating current
A-K model	Alpkvist and Klapper model
AI-2	autoinducer-2
ATCC	American Type Culture Collection
<i>B</i>	biofilm domain
BFC	biofilm control
BFS	bacteria in biofilm stimulated
BFNS	bacteria in biofilm not stimulated (control)
BHI	Brain Heart Infusion
BHIV	Brain Heart Infusion with 10 µg/mL vitamin K
BHISV	Brain Heart Infusion with 5% sucrose and 10 µg/mL vitamin K
CDT	cytolethal distending toxin
CFU	colony forming unit
cAMP	cyclic adenosine monophosphate
cDNA	complementary DNA
cGMP	cyclic guanosine monophosphate
CLSM	confocal laser scanning microscopy
<i>d</i>	reactor diameter
<i>D</i>	diffusion coefficient
DBL	diffusion boundary layer
DC	direct current
DEB	discrete element based
DNA	deoxyribonucleic acid
ds	double stranded
DSMZ	German Collection of Microorganisms and Cell Cultures
EDTA	ethylenediaminetetraacetic acid
EPS	extracellular polymeric substance
FEMS	Federation of European Microbiological Societies
FIC	finite increment calculus
FISH	Fluorescence <i>in situ</i> hybridization
Gn	GalNAcβ1-3Gal

gPS	gProcessedSignal
GTase	Glycosyltransferases
<i>H</i>	heights of the computational domain
<i>H<sub>b</sub></i>	thickness of boundary layer
<i>h</i>	biofilm height
<i>K<sub>i</sub></i>	inactivation rate
<i>k<sub>s</sub></i>	monod half-rate constant
LUH	Leibniz University Hannover / Leibniz Universität Hannover
MARIO	Multifunctional Active and Reactive Interfaces and Surfaces
Mbp	mega base pairs
OD <sub>600</sub>	optical density
ORF	open reading frame
$\rho$	density of biofilm
PCR	polymerase chain reaction
PDE	partial differential equation
<i>P. gingivalis</i>	<i>Porphyromonas gingivalis</i>
PLoS	Public Library of Science
PMA	propidium monoazide
PN	polymorphonuclear neutrophils
PRR	pattern recognition receptor
PRPP	5-phospho-alpha-D-ribose 1-diphosphate
PTS	phosphoenolpyruvate-dependent phosphotransferase systems
PurM_cligase	phosphoribosylformylglycinamide cyclo-ligase
PyrD	dihydroorotate dehydrogenase electron transfer subunit
PyrE	orotate phosphoribosyltransferase
PyrF	orotidine 5'-phosphate decarboxylase
RANKL	receptor activator of nuclear factor $\kappa$ B ligand
<i>r</i>	reaction term
RIN	RNA integrity number
RNases	ribonucleases
rpm	rounds per minute
RPS	polysaccharide receptors
ROS	reactive oxygen species
RT	room temperature

$s$	substrate concentration
<i>S. aureus</i>	<i>Staphylococcus aureus</i>
<i>S. gordonii</i>	<i>Streptococcus gordonii</i>
$Sh$	sherwood number as dimensionless number of mass transport
$s_{max}$	maximum input medium concentration (1 x TSB medium)
<i>S. oralis</i>	<i>Streptococcus oralis</i>
<i>S. salivarius</i>	<i>Streptococcus salivarius</i>
SNS	bacteria in the supernatant simulated
SNNS	bacteria in the supernatant not simulated (control)
SPH	smoothed-particle hydrodynamics
$S_t$	substrate transport domain
SV	anaerobic Schaedler bouillon with 10 $\mu\text{g}$ /mL vitamin K
TA	toxin-antitoxin
TDG	time discontinuous Galerkin method
TSB	Tryptic Soy Broth
TSBY	Tryptic Soy Broth with 10% yeast extract
TSBYG	Tryptic Soy Broth with 10% yeast extract and 50 mM glucose
$u$	flow velocity
UMP	uridine monophosphate
$\nu$	kinematic viscosity
$W$	length of the computational domain
XFEM	extended finite element method
$Y$	biofilm yield coefficient of biofilm
$\mu_{max}$	growth rate
$\mathbf{n}_b$	normal vector of the boundary of the computational domain $\partial\Omega$
$\mathbf{v}$	volume fractions of different biomass components
$\theta^2$	Thiele modulus

## 1. Introduction and Objectives

The demographic change we experience today inevitably leads to an increased proportion of older people in our society. This shift is directly associated with new demands in the medical sector and financial challenges to afford an appropriate health care system for patients of every age.<sup>4</sup> A special attention is devoted to the field of implantology, since the need for specific body part replacements is also increasing. Prominent examples are artificial knees and hip joints, cardiac pacemakers, vascular prosthesis as well as cochlear and dental implants. The tooth implantation is one of the main incidences among these medical treatments. In Germany, about one million dental prostheses are implanted annually. Unfortunately, the integration of a dental implant into the oral cavity is often followed by bacterial-induced inflammations that are responsible for severe diseases like endocarditis as a secondary infection.<sup>2</sup> Studies conducted in 2012 have shown that the prevalence of a tooth implant infection was 20% due to the bacterial infection termed “peri-implantitis”.<sup>1,2</sup> These inflammations are most commonly associated with implant and tissue loss, physically demanding reoperations, secondary infections and life-threatening or fatal health situations.<sup>2</sup> In addition, the costs for the health care system are dramatically increased. The main focus for clinicians and researchers is on the development of more precise, non-invasive implementation procedures, the personalization of implants, the design of more cell-attracting implant surfaces and the prevention of bacterial infections.<sup>1,5,6</sup>

The main reason for peri-implantitis are bacterial infections that in a progressed state lead to the formation of so-called biofilm. These are microbial communities embedded in a self-secreted extracellular polymeric substance (EPS) that shields the bacteria from external hazards. These communities are hard to treat with standard medical therapeutics. Although the research efforts on peri-implantitis have increased tremendously over the last decades, there is still no satisfying treatment available. Therefore, a basic understanding of the bacterial biofilm behavior is required to facilitate a directed development process.

The present thesis is one of 15 projects within the framework of the doctoral program Multifunctional Active and Reactive Interfaces and Surfaces (MARIO). This program investigates in the behavior of liquids on structured surfaces with a broad range of different techniques such as numerical simulations, chemical modification of surfaces and composite materials, and bio-medical applications. The doctoral program was structured in three main blocks: A) surfaces within biomedicine, B) high performance contact pairings, and

C) intermaterial contact surfaces.

The present thesis is part of block A and is based on the cooperation with three doctoral students from the identical block. This work is structured into two main categories: 1) development of an experimental set-up for biofilm growth under physiological-like flow conditions for the calibration and validation of numerical biofilm models and 2) determination of electrical stimulation parameters for the inhibition of bacterial growth on piezoelectric membranes.

The development of the experimental fluid flow set-up for the calibration and validation was carried out in a cooperation together with Dianlei Feng from the Institute of Fluid Mechanics and Environmental Physics in Civil Engineering directed by Prof. Insa Neuweiler, and with Meisam Soleimani from the Institute of Continuum Mechanics led by Prof. Peter Wriggers. Both institutes are affiliated with the Leibniz University Hannover (LUH).

The main goal of both cooperation projects was the evaluation of the biofilm growth behavior on the defined implant-relevant substratum titanium. The studies differed in the application of the numerical model, such as continuous and discrete element based (DEB) model under smoothed-particle hydrodynamics (SPH), and the investigated implant infection-associated bacteria *S. gordonii* and *S. aureus*. The analyzed calibrators for the continuous model were the influence of different flow rates and nutrient concentrations on the biofilm growth, as well as the spatial distribution of active (vital) and inactive (dead) bacteria in the biofilm over a period of 24 h for *S. gordonii* (section 4.2). The *S. aureus* biofilm growth behavior was analyzed under different flow velocities (section 4.3) for SPH model. Two flow chamber systems were designed and established for the biological investigations. First, a continuous flow circuit system for five dental implant-relevant bacteria was evaluated and established: *S. gordonii*, *Streptococcus oralis*, *Streptococcus salivarius*, *Porphyromonas gingivalis*, and *Aggregatibacter actinomycetemcomitans*. The biofilm heights were significantly reproducible (section 4.1). Second, an open flow chamber system with continuous feed was investigated to improve the consistency of culture conditions for the biofilm growth throughout the experiments. The experimental calibration and validation for both numerical models were successfully.

Next to the two numerical simulation model projects of the MARIO program, an international cooperation was initiated with Prof. Nick Cogan from the Department of Mathematics of the University of Florida and Nadine Kommerein from the Department of Prosthetic Dentistry and Biomedical Materials Science of the Hannover Medical School. The aim of the present study was the experimental validation of a numerically developed disinfection protocol for persister

cells. These cells are genetically identical to the bacteria of the same species, but have different phenotypical characteristics. These persister cells are dormant and halt their cellular and metabolic processes under the presence of antibiotics. Therefore, this specific type of bacteria is assumed as the main cause of chronic diseases.<sup>7</sup> As those persister cells reactivate their essential mechanisms after the antibiotic treatment was ceased, the cells are susceptible in this stage. Prof. Nick Cogan investigated in a numerical model based disinfection protocol under three different regimes of antibiotic treatment to determine this susceptible phase for persister cell eradication. The experimental set-up for the antibiotic regimens were designed and evaluated for planktonic *S. aureus* cultures. Hence, one antibiotic regime was effective in eradicating the persister cells, as predicted by the numerical simulation (*section 4.4*).

The second part of this thesis was a cooperation with Bastian Dreyer from the Department of Materials Science directed by Prof. Ralf Sindelar of the University of Applied Science and Arts Hannover and Prof. Franz Renz from the Institute of Inorganic Chemistry, LUH. The objective of this project was the determination of electrical stimulation parameter for the inhibition of bacteria growth on the piezoelectric material polyvinylidene fluoride (PVDF). As piezoelectricity is characterized by the electric charge resulting from mechanical deformation of a material, PVDF is assumed to be applicable for the oral implantology. Dental implants are constantly exposed to pressure by usual mastication.<sup>8,9</sup> Bastian Dreyer successfully manufactured PVDF membranes with piezoelectric character. For the biological investigations, two different experimental set-ups were evaluated: 1) a stimulation system under static cultivation with a self-designed stimulation lid and 2) a stimulation under fluid flow conditions in an flow chamber system equipped with platinum electrodes. Three dental-relevant bacterial species were analyzed: *S. gordonii*, *S. salivarius* and *P. gingivalis*. Initially, the electric stimulation parameters were determined on polystyrene and afterwards verified on the PVDF membranes. The biofilm formation of these three species was successfully inhibited under static and dynamic culture conditions. Furthermore, the viability of the bacteria was quantified and the genetic expression patterns of control and stimulated bacterium of *S. gordonii* were analyzed. The gene expression of the stimulated bacteria was altered compared to the control, indicating that, at least in parts, electric stimulation had a direct influence on the expression level of biofilm forming related genes. Furthermore, the electrical stimulation led to the electrolysis of the nutrient medium as gaseous hydrogen was produced and soared up as bubbles that inhibited the bacterial attachment process (*section 4.5 and 4.6*).





## 2. Fundamentals

This chapter aims to elucidate the basics of dental implant-associated infections. In detail, it focuses on the cause for the implant infections: biofilms. The formation process, occurrence, the composition and growth behavior of biofilms are explained and oral bacteria involved in the development and progression of implant infection are introduced in detail. The host immune response to bacterial-induced inflammations is outlined and the phenomenon of bacterial persistence presented. Furthermore, experimental strategies such the experimental set-up of the flow chamber systems and the antimicrobial strategies of electrical stimulation are presented in detail. At last, numerical biofilm modeling is explained as a strategy to supplement biofilm etiology and disinfection strategies.

### 2.1 The tooth and dental implants

The natural tooth is divided in two segments: the crown and the root. The crown extends into the oral cavity and the root stretches into the gingiva. Both segments are connected by the tooth neck.<sup>10</sup> The tooth is composed of dentin, a bone-like structure that surrounds the pulp. The dentin is protected by enamel and covered by the cementum, which is a part of the periodontium. The periodontal ligamentum fixes the tooth through a connection of the lamina dura and the cementum.<sup>10</sup> A healthy tooth is anchored into the bone via the periodontal ligaments.

In the last four decades the restoration and the replacement of missing teeth has increased.<sup>11,12</sup> Tooth implantation was introduced in 1947 and has been in the focus of research since.<sup>13</sup> Nowadays, dentists implant a root-like endosseous implant composed of a titanium ligation to fully replace the human root and tooth. The osseo-integrated implant is connected to the crown via a metal or ceramic abutment. This implant ensures the direct contact to the jaw bone structure and function of the bone that is adjacent to the implant.<sup>14</sup>

#### 2.1.1 Tooth disease and implant-associated infections

##### *2.1.1.1 Periodontitis and peri-implantitis*

Periodontitis is a degenerative disease of the periodontium including the gingival, cementum, alveolar bone, and the periodontal ligamentum.<sup>15</sup> This is one of the most concerning human infective diseases and is the main reason for tooth loss.<sup>15-18</sup> Periodontitis is characterized by the

fast destruction of tissue supporting the tooth. Globally around 10 - 15% of all adults are affected.<sup>19</sup>

The disease starts with an acute inflammation of the periodontal tissue, without treatment, leads to the pathogenic deepening of the periodontal pockets, ultimately resulting in tooth loss. There are two types of periodontitis: the aggressive variant, often beginning in young ages and the more frequent chronic disease.<sup>13,20-22</sup> Progression in both forms is identical. Typically, symptoms are redness and swelling of the periodontium, regression of the gingiva, purulence and tooth movement in the jaw bone. The cause of periodontitis is the irreversible inflammation of the gingiva caused by bacterial biofilm, leading to the destruction of the periodontal ligaments and the alveolar bone. Once it proceeds into the epithelial ligamentum, periodontal pockets are deepened and are a clear evidence of periodontitis, since it provides an ideal environment for the formation of subgingival plaque.<sup>23</sup>

The main reason for periodontitis is the propagation of bacterial products released from so-called biofilms in the subgingival area.<sup>24-26</sup> This community composes over more than 700 bacterial species with *P. gingivalis* and *A. actinomycetemcomitans* being the main reason causing this severe disease.<sup>27,28</sup> Further important candidates are *Capnocytophaga*, *Treponema denticola*, *Tannerella forsythia*, *Prevotella intermedia*, *Campylobacter rectus*, *Fusobacterium* spp., *Parvimonas micra*, *P. nigrescens*, and *Filifactor*.<sup>28</sup> In 2014, Pérez-Chaparro reported the relationship between periodontitis and following organisms: members of the bacteroidetes, firmicutes, proteobacteria, and archaea and *Candidatus saccharibacteria* spp.<sup>29</sup>

Often periodontitis patients are predisposed by suboptimal tooth restoration, tooth abnormalities, and mechanical pressure of the gingival caused by growing tooth. Smoking, diabetes or immune-suppressions are additional factors for the onset of periodontitis.<sup>10</sup>

Peri-implantitis disease is a polymicrobial infection of the implant and its surrounding environment and is characterized by an infected mucosa, ultimately resulting in bone loss.<sup>30</sup> The preliminary stage is called mucositis and is described as the inflammation of the oral implant surrounding tissue. Typical symptoms are tissue reddens, swells and bleeds under little mechanical pressure. Mucositis is seamlessly followed by peri-implantitis.<sup>31</sup> The peri-implantitis is defined as bone loss in connection with bleeding, purulence, pathogenic deepening of the periodontal pocket, bone resorption, loss of osseointegration and the prosthesis.<sup>13,32</sup> The implant loss is separated into early and delayed failure.<sup>31</sup> The bacterial attachment on a dental implant starts seconds after implantation and reaches its climax after about two weeks later.<sup>33</sup> Peri-implantitis and periodontitis can be compared to each other, at least concerning the deepening of the periodontal pocket, bone loss and the biochemical

response, even though lesions from peri-implantitis are twice as high as compared to periodontitis.<sup>13</sup> This changes the wound behavior, cell-cell adhesion and reaction of the immune system. Although, the composition of bacteria associated with peri-implantitis is often described as resembling periodontitis.<sup>34,35</sup> Furthermore, other properties that influence the biofilm composition are: A) material of the implant, B) roughness, C) morphology, and D) surface energy.<sup>13</sup> The pre-dominant species in peri-implantitis are *P. gingivalis*, *P. intermedia*, *P. nigrescens*, *S. constellatus*, *A. actinomycetemcomitans*, *T. denticola* und *T. forsythia*, *Peptostreptococcus micros* and *F. nucleatum*.<sup>36,37</sup> In contrast to the periodontitis, *S. aureus* is predominant concerning the affinity to titanium in peri-implantitis.<sup>38</sup>

There are causalities leading to peri-implantitis such as a history of periodontitis, smoking, diabetes, systemic diseases, low bone quality, surgical trauma, wrong implant design, and low oral hygiene.<sup>31,32,39-46</sup> Additionally to microbial infection, Wilson *et al.* indicated that the filling component cement can also cause peri-implantitis without any occurrence of bacteria. Here, mechanical irritation can cause the inflammation.<sup>2,47</sup>

### **2.1.1.2 Tooth decay and pulpitis**

Tooth decay is one of the most common diseases of the global human population. About 80% of people in the industrial countries are affected.<sup>48</sup> It is an opportunistic infective disease and initiated by bacterial infection.<sup>49</sup> Some of the involved bacteria secrete acids produced via fermentation of carbohydrates that demineralize the enamel and dentin of the natural tooth in the process.<sup>50</sup> Those bacteria are incorporated with food. The main cause is *Streptococcus mutans* attacking the dentin with the release of acids (mainly carboxylic acid).<sup>51-53</sup> Tooth decay often occurs between adjacent teeth, with the resulting structure resembling a mushroom. The „stem“ starts from the peripheral enamel and the demineralization site resembles the head of the mushroom.<sup>54</sup>

Serious tooth decay can lead to pulpitis. Here, the bacteria pass the dentin and enter the pulp, the neurovascular part of the tooth, leading to pulp infection, called pulpitis. This inflammation is often irreversible and leads to necrosis of the pulp and death of a tooth.<sup>10</sup>

## **2.2 Biofilm**

### **2.2.1 Definition and composition**

According to Hale *et al.* a biofilm is defined as “a collection of microbial cells covered by and embedded in a matrix of extracellular microbial polymers such as mucilage or slime, at an

interface. Biofilms are found, for example, on the surface of stones in rivers and ponds, in water pipelines, as dental plaque on teeth and on surgical implants. Microorganisms within biofilms appear to be less susceptible to biocides than their planktonic counterparts. The extracellular polymer and/or nutrient limitation associated with position of organisms in the film may alter sensitivity. Biofilms allow for the rapid spread of genetic material between the component microorganisms. Biofilm formation can have serious implications in industrial, environmental, medical and public health situation.<sup>55</sup>

Biofilms contain a defined microbiome or mycobiome and are embedded in an EPS that is self-produced by the bacteria or fungi.<sup>56,57</sup> Furthermore, the EPS forms channels for water, nutrients, waste or signal transport. The latter is for the intra- or interspecies communication, which leads to altered gene expression, biofilm formation and maturation.<sup>7,58</sup> The EPS establishes the functional and structural integrity of biofilms. It is composed of polysaccharides such as alginate, dextran, lean and/or celluloses. Furthermore, it comprises liposaccharides, lipids, phospholipids, glycolipids, proteins, glycoproteins, and extracellular DNA.<sup>59,60</sup> The main component with about 97% is water.<sup>61</sup> The stability of a given biofilm is determined by the hydrophobic interaction, the cross linkage between polysaccharide structures and multivalent cations.<sup>60</sup> The EPS also defines the conditions for the biofilm such as hydrophobicity, water content, nutrient ingestion, charges, density, and porosity.<sup>60</sup> EPS are the construction material of bacterial settlements and either remains attached to the cell's outer surface, or are secreted into its growth medium. Biofilms occur in different shapes, whereby four shapes are the most common: 1) mushroom-like, 2) pillar-like, 3) hilly-like, and 4) homogenous flat.<sup>62</sup> The shape of a biofilm is defined by the compositions of polysaccharides, protein, products of cell lysis, or extracellular DNA.<sup>62-64</sup> Furthermore, the EPS protects the bacteria from osmotic shock, desiccation, predators and toxic substances like antimicrobials. The advantage of this specific matrix for the bacterial community is a robust shielding against external hazards that increases antibiotic resistance up to 5000-fold compared to planktonic bacteria.<sup>63,65</sup> The EPS protects the bacteria from antimicrobial threats through two mechanisms: 1) growth of bacterial cells within the biofilm is reduced compared to planktonic bacteria. Antimicrobials predominantly affect bacterial cell cycles and their reproductive machinery. With reduced growth both mechanisms are not attacked as in fast growing planktonic bacteria, 2) EPS offers a natural diffusion barrier that limits the transportation rate of antibiotics through the matrix.<sup>66-69</sup>

### 2.2.2 Appearance

Biofilms are mainly formed in hydrophilic environments such as wastewater pipes, ship hulls, soil, oil or gas installations, on stones, food manufacturing units, contaminated surgical equipment, infected wounds, tooth or implant surfaces.<sup>62</sup> Additionally, there are biofilms colonizing extreme environments as in frost or permafrost, high pressure, alkaline or acidic, and salty environments. Furthermore, some biofilms can survive high UV-illumination and radioactivity.<sup>68,70-72</sup>

### 2.2.3 Biofilm formation and communication

A biofilm is formed in four steps: 1) attachment of planktonic bacteria to the substratum, 2) cell-cell adhesion on the substratum, 3) proliferation and maturation and 4) detachment and dissemination to other substrata (Figure 1).<sup>70</sup>

In the human body, assembly of the bacteria to the host cells is performed through the specific binding of the microbial surface receptors to the host protein receptors. This connection depends on the pH value of the surrounding environment, temperature, flow-velocity, oxygen concentration, nutrient concentration, iron content and osmolarity.<sup>70</sup> After attachment of pioneer bacteria, the bacterial cells adhere and form macrocolonies, transiting from the planktonic stage to the biofilm stage. This process is conducted by van der Waals forces, electrostatic attraction and hydrogen bonds and stimulates the multiplication of the planktonic cells and the secretion of EPS is initiated to surround the planktonic cells. Furthermore, signaling molecules for the communication via quorum sensing are initiated. This is a signal and response mechanism enabling intra- and interspecies communication. Signal molecules are transported through the EPS, while achieving many tasks as gene expression, information of growth conditions, attachment and detachment processes, host infiltration, coexistence with different bacterial species, and predator or antimicrobial penetration.<sup>73-76</sup>

The biofilm proliferates, matures and at last, single cells or biofilm clusters detach and colonize other substrata. This is controlled by limiting concentrations of nutrients, enzymes digesting the EPS, and mechanical stress.<sup>57,70,77-80</sup>

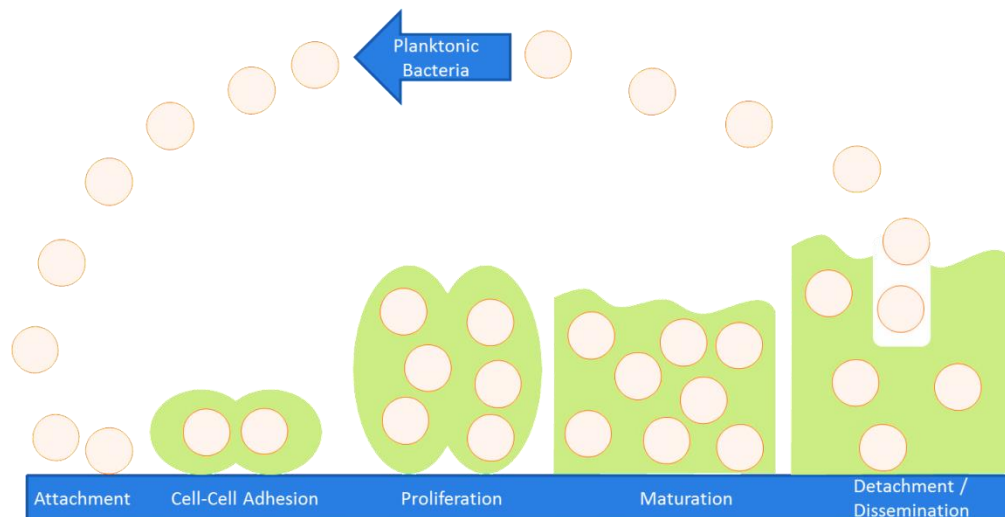


**Figure 1: Biofilm formation cycle on a surface.**

### 2.2.4 Biofilm in the human oral cavity

The human oral cavity is the second most diverse microbial habitat of the human body.<sup>81</sup> This habitat hosts a wealth of over six billion bacteria, with a diversity that is represented by approximately 700 different bacterial species.<sup>82</sup> Apart from bacteria, fungi, protozoa and viruses inhabit the cavity.<sup>83</sup> The normal pH of the saliva is neutral (pH 7.0) and the general temperature is between 34-37°C.<sup>84</sup> Bacteria communicate inter- and interspecifically. The main part of the bacterial diversity is commensal and harmless to the host. A minor part of this bacterial diversity is opportunistic pathogenically and initiates diseases as periodontitis, peri-implantitis and tooth decay.<sup>82,85</sup> The dental biofilm is a multispecies community.<sup>86</sup>

The initial bacteria attach to proteins, carbohydrates, lipids, and glycoproteins from the saliva that forms a thin layer on the tooth called the pellicle.<sup>87</sup> The main tasks of the pellicle are the protection from erosion, ion depot, mineral balance, and lubricant between adjacent teeth. The pellicle forms a protective layer for the host since it contains lysozymes and proteins, however it provides the receptors for bacterial attachment and adhesion as well as proteins, amylases and glycosyltransferases.<sup>88-90</sup> The pellicle is characterized by its adsorption after a few seconds. The phosphoproteins, predominantly proline rich proteins, build the precursor layer of the pellicle that adsorbs calcium ions of the enamel surface.<sup>88</sup> This layer protects the pellicle from saliva proteases.<sup>88,91</sup> The precursor's layer is settled by the continual adsorption of biomolecules.<sup>88,92</sup> The bacterial colonization is secondary and fimbriae-mediated. The main components are adhesins that mediate further colonization.<sup>92,93</sup> Additionally, amylases and glycosyltransferases are important for the biofilm formation, since they are critical for energy absorption and consumption.<sup>88,94</sup>

About 80% of pioneering bacteria belong to the *Streptococcus* group after eight hours of biofilm formation.<sup>95</sup> Those bacterial species predominantly bind to glycoprotein receptors.<sup>96</sup> Furthermore, they initiate the coaggregation of other species like veillonellae and actinomycetes.<sup>95</sup> For intraspecies coaggregation, the bacteria mediate the adhesion through lectin-like cell surface receptors and polysaccharide receptors (RPS) of other streptococci.

The adhesion conveys the identification of the polysaccharide in the presences of the host-like character of the GalNAc $\beta$ 1-3Gal (Gn) in the repetition unit of the RPS.<sup>97</sup> The streptococci carrying this specific character are the main reason for the development of the pioneer colonization in the oral cavity.<sup>98</sup> The initial biofilm colonization is followed by secondary and late colonizing bacteria. One of the transitional bacteria between the initial and the secondary phase is *F. nucleatum*. This threadlike bacterium is capable of cross connecting throughout the whole biofilm.<sup>99</sup> Further predominating species are *P. intermedia*, *P. loescheii* and *Capnocytophaga* spp. Late colonizers are *P. gingivalis*, *T. denticola*, and *T. forsythia*.<sup>86,100,101</sup> The secondary and late colonizers congregate with the bacterial surface of the initial colonizers via stereo-chemical interactions of proteins and carbohydrates and van der Waals forces.<sup>102</sup> Late colonizers are able to initialize the cell death of the pioneer or secondary bacteria, contribute to the alteration of the biofilm composition and trigger the pathogenicity.<sup>103</sup>

The oral biofilm is not only characterized by the order of the substratum colonization, but is also organized in five distinctive complexes (green, purple, red, orange, and yellow, as shown in Figure 3). Bacteria that cannot be assigned do not have complex. Originally, Socransky *et al.* subdivided the subgingival plaques that were associated with the periodontopathic diseases in the five categories.<sup>104</sup> Figure 2 shows the classification of the complexes. The orange and red complex are the predominate bacteria for periodontitis. Additionally, over 90% of the pathogenic bacteria are from the red complex.<sup>105</sup>

<i>Aggregatibacter actinomycetemcomitans</i> (serotype a) <i>Eikenella corrodens</i> <i>Campylobacter concisus</i> <i>Capnocytophaga</i> species	
<i>Veillonella parvula</i> <i>Neisseria mucosa</i>	<i>Prevotella intermedia</i> <i>Prevotella nigrescens</i> <i>Fusobacterium nucleatum</i> <i>Fusobacterium periodonticum</i> <i>Fusobacterium polymorphum</i>
<i>Porphyromonas gingivalis</i> <i>Tannerella forsythia</i> <i>Treponema denticola</i>	<i>Campylobacter gracilis</i> <i>Campylobacter rectus</i> <i>Campylobacter showae</i> <i>Eikenella nodatum</i> <i>Peptostreptococcus micros</i> <i>Streptococcus constellatus</i>
<i>Actinomyces</i> species	<i>Streptococcus mitis</i> <i>Streptococcus oralis</i> <i>Streptococcus sanguis</i> <i>Streptococcus gordonii</i> <i>Streptococcus intermedius</i>

**Figure 2: Complex classification of oral bacteria.** The bacteria are divided into green, purple, red, orange and yellow complexes. The grey-marked group accounts as undefined. Figure adapted and modified from Socransky *et al.* and Aruni *et al.*<sup>104,106</sup>

In a healthy oral cavity, the bacteria are in a microbial balance to protect the host environment. With a sensitive shift of this balanced system, the microbial composition of the biofilm changes from predominantly aerobic gram positive bacteria to gram negative anaerobic pathogenic bacteria.<sup>60,107,108</sup> Consequently, diseases such as periodontitis, peri-implantitis, and tooth decay occur.<sup>82,109</sup> A major factor for this microbial imbalance is the shift in pH value. Most orally relevant bacteria have a specific limit within acidic or alkaline surroundings. If their environment is too acidic or too alkaline, their metabolisms are negatively influenced and ultimately die. One of the pH-shifting bacteria is *S. mutans*, an acidophilic bacterium that acidifies its surrounding environment to a pH of 1.<sup>85</sup> Alkaline bacteria such as *P. gingivalis* are not able to stay viable in this environment. For the enhanced understanding of the oral pathogenic bacteria, the relevant bacteria *S. gordonii*, *S. oralis*, *S. salivarius*, *P. gingivalis*, and *A. actinomycetemcomitans* are introduced in detail. Additionally, for implant-associated infection, *S. aureus* is described in detail.

#### 2.2.4.1 *Streptococcus gordonii*

*S. gordonii* is an opportunistic pathogen bacterium. It is gram positive, facultative anaerobe and non-motile. It has a genome size of 2.2 mega base pairs (Mbp).<sup>110-112</sup> It is one of the pioneer colonizers that adheres to tooth or implant substratum providing the ideal attachment site for secondary and late colonizers.<sup>113,114</sup> If this bacterium enters the human circulatory system by chance, it infects the endocardium of the heart leading to endocarditis.<sup>79,115,116</sup>

#### 2.2.4.2 *Streptococcus oralis*

*S. oralis* is an opportunistic pathogenic bacterium with a genome size of 2.0 Mbp. *S. oralis* is gram positive, facultative anaerobe and non-motile. If the oral cavity is in balance, *S. oralis* has a protective and probiotic character. It is involved in the initial colonization of surfaces in the



oral cavity.<sup>117</sup> As *S. gordonii*, it provides the attachment sites for secondary and late colonizing bacteria.<sup>113,114</sup> *S. oralis* produces glycosyltransferases (GTPase), which synthesize glucan from sucrose. This is indispensable for the localization of the bacteria and biofilm development.<sup>118-120</sup> Furthermore, *S. oralis* produces sialidase. This enzyme cuts the binding between a sialic acid residue and the hexose- or hexamine acid at the terminal end of the oligosaccharides of glycolipids or glycoproteins. This negatively influences the cellular processes of the host defense mechanism.<sup>121-124</sup> Moreover, *S. oralis* has negative effect on immunosuppressed patients and initiates endocarditis.<sup>122,125-129</sup>

#### **2.2.4.3 *Streptococcus salivarius***

*S. salivarius* is a gram positive and opportunistic pathogenic bacterium. It is facultative anaerobe with a genome size of 2.4 Mbp.<sup>130</sup> *S. salivarius* produces flexible peritrichously fimbriae for the initial attachment and adhesion.<sup>131-134</sup> *S. salivarius* colonizes preferably the tongue and the oral mucosa.<sup>135</sup> It also provides the ideal attachment sites for secondary and late colonizers.<sup>113,114</sup> *S. salivarius* produces extracellular GTPases and induces tooth decay and halitosis.<sup>136,137</sup>

#### **2.2.4.4 *Porphyromonas gingivalis***

*P. gingivalis* is a gram negative rod-shaped, anaerobic, and non-motile bacterium. It has a genome size of 2.3 Mbp. *P. gingivalis* ferments amino acids as energy source providing the opportunity to inhabit the anaerobic epithelia cells of the periodontal pocket.<sup>138</sup> Next to the periodontal pocket, *P. gingivalis* inhabits the oral mucosa and the sulcus.<sup>105,139-144</sup> *P. gingivalis* is an opportunistic periodontopathogen described as the main cause of periodontitis and peri-implantitis.<sup>18,145,146</sup> It is characterized as a late colonizer of the red complex.<sup>24,147,148</sup> It has fimbriae and capsule mechanisms to adhere and colonize surfaces facilitating the host invasion.<sup>84,149,150</sup> Furthermore, it provides the coaggregation sites for other bacterial species as *S. gordonii*.<sup>151</sup> *P. gingivalis* produces virulence factors as liposaccharides, phosphoserine phosphatase (serB protein) and cysteine proteases for the attack of the host tissue. The main virulence factors of the periodontopathogenic bacterium are lysine and arginine gingipains. These are proteases that harm the host's tissue severely.<sup>152</sup> Additionally, *P. gingivalis* affects osteoblasts and gingival fibroblasts.<sup>153</sup>

#### **2.2.4.5 *Aggregatibacter actinomycetemcomitans***

*A. actinomycetemcomitans* is a pathogenic, gram negative, rod-shaped, and facultative anaerobic bacterium. It has a genome size of 2.2 Mbp. It has fimbriae and is organized in six serotypes (a-f).<sup>20,27</sup> These serotypes differ in their composition of polysaccharide antigens and

the cell surface.<sup>154</sup> In Germany, the main serotypes are type a and b with around 33%.<sup>155</sup> Additionally to *P. gingivalis*, *A. actinomycetemcomitans* triggers periodontitis and peri-implantitis.<sup>18</sup> It produces virulence factors facilitating the migration and invasion mechanisms. These factors are characterized in three categories: 1) inhibition of tissue repair with the chemotactic peptide *N*-Formylmethionine-leucyl-phenylalanine; 2) modulation of inflammation with leucotoxins, cytolethal distending toxin (CDT), super antigens and 3) introduction of tissue damage with lipopolysaccharides and cell-stress responding proteins like chaperonin.<sup>27,156-162</sup> *A. actinomycetemcomitans* binds to saliva receptors of teeth, extracellular matrix, fibronectin and epithelial cells.<sup>27</sup> Moreover, *A. actinomycetemcomitans* is responsible for severe inflammatory diseases like endocarditis, meningitis, sepsis, osteomyelitis and brain abscess.<sup>27,163</sup>

#### 2.2.4.6 *Staphylococcus aureus*

The opportunistic pathogen *S. aureus* is a gram positive, 2.8 Mbp genome sized and aerobic bacterium that is often associated with implant infections.<sup>58,164-168</sup> *S. aureus* produces virulence factors and rapidly acquires resistance against potent antibiotics e.g. methicillin-resistant *S. aureus*.<sup>169</sup> Moreover, it initiates inflammatory diseases like endocarditis, pneumonia, osteomyelitis and bacteremia.<sup>165,170-173</sup>

### 2.3 Interaction of bacterial infections and the host immune response

As soon as a biofilm becomes pathogenic, it is deleterious to the host and the immune system is activated. The system can be divided into an innate and an adaptive system. The innate system is the first to respond to the bacterial attack and acts as the general defense mechanism. The adaptive immune system targets specific pathogens. Both systems are communicating via cytokines and cell-cell interaction.<sup>174-177</sup>

The innate immune response is triggered by the pattern recognition receptor (PRR) that binds to a pathogen-associated molecular pattern receptor. Those specific PRRs are characterized as toll-like receptors and nucleotide-binding oligomerization domain proteins.<sup>178,179</sup> These receptors are present in dendritic cells, macrophages, lymphocytes and the epithelium. They are expressed in the periodontal tissue.<sup>178-183</sup> The PRRs recognize the different lipoprotein and peptidoglycan patterns and activate the migration of cytokines for the destruction of surrounding specific bacteria. A permanent stimulation of these receptors by bacteria results in the destruction of the host tissue.

Another essential group of immune response mechanisms are the polymorphonuclear

neutrophils (PN). These neutrophils are released by the immune system few minutes after the damage to the tissue and are necessary for protection, facilitating phagocytosis of bacteria and induce the release of soluble antimicrobials. The PNs contain enzymes for tissue destruction as a defense mechanism.<sup>105,184,185</sup> *P. gingivalis* is able to alter the phagocytosis and chemotaxis response of neutrophils and initiate the tissues self-destruction.<sup>184</sup>

A further mechanism of the initial immune response is the inflammasomes that are essential for the subsequent activation of caspase proteases. Those proteases modulate the maturation and release of the cytokines.<sup>186-188</sup> Moreover, the inflammasome controls the regulation of further cytokines and chemokines reactions through other immune cells. This mechanism mainly protects the host from sepsis, however if this system is unbalanced it results in auto immune diseases.<sup>187,189</sup>

Furthermore, the secretion of cytokines by T-helper cells and CD4<sup>+</sup>T- cells is an important part of the adaptive immune system. They regulate the release of cytokines and upregulate or suppress the immune response, and activate the cytotoxic T-cells and macrophages. The release of cytokines is used for cell signaling and controlling other components of the immune system by influencing maturation and growth.<sup>190-192</sup>

The bacterial-induced inflammation causes the distribution of cytokines resulting in the release of chemokines from the gingival epithelium surrounding the tooth. Consequently, this activates adhesion molecules of the invading bacteria, resulting in the migration of the bacteria through the gingival capillary vessels. This triggers the increase of further chemotaxis and the neutrophils pass the junctional epithelium and the sulcus gingivae.<sup>105,193-195</sup> The sulcus gingivae is a depression between the tooth neck and the gingiva. Without inhibition of this process, the inflammation continues affecting the connective tissue and the alveolar bone resulting in the formation of a periodontal pocket and ultimately leading to periodontitis.<sup>105</sup> The immune response of the host is triggered by virulence factors of bacteria from the red complex. *P. gingivalis* ferments amino acids of host proteins and degrades macrophages.<sup>196</sup> Furthermore, the bacteria form capsules, containing mainly negatively charged polysaccharides that surround their cells and protect them from disassembly by host's immune cells.<sup>197,198</sup> Moreover, leukotoxins and CDT that inhibit the host lymphocyte function by interfering with the cell cycle progress, damage the lympholytical development.<sup>105,162</sup> The bacteria produce cysteine proteases facilitating hemolysis and induce cell apoptosis.<sup>162,199,200</sup>

## 2.4 Flow chamber systems

Most biofilm models focus on the biofilm formation behavior under static growth conditions. Although those studies are time-saving and often easier for laboratory-based investigations, the results often do not reflect the physiological biofilm situations.<sup>201</sup> The flow velocity has a major impact on the growth behavior, structure, composition, morphology and formation of a biofilm. The flow influences the transport of nutrient, oxygen, signal molecules as quorum sensing messengers and defines the morphology and physiology of the biofilm.<sup>202-207</sup> Furthermore, it controls the cellular processes for the alteration of gene expression and EPS content.<sup>208</sup> The flow coordinates the energy loss, heat and mass transfer, and transformation reactions from active to inactive bacteria.<sup>203</sup> Moreover, shear stress negatively influences the development of the biofilm matrix, but is also important for the progress of the biofilm formation as it increases the biofilms mobility. At last, the flow velocity is a major coordinator of attachment and detachment processes.<sup>208</sup>

In 1994 Wolfaardt *et al.* first introduced a flow chamber system for the *in vitro* analysis of bacterial biofilm growth behavior in a fluid dynamic environment.<sup>209</sup> In general, the main scientific issues investigated by this device are: 1) cell-cell interaction within the biofilm, 2) cell number and biovolume, 3) species compositions, biofilm morphology and biofilm growth behavior of multispecies biofilms, 4) antimicrobials efficacy testing, 5) influence of growth conditions, e.g. nutrient and oxygen concentrations on biofilm formation, 6) spatial distribution of vital and dead bacteria in biofilms, 7) bacterial attachment and detachment behavior and 8) interactions between eukaryotic cells and bacteria (co-culture).<sup>210-220</sup> Most flow chamber systems are analogically constructed: a bioreactor for bacterial cultivation, flow cell(s) and a peristaltic pump to pass the bacterial suspension and/or growth medium through the system. The bacteria form the biofilm on a substratum in the flow chamber and non-adhering bacteria are either recirculated to the bioreactor (continuous flow circuit system) or pumped in a waste bottle (open flow chamber system with continuous feed of nutrients).<sup>221,222</sup> Often a bubble trap is mounted upstream the flow chamber to avoid the accumulation of air bubbles on the substratum as they impair the biofilm growth.<sup>62</sup> The most commonly tested substratum for biofilm growth under flow conditions is glass, followed by ceramics and titanium. Typically, silicone or metal tubing are utilized for the connection of the device's components. The systems are frequently designed for direct macroscopic and microscopic investigation of the biofilm formation throughout the experiments.

## 2.5 Persistence in the biofilm

In the 1940s, the survival of a small bacterial fraction after antibiotic treatment was described by Bigger.<sup>223,224</sup> This phenomenon was first investigated with different concentrations of penicillin and treatment durations resulting in the eradicating a great number of bacteria while a tolerant subpopulation remained. This was true for planktonic and sessile bacteria. In 1999 Costerton *et al.* introduced the term of persistence.<sup>7</sup> Persistence is described as a genetically identical type of bacteria within a species with phenotypical different behavior. Persistence is not inheritable in contrast to resistance.<sup>225</sup> Persister cells are small, and form slow-growing colonies compared to non-persistent cells as detected on agar plates. Those bacteria are insusceptible to antibiotics.<sup>226</sup> Lewis assumed that the emergence of bacterial persistence ensures the survival of non-growing populations in severe situations.<sup>223</sup> The cells are dormant with little or no cell wall synthesis, translation and topoisomerase activity. The persister bacteria will not proliferate in this state, but restart their metabolism after antibiotic treatment to reassemble the bacterial population.<sup>223,227</sup> This includes the release of planktonic bacteria to recolonize new surfaces.<sup>7,223,226,228</sup> The down-regulation is controlled by yet uncharacterized persister proteins. Their expression rates are regulated by population density and environmental conditions.<sup>225</sup> Experiments indicated that specific motility and energy metabolism genes are down-regulated supporting the dormancy of the persisters.<sup>227</sup> Furthermore, genes were detected that are induced during dormancy and operate as translation inhibitors, septation inhibitors and toxin-antitoxin (TA) genes. The TA protein inhibits replication via the production of antitoxin complexes.<sup>229,230</sup> Those persister cells are assumed to be the main reason for chronic diseases stimulated by bacterial invasion.<sup>7</sup>

## 2.6 Electrical stimulation

Since the first electrical sterilization of milk in the 1920<sup>th</sup>, electrical stimulation has evoked an increasing interest for the application of bacterial eradication.<sup>231</sup> In general, two different mechanisms of electrical stimulation were investigated: 1) direct current (DC) and 2) alternating current (AC). DC is defined as the unidirectional current flow. Voltage and current vary over time until the flow of direction is changed. The AC is defined as a flow of charges that changes its direction periodically, resulting in the reversed voltage along with the current. The AC has different waveforms, such as sine, square, triangular or complexes waves, whereby the sine and squared waves are the common forms.

In 1972, Rowley and McKenna initially investigated the bacterial static effect by electrical stimulation of *E. coli*.<sup>232</sup> As their stimulation was successful, the interest in electrical eradication was decisively raised, even though a medical application was not possible as the 300 V used in the study would have been painful for the patient.

It is not yet completely understood how bacteria react to electric current in detail.<sup>233</sup> Summarized, the electrical stimulation has a direct and/or indirect effect on the bacteria as described in Figure 3, both resulting in bacterial death as presented in Figure 3.

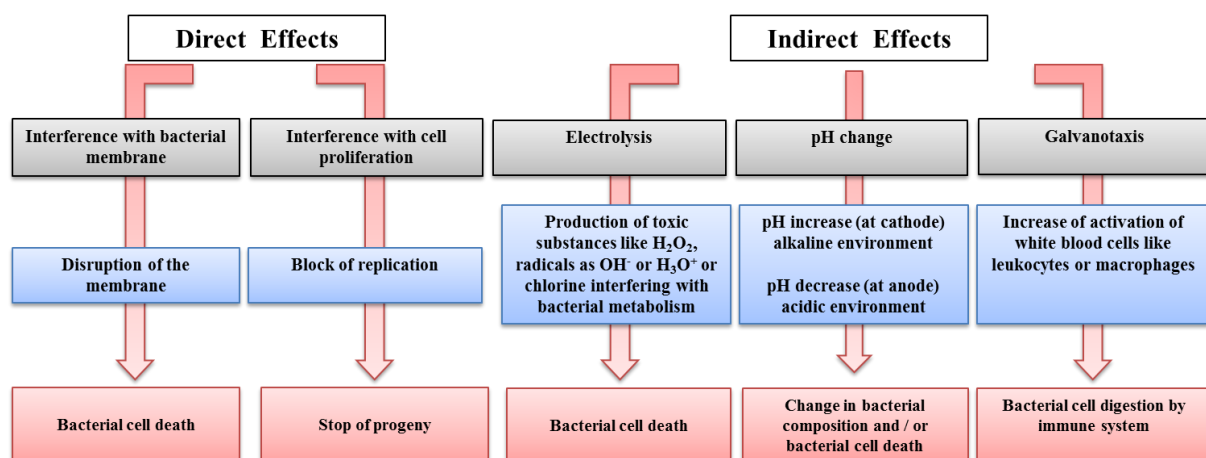


**Figure 3: Potential mechanisms of electrical stimulation.** Figure adapted and modified from Karba *et al.*<sup>234,235</sup>

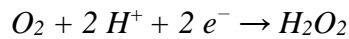
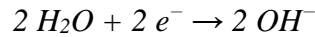
The direct effect of the electric current results in the disruption of the bacterial cell membrane or the destruction of bacterial surface molecules by electrolysis, leading to bacterial cell death.<sup>234-237</sup> Bacterial membrane potentials are essential for the main metabolic mechanisms in the cell. Cevc noticed in his study that the bacterial membrane proteins were affected by an external field influencing the membrane potentials.<sup>238-240</sup> Furthermore, electric currents influenced the bacterial growth processes, the proportion of the bacterial glycocalyx and the structure of bacterial membranes.<sup>241,242</sup> Furthermore, the DC stimulation blocks the bacterial replication and inhibits the growth. The indirect effect is assumed to be triggered by the electrolytic generation of toxic substances, e.g. hydrogen, hydroxide, hydrogen peroxide and chlorine, which interfere with the bacterial metabolism.<sup>236,237</sup> Additionally, the pH is altered by electrical stimulation, causing cell death and/or reorganization of the microbial community structure.<sup>234,235,243-245</sup> However, there are studies that disprove this effect.<sup>245</sup> Furthermore, electrical stimulation can have a galvanotaxis effect on macrophages and leukocytes, causing increased bacterial cell digestion.<sup>246-248</sup> For coccoid and rod-shaped bacteria there is a typical phenomenon called “controlled electrophoretic deposition”.<sup>249,250</sup> It describes the formation of

ordered clusters by inducing an electric field. Additionally, it was observed that AC stimulation leads to a parallel alignment of the rod-shaped bacteria to the direction of the electric field.

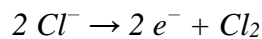
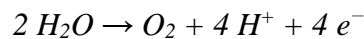
Two main effects have been described for the electrical inhibition in literature. First, the electrical eradication of bacteria was explained by the “bioelectric effect” as it describes the strong bactericidal effect caused by the combination of electrical stimulation and antimicrobial agent treatment.<sup>65,251</sup> The mechanism of the “bioelectric effect” was discussed by many researchers and they concluded the following: the bacteria are not damaged or killed by the electric current, but increased the metabolic activity of the cells sensitizing the bacteria for antibiotics.<sup>252,253</sup> Furthermore, increased oxygen concentrations lead to a reduction in cell numbers.<sup>253,254</sup> Furthermore, a pH change from alkaline to acidic at the cathode decreases the bacterial adhesion. It was stated that protons are produced by anodic oxidation of water at the anode resulting in a pH decrease. At the cathode, hydroxyl ions are produced and lead to an alkaline pH value. This indicated the first proof of electrochemical reactions under electric stimulation (equation 1).<sup>255</sup>

**Equation 1: Chemical reactions of electric stimulation**

*Cathode electrode:*



*Anode electrode*



The hydrogen ions influence a potential disruption of the bacterial membrane and the EPS resulting in an enhanced electrostatic repulsion force between bacteria and the colonized surface.<sup>250,256</sup> Moreover, by the alteration of the ionic strength or the application of an electrical field, electrostatic interactions in the cells are rearranged. As a consequence, adherent bacteria detach by overcoming the van der Waals forces.<sup>257</sup> In other experiments, reactive oxygen species (ROS) were formed by electrolysis leading to the inhibition of the bacterial cell division. Interestingly, the remaining bacteria grew 300 times in length.<sup>258</sup> Moreover, mechanical eradication has an effect on the EPS by radio frequency. The vibrations are assumed to weaken the biofilms' structure and increase the fluidity of the matrix. This favors the penetration of antibiotics into the biofilm.<sup>79,259,260</sup>

Two decades after the introduction of the “bioelectric effect”, the term “electricidal effect” was first established, since the bactericidal action is solely mediated by electrical stimulation.<sup>245</sup> It was verified that the electrical stimulation without antibiotics has an inhibiting effect on the bacterial growth.<sup>245,261,262</sup>

In 2006, the first piezo-electric ceramic elements for bactericidal methods were introduced by Hazan *et al.*<sup>263</sup> Mechanically generated vibrations were evaluated for bacterial surface detachment.<sup>263</sup> For the medical investigation of the electric stimulation, the acoustic energy frequencies are the most promising candidates. However, for the application of electrical currents in patients, acoustic energies at specific frequencies were introduced.<sup>263,264,265,266</sup> Even though intensive efforts have been made in the past 60 years, the complete mechanism of the antibacterial effect is still not completely understood. Also, the knowledge about the electrical stimulation parameters is limited and is available for a few numbers of bacterial species. It is still questionable whether the current passes through the biofilm or simply spreads an electrical field across the electrode surface, because the resistance of a biofilm cannot be determined.<sup>233</sup>

### 2.6.1 Piezoelectricity

Piezoelectricity is translated as “piezo” from the Greek word “piezin” meaning “to press tight, squeeze” and “electricity” from the word *elektron*, the Greek word for “amber”, a source of energy.<sup>267</sup> Therefore, the direct translation of piezoelectricity is pressure-driven electricity. Piezoelectricity is the ability of certain solid materials to transform mechanical displacement into electrical energy (piezo-electric effect). The inverse piezoeffect is the mechanical deformation of a material under the application of an electric field.<sup>268</sup>

It was firstly detected in crystals of quartz by Pierre and Jacques Curie, even though the effect was already described in theory by Charles Coulomb in 1817.<sup>269-271</sup> Lippmann assumed that the piezoelectric material is able to generate electrical charge under pressure and that the inverse effect appears when mechanical strain is developed as electric charges are applied.<sup>272</sup> This was proven in 1881.<sup>273</sup> This study already conducted the direct and the inverse effect of the piezoelectricity (Figure 4).



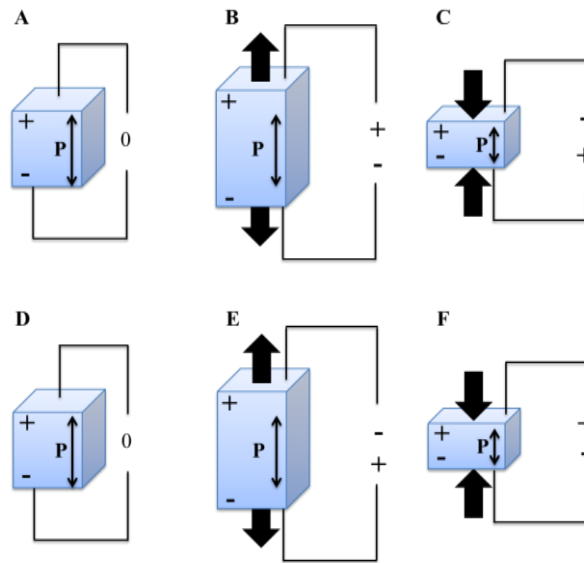


**Figure 4: The piezoelectric effect. A-C direct-, and D-F inverse effect** A) + D) Piezoelectric material without external stress, B) Tension generating energy, C) compression generating energy, E) Electric charge applied for dimensional change, and F) Opposite electric charge applied for dimensional change; Schemata adapted from Vatansever.<sup>274</sup>

The mechanism of the piezoelectricity is the separation of positive and negative electric charges resulting in a dipole moment, It is typically shown as a vector extending from the negative charge to the positive charge.<sup>268</sup> In the piezoelectric effect, piezoelectric crystals are mechanically stressed and the molecular dipole moments re-orient themselves causing a variation of surface charge density and thus a voltage.<sup>275</sup> In the inverse piezoelectric effect, an electric field is applied cross a piezoelectric medium resulting in a change in the shape of the dipoles causing a significant change in the material.

Furthermore, there are materials that have spontaneous electric polarizations, called ferroelectrics.<sup>276</sup> The dipole moments can be reoriented by an external electric field. All ferroelectric materials are piezoelectric, but not all piezoelectric materials are ferroelectric. In nature many piezoelectric materials with different structures are known, e.g. quartz, tourmaline, wood, potassium sodium tartrate (Rochelle salt), DNA and RNA, bone and tendon, keratin and silk, enamel, and myosin.<sup>271,277-285</sup> Known piezoelectric ceramic materials are lithium niobate and lithium titanate, barium titanate, lead titanate, lead zirconate titanate and potassium niobate.<sup>286-293</sup> But also polymers can have oriented dipole structures such as polyvinyl fluoride, PVDF, polysulfone, aromatic polyamides and synthetic polypeptides.<sup>294</sup> The latter materials are produced as fibers or membranes and can be produced in various shapes. At present, the piezoelectricity is exploited in the medical sector as biomedical implants, piezoelectric surgery, microelectromechanical systems and ultrasound imaging and therapies.<sup>268,295-298</sup>

## 2.6.2 Polyvinylidene fluoride as piezoelectric material

PVDF is a ferroelectric, biocompatible thermoplastic fluoropolymer that is resistant against thermal and chemical stress.<sup>299</sup> It withstands UV radiation, has a plane surface and low protein adsorption characteristics.<sup>300</sup> Therefore, this material is one of the most important polymers in engineering.<sup>301</sup> PVDF is mechanically stretched for the orientation of molecular chains and poled under tension for the generation piezoelectric characteristics.<sup>302</sup>

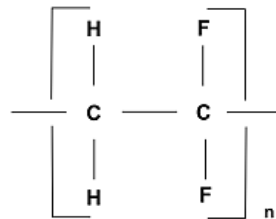


Figure 5: Structural formula of polyvinylidene fluoride.<sup>303</sup>

In the industry, PVDF has many applications, e. g. as separators in batteries or membranes in water treatment.<sup>301,304</sup> The application of piezoelectric PVDF for medical treatment has been evaluated for the stimulation of new bone formation. Reis *et al.* implanted the polymer in an osteotomy cut of sheep femur and tibia and detected an increased bone formation around the areas that have been mechanically stimulated to induce a piezoelectric effect.<sup>305</sup> Additionally, other studies observed increased proliferation, differentiation, and bone remodeling *in vitro* and *in vivo*.<sup>306-310</sup> The bone density depended on the mechanical strain magnitude, frequency and loading duration. This design of a smart medical device is also transferable to dental implants.<sup>311</sup>

## 2.7 Biofilm modeling

Biofilm modeling is a mathematical way to understand the etiology of biofilm-related infections. The modeling of *in vitro* biofilm conditions is economically and less time-consuming than the performance of long-term practical experiments. This field of research is predominated by mathematicians, physics and engineers.

In the 1970s the first bacterial biofilms were simulated by 1 D models for simple reaction/diffusion analysis.<sup>312-315</sup> These models were improved by the implementation of mass transfer at the biofilms surface. Detachment processes and biomass transfer have been included. With the introduction of biological methods as confocal laser scanning microscopy (CLSM), Fluorescent *in situ* hybridization (FISH) and polymerase chain reaction (PCR) in the 1990's, the improved knowledge of biology was conducted to biofilm simulation. The main focus was

drawn on biofilm mechanical / biochemical behavior, morphology, composition and distribution.

In general, biofilm models are categorized in two main groups: 1) DEB models and 2) continuous models.<sup>316-329</sup> The DEB models investigate single particle-based assumption of the individual bacterium. Those particles are described as sphere shaped.<sup>327,330</sup> Therefore, these models can simulate different *in vitro* biofilm configuration of single bacteria. In 2005 Xavier *et al.* modeled the biofilm formation under physiological flow conditions in a particle based model. They solved the Navier-Stokes equation for the flow field and calculated the laminar flow above the biofilm structure. Furthermore, the detachment behavior was implemented to the numerical simulation.<sup>331,332</sup>

Due to computational expense, the DEB models are capable to model micro scale difficulties concerning 3 D issues, but cannot be considered for modeling of multi-physical processes. The continuous models are suitable to simulate numerous scales problems and model physical progressions. Furthermore, the continuous models are capable to model mechanical biofilm behavior within a fluid interphase and bacterial structure interaction. In 1986, Wanner and Gujer invented the one-dimensional biofilm model called W-G model.<sup>320</sup> This model is based on the advective assumption. It describes the biofilm growth rate as a sigmoidal shaped Monod curve of growth limited by the nutrient concentration.<sup>320,333</sup> To further describe the interactions between the structures of the biofilm as the EPS, the internal fluid flow and pores, Alpkvist and Klapper developed the A-K model in 2007.<sup>322</sup> They implemented the biofilm pressure field, called ball-spring method that leads to fluid structure interactions. With this model the simulation of the mechanical response and detachment processes of biofilm mass in a dynamic flow system was accomplished.<sup>322</sup>

The layer between the biofilm and the laminar-flow layer is described as the diffusion boundary layer (DBL).<sup>334,335</sup> Within the A-K model the diffusion of the substrates through the DBL was considered. Next to the thickness of the DBL, other parameters are important for the biofilm simulation: average flow velocity  $u$ , kinematic viscosity  $\nu$ , substrate concentration  $s$ , reactor diameter  $d$ , diffusion coefficient  $D$ , growth rate  $\mu_{\max}$ , biofilm yield  $Y$ , biofilm density  $\rho$ , inactivation rate  $K_i$ , and Sherwood number  $Sh$  as the dimensionless number of mass transport.

In 2009, Duddu *et al.* applied the extended finite element method (XFEM) to this mathematical description of a biofilm that facilitates the investigation of a *S. aureus* biofilm in 2013 for clinical research.<sup>336,337</sup>

Even though there are a lot of studies dealing with the modeling of biofilms, only few is known about numerical simulation of pathogenic biofilms involved in implant-associated infections.

### 3. Materials and Methods

#### 3.1 Nutrient broth, buffer, chemicals, enzymes, kits, devices and laboratory equipment

##### 3.1.1 Nutrient broth and buffer

The nutrient broths and the buffers for the experiments are listed in Table 1.

**Table 1: Nutrient broth and buffer supply.**

<b>nutrient broth / buffer</b>	<b>company</b>	<b>city and country</b>
Tryptic Soy Broth (TSB)	Oxoid, Thermo Fisher Scientific	Waltham, USA
Brain Heart Infusion (BHI)		
Anaerobic Schaedler bouillon		
Yeast extract	Carl Roth	Karlsruhe, Germany
TRIS ( $\geq 99\%$ )		
ethylenediaminetetraacetic acid (EDTA)		
Phosphate-buffered saline (PBS)	Dulbecco's Media, Sigma Aldrich	St. Louis, USA

In the following special mediums were prepared as TSB with 10% yeast extract (TSBY) and TSBY supplemented with 50 mM glucose (TSBYG), BHI with 10  $\mu\text{g}/\text{mL}$  of vitamin K (BHIV) and BHIV added with 5% sucrose (BHIVS), and anaerobic Schaedler bouillon medium supplemented with 10  $\mu\text{g}/\text{mL}$  vitamin K (SV).

### 3.1.2 Chemicals and enzymes

The chemicals and enzymes used in this thesis are listed in Table 2.

**Table 2: Chemicals and enzymes supply.**

<b>chemical / enzyme</b>	<b>company</b>	<b>city and country</b>
D(+)-sucrose	Carl Roth	Karlsruhe, Germany
$\alpha$ D(+)-glucose monohydrate		
vitamin K		
crystal violet (p.a.)		
denatured ethanol ( $\geq 99.8\%$ )		
10% hydrochloric acid		
12% sodium hypochlorite		
sodium thiosulfate pentahydrate ( $\geq 98.5\%$ )		
2-propanol (p.a.)		
$\beta$ -mercaptoethanol		
glycerol ( $\geq 98\%$ )		
25% glutaraldehyde		
lysozyme		
ethylenediaminetetraacetic acid (EDTA)		
100% ethanol (p.a.)	J. T. Baker	Deventer, Netherlands
RNAse-free H <sub>2</sub> O	Qiagen	Hilden, Germany
RNA protect bacteria Reagent		
Agarose	AppliChem GmbH	Darmstadt, Germany
RNA-Protect bacteria reagent	Qiagen	Hilden, Germany
Helibond	Ivoclar Vivadent	Hamburg, Germany
All primers	Eurogentec GmbH	Köln, Germany
propidium monoazide	Biotium	Hayward, USA
mutanolysine	Sigma-Aldrich	St. Louis, USA
ofloxacin	MP Biomedicals	Santa Ana, USA

### 3.1.3 Molecular biology kits

The Table 3 shows all molecular kits used for fluorescence microscopy, RNA- and DNA extraction, real-time PCR, and microarray analysis.

**Table 3: The supplier and manufacture of the kits.**

<b>kit</b>	<b>company</b>	<b>city and country</b>
RNAse-free DNase Set	Qiagen	Hilden, Germany
QuantiTect Reverse Transcription Kit RNeasy Mini Kit		
FastDNA SPIN Kit for Soil	MP Biomedicals	Eschwege, Germany
LIVE/DEAD BacLight Bacterial Viability Kit	Life Technologies	Darmstadt, Germany
Quick Amp Labeling Kit, one color Kit	Agilent Technologies	Ratingen, Germany
SYBR GREEN Maser Mix (dNTPs, MgCl <sub>2</sub> , and DNA polymerase)	Bio-Rad Laboratories	Hercules, USA

### 3.1.4 Experimental devices and laboratory equipment

The experimental devices and the laboratory equipment necessary for the experimental part are listed in Table 4.

**Table 4: Experimental devices and laboratory equipment.**

<b>experimental devices / materials</b>	<b>company</b>	<b>city and country</b>
Oscilloscope DSO 1004A	Agilent Technologies Deutschland GmbH	Ratingen, Germany
Bioanalyzer Agilent microarray, 60-mer Agilent Micro Array Scanner G2565CA		
Incubator SM-30	Bühler	Utzwil, Switzerland
BioPhotometer	Eppendorf	Hamburg, Germany
Inline-Photometer Elo-Check	biotronix GmbH	Hennigsdorf, Germany
Stimulus Generator STG 4008	Multichannel Systems	Reutlingen, Germany
pH-meter	SI Analytics GmbH	Mainz, Germany
Zeiss Leo 1455VP scanning electron microscope	Zeiss	Oberkochen, Germany
Leica NP microscope equipped with a TCS SP2 AOBS scanning head	Leica	Wetzlar, Germany
peristaltic pump IPC-16	Ismatec	Wertheim, Germany
Sigma E140DG camera	Nikon	Tokyo, Japan
NanoDrop ND-1000 spectrophotometer	NanoDrop Technologies	Wilmington, USA
PCR Multicolor detection system	Bio-Rad	Hercules, USA
6-well plates	Greiner, bio one	Frickenhausen, Germany
cell scraper	Sarstedt	Nümbrecht, Germany
MQuant test sticks for Cl <sub>2</sub> and H <sub>2</sub> O <sub>2</sub>	Merck	Darmstadt, Germany
28 mm glass cover slip	Thermo Scientific	Waltham, USA
Imaris 3D image software processing (Version 6.2.1)	Bitplane, Instruments	Oxford Zürich, Switzerland



SSCP software (Version v23.0.0)	International Business Machines	Armonk, USA
Qlucore Omics Explorer (Version 3.2.)	Qlucore	Lund, Sweden

### 3.2 Bacterial strains

The bacterial strains used for the experiments of this thesis are listed in Table 5.

Table 5: The origin of the respective bacterial strains.

bacterial strain	company	city and country
<i>Streptococcus gordonii</i> DSM 20568	German Collection of Microorganisms and Cell Cultures (DSMZ)	Braunschweig, Germany
<i>Streptococcus salivarius</i> DSM 20067		
<i>Staphylococcus aureus</i> DSM 20231		
<i>Porphyromonas gingivalis</i> DSM 20709		
<i>Streptococcus oralis</i> ATCC 9811	American Type Culture Collection (ATCC)	Manassas, USA
<i>Aggregatibacter actinomycetemcomitans</i> ATCC 2474		

### 3.3 Culture conditions

The bacteria *S. gordonii*, *S. salivarius*, *S. oralis* and *S. aureus* were cultured aerobically in TSBY at 37°C under agitation (200 min<sup>-1</sup>) for 18 h (*S. gordonii*, *S. salivarius*, *S. aureus*) or 24 h (*S. oralis*). *P. gingivalis* was cultured anaerobically (10% carbon dioxide, 10% hydrogen, 80% nitrogen) in BHIV over 72 h (*P. gingivalis*) at 37°C without agitation. *A. actinomycetemcomitans* was anaerobically cultured in SV medium over 48 h at 37°C under agitation (200 min<sup>-1</sup>). Subsequently, the bacterial solution was transferred to a round-bottom flask and cultivated anaerobically for a further 48 h at 37°C under stirring. Media containing vitamin K were protected from light to avoid decay of the compound.

### 3.4 Biofilm experiments

Biofilm experiments were performed in static 6-well plates or in flow chamber systems. The culture conditions were as follows:

#### 3.4.1 Aerobic biofilm cultivation

For the biofilm experiments of *S. gordonii* and *S. salivarius*, overnight cultures were adjusted to a starting optical density (OD<sub>600</sub>) of 0.016 with TSBYG. This OD<sub>600</sub> corresponds to  $1.94 \times 10^6$  and  $4.19 \times 10^6$  colony-forming units per ml (CFU/mL), respectively. The biofilm growth of *S. oralis* was performed with a starting OD<sub>600</sub> of 0.026 with BHIVS corresponding to  $3.5 \times 10^6$  CFU/mL. The biofilm cultivation of all three species was conducted for 24 h at 37°C under aerobic conditions. The *S. aureus* overnight cultures were adjusted to an OD<sub>600</sub> of 0.2 with TSBYG, corresponding to  $3.33 \times 10^7$  and cultivated aerobically under agitation at 37°C for 24 h.

#### 3.4.2 Anaerobic biofilm cultivation

*P. gingivalis* suspensions were adjusted to a starting OD<sub>600</sub> of 0.0375 with BHISV. This corresponds to  $7.88 \times 10^6$  CFU/mL. The biofilm growth was performed over 48 h in BHIVS anaerobically. *A. actinomycetemcomitans* biofilm cultivation was performed in SV medium with a starting OD<sub>600</sub> of 0.0319. This corresponds to a bacterial concentration of  $1.25 \times 10^6$  CFU/mL. The biofilms were cultured anaerobically over 72 h. For the biofilm formation in the flow chamber system, the bioreactor was vacuumized twice and subsequently flushed with anaerobic gas (10% hydrogen, 10% carbon dioxide, 80% nitrogen) before inoculation of the bacteria. A balloon connected to the interior of the biofilm reactor served as gas content control.

### 3.5 Determination of colony-forming units

Bacterial suspensions were serially diluted up to 1:10.000. Defined volumes from all dilution steps were plated on solid media and cultured aerobically over 24 h or microaerophilically/anaerobically over 48 h at 37°C. The colonies were subsequently counted and amounts extrapolated according to the dilution series to define the number of vital bacterial cells per mL of culture medium.

## **3.6 Microscopic investigations**

### **3.6.1 Scanning electron microscopy**

For scanning electron microscopy (SEM) imaging, the bacterial colonized PVDF membranes were fixed after stimulation with 2.5% glutardialdehyde solution for 30 min. To prevent electrical charging effects the samples were coated with a layer of Au/Pd (5-10 nm). This process is called sputter coating. The imaging was performed on a Zeiss Leo 1455VP scanning electron microscope.

### **3.6.2 Staining protocol**

For fluorescence microscopy of biofilms, bacteria were stained beforehand. For the removal of planktonic bacteria, biofilms in the static systems were washed twice with PBS. In the dynamic systems, PBS was flushed through the system at constant flow velocity of 100  $\mu\text{L}/\text{min}$  over 15 min. Subsequently, the biofilm was stained with a 1:1000 LIVE/DEAD staining stocks solution. The kit contains two components: Syto 9 and propidium iodide. Syto 9 is a green-fluorescent dye with an excitation and emission spectrum at 480 and 500 nm respectively. Since it is a small molecule, it passes through the bacterial membrane and intercalates with unspecific DNA. The red-fluorescent dye propidium iodide with an excitation/emission spectrum at 490/635 nm is a large molecule that is incapable of passing bacterial cell membranes. It is capable to passes damaged membranes though and thus labels only the DNA of membrane-damaged or dead cells and simultaneously supersedes the Syto 9 dye. Hence, conclusion of the viability of cells can be drawn by the type of fluorescence signal.

Static biofilms also as biofilms that have formed in the flow chamber were stained for 15 min. In the latter case, the dye solution was pumped through the flow chamber system at constant flow rate of 100  $\mu\text{L}/\text{min}$ . Both systems were protected from light since the fluorescent stain is photosensitive. Finally, the biofilm was fixed with 2.5% glutardialdehyde for further 15 min. The static system was subsequently washed twice with PBS.

### **3.6.3 Confocal laser scanning microscopy**

CLSM is an optical imaging technique to provide fluorescence images in high resolution and is characterized by the serial sectioning of a sample with depth selectivity. This enables the 3D-biofilm reconstruction of the specimen in post preparation. Images of biofilms were obtained

with an upright Leica NP microscope equipped with a TCS SP2 AOBS scanning head. Z- stacks images (20-50 images/stack, 1  $\mu\text{m}$  size) of each specimen were acquired at five independent positions (middle, up, down, right, and left). The biofilms were scanned each with 10 x, 40 x, or 63 x magnification, corresponding to a recording area of 1200 x 1200  $\mu\text{m}$ , 300 x 300  $\mu\text{m}$ , or 120 x 120  $\mu\text{m}$ , respectively. The image resolution was 1024 x 1024 pixels.

### 3.6.4 Calculation of biofilm height

For the calculation of average biofilm height (z) the 3D-biofilm reconstructions were analyzed with the Imaris 3D image processing. The biofilm height was calculated by dividing the biofilm volume (V) by the respective recording area (X \* Y).

## 3.7 Flow chamber experiments

The flow chamber has a dimension of 7.0 cm x 5.5 cm x 3.5 cm and is equipped with a 28 mm glass cover slip above the specimen holder, used as an observation window. A 12 mm titanium disc (grade 4) is used as a test specimen. The discs were made uniform with a 45  $\mu\text{m}$  diamond abrasive grinding. Within the first established flow chamber system, the bacterial suspension was pumped circulatory through the flow chamber system, starting from the bioreactor containing the initial bacterial culture. The bacteria were pumped through the system with a peristaltic pump passing a bubble trap before entering the flow chambers. The bubble trap kept the system free from bubbles to guarantee a frictionless biofilm formation on the test specimens. After passing the flow chambers, the bacterial suspension was pumped circulatory into the bioreactor. Throughout the whole experiment, the OD<sub>600</sub> was recorded with an inline-photometer to analyze and control the bacterial behavior and viability. The flow velocity for the continuous circuit flow chamber system was 100  $\mu\text{L}/\text{min}$ . All experiments were performed five times with at least three technical replicates of *S. gordonii*, *S. oralis*, *S. salivarius*, *P. gingivalis*, and *A. actinomycetemcomitans*.

In contrast to first flow chamber system, a second open flow system with continuous feed of nutrients was established. Here, the bacterial suspension was not circulated back into the bioreactor. Any non-adhering bacteria were pumped into a waste bottle. The flow velocities varied between 100-400  $\mu\text{L}/\text{min}$  according to the experimental set-up for the subsequent performance of the biofilm modeling of *S. gordonii* and *S. aureus*. Additionally, the open flow chamber system was supplied by fresh medium throughout the whole experiment to guarantee constant growth conditions for the bacteria.

Both systems were cleaned as follows: 1) 12% sodium hypochlorite for at least 1 h; 2) neutralization with sodium thiosulfate pentahydrate for 1 h; and 3) finally rinsing with tridest. H<sub>2</sub>O. Afterwards, the complete systems were autoclaved at 121°C for 15 min before use.

### 3.8 Electrical stimulation

The electrical simulation was performed with two different devices. For the stimulation under static growth conditions, an electrical stimulation lid was designed and afterwards manufactured by the “Zentrale Forschungswerkstätten” of the Hannover Medical School. The lid was equipped with two platinum electrodes (Figure 19A). It perfectly fits to commercial available six-well plates from Greiner. Each single well was controlled separately. For the stimulation under dynamic bacterial growth, one flow chamber was equipped with platinum electrodes at the inlet and outlet of the flow chamber (Figure 19B).

A stimulus generator STG 4008 was utilized for electrical stimulation. The stimulation parameters were controlled with an Oscilloscope DSO 1004A. Both instruments were gratefully borrowed from the department of “Experimental Neurosurgery, Hannover Medical School” directed by Prof. Kerstin Schwabe.

The initial static trials were conducted on polystyrene (six-well plates) to define the appropriate stimulation parameters. The main experiments were performed on PVDF membranes produced by Bastian Dreyer. Those membranes were fixed on the polystyrene (static) and titanium discs (dynamic) by Heliobond. For polymerization, the Heliobond was illuminated with a blue light (intensity = 1000 mW/cm<sup>2</sup>) for a total of 30 s. Bacterial cultivation was conducted as described in *section 3.4*. For static cultured experiments, 3 mL bacterial suspension was used. Four of the six wells were utilized for electrical stimulation of the bacterial suspension. One well was used as biofilm control without stimulation (BFNS) and the sixth well was utilized for stimulation of the growth medium.

#### 3.8.1 Production of PVDF membranes

The development and production of the PVDF membranes was the main goal of the doctoral thesis of Bastian Dreyer: “Development of tooth implants with inherent electrical stimulation of the bone by piezoelectric”. The thesis has not yet been submitted. In short, PVDF (20 wt%, 275.000 Mw) was dissolved in N,N-Dimethylformamide and stirred at 60°C for 12 h. Thin film preparation was performed via the standard doctor blade method. Afterwards, the produced PVDF membranes were dried at 60°C overnight. After production, the PVDF films were

autoclaved at 121°C for 20 min to guarantee sterile conditions for the experimental observation. An example of a PVDF film is shown in Figure 6.



**Figure 6: Example of a PVDF film.** The membrane was produced by Bastian Dreyer.

### 3.8.2 Determination of pH values

The pH values of the supernatants of the stimulated samples under static growth conditions were determined with a pH-meter. The pH of the supernatants was measured before and after electrical stimulation.

### 3.8.3 Determination of chlorine and hydrogen peroxide content

The determination of the chlorine concentration in the unstimulated and the stimulated supernatants were analyzed with MQuant test sticks. The tests were performed according to the manufacturers' instructions. The sensitive range was 0.5-1-2-5-10-20 mg/L for Cl<sub>2</sub> and 0-0.5-2-5-10-25 mg/L for H<sub>2</sub>O<sub>2</sub>.

### 3.8.4 Agar plates

The agar plates were either prepared with TSBY (*S. gordonii*, *S. oralis*, *S. salivarius* and *S. aureus*) or BHI (*P. gingivalis* and *A. actinomycetemcomitans*) with 1.5% agar. The agar was autoclaved at 121°C for 15 min and transferred into 9 mm petri dishes (20 mL/dish). After cooling down to 55°C, BHI plates were supplemented with 10 µg/mL vitamin K and stored in the dark.

### 3.8.5 Viability test on agar plates

The viability of the bacteria after electrical stimulation was determined by plating 100  $\mu$ L each of supernatant, medium and control on agar plates after the stimulation. The plates were incubated at 37°C for 24 h (aerobic, *S. gordonii* and *S. salivarius*) and 48 h for *P. gingivalis* (anaerobic). Plates were recorded with a Sigma E140DG camera.

## 3.9 Molecular investigations

### 3.9.1 Isolation of DNA

The DNA of electrically stimulated and control bacteria was isolated with a Fast DNA SPIN Kit for Soil according to manufacturer's instructions and eluted in 100  $\mu$ L tridest. water. The concentration was measured with a NanoDrop ND-1000 spectrophotometer and stored at -20°C for further processing.

### 3.9.2 Isolation of RNA

The RNA isolation protocol was modified from a previously published RNA-isolation protocol.<sup>338</sup> After the electrical stimulation, the supernatant (3 mL) and biofilm of each well were transferred separately to 15 mL reaction tubes each. The biofilm was resolved from the PVDF membrane surface with a cell scraper and transferred to 3 mL PBS. RNA-Protect bacteria reagent was added directly to the supernatants and biofilms in a 2:1 ratio. Afterwards, the reaction tubes were closely sealed vortexed for 1 min full speed and incubated for 15 min at RT. The suspensions were pelleted by centrifugation (5 min, 4000 x g, RT). The supernatant was discarded. For chemical cell disruption, the bacterial pellets were resuspended in 400  $\mu$ L lysis buffer (10 mM Tris, 1 mM EDTA, pH 8.0, 15 mg/mL lysozyme and 500 U/mL mutanolysine) and incubated for 90 min at RT under agitation (350 rpm). Subsequently, 700  $\mu$ L RLT Buffer supplemented with 1% (v/v)  $\beta$ -mercaptoethanol were added to the bacterial solutions and vortexed for 10 s at full speed. For mechanical disruption of the bacteria, 50 mg acid-washed glass beads (diameter 106  $\mu$ m) were added to the suspensions. The mixture was vortexed for 30 s at full speed and allowed to cool down on ice for 30 s to protect the RNA from heat disruption. This procedure was repeated 10 times. Afterwards, samples were centrifuged (2 min, 13.000 rpm, RT). The supernatants were supplemented with 100% ice-cold ethanol, gently mixed and centrifuged (1 min, 13.000 rpm, RT). The pellets were discarded.

The resulting total RNA was isolated with the RNeasy Mini Kit following the manufacturer's instructions. The remaining DNA was removed with an RNase-free DNase set according to the manufacturer's instructions. The procedure of total RNA-isolation and DNA removal was repeated twice. Finally, the RNA was eluted in 50  $\mu$ L RNase-free H<sub>2</sub>O. The concentrations were measured with a NanoDrop ND-1000 and stored at -80°C. The integral quality of the RNAs was identified on a Bioanalyzer chip for RNA.

### 3.9.3 Propidium monoazide assay

Propidium monoazide (PMA) is a photo-reactive DNA dye predominantly binding to double-stranded (ds) DNA. It is used for the quantification of vital and dead bacterial cells. Through photolysis reactive acid groups of the PMA are converted to nitrene radicals. These radicals react with any carbohydrate residual, leading to a stable covalent nitrogen-carbon binding. PMA is incapable of passing the bacterial membrane. Hence, it only binds to dsDNA in membrane-damaged or dead cells. The PMA intercalates to the DNA by covalent binding. Thus, in a PCR the damaged/dead cells are inhibited and cannot be amplified by DNA-polymerase. The following protocol was modified according to Kommerein *et al.*<sup>339</sup> After stimulation, supernatants and biofilms (via cell scraper and resuspended in 3 mL PBS) were transferred to a 15 mL reaction tube each and pelleted by centrifugation (5 min, 4000 x g, RT). Afterwards, the supernatants were discarded and the pellets resuspended in 1 mL PBS. The suspension was divided in equal parts for vital/dead samples. The vital samples were supplemented with 4 mM PMA and incubated at 4°C for 10 min. Afterwards, photolysis was triggered with a 470 nm 3 W LED light source for 20 min. Subsequently, the sample was centrifuged (5 min, 5.000 x g, RT) and washed once with PBS. After the last centrifugation, supernatants were discarded and the pellets stored at -20°C.

The dead samples/controls were supplemented 1:10 with ice cold 70% 2-propanol, vortexed for 1 min at full speed, and incubated for 15 min at RT. Afterwards, the bacterial suspensions were pelleted (10 min, 5.000 x g, RT) and the supernatants were discarded. Subsequently, the samples were washed twice with PBS and pelleted again (10 min, 5.000 x g, RT). The bacterial pellets were resuspended in 50  $\mu$ L PBS and incubated for 10 min at 95°C under agitation (350 rpm). At last, the samples were incubated at -80°C for 10 min. Afterwards, the bacterial solutions were supplemented with 4 mM PMA and treated equally to live samples. The PMA assay was followed by DNA-isolation.



### 3.9.4 Quantitative real-time PCR

The quantitative real-time PCR (qRT-PCR) was performed with the iQ5 real time PCR Multicolor detection system. The primer sequences are listed in Table 6. The respective qRT-PCRs were performed in a total volume of 25  $\mu$ L containing 12.5  $\mu$ L iQ SYBRGreen supermix 0.2  $\mu$ M forward and reverse primers and 10 ng of the template DNA. The PCRs were performed with an initial incubation of 3 min at 95°C, followed by 40 cycles of denaturation for 10 s at 95°C. The annealing was performed for 20 s. The respective annealing temperatures are listed in Table 6. It was followed by the amplification at 72°C for 20 s and a melting curve analysis. The genomic DNA was calculated by a standard curve. The curves were generated with defined concentrations in a dilution series. The corresponding number of bacterial cells was determined by the division of the measured DNA and the total genome weight per cell listed in Table S 4. The experiments were performed in biological and technical triplicates. Here, the respective bacteria in the supernatants and biofilms samples were pooled from six-wells, respectively.

**Table 6: Primer for real- time PCR of *S. gordonii*, *S. salivarius*, and *P. gingivalis*.**

<b>bacterium</b>	<b>primer name</b>	<b>primer sequence 5' → 3'</b>	<b>annealing temperature</b>
<i>S. gordonii</i>	<i>S.g.</i> forward	AACGGAATGCACGATGGAGT	56°C
<i>S. gordonii</i>	<i>S.g.</i> reverse	TCGTTCCAATGGAGCCTAGC	
<i>S. salivarius</i>	<i>S.s.</i> forward	GTTGCCACATCTTCACTCGCTT	58°C
<i>S. salivarius</i>	<i>S.s.</i> reverse	CGTTGATGTGCTTGAAA GGCACCATT	
<i>P. gingivalis</i>	<i>P.g.</i> forward	AGGCAGCTTGCCATACTGCG	56°C
<i>P. gingivalis</i>	<i>P.g.</i> reverse	ACTGTTAGCAACTACCGA TGT	

### 3.9.5 Microarray analysis

The *S. gordonii* microarray chip (Design-ID: 077018) was based on the array with GEO accession number: GPL5736.<sup>340,341</sup> The design is based on the genome of *S. gordonii* str. Challis substr. CH1.<sup>342</sup> The original microarray assay was performed with a 70-mer array. Here, a 60-mer Agilent microarray chip was designed with three variants of the probe: 1) removal of the first ten nucleotides, b) removal of the last ten nucleotides, and c) and removal of five nucleotides at the beginning and end each. The procedure is visualized in Figure 7.

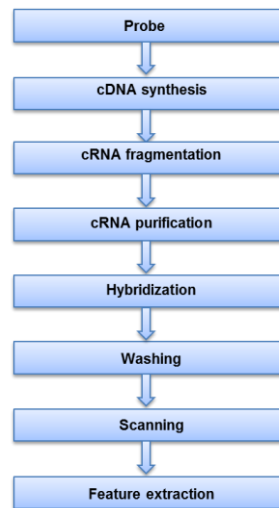


**Figure 7: Flow chart of the sample preparation for a microarray assay.**

In essence, Microarray experiments were performed as described in the application note ‘Gene Expression Profiling of Prokaryotic Samples using Low Input Quick Amp WT Kit’ (Publication Number 5991-0879EN, Agilent Technologies 2012). The cRNA synthesis and fragmentation as well as hybridization and washing steps were carried-out as recommended in the ‘One-Color Microarray-Based Exon Analysis-LIQA WT Labeling Protocol’ (publication G4140-90042, Version 1.0, November 2010), except that 2500 ng of each fluorescently labeled cRNA population were used for hybridization. The slides were scanned on the Agilent Micro Array Scanner G2565CA (pixel resolution 3  $\mu\text{m}$ , bit depth 20). Data extraction was performed with the ‘Feature Extraction Software V10.7.3.1’ using settings outlined in the extraction protocol file ‘GE1\_107\_Sep09.xml’, except for the inactivation of the ‘Multiplicative detrending’ algorithm. The measurements of on-chip replicates (quintuplicates) were averaged using the geometric mean of processed intensity values of the green channel, ‘gProcessedSignal’ (gPS) to retrieve one resulting value per unique non-control probe. Single features were excluded from averaging, if they 1) were manually flagged, 2) were identified as outliers by the Feature Extraction Software, 3) lay outside the interval of ‘1.42 x interquartile range’ regarding the normalized gPS distribution of the respective on-chip replicate population, or, iv) outlined a coefficient of variation of pixel intensities per feature that exceeded 0.5. Averaged gPS values were normalized by a quantile normalization approach. The preparation and experimental performance was done by the research unit of “Transcriptomics” directed by Dr. Oliver Dittrich-Breiholz of the Hannover Medical School. For the evaluation of the data, the excel-based program RCUTAS (Version 2012) was employed.

### 3.10 Antibiotic treatment of *S. aureus*

The *S. aureus* overnight culture was adjusted to a starting OD<sub>600</sub> of 0.2 corresponding to  $3.33 \times 10^7$  CFU/mL. The bacterial cultures were supplemented with the antibiotic fluoroquinolone ofloxacin (600 µg/mL). An untreated *S. aureus* culture was used as control. The bacterial growth was investigated for three different antibiotic regimes: 1.) 8 h antibiotics and 16 h recultivation in fresh TSBY medium; 2.) 15 h antibiotics and 9 h recultivation in fresh medium; and 3.) 20 h antibiotics, and 4 h recultivation in medium. To guarantee the removal of ofloxacin within the recultivation period, the samples were washed twice with PBS and centrifuged (15 min, 4,000 x g, 4°C) after antibiotic treatment. All experiments were performed in quadruplicates over a period of five to six days. The OD<sub>600</sub> of the three regimes was determined five times within 24 h. The viability of the cultures and the controls were controlled by plating the bacterial suspension in dilution series on agar plates (10 µL). The plates were cultivated aerobically at 37°C over 24 h and recorded. Afterwards, the plates were cultivated for further 48 h to exclude false negative results due to growth impairment. Additionally, the susceptibility of ofloxacin was tested on TSBY agar plates supplemented with 600 µg/mL ofloxacin. Bacterial cultures and controls (both 10 µL) were plated and incubated for 48 h at 37°C to exclude false negative results.

### 3.11 Statistical analyses

The statistical analyses were performed with the SSCP Software. Average biofilm heights and standard deviations of the independent biological replicates were analyzed with a one-dimensional ANOVA Test. The significance level was set to  $p \leq 0.05$ .

### 3.12 Numerical simulation

The numerical simulations were performed by Dianlei Feng as described in Feng *et al.* and the according doctoral thesis “Numerical modeling of biofilm growth and detachment on interfaces in flow fluids using DG FEM” (not submitted).<sup>343</sup> The simulation developed by Dianlei Fang is based on the model of Alpkvist and Klapper.<sup>322</sup> The DEB model was based on the SPH method used for simulating fluid flows and utilized by Meisam Soleimani’s simulation.<sup>344,345</sup>



## 4. Results and Discussion

### 4.1 Development of a flow chamber system for the reproducible *in vitro* analysis of biofilm formation on implant materials

#### *Preface*

This work describes the development and evaluation of a dynamic flow chamber system for quantitative analysis of bacterial attachment to dental implant materials. Studies focusing on biofilm formation of oral commensals and periodontopathogens under physiological flow conditions have been rarely reported. Furthermore, the few existing devices and experimental procedures have not been designed for targeted implant material testing. Here, we describe a flow chamber design, experimental set-up and a microscopic analysis method for this purpose. First, we have chosen a panel of orally relevant bacteria, consisting of commensals and periodontopathogens (*S. gordonii*, *S. oralis*, *S. salivarius*, *P. gingivalis* and *A. actinomycetemcomitans*) for our experiments. In the following, we have adapted the individual cultivation conditions and the flow chamber set-up to give a reproducible biofilm formation under physiological flow conditions. Finally, biofilm quantification by CLSM analysis have been established. According to our requirements, we have successfully developed a robust and reproducible implant material test system to be used with oral bacteria under physiological flow conditions. This study was the initial investigation of flow chamber systems and has been further improved as described in *section 4.2*.

The initial study was initiated by Prof. Dr. MEIKE STIESCH. The flow chamber set-up was developed by HENRYKE RATH and Dr. SASCHA NICO STUMPP, Medical School Hannover. Manufacturing of technical devices was carried out in the “Zentrale Forschungswerkstätten” department of the MHH. The biological experiments, data analysis and evaluation was performed by HENRYKE RATH guided by Dr. SASCHA NICO STUMPP. The initial manuscript was written by HENRYKE RATH and refined together with Dr. SASCHA NICO STUMPP and Prof. Dr. MEIKE STIESCH. The manuscript was submitted to the Journal *Public Library of Science (PLoS) One*.

## **Development of a Flow Chamber System for the reproducible *in vitro* Analysis of biofilm Formation on Implant Materials**

Henryke Rath<sup>1</sup>, Sascha Nico Stumpp<sup>1</sup>, Meike Stiesch<sup>1</sup>

<sup>1</sup>Clinic for Prosthetic Dentistry and Biomedical Materials Science, Hannover Medical School,  
Hannover, Germany

### **4.1.1 Abstract**

Since the introduction of modern dental implants in the 1980s, the number of inserted implants has steadily increased. Implant systems have become more sophisticated and have enormously enhanced patients' quality of life. Although there has been tremendous development in implant materials and clinical methods, bacterial infections are still one of the major causes of implant failure. These infections involve the formation of sessile microbial communities, called biofilms. Biofilms possess unique physical and biochemical properties and are hard to treat conventionally. There is a great demand for innovative methods to functionalize surfaces antibacterially, which could be used as the basis of new implant technologies. Present, there are few test systems to evaluate bacterial growth on these surfaces under physiological flow conditions. We developed a flow chamber model optimized for the assessment of dental implant materials. As a result, it could be shown that biofilms of the five important oral bacteria *S. gordonii*, *S. oralis*, *S. salivarius*, *P. gingivalis*, and *A. actinomycetemcomitans*, can be reproducibly formed on the surface of titanium, a frequent implant material. This system can be run automatically in combination with an appropriate microscopic device and is a promising approach for testing the antibacterial effect of innovative dental materials.

### **4.1.2 Introduction**

More than 700 bacterial species inhabit the human oral cavity.<sup>82</sup> While a large proportion of these bacteria are harmless commensals, opportunistic bacteria can trigger common oral diseases like caries, peri-implantitis and the chronic inflammatory disease periodontitis.<sup>82,85</sup> Most bacteria within the oral cavity are sessile and form highly organized microbial communities, referred to as biofilm, on the surfaces of soft and hard tissues. Bacteria are embedded in a matrix of self-secreted EPS that determine the three dimensional structure of the

biofilm.<sup>346</sup> As the EPS matrix shields cells in the biofilm from antimicrobials as well as from the host immune response, sessile bacteria can exhibit up to 5000-fold greater resistance to antibiotics than free floating (planktonic) cells.<sup>63</sup> There are three mechanisms that increase antibiotic resistance: First, the EPS acts as a potent diffusion barrier that antagonizes antibiotic penetration into the biofilm.<sup>68,69</sup> Second, the sessile life cycle stage is accompanied by a metabolic activity change that reduces the antibiotic uptake.<sup>66,67,347-349</sup> Third, via horizontal gene transfer resistance genes can be exchanged between bacteria in biofilms as reported by Roberts *et al.*<sup>350</sup> The high antibiotic tolerance makes biofilm infections hard to treat. Despite intensive research, these bacterial communities still pose a severe medical complication. Therefore, the biofilm-related infections belong to the main reasons for early and late implant loss in dental implantology, as well as in other medical disciplines.<sup>351</sup> Therefore, studies are necessary investigating oral biofilm formation in order to develop implant surfaces that reduce biofilm formation and the risk of implant failure.

Even though flow chamber systems have been used to study biofilm formation in oral implants research, most studies were conducted under static conditions.<sup>209,352-355</sup> These require a less sophisticated experimental set-up and show greater ease of handling.<sup>201</sup> However, the physiological flow conditions, as they are found at the dental implantation site, are not considered in these systems. Even though, the application of a static or dynamic system depends on the considered scientific question. The microenvironmental conditions have substantial impact on biofilm morphology and growth behavior as they influence: A) oxygen and nutrients transport processes through the biofilm, B) transport of signal molecules, e.g. quorum sensing messengers that alternates the biofilm morphology and physiology, C) heat and mass transfer that coordinates the biotransformation reaction and energy losses, D) gene expression and EPS content and E) spreading of biofilms through increasing the mobility of pioneering bacterial cells.<sup>202-208</sup>

Sternberg *et al.*, Besemer *et al.*, Purevdori *et al.*, and Zhang *et al.* focused on a variety of features of biofilms, including the influence of flow velocity on biofilm morphology and the distribution of bacterial growth activity within a flow chamber system.<sup>205,356-359</sup> Biofilm behavior was also tested under different chemical and physiological conditions as the pH or the different nutrient and oxygen concentrations in a flow environment.<sup>202,203,205,355-358</sup>

Clinical research with flow chamber systems has increased rapidly within the last decade. For example, Zhao *et al.* developed a model to investigate different implant materials for the suppression of biofilm formation and Chin *et al.* used a flow chamber system to test the effects

of antibacterial agents on orthodontic binding materials.<sup>360,361</sup> In 2013, da Silva Domingues *et al.* developed a parallel flow chamber system to elucidate the adherence mechanisms of *S. aureus* and quantify phagocytosis by murine and human macrophages.<sup>193</sup> Even though, dynamic studies of oral biofilm formation and characterization have to be improved. These studies have to include the implant material, implant failure relevant bacteria, reproducible culture and flow conditions.

Biofilm architecture is greatly influenced by the colonizing bacterial species or the species composition. The present study focused on a selection of oral biofilm formers that reside within the oral cavity during health and/or disease: *S. gordonii*, *S. oralis*, *S. salivarius*, *P. gingivalis*, and *A. actinomycetemcomitans*. The gram-positive streptococci *S. gordonii*, *S. oralis* and *S. salivarius* are commensal bacteria that, as pioneer colonizers, provide adhesion sites to middle and late colonizing bacterial species.<sup>113,114</sup> *S. salivarius* is an opportunistic pathogen that may occasionally cause infections such as caries in man and which is involved in the development of halitosis.<sup>136,137</sup> One of the most virulent opportunistic pathogenic streptococci is *S. oralis*. This bacterium expresses a sialidase, an enzyme that hydrolyses the bonds between sialic acids residues and the hexose or hexosamine residues at the terminal side of the oligosaccharides in glycolipids and glycoproteins. In the bacterial host, the enzyme cleaves target structures and thus unfavorably influences cellular processes.<sup>121-124</sup> Moreover, *S. oralis* causes infective endocarditis and is a major pathogen in immunosuppressed patients.<sup>125-127,145</sup>

*P. gingivalis* and *A. actinomycetemcomitans* are rod-shaped, anaerobic, gram-negative bacteria that can cause severe diseases, including periodontitis.<sup>18,145,146</sup>

*P. gingivalis* secretes inflammatory compounds and toxins that attack host tissue and can lead dysbiosis of the microbial flora.<sup>139</sup> *A. actinomycetemcomitans* produces virulence factors that allow the migration and invasion of other bacteria, e.g. the expression of leukotoxins. Thus, host periodontal tissue is damaged and the immune response severely weakened.<sup>158,160</sup>

For oral implant materials testing a standardized *in vitro* biofilm model for a panel of relevant bacterial species is missing. The aim of the study was to establish and evaluate a flow chamber system for this purpose. The experimental parameters growth environment, cultivation duration and nutrient supply had to be optimized for the biofilm formers, *S. gordonii*, *S. oralis*, *S. salivarius*, *P. gingivalis* and *A. actinomycetemcomitans* to give a reproducible and robust biofilm formation *in vitro*.



### 4.1.3 Materials and methods

#### 4.1.3.1 Bacterial strains

*S. gordonii* DSM 20568, *S. salivarius* DSM 20067 and *P. gingivalis* DSM 20709 were obtained from the German Collection of Microorganisms and Cell Cultures (DSMZ). The bacterial strains *S. oralis* ATCC 9811 and *A. actinomycetemcomitans* ATCC 2474 were purchased from the American Type Culture Collection (ATCC).

#### 4.1.3.2 Bacterial cultivation and biofilm formation

*S. gordonii*, *S. salivarius* and *S. oralis* were routinely precultured in TSB supplemented with 10 % yeast extract), aerobically at 37°C in an incubator shaker for 18 h (*S. gordonii*, *S. salivarius*) or 24 h (*S. oralis*). For the induction of biofilm formation, *S. gordonii* and *S. salivarius* cultures were adjusted to an of 0.016 in TSB medium modified by addition of 50 mM glucose and stirred for 24 h at 37°C for biofilm formation. This OD<sub>600</sub> corresponds to an inoculum of: 1.94 x 10<sup>6</sup> CFU/mL for *S. gordonii* and 4.19 x 10<sup>6</sup> CFU/mL for *S. salivarius*, respectively. For *S. oralis*, the procedure was identical, except that an OD<sub>600</sub> of 0.026 was chosen (3.5 x 10<sup>6</sup> CFU/mL) and that BHI medium supplemented with 5 % sucrose and 10 µg/mL vitamin K was used as nutrient broth. *S. oralis* was also cultured for 24 h.

*P. gingivalis* was cultured anaerobically (10 % carbon dioxide, 10 % hydrogen, 80% nitrogen) in BHI medium modified with 10 µg/mL of vitamin K for 24 h without agitation at 37°C, followed by culture in an incubator shaker (200 min<sup>-1</sup>) for 48 h. For biofilm formation experiments, the cultures were adjusted to an OD<sub>600</sub> of 0.0375 (7.88 x 10<sup>6</sup> CFU/mL) in BHI medium supplemented with 5 % sucrose and 10 µg/mL vitamin K. The bacterial suspension was anaerobically grown under continuous stirring for 48 h at 37°C for biofilm formation.

*A. actinomycetemcomitans* was routinely cultured anaerobically in Schaedler bouillon supplemented with 10 µg/mL vitamin K at 37°C under agitation (200 min<sup>-1</sup>) for 48 h and was then transferred to an Erlenmeyer flask to be cultured for an additional 48 h under continuous stirring. To induce biofilm formation by *A. actinomycetemcomitans*, cultures were adjusted to an OD<sub>600</sub> of 0.0319 (1.25 x10<sup>6</sup> CFU/mL) in Schaedler bouillon supplemented with 10 µg/mL vitamin K and anaerobically cultured for 72 h at 37°C under continuous stirring for biofilm formation.

All experiments modified with vitamin K were protected from light to avoid the destruction of the compound by light. For the anaerobic cultivation of *P. gingivalis* and *A. actinomycetemcomitans*, the bioreactor and the flow chamber system were evacuated twice

and subsequently flushed with anaerobic gas mix. The system was kept pressurized by connecting a gas filled balloon to the bioreactor. Thus, the inflow of oxygen was inhibited throughout the experiment.

#### **4.1.3.3 Flow chamber system**

The flow chamber devices were 7.0 cm x 5.5 cm x 3.5 cm in size and were equipped with a 28 mm glass cover to allow direct macro- and microscopic analysis of biofilm formation on test surfaces Figure 8. Titanium discs (grade 4) with a diameter of 12 mm were used as specimens. Each of these underwent surface treatment with a 45  $\mu\text{m}$  diamond abrasives grinding disc to generate a uniform surface pattern for bacterial adhesion. The bacterial suspension was recirculated from the bioreactor to the flow chambers and back at a flow rate of 100  $\mu\text{L}/\text{min}$ . The flow chamber system was kept air-free by use of bubble traps. To monitor bacterial growth in the bioreactor, the  $\text{OD}_{600}$  was continuously recorded during the experiment using an inline photometer. Each flow chamber experiment was repeated independently five times with at least three technical replicates.

#### **4.1.3.4 Biofilm imaging and analysis**

The flow chambers were separated from the system by surgical clamps at the collector's site. New sterile tubings were connected to the tubings of the peristaltic pump. Biofilms were washed by pumping PBS through the flow chambers to remove planktonic bacteria. The biofilms were specifically stained live/dead by flushing with a 1:1000 dilution of BacLight staining mix. Syto 9 is a green fluorescent dye that passes bacterial cell membranes by diffusion and intercalates unspecifically into bacterial DNA. Propidium iodide is a red fluorescent dye that, due to its size, cannot pass intact cell membranes. Dye intercalation is only observed in dead cells in which membrane integrity is impaired. The bacteria were stained for 15 min at a flow rate of 100  $\mu\text{L}/\text{min}$  in the dark and subsequently examined by CLSM. From each specimen, image stacks were acquired at five different positions; center, right, left, top and bottom, using 10x magnification. The Imaris 3D image processing was used to calculate mean biofilm height.

#### **4.1.3.5 Statistical analysis**

The experiments were performed five times for each bacterial species, and the mean biofilm height and standard errors were calculated. The mean biofilm heights between independent biological replicates were compared using the univariate ANOVA test with a significance level of 0.05. All statistical analyses were conducted using the software package SPSS.

## 4.1.4 Results

### 4.1.4.1 The flow chamber system

The flow chamber system was successfully manufactured according to the construction plans. An assembly drawing of the chamber is presented Figure 8. A. As test specimen titanium discs were used. To allow for macro-and microscopically specimen observation, the stainless steel cover plate had been manufactured with a circular recess, housing a microscopic cover glass. In Figure 8B, the complete set-up of a flow chamber in a continuous flow circuit is depicted. The growth conditions were successfully adjusted under aerobic and anaerobic conditions as seen by the formation of stable, mature biofilms on the titanium specimens (Figure 9).

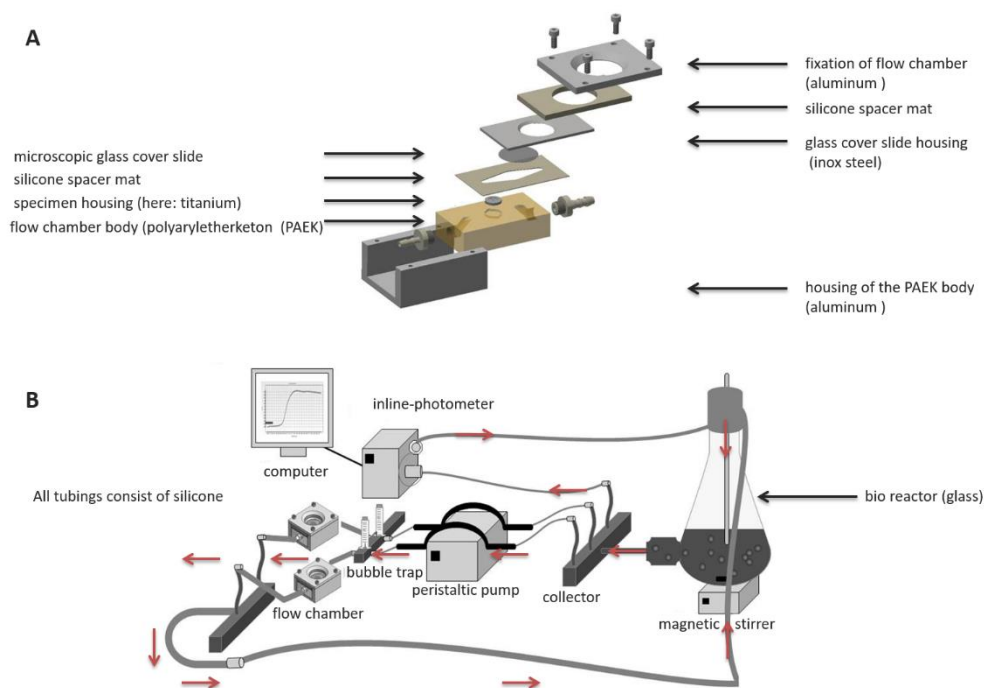


**Figure 8: Sketch of the flow chamber and flow chamber system.** A) Assembly drawing with test specimen; B) General set-up of the closed circuit system. The red arrows indicate the direction of the flow.

### 4.1.4.2 Micro- and macroscopic evaluation of biofilm formation

Biofilm formation of *S. gordonii*, *S. oralis*, *S. salivarius*, *P. gingivalis* and *A. actinomycetemcomitans* was evaluated under constant flow conditions. A confluent biofilm formation was observed for all tested bacterial species. The bacterial cultures in the bioreactor showed normal growth behavior during the experiment and the resulting biofilms were structurally intact and composed of predominantly vital cells (Figure 9 A-E). For all species, biofilm formation was highly reproducible between independent experiments. However, the observed biofilm morphologies were unique to the individual species. In detail, *S. gordonii* (A)

and *S. salivarius* (C) biofilms showed relatively homogenous surface pattern interspersed with a few tower-like structures. *S. oralis* (B) biofilms demonstrated an uneven surface pattern with numerous tower-like structures. The *P. gingivalis* (D) biofilm showed a rough biofilm surface with macrocolonies. The biofilm of *A. actinomycetemcomitans* (E) demonstrated an open and loose microbial biofilm structure.

Throughout all experiments, the biofilms exhibited high structural stability and no visible detachment was detected during sample preparation for microscopic analysis.

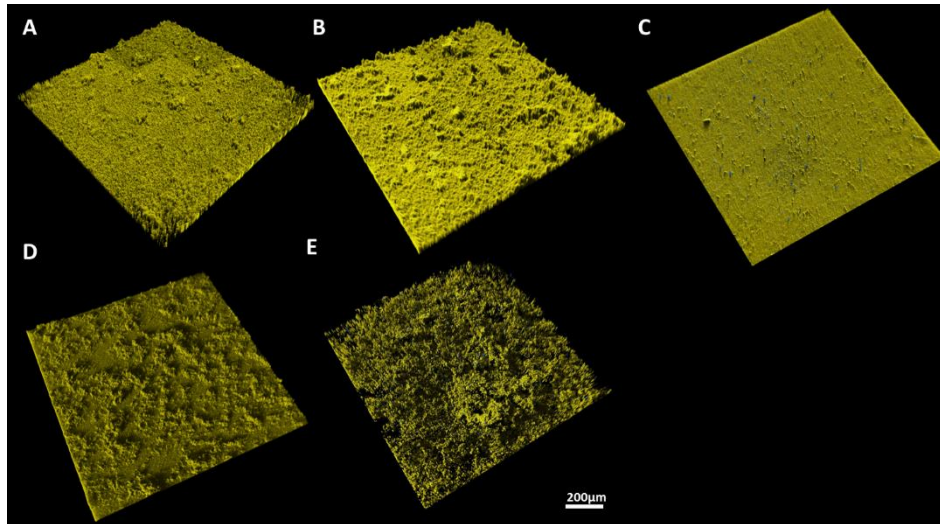


**Figure 9: 3D reconstruction of biofilms in side view.** The cells were stained live/dead and analyzed by CLSM. Vital cells are depicted in yellow, viable cells in blue. A) *S. gordonii*, B) *S. oralis*, C) *S. salivarius*, D) *P. gingivalis*, and E) *A. actinomycetemcomitans*.

#### 4.1.4.3 Calculation of mean biofilm height

Mean biofilm heights were determined for the five bacterial species tested. For each species, the reproducibility of biofilm formation between the independent experiments was statistically significant (Figure 10). The greatest mean biofilm height was observed for *P. gingivalis* with 38.85  $\mu\text{m}$  ( $p=5.2 \times 10^{-13}$ ), followed by *A. actinomycetemcomitans* with 28.9  $\mu\text{m}$  ( $p=0.01$ ), *S. oralis* with 28.5  $\mu\text{m}$  ( $p=0.003$ ), *S. salivarius* with 26.5  $\mu\text{m}$  ( $p=0.008$ ), and *S. gordonii* with 21.1  $\mu\text{m}$  ( $p=0.000009$ ).

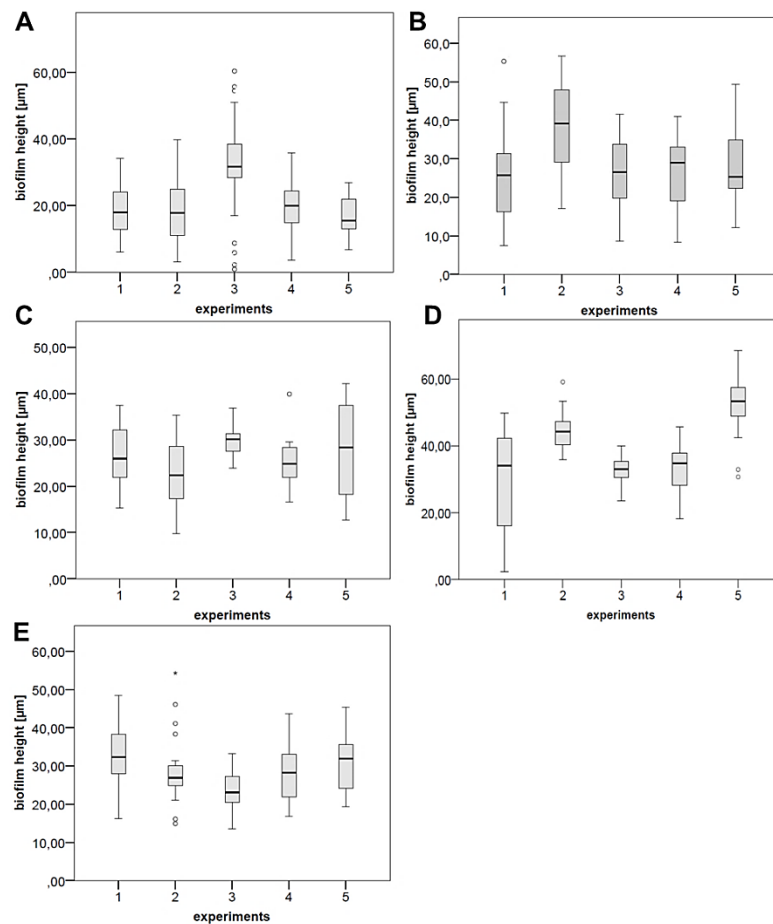


**Figure 10: Biofilm heights on titanium substrata in the flow chamber system.** In each diagram, the mean biofilm heights for five independent experiments are shown. A) *S. gordonii*, B) *S. oralis*, C) *S. salivarius*, D) *P. gingivalis*, and E) *A. actinomycetemcomitans*.

#### 4.1.5 Discussion

Many flow chamber systems have been developed within recent decades to analyze biofilm formation and dynamics in a fluid system. Our flow chamber system was optimized for the experimental investigation of dental relevant bacteria on the implant material titanium, as this is an important approach to prevent implant failure due to biofilm-associated infections. Within the presented flow chamber system, the replacement of the titanium disc with other disc-shaped sample materials of interest is applicable without time-consuming reconstruction measures. The complete flow chamber system is reusable and fully autoclavable. The cultivation set-up can easily be modified according to the optimal growth conditions of the respective bacterial species under aerobic as well as anaerobic conditions.

We focused on a group of bacteria, consisting of oral commensal and periodontopathogenic bacteria: *S. gordonii*, *S. oralis*, *S. salivarius*, *P. gingivalis*, and *A. actinomycetemcomitans*. Previous studies have mostly described biofilm formation under static test conditions, but *in*

*vivo* the flow has great influence on the of the biofilm behavior.<sup>362,363</sup> Therefore, fluid systems have been established to mimic the physiological flow conditions within the oral cavity.<sup>364</sup> To achieve a realistic experimental set-up, we chose a flow speed of 100  $\mu\text{L}/\text{min}$ , as it is described for the natural saliva flow in the hibernation mode.<sup>365</sup> The bacterial suspension was pumped continuously over the test specimens as in the oral cavity bacteria-contaminated saliva is permanently flooding the implant.

All bacterial species exhibited reproducible and homogenous growth behavior under the given flow conditions, as confirmed by 3D biofilm reconstruction from CLSM image stacks and statistical analyzes.

In contrast to the flow chamber systems of Weiger *et al.*, Hauser-Gerspach *et al.*, Meier *et al.*, and Diaz *et al.*, our test procedure allows direct investigation of biofilm formation for five bacterial species.<sup>366-373</sup> The test specimens were not removed from the chambers for microscopic observation, so that detachment effects were minimized and biofilm quantification was highly precise. Only a few studies have analyzed biofilm development for oral health relevant bacteria in a flow system.<sup>366-373</sup> To the best of our knowledge, no other study has focused on the described group of bacteria for microbial adhesion testing in one flow chamber system.

The biofilm morphologies of the applied bacterial species have already been in other studies: In accordance to the study of Diaz *et al.*, a homogeneously flat biofilm morphology with a few tower-shaped structures was observed for *S. gordonii*. However, contrasting to our study the bacteria were visualized by fluorescent in situ hybridization (FISH).<sup>369</sup>

For *S. oralis* Paramonova *et al.* designed a flow chamber system to analyze the influence of shear stress on biofilm formation.<sup>370</sup> The biofilm height of *S. oralis* was enhanced with increasing shear stress. The observed biofilm morphology of *S. oralis* showed a typical tower-like biofilm with a rough surface comparable to our study.

The *S. salivarius* biofilm morphology was homogeneously flat, as also shown in the study of Gashti *et al.*<sup>374</sup> However, they used microfluidic flow chambers, and focused primarily on the influence of pH on biofilm formation.

Davey *et al.* designed their flow chamber model for *P. gingivalis* according to Christensen *et al.*<sup>373,375</sup>. They also observed a rough surface morphology with macrocolonies within the biofilm. Analogously to our experiments, the biofilm was grown under anaerobic conditions. However, the mean biofilm height was about five times higher compared to our study. These findings can be attributed to the different flow chamber design and the differing cultivation conditions. Davey *et al.* grew biofilms for 96 h compared to 48 h in our experiment.<sup>373</sup>

Additionally, Davey *et al.* analyzed the living fraction of the biofilm by staining with SYTO 9. The biofilm morphology of *A. actinomycetemcomitans* showed an open and soft microbial architecture on the titanium substratum. The same findings were described by Sliepen *et al.*<sup>372</sup> In contrast to our method, they tagged *A. actinomycetemcomitans* with a green fluorescent protein to analyze the biofilm formation by CLSM. However, it cannot be completely ruled out that this genetic modification may have influenced the adhesion behavior and biofilm formation.

Finally, in the present study, the reproducibility of the bacterial biofilm height was given in all our experiments.

Biofilm formation takes places throughout the whole oral cavity. However, daily oral hygiene measures reduce the amount of attached biofilm in the oral cavity. Especially at the interfaces gum/tooth or gum/implant, bacteria begin to accumulate and form a biofilm. If not removed, biofilm causes swelling and detachment of the gums from the teeth or the implants. Biofilm further proliferates in the formed periodontal pockets. As these are not isolated compartments but are connected to the oral cavity, biofilms are exposed to a low flow environment rather than static conditions. Therefore, the described flow chamber model approximates the *in vivo* situation, which is crucial for evaluation of surfaces intended to be used in the oral cavity.

In conclusion, the here developed flow chamber system, in combination with CLSM-based biofilm quantification, proved to be a reliable instrument for the analysis of biofilm height and the formation of bacterial biofilms that are relevant in dentistry. Under the given experimental setting, the flow chambers can be used for evaluation of bacterial colonization behavior of implant materials for the oral cavity. In further studies, the system will be optimized for studies of the formation of oral multispecies biofilms, which is closer to the actual situation in the human mouth. Other interesting aspects will be the investigation of the influence of different flow velocities, nutrient concentrations and substrata on the biofilm formation.





## 4.2 Biofilm formation by the oral pioneer colonizer *Streptococcus gordonii* an experimental and numerical study

### *Preface*

The aim of this work was to determine biological parameters, describing oral biofilm formation and setting up a basic numerical simulation model of this process. For this purpose, the flow chamber model of *section 4.1* has been modified in a way that variations in the course of bacterial cultivation were minimized. The main focus has been drawn on the influence of the flow rates (100 to 400  $\mu\text{L}/\text{min}$ ) and different nutrient concentrations (0.01 to 1.0 x) on the biofilm behavior of the oral commensal bacterium *S. gordonii*. Furthermore, the spatial distribution of vital and dead bacteria in the biofilm after 24 h of growth has been analyzed. The experimental data have been evaluated by CLSM imaging. Based on the acquired data set, a numerical model of biofilm formation has been successfully developed, calibrated and validated by DIANLEI FENG, a PhD-student participating in the MARIO doctoral program at LUH.

The study was initiated by Prof. Dr. INSA NEUWEILER, Prof. Dr. UDO NACKENHORST, and Prof. Dr. MEIKE STIESCH. The biological experiments have been developed and performed by HENRYKE RATH and guided by Dr. SASCHA NICO STUMPP and Prof. Dr. MEIKE STIESCH. The evaluation of the numerical simulation has been supported by Prof. Dr. INSA NEUWEILER and Prof. Dr. UDO NACKENHORST. The initial manuscript has been written by HENRYKE RATH and DIANLEI FENG and refined with the help Dr. SASCHA NICO STUMPP, Prof. Dr. INSA NEUWEILER, Prof. Dr. UDO NACKENHORST, and Prof. Dr. MEIKE STIESCH. This work was a cooperation study of the MARIO program. The manuscript has been submitted with shared first authorship between HENRYKE RATH and DIANLEI FENG to the Journal *Federation of European Microbiological Societies (FEMS) Microbiology Ecology*.

As an additional work of this topic a book chapter manuscript was written that aimed for a more detailed study of the numerical simulation: “A deeper insight of a multi-dimensional continuous biofilm growth model: experimental observation and parameter studies” by DIANLEI FENG; HENRYKE RATH, Dr. SASCHA NICO STUMPP, Prof. Dr. INSA NEUWEILER, Prof. Dr. UDO NACKENHORST, and Prof. Dr. MEIKE STIESCH submitted to *Lecture Notes in Applied and Computational Mechanics*, Springer Verlag, 2016 presented in *section 7.1*.

## **Biofilm formation by the oral pioneer colonizer *Streptococcus gordonii* an experimental and numerical study**

Henryke Rath<sup>1\*</sup>, Dianlei Feng<sup>2\*</sup>, Insa Neuweiler<sup>2</sup>, Sascha Nico Stumpp<sup>2</sup>, Udo Nackenhorst<sup>3</sup>,  
Meike Stiesch<sup>1</sup>

<sup>1</sup> Clinic for Prosthetic Dentistry and Biomedical Materials Science, Hannover Medical School,  
Hannover, Germany

<sup>2</sup> Institute of Fluid Mechanics and Environmental Physics in Civil Engineering, Leibniz  
University Hannover

<sup>3</sup> Institute of Mechanics and Computational Mechanics, Leibniz University Hannover

\* authors contributed equally

### **4.2.1 Abstract**

For decades, extensive research efforts have been conducted to improve the functionality and stability of implants. Especially in dentistry, implant treatment has become a standard medical practice. The treatment restores full dental functionality, helping patients to maintain high quality of life. However, about 10% of the patients suffer from early and late device failure due to peri-implantitis, an inflammatory disease of the tissues surrounding the implant. Peri-implantitis is caused by progressive microbial colonization of the device surface and the formation of microbial communities, so-called “biofilms”. This infection can ultimately lead to implant failure. The causative agents for the inflammatory disease, periodontal pathogenic biofilms, have already been extensively studied, but are still not completely understood. As numerical simulations will have the potential to predict oral biofilm formation precisely in the future, for the first time, this study aimed to analyze *S. gordonii* biofilms by combining experimental studies and numerical simulation for the first time. The study demonstrated that numerical simulation was able to precisely model the influence of different nutrient concentration and spatial distribution of active and inactive biomass of the biofilm in comparison with the experimental data. This model may provide a less time-consuming method for the future investigation of any bacterial biofilm.

**Keywords:** bacterial biofilm, numerical simulation, model validation, implant-associated infection, *S. gordonii*, flow chamber system

## 4.2.2 Introduction

Dental implantation is now a routine medical treatment throughout developed countries and improves patients' quality of life.<sup>376</sup> In light of increasing life expectancy, the number of patients receiving dental implants is also increasing as are the number of associated infections. Treatment of implant infection poses major challenge to physicians and health care systems, as therapeutic interventions are frequently ineffective.

The oral cavity is inhabited by more than 700 different bacterial species.<sup>82</sup> Most bacteria are harmless commensal inhabitants, as long as microbial homeostasis is maintained.<sup>107,108,377,378</sup> If there is a shift in this sensitive equilibrium, pathogenic bacteria begin to prevail and induce oral diseases like periodontitis, peri-implantitis or caries.<sup>82,85,109</sup> Oral bacteria are able to form biofilms. Biofilms are complex microbial communities that are embedded in a self-produced EPS. The EPS matrix shields against external hazards and can increase antibiotic resistance by up to 5000-fold.<sup>65</sup>

*S. gordonii* is a commensal bacterium of the oral cavity. As a pioneer colonizer, the bacterium initiates biofilm formation by adhesion to tooth and implant surfaces, thus providing attachment sites for secondary and late colonizing bacterial species.<sup>95,379-383</sup> Furthermore, it can lead to acute bacterial endocarditis if it enters the circulatory system.<sup>79,115,116</sup>

In this study, we investigated *S. gordonii* biofilm formation by using both experimental methods and numerical simulation. In summary, a bacterial suspension was flowed over titanium specimens in dedicated flow chambers. Biofilms were allowed to develop under controlled experimental conditions. Applied numerical modeling possesses many attractive advantages, as has been shown in recent decades in traditional fields of engineering. For instance, numerical modeling is generally more economical than experimental studies and can clearly shorten product development. However, no numerical model can be built without experimental studies, especially when the underlying mechanism is not well understood and when the model parameters are not known. Therefore, studying biofilm formation by combining experimental studies together with numerical modeling is a promising strategy for the investigation of microbial biofilms. There are several published reports on the use of this combined strategy. Horn and Hempel studied substrate utilization and mass transfer in an autotrophic biofilm by using a one dimensional empirical equation to model biofilm height.<sup>384</sup> The parameters used in the model were calibrated from the corresponding experimental results. Rittmann and Manem developed a steady state model with multi-species biomass and substrate utilization features.<sup>385</sup> The model was further evaluated by experimental studies. Clement *et al.* investigated soil

column experiments to study bacterial growth and transport process in porous media.<sup>386</sup> The experimental results were further applied to calibrate the detachment coefficient and initial biomass value with a one dimensional numerical model. Peszynska *et al.* also studied biofilm growth in porous media by combining experimental studies and numerical simulation and this study mainly focused on how the influences of porosity, permeability and mass transport processes in porous media to biofilm formation.<sup>387</sup>

In this paper, we studied development of *S. gordonii* biofilms using in vitro experiments and used the resulting data to calibrate and validate a model for the process. Based on the experimental observations, a mathematical model developed by Alpkvist and Klapper is used to model formation of *S. gordonii* biofilms.<sup>322</sup> The model described the growth of biofilm as a result of consuming medium and two components of biomass - active and inactive biomass - were considered. The calibrated parameters were applied to model the biofilm formation process over time under specific input medium concentrations and the simulation results are validated by spatial active and inactive biomass distribution experiments over 24 h.

The study aimed to successfully combine experimental and numerical investigations on *S. gordonii* biofilms.

### **4.2.3 Material and methods**

#### **4.2.3.1 Bacterial strain**

*S. gordonii* DSM 20568 was obtained from the German Collection of Microorganisms and Cell Cultures (DSMZ).

#### **4.2.3.2 Bacterial cultivation and biofilm formation**

*S. gordonii* was precultured in Tryptic Soy Broth (TSB; Oxoid, Unipath Ltd., Wesel, Germany with 10% yeast (TSBY; Roth, Karlsruhe, Germany). The bacterial culture was incubated for 18h under agitation (200 min<sup>-1</sup>, SM-30, Bühler, Uzwil, Switzerland) at 37°C. For biofilm formation in the flow chamber system, the OD<sub>600</sub> of *S. gordonii* was adjusted to 0.016 with modified TSB supplemented with 50 mM glucose (TSBYG; Roth, Karlsruhe, Germany). This equaled an inoculum of 1.94 x 10<sup>6</sup> CFU/mL. The biofilms were grown for 24 h at 37°C.

#### **4.2.3.3 Open flow chamber system**

The flow chamber type used in this study was designed and manufactured in-house, its dimensions were as follows: 7.0 cm x 5.5 cm x 3.5 cm instrument for the dynamic growth of bacteria. For microscopic and macroscopic analysis, the device was equipped with a 28°mm

cover slip. As test specimens, 12 mm titanium discs (grade 4) were used to guarantee uniform surface pattern. The bacterial solution was driven through the system at constant flow velocity (100 – 400  $\mu\text{L}/\text{min}$ ) using a peristaltic pump and collected in a waste bottle. The bioreactor was constantly fed with fresh medium, so that the level was kept constant (Inflow volume = outflow volume). A schematic description is presented in Figure 11.

The dynamic experiments were performed with varying flow velocities in the range of 100 – 400  $\mu\text{L}/\text{min}$ . Different concentrations of TSBG were used: 0.01x; 0.03x; 0.05x; 0.06x; 0.07x; 0.1x; 0.3x; 0.5x; 0.7x; 1.0x). For data acquisition, three independent biological experiments were performed. Each experiment consisted of at least three technical replicates. For the analysis of the active and inactive distribution of a *S. gordonii* biofilm over 6, 12, 18, and 24 h, the flow velocity was set to 100  $\mu\text{L}/\text{min}$ . Here, the nutrient concentration was 1 x modified TSB. For each time point, two independent flow chambers were used. The experiments were performed in triplicate.

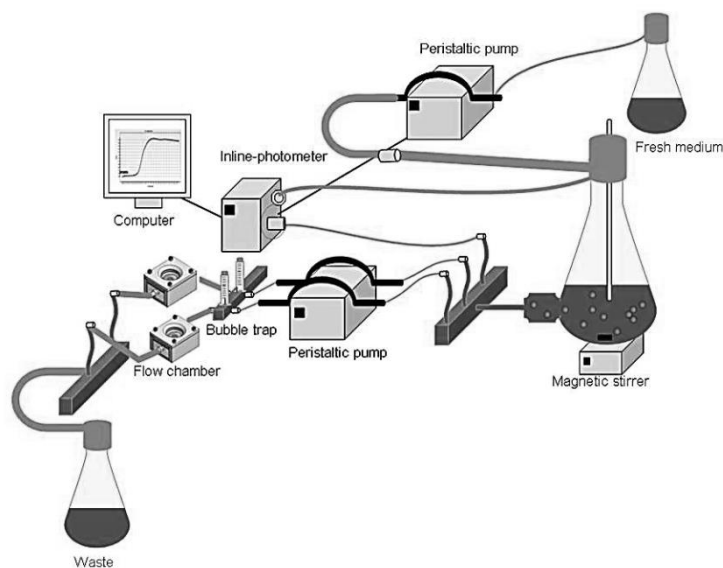


**Figure 11: Schematic description of an open flow chamber system.** The bacterial solution is pumped through the system by peristaltic pump. Air bubbles are avoided with a bubble trap. Bacteria adhere to the titanium disc in the flow chamber. Non-adhering bacteria are pumped into the waste bottle. The flow velocity varies between 100 to 400  $\mu\text{L}/\text{min}$ . The fresh medium is pumped into the system at the corresponding velocity. Optical density is visualized with an inline-photometer.

#### 4.2.3.4 Biofilm imaging and analysis

After biofilm formation, the biofilm in the flow chambers was washed once with phosphate buffered saline for 15 min to dispose of planktonic bacteria. The biofilm was then stained live/dead with a 1:1000 dilution of BacLight staining for 15 min in the dark. Live staining was performed with Syto 9. This is a green fluorescent dye that intercalates into the bacterial DNA

after diffusion through the bacterial membrane. The dead staining was carried out with propidium iodide, a red fluorescent dye that is too large to pass the bacterial membrane, unless membrane integrity is impaired. Additionally, biofilms were carefully fixed with 2.5% glutaraldehyde (Roth, Karlsruhe, Germany) for 15 min. A washing step was not used to avoid further shear stress to the biofilm. As the tubing had a small diameter (0.8mm), the staining dye was completely displaced by the glutaraldehyde. For the analysis of the live / dead distribution within a biofilm, biofilms were washed 15 min, stained live/dead over 25 min and fixed for a further 15°min.

For imaging, the biofilm was analyzed by CLSM, (Leica-Upright MP microscope connected to a TCS SP2 AOBS scan head). Z-stack images (30 images in z-plane/position, '40 objective lens magnification', 300 x 300  $\mu\text{m}$  area, Figure 12) were acquired at five different positions (top, center, bottom, left, right) on each specimen. To calculate the spatial geometry parameters of the biofilms, they were analyzed by Imaris Scientific 3D image processing software.

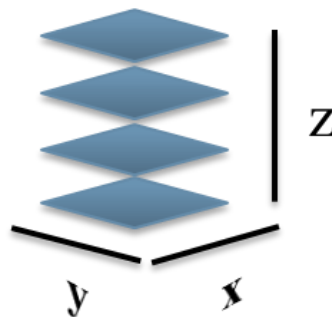


**Figure 12:** The biofilm is imaged at different focal planes by gradual scanning across the sample (here: step-size 1  $\mu\text{m}$ ). The 3D-biofilm, reconstructions are processes from the acquired z-stack images by the Imaris software. Adapted from Rath *et al.*<sup>388</sup>

## 4.2.4 Biofilm formation modeling

### 4.2.4.1 Selection of a mathematical model

Many mathematical models have been developed for modeling biofilm growth. Whether a mathematical model can describe the process or not, is highly dependent on the bacterial species, given environmental conditions, as well as the time and space scales. To the best of the authors' knowledge, there is no universal model that can be applied to model all kinds of biofilm under different environmental conditions. For instance, DEB models are generally preferred to continuous models when the biological or mechanical behaviors of individual bacteria are the issue.<sup>327,329</sup> Such models are applicable only at the scale of a single bacterium. As presented in the previous section, we focused on biofilm height, instead of on a single bacterium. Therefore, in the present study, we preferred continuous models with sharp biofilm-fluid interface.

A comprehensive continuous model should be capable of describing the relevant physical and biological processes as well as possible. However, properly simplified models were always preferred from a practical perspective. In general, the biofilm system could be described as a mass transport problem in a fluid environment.<sup>389</sup> The mass transport process was definitely the most important property of the system, because it described both biofilm formation as well as transformations of different components of biomass. However, whether the flow environment influenced the biofilm differed between cases. This was dependent on the bacterial properties, flow velocity and many other environmental factors. For this reason, we have carried out a group of experiments to study influence of different flow rates.

As described in the previous section, experiments were carried out to study the height of *S. gordonii* biofilms after 24 h under flow rates of 100  $\mu\text{L}/\text{min}$ , 200  $\mu\text{L}/\text{min}$ , 300  $\mu\text{L}/\text{min}$  and 400  $\mu\text{L}/\text{min}$ . If the fluid property is approximated by those of water (kinematic viscosity of  $10^{-6}$   $\text{m}^2/\text{s}$ ) and the tubing diameter is about 0.8 mm, a flow discharge of 100  $\mu\text{L}/\text{min}$  yields a Reynolds number about  $\text{Re}_{100} \approx 2.7$ . With the other larger flow discharge rates used in the experiments, the Reynolds number will be several times higher than  $\text{Re}_{100}$ . However, the flow is clearly laminar in the tubing with all flow discharge rates adopted in the experiments. Moreover, the Reynolds number will be even smaller in the flow cell as the cross section of the cell is much larger than the tubing. Therefore, there was only laminar flow in the flow chamber system. Experimental results (Figure 13) indicate that there was no significant difference in biofilm height for flow rates of 100 and 200  $\mu\text{L}/\text{min}$ . The active biofilm heights varied between 10.1 and 9.9  $\mu\text{m}$  respectively. This means that, in the normal human oral environment (with an approximate flow rate of 100  $\mu\text{L}/\text{min}$ ), flow velocity was slow enough to ignore detachment of the biofilm due to fluid erosion. It is then justifiable to model the biofilm system without explicitly considering structural interactions between the *S. gordonii* biofilm and fluid. As a remark, such assumption does not hold in general. When flow velocity increased to  $>200$   $\mu\text{L}/\text{min}$ , biofilm height was reduced to 4.2  $\mu\text{m}$  (300  $\mu\text{L}/\text{min}$ ) and 3.1  $\mu\text{m}$  (400  $\mu\text{L}/\text{min}$ ). The Figure 13 displays biofilm height with different flow velocities. Only a few publications have reported that biofilm formation acutely decreased with increasing flow velocity.<sup>390-393</sup> In contrast, there have been reports that biofilm increases with increasing flow velocities.<sup>394</sup> None of these publications examined the behavior of *S. gordonii* in an open flow chamber system with increasing flow velocities. It was interesting that the inactive portion of the biofilm formed at 400  $\mu\text{L}/\text{min}$  was a quarter of the total biofilm height. This was a tremendous increase compared to the other flow velocities.

A reason for the large inactive portion at 400  $\mu\text{L}/\text{min}$  might be that shear stress led to

physiological stress and morphological changes during biofilm formation.<sup>58,203,204,395</sup> Additionally, in *S. aureus*, for example, increasing fluid stress has led to lower protein expression of “proteins associated with metabolic function such as carbohydrates protein synthesis and stress tolerance significantly changed”.<sup>359</sup> Inactive bacteria were also observed in our experiments. For this reason, the inactivation process shall also be considered in the mathematical model. However, the mechanism of inactivation was still not clear, which made it difficult to build a physically correct model to describe the process. We simply used an inactivation model, which assumes that the production of the inactive biomass was proportional to the mass of active biomass and a deeper insight into the inactivation process is discussed in the following section.

On the basis of these arguments, a multi-species multi-dimensional biofilm model developed by Alpkvist and Klapper (A-K model) was used to model *S. gordonii* biofilm formation.<sup>322</sup> Biofilm growth was modeled as convective movements with a potential flow driven by biochemical reactions in the biofilm. We assumed that biofilm growth was limited by the concentration of the TSB medium, which is a mixture of many components. The growth limiting substrate (TSB medium) diffused through a DBL of constant thickness above the biofilm-fluid interface. The DBL was the only influence of the fluid above the biofilm in the model. Attachment and detachment processes related to flow were not taken into consideration here. The mathematical model is introduced in the following section, as well as the numerical methods used to solve the model.

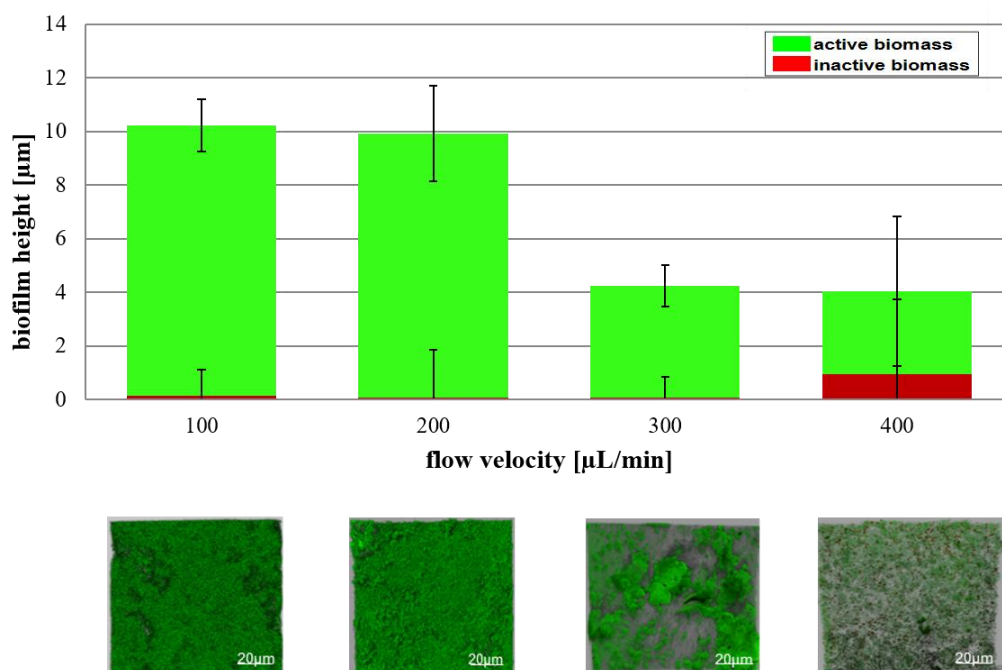


**Figure 13:** Mean height of *S. gordonii* biofilms after 24 h of cultivation at flow velocities between 100-400  $\mu\text{L}/\text{min}$ . The vitality of the bacteria is indicated by green (active) and red (inactive) staining.



#### 4.2.4.2 Mathematical model

For the two dimensional A-K model, the biofilm was considered within a computational domain, as illustrated in Figure 14. The biofilm-fluid interface  $\Gamma_{\text{int}}$  denoted the intersection line of the time dependent fluid domain  $F_t$  and biofilm domain  $B_t$ . A boundary layer of constant thickness  $H_b$  was assumed above the biofilm-fluid interface and the growth limiting substrate diffused from the top of the boundary layer  $\Gamma_h$  into the biofilm. The domain below  $\Gamma_h$  refers to the substrate transport domain  $S_t$ .

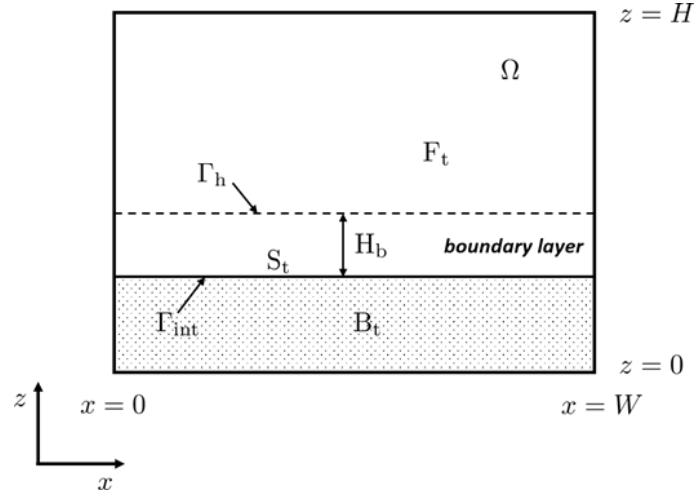


Figure 14: Two dimensional illustration of the computational domains.

We assumed that the biofilm growth limiting substrate is the mixture of the TSB medium with an input concentration of  $\bar{s}$  [ $ML^{-3}$ ]. It was further assumed that the domain above  $\Gamma_h$  was fully mixed and that the medium concentration equaled the input concentration. The medium concentration  $s = s(\mathbf{x})$  in the domain  $S_t$  was governed by the mass balance equation with boundary conditions

$$-D\nabla^2 s = -v_1 \rho \frac{1}{Y} \frac{\mu_{\max} s}{k_s + s}, \quad \mathbf{x} \in S_t,$$

$$s = \bar{s}, \quad \mathbf{x} \in \Gamma_h, \quad (2)$$

$$\frac{\partial s}{\partial \mathbf{n}_s} = 0, \quad \mathbf{x} \in \Gamma_s,$$

The transport process of the medium was considered as a stationary diffusive-reaction process with a constant diffusive coefficient  $D$  and the reaction term of the right hand side of the equation followed the Monod equation, which described the consumption of the medium by the active biomass.  $\mathbf{v} = (v_1, v_2, \dots, v_n)$  referred to the volume fractions of  $n$  different components of biomass. In this study,  $n = 2$  and index “1” refer to the active biomass and “2” referred to

the inactive biomass.  $\rho$  and  $Y$  were the density and yield the coefficient of the biofilm;  $\mu_{\max}$  and  $k_s$  are constant Monod parameters.

Both active biomass and inactive biomass were assumed to move with the same velocity  $\mathbf{u}$ . The movement of biofilm is modeled as a potential flow; thus  $\mathbf{u}$  is described as the gradient of the potential

$$\Phi \mathbf{u} = \nabla \Phi. \quad (3)$$

Biofilm growth was modeled as self-reproduction of the active biomass by consuming the growth limiting substrate. The production of biofilm material caused a source term in the flow (so that the whole biofilm moves depending on production). The corresponding divergence of the growth velocity is given as

$$\nabla \cdot \mathbf{u} = \nabla^2 \Phi = v_1 \mu, \quad \mathbf{x} \in B_t \quad (4)$$

where  $\mu = \mu(s)$  is the biofilm growth rate

$$\mu = \frac{\mu_{\max} s}{k_s + s}, \quad \mathbf{x} \in B_t. \quad (5)$$

The inactive biomass was produced without consuming any substrate, but only through transformation of the active biomass. We referred to this transformation here specifically as an inactivation process and the inactivation rate is assumed to be a constant  $\kappa_i$ . The mass balance equations of the active biomass as well as inactive biomass and the boundary conditions was given as

$$\begin{aligned} \frac{\partial v_1}{\partial t} + \nabla \cdot (\mathbf{u} v_1) &= v_1 (\mu - \kappa_i), \quad \mathbf{x} \in \Omega, \\ \frac{\partial v_2}{\partial t} + \nabla \cdot (\mathbf{u} v_2) &= v_1 \kappa_i, \quad \mathbf{x} \in \Omega, \quad (6) \\ \frac{\partial v_1}{\partial \mathbf{n}_b} &= 0, \quad \frac{\partial v_2}{\partial \mathbf{n}_b} = 0, \quad \mathbf{x} \in \partial\Omega, \end{aligned}$$

$\mathbf{n}_b$  was the normal vector of the boundary of the computational domain  $\partial\Omega$ . Equations (2), (4), (5) and (6) compose the full mathematical model used to describe the biofilm system in this paper.

#### 4.2.4.3 Numerical methods

The mathematical model presented above is a free boundary problem. The location of the biofilm-fluid interface is also unknown as the solutions of the equations. We determined the interface by using an isoline of the total biomass volume fraction as

$$\Gamma_{\text{int}} : \rightarrow \text{contour}\{\sum_{i=1}^2 v_i = v^*\}, \quad 0 < v^* < 1 \quad (7)$$

In this paper, we use  $v^*=0.7$ .

Mass balance equation of the TSB medium (1), potential equation (3) and the mass balance equation of the biomass (5) were solved in sequence within single time interval. As the location of the biofilm-fluid interface only depends on the solutions of equation (5), equations (1) and (3) are solved in the configuration of the previous time point.

Because of the non-linear reaction terms, obtaining an accurate and robust solution of the mathematical model was challenging. A numerical strategy recently presented by Feng *et al.* with detailed description on the numerical aspects was applied in this study to solve the model.<sup>343</sup> All the governing equations were solved by finite element methods. The substrate transport equation and the potential equation were solved with the standard finite element method by using  $100 \times 100$  first order and second order elements, respectively. Time discontinuous Galerkin (TDG) methods and finite increment calculus (FIC) were applied for solving the mass balance equation of each component of biomass.<sup>396,397</sup> A time-space element of fifth order time accuracy (with a time step of  $\Delta t = 0.24$  h) and second order accuracy in space ( $100 \times 100$  elements) was used in the TDG-FIC scheme.<sup>398</sup> A rolling ball algorithm was used to determine the position of the top of the DBL. For more details on the numerical strategy we refer the reader to Feng *et al.*<sup>343</sup>

## 4.2.5 Results and discussion

### 4.2.5.1 The influence of the medium concentration on the biofilm height

The influence of the medium concentration on the biofilm height after 24 h and the biofilm formation profile over time were studied experimentally and numerically in this section. The biofilm formation was examined at a flow rate of  $100 \mu\text{L}/\text{min}$ , as defined by Dawes *et al.* as this is equivalent to normal physiological conditions of the oral cavity.<sup>365</sup> This is the flow rate used in many flow chamber studies.<sup>399-402</sup> For the numerical simulation, 2D simulations were carried out with an initial biofilm fluid interface is set as

$$\Gamma_{\text{int}}^0: \rightarrow 1(\mu\text{m}). \quad (8)$$

As no perturbation was introduced initially, the flat interface maintains during the biofilm growth. Therefore, the distance between the flat surface and the bottom of the computational domain denotes to the total biofilm height  $h_{\text{biofilm}}$ . Some of the simulation parameters used were taken from the literature, whilst others were calibrated by using the experimental results of the biofilm heights over different input medium concentrations (as listed in Table 7). We define the active biofilm height  $h_1$  and inactive biofilm height  $h_2$  mentioned below as

$$h_i = \vartheta_i h_{\text{biofilm}}, \quad (9)$$

where the index  $i=1$  and  $i=2$  refer to the active biomass and inactive biomass respectively,  $\vartheta_i$  is the mass (volume) fraction of each component of biomass in the computational domain and  $h_{\text{biofilm}}$  here refers to the total biofilm height from the simulation results.

Experiments on the evolution of both active and inactive biomass heights over different input TSB medium concentrations was firstly carried out and numerical parameters (as shown in Table 7) used in the model were calibrated from the experimental results. As illustrated in Figure 16, the mathematical model used in this paper is capable of describing the live biofilm height after 24 h growth over different nutrient concentrations. As one numerical simulation run takes hours, global search algorithms were not feasible for parameter estimation. Therefore, we determined the parameters with a gradient based method using an objective function

$$f = \frac{1}{2} (h_1^{\text{sim}} - h_1^{\text{exp}})^T \mathbf{C}^{-1} (h_1^{\text{sim}} - h_1^{\text{exp}}), \quad (10)$$

where  $h_1^{\text{sim}}$  and  $h_1^{\text{exp}}$  are the numerical results and the mean experimental results of the active biofilm height vector with 10 different TSB medium concentrations respectively.  $\mathbf{C}$  is a diagonal matrix with the standard deviations of each point placed along the diagonal. The calculated objective function values with different combination of the parameters are illustrated in Figure 15. Clearly, our calibrated parameters set results in a minimum value of the objective function.

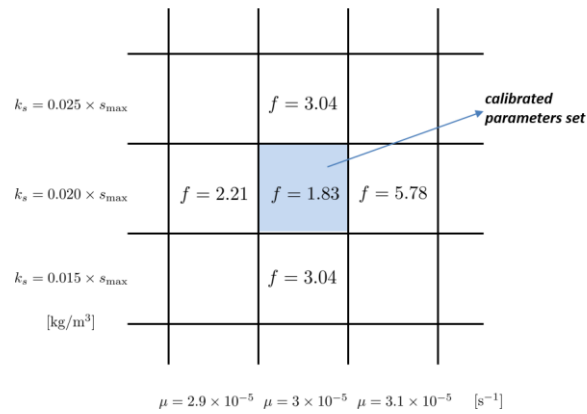


**Figure 15: Illustration of the objective function values with different parameters sets.**

As a remark, only the active biofilm height is used in the objective function. However, the inactivation rate also influences the active biofilm height indirectly. We can also not be sure that our parameter estimation corresponds to a local minimum of the objective function, however, we consider this method as a reasonable compromise. The active biofilm height was significantly increased when low media concentrations (0 to 0.3) were used. At higher media concentrations, the biofilm height increased to a constant level. This phenomenon is widely known as the Monod growth form, and is limited by the growth limiting substrate concentration; the simulation results also show the same trend.<sup>333</sup> Both the experimental results and simulation results indicate that it is reasonable to take the TSB medium as the only growth limiting substrate in the case of *S. gordonii* biofilm formation. The standard deviation of biofilm height varies within a range of  $\pm 1 \mu\text{m}$ . This actually only equals the size of one bacterium.<sup>403</sup> Therefore, the standard deviation for the experimental part is negligible or marginal.

For the inactive biofilm part, the experimental data also showed a standard deviation comparable to that of the active biofilm. It should be noted that inactivation of active bacteria is still an unclear process in biology, even though there are some literature references that attempt to describe the behavior of the inactive bacterial biomass.<sup>379,404-407</sup> In this study, we found that the experimental results of the mean inactive biofilm height lie in a range of 0 to  $2.0 \mu\text{m}$  and the simulation results are in the same range. It was at least shown that there were no outliers within the experimental results. As shown in Figure 16, the simulated inactive biofilm was close to the experimental data. It should, however, be noted that the inactive biofilm mass was very low, so that it is impossible to draw conclusions on the inactivation process.

Table 7: Parameters for the numerical simulation.

quantify name	symbol	value	unit	source
<b>Diffusive boundary layer thickness</b>	$H_b$	15	$\mu\text{m}$	estimated according to Alpkvist and Klapper 2007 <sup>322</sup>
<b>Diffusion coefficient of medium</b>	$D$	$5 \times 10^{-10}$	$\text{m}^2/\text{s}$	Estimated according to Corbin <i>et al.</i> 2011 <sup>408</sup>
<b>Biofilm density</b>	$\rho$	1100	$\text{kg}/\text{m}^3$	estimated according to Duddu <i>et al.</i> 2009 <sup>336</sup>
<b>Maximum growth rate of biofilm</b>	$\mu_{\text{max}}$	$3 \times 10^{-5}$	$\text{s}^{-1}$	calibrated
<b>Maximum input medium concentration (1x TSB)</b>	$s_{\text{max}}$	43.9	$\text{kg}/\text{m}^3$	Fixed by experimental set-up
<b>Monod half-rate constant</b>	$k_s$	$0.020 \times s_{\text{max}}$	$\text{kg}/\text{m}^3$	calibrated
<b>Biofilm yield</b>	$Y$	0.1	—	estimated according to Alpkvist and Klapper 2007 <sup>322</sup>
<b>Inactivation rate</b>	$\kappa_i$	$4 \times 10^{-6}$	$\text{s}^{-1}$	calibrated

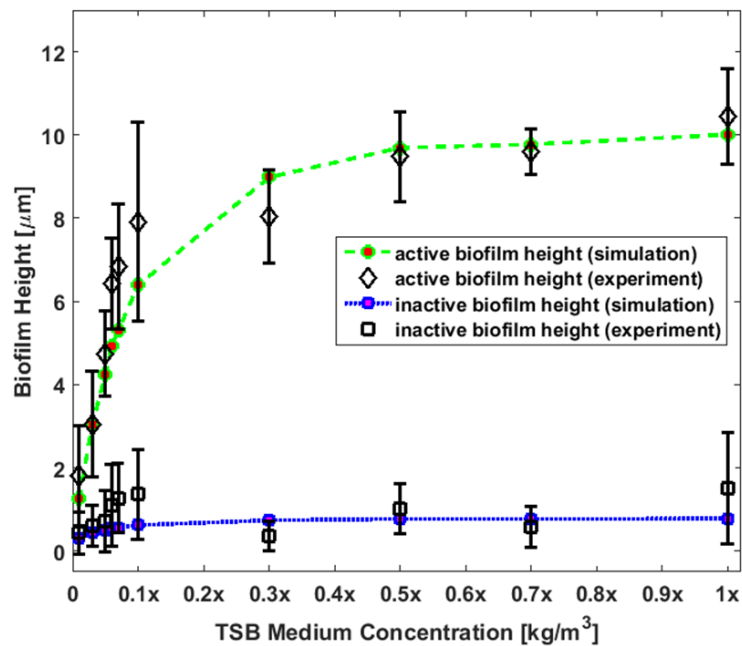


**Figure 16: The biofilm height of *S. gordonii* after 24 h with increasing nutrient concentrations.** The vitality of the bacteria is indicated by green (active) and red (inactive) staining. The diagram shows the mean value of the biofilm height for the experiments.

#### 4.2.5.2 Time dependent spatial distribution of active / inactive biomass within a biofilm

The modeling parameters (as shown in Table 7) as calibrated from the experimental results presented in the previous section are further validated by experiments on *S. gordonii* biofilm formation at different times. Figure 17 shows the experimental and simulation results of the active biofilm height and inactive biofilm height at 6, 12, 18 and 24 h for a TSB medium concentration of 1 x. As shown by the CLSM images in Figure 16, the 6 h data did not indicate the presence of a biofilm. At this time, it was a monolayer of bacteria. This was also indicated by the biofilm height that was around 1  $\mu\text{m}$ , corresponding to the size of one bacterium. After 12 h, microscopic examination showed accumulation of organic matter around the cells, indicating an initial stage of biofilm formation through bacterial EPS secretion. After 18 h, the biofilm already exhibited an active biofilm structure. However, the surface still exhibited free areas on the titanium disc. After 24 h, the bacterial biofilm was confluent, mature and vital. The biofilm height was around 10  $\mu\text{m}$ . The experimental biofilm formation in a dynamic system behaved as expected from the literature. The standard deviations varied within a range of  $\pm 1 \mu\text{m}$  and were negligible.

The inactive biomass increased to 1  $\mu\text{m}$  after 18 h. Just as for the active biofilm, the inactive bacteria were also organized in a monolayer and did not comply with the criteria of a biofilm.

However, it was obvious that the inactive biomass of the bacteria increased until 18 h, and afterwards the experimental data showed a decrease in the height of inactive bacterial biofilm. This phenomenon of bacterial inactivation has already been explained: bacteria in a static or dynamic system need time, firstly to adhere to the substratum irreversibly and afterwards, to adapt to the new situation and start to change their physiology according to the environment. This is an energy consuming procedure and leads to localized bacterial cell death.<sup>58,78,79,94,346,391,409-414</sup> Furthermore, cell death is a normal phenomenon of bacterial cohabitation.<sup>415-418</sup> Additionally, bacteria within a biofilm will be killed by the bacterial community, in order to use the inactive bacteria for biofilm architecture.<sup>414,416,419-423</sup> Additionally, inactive bacteria have been proposed to increase bacteria resistance to external hazards.<sup>21,424-426</sup> Furthermore, it is known that bacteria use the active and the inactive biomass for inter- and intraspecies communication; this is called “quorum sensing”.<sup>73,76,86,421,427-431</sup> After 18 h, the fraction of inactive bacterial decreased. This indicated the time, when the bacteria in the biofilm have fully adhered and settled on the titanium. From this time, the biofilm just matures. This does not necessarily include additional cell death.

It is experimentally observed that the height of the active biofilm increases exponentially over time and the numerical simulation results present the same trend. As can be seen from the model equations, it is not surprising that the numerical solution also behaves as an exponential function. The equations governing the mass balance of both components of biomass are typically hyperbolic PDEs and the solutions (analytically or numerically) are exponential functions for linear systems.

Although the growth rate in the experiments is slightly faster than predicted with the calibrated model, the simulation results generally match the experimental observations very well. This again demonstrates that the A-K model is appropriate to describe *S. gordonii* main biofilm formation process (patchy structures at early times are of course not reproduced). Moreover, it indicates that the parameters calibrated from the previous experiments are useful for modeling the *S. gordonii* biofilm under the situation of the experimental set-up.



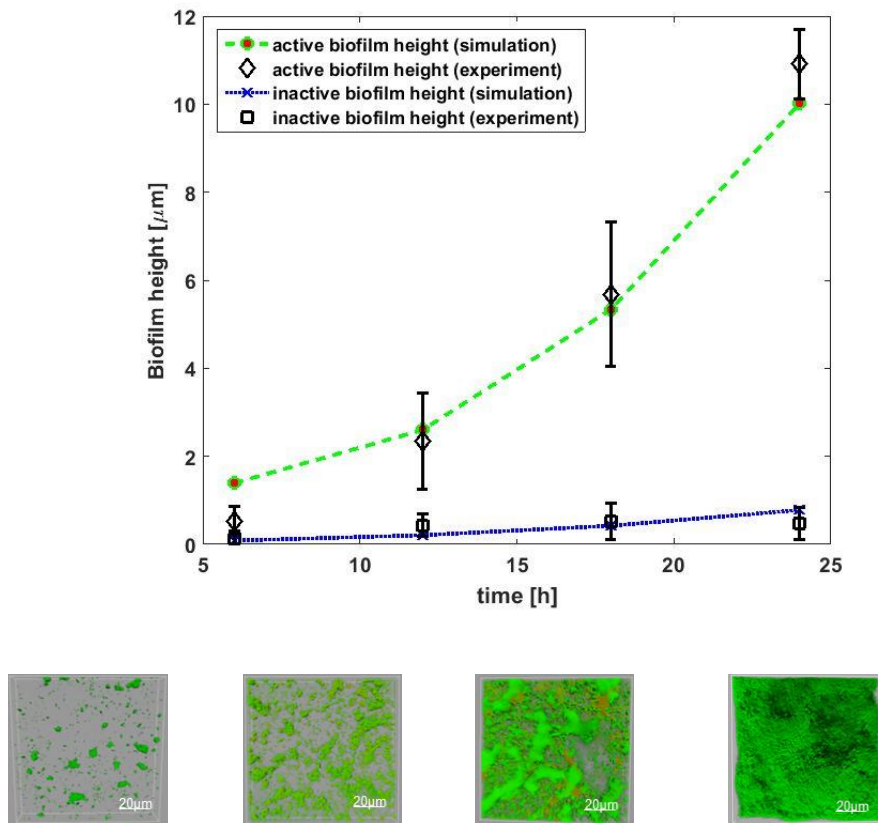


**Figure 17: Height of *S. gordonii* biofilm in a time dependent open flow chamber experiment.** Biofilm images were taken by CLSM and represented the respective time point after 6, 12, 18, and 24 h. The active bacteria are depicted in green and the inactive bacteria in red.

## 4.2.6 Conclusion

This study establishes a new strategy to evaluate the biofilm behavior of *S. gordonii* by numerical and experimental methods. For this purpose, a flow chamber system was successfully designed for direct microscopic observation of biofilm formation. The biological results were successfully used to calibrate and validate the numerical simulation parameters.

The results show the potential of studying the medical biofilm formation in general by using numerical simulations together with experiments. The A-K model used in this paper is shown to be capable of representing the biological process of *S. gordonii* biofilm formation, under moderate flow velocities. It also shows that it is possible to consider the full mixture of the medium as single growth limiting substrate when detailed components of the growth limiting substrates are complex or unclear.

Although we validated our model by a set of time behavior experiments and drew the conclusion that the mathematical model presented in the paper was able to predict the *S. gordonii* biofilm formation in oral environment, we cannot exclude that other model

formulations could also be used to reproduce the results. However, the model we set up in this paper is the simplest model we could formulate and still reproduce the measurements. The mathematical model can be further applied for modeling other biofilms, such as those cultured anaerobically or comprising of multi-species. However, more experimental studies are needed to understand the mechanism of biofilm formation in specific systems. In these instances, this model will likely require appropriate modification. For modeling the multi-species biofilm, one challenge among many is the high computation expense, especially for 2D or 3D simulations. Meanwhile, interactions between different species of bacteria could result in more complicated mathematical description of the metabolic processes. This also increase the difficulty of solving the system numerically.

### **4.3 Numerical simulation and experimental validation of biofilm in a multi-physics framework using an SPH based method**

Meisam Soleimani, Peter Wriggers, Henryke Rath, Meike Stiesch

Comput Mech, **2016**, 58, 1-15

DOI 10.1007/s00466-016-1308-9

The final publication is available at

<http://link.springer.com/article/10.1007%2Fs00466-016-1308-9>

Reprinted from Computational Mechanics, 58, Meisam Soleimani, Peter Wriggers, Henryke Rath, Meike Stiesch, Numerical simulation and experimental validation of biofilm in a multi-physics framework using an SPH based method, Copyright (2016), with permission from Springer.

## ***Preface***

This study aimed for the experimental and numerical investigation of the biofilm formation of *S. aureus* in a fluid flow system under physiological conditions. The numerical simulation has been based on the SPH model, thus analyzing the biofilm growth on the particle scale. As *S. aureus* is a round shaped bacterium it has been qualified for this study. The experimental biofilm formation has been performed in an open flow system with continuous feed of nutrients modified from the invented flow chamber system in *section 4.1*. In the presented study, the focus has been drawn on the influence of the flow velocity on the biofilm formation. The biofilm formation was investigated at 100, 200, and 400  $\mu\text{L}/\text{min}$  over a period of 24 h. The experimental data have been analyzed by CLSM imaging and the average biofilm height results have been fed into the numerical simulation of MEISAM SOLEIMANI, a PhD-student participating in the MARIO doctoral program at LUH for validation. The numerical model and experimental set-up for the investigation of *S. aureus* biofilm formation have been successfully developed.

This cooperation has been initiated and guided by Prof. PETER WRIGGERS and Prof. MEIKE STIESCH. The numerical simulation was developed and investigated by MEISAM SOLEIMANI. The experimental set-up, the investigation with the CLSM and the analysis have been performed by HENRYKE RATH. The initial manuscript has been written by MEISAM SOLEIMANI and refined with the help of Prof. PETER WRIGGERS.

The manuscript of this cooperation project has been accepted by *Computational Mechanics* for publication and is depicted in the following. Furthermore, the biological experiments are presented in detail subsequent to the manuscript.



## Numerical simulation and experimental validation of biofilm in a multi-physics framework using an SPH based method

Meisam Soleimani<sup>1</sup> · Peter Wriggers<sup>1</sup> · Henryke Rath<sup>2</sup> · Meike Stiesch<sup>2</sup>

Received: 6 April 2016 / Accepted: 13 June 2016  
© Springer-Verlag Berlin Heidelberg 2016

**Abstract** In this paper, a 3D computational model has been developed to investigate biofilms in a multi-physics framework using smoothed particle hydrodynamics (SPH) based on a continuum approach. Biofilm formation is a complex process in the sense that several physical phenomena are coupled and consequently different time-scales are involved. On one hand, biofilm growth is driven by biological reaction and nutrient diffusion and on the other hand, it is influenced by fluid flow causing biofilm deformation and interface erosion in the context of fluid and deformable solid interaction. The geometrical and numerical complexity arising from these phenomena poses serious complications and challenges in grid-based techniques such as finite element. Here the solution is based on SPH as one of the powerful meshless methods. SPH based computational modeling is quite new in the biological community and the method is uniquely robust in capturing the interface-related processes of biofilm formation such as erosion. The obtained results show a good agreement with experimental and published data which demonstrates that the model is capable of simulating and predicting overall spatial and temporal evolution of biofilm.

**Keywords** Biofilm · Multi-physics · Smoothed particle hydrodynamics · Fluid-solid interaction

**Electronic supplementary material** The online version of this article (doi:10.1007/s00466-016-1308-9) contains supplementary material, which is available to authorized users.

✉ Meisam Soleimani  
soleimani@ikm.uni-hannover.de

<sup>1</sup> Institute of Continuum Mechanics, Leibniz Universität at Hannover, Hannover, Germany

<sup>2</sup> Hannover Medical School, Hannover, Germany

### 1 Introduction

Although Biofilm could be simply described as the aggregation of microorganisms, for example bacteria, on a surface, its formation and evolution is quite complex due to the fact that several physical phenomena account for that. Indeed, bacteria tend to grow in clustered populations instead of individually wandering because this type of living make them more resistant to environmental and external threats. They anchor themselves to a solid surface where sufficient nutrient is available to feed them. An internally secreted matrix called extra polymeric substance (EPS) keep them together and forms a spatially heterogeneous solid like material.

Biofilms may be either beneficial or detrimental to human's life. In some industrial applications, for example water treatment units, one can take the advantage of biofilms whereas in medical application they are considered to be infectious and harmful. In this research, the focus is on the formation of biofilms on the surface of teeth as well as dental implants. In fact biofilm formation in the mouth cavity significantly contributes to later dental plaque emergence. Aside from their role in human's life, a great deal of attention has been drawn especially over the last three decades to simulate their formation in order to predict and finally control their behavior.

Early attempts to mathematically model the biofilms date back to 1980s, see [1, 2]. Here it was tried to develop a one dimensional system of partial differential equation describing biofilm growth. Since then, a variety of methods have been proposed to model two and three dimensional biofilm, all of which fall into either continuum-based [3–7] or Hybrid discrete-continuous models that are known as individual-based methods (IBM) [8–10]. There are also some cellular automaton (CA) models which are conceptually more or less similar to IBM in this sense that the overall behavior and spa-

tial structure of biofilm comes out of biological interactions taking place at the individual level between discrete agents [11–13]. In spite of being simple, such agent based models are capable of reproducing quite complex morphologies such as finger like and fractal shape of biofilm in case that biofilm growth is governed by diffusion-limited aggregation (DLA) model in which the nutrient diffusion is the dominant process [14].

It might be noteworthy to mention that agent based methods are more appealing to biologist because of their inherent simplicity and their capacity to incorporate new local ad hoc rules being inspired from biology such as bacterial binary division, attachment and detachment of bacteria. Furthermore, handling multi species biofilm is not a big deal by defining local interactions between different agents [15]. Nevertheless drawbacks of these methods are introduced stochastic effects and geometrical anisotropy which make the results less physical. So many parameters challenge predictiveness of the model. Non-trivial error estimation and more aesthetically driven results oppose mathematical and physical based predictions [16].

To discuss concisely what has been done with regard to biofilm simulation in the literature, the physics behind the process needs to be deeply understood. Biofilm models are based on three principal concepts. First transport mechanisms (diffusion–advection) which bring nutrients to biofilms, second biological consumption and consequently growth mechanisms which directly contribute to biofilm structural form and third biofilm–fluid interface related mechanisms that account for the effect of a surrounding fluid on biofilms in terms of surface erosion (detachment) or the attachment of planktonic bacteria.

The first mechanism has been well developed in a continuum-based frame work in all existing above mentioned references.

The second mechanism is exactly the point where two different approaches, i.e Individual-based and continuum based methods, branch. The main idea of agent-based methods for growth is that discrete elements mimicking bacteria grow and afterward a contact model handles the overlap between agents and results in overall expansion of the system which is called shoving mechanism. The most recent open source simulator for biofilms is called iDynoMiCS (Individual based Dynamics of Microbial communities Simulator) developed in Java Language [17]. When it comes to a continuum framework for biofilm growth, almost all researcher assume the biofilm to behave like a viscous fluid with a mass source term [18–20]. This assumption is favourable although the biofilm is apparently a solid-like material. The fact is that the characteristic time scale of biofilm growth is so larger than its relaxation time scale. Hence in practice no residual stresses remains inside the biofilm and it is fully relaxed like a viscous fluid [21]. It should be noted that the residual stresses

are generally an inevitable resultant of biological soft tissues growth when they are assumed to behave like a viscoelastic solid. This has been extensively studied by researchers in a robust continuum framework [22–26].

The third and the least understood mechanism is the one occurring at the interface of fluid and biofilm [27]. The fluid flow exerts forces to the biofilm and erodes or sloughs it which change its architecture significantly. This process is of great importance since it contributes to biofilm development in an opposite way in comparison to biological growth. Thus it results in material removal and in some cases a final balance between detachment and growth process is reached which keeps the overall biofilm architecture more or less constant [28]. Although the induced stresses and deformation and even triggered small vibrations in biofilm are not an important factor in its shape, it is necessary to do a stress analysis embedded in a fluid–structure interaction (FSI) analysis in order to correctly capture failure and detachment process in biofilms [29,30]. Furthermore, the effect of detached material forming streamers and also its oscillation characteristics, has been taken into account by some authors [32,33]. In general, the biofilm response to external forces has been modeled using FEM in conjunction with a fluid flow solver [31]. However some researchers preferred to use particle based methods such as discrete breakable spring–damper elements to simulate biofilm interaction with the fluid flow [34] and also dissipative particle hydrodynamics (DPD) as a Lagrangian stochastic approach [35]. Besides these approaches some models are relied on empirical or semi analytical detachment description inspired from a 1D biofilm model in which the detachment rate is proportional to  $h^2$  where  $h$  is the local biofilm thickness. Of course this method introduce some unknown parameters that need to be identified for each problem [36]. It is noteworthy that in iDynoMiCS, the fluid flow is not resolved and a constant boundary layer for nutrient diffusion in fluid along with such detachment functions has been implemented, instead [17].

Regardless of the method, the presence of moving boundaries in biofilm–fluid interface and how to handle it is a complex task—especially in 3D— in grid based schemes and needs to be dealt with in an accurate and efficient way. In [37] this issue has been addressed using level set methods in the extended finite element framework (XFEM).

The aim of this paper is to develop and present a unified computational approach for biofilm formation modeling based fully on the SPH method. SPH was firstly introduced in [38] and [39] for astrophysical application and nowadays has been applied to simulate several physical processes such as diffusion–advection [40–42], fluid flow [43,44], hydraulic terrain erosion [45], reactive transport and precipitation [46], solid deformation [47,48] and FSI analysis [50]. Although most of these process are conceptually involved in biofilm formation, to the best of author’s literature surveying, this

Comput Mech

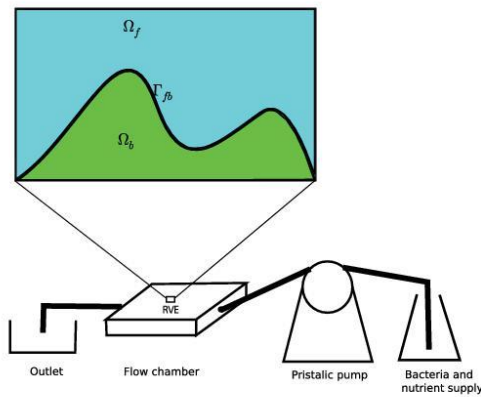


Fig. 1 Schematics of experimental set up and subdomains of RVE

work is the first one in which biofilm formation as a multi-physics phenomenon has been modeled using a fully SPH based method. Furthermore, a novel SPH expression for biological growth inspired by astrophysical gravitational wind accretion [51] was developed based on soft tissue growth mechanics [52]. Considering the superiority of SPH in terms of handling the before-mentioned issues due to its meshless Lagrangian adaptive nature and also its attractive capacity for parallel computation, a computational FORTRAN code in SPH framework was developed by the author from scratch. Furthermore, parallelized computation was realized using OpenMP to benefit from multi-thread execution.

## 2 Mathematical framework and model description

### 2.1 Spatial domain and geometry

In this study, The predictions based on the developed SPH method for biofilm growth will be validated by experimental results. The main part of experimental set-up conducted by colleagues of the medical school is a flow chamber which is fed with a peristaltic pump. At the center of it, there is titan plate where the biofilm can form. The size of the titan plate is  $12 \times 12$  mm. See Fig. 1. Due to computational costs of resolving the full macro scale, the simulation is limited to several hundred microns in each spatial direction which could be considered as a representative volume element (RVE) at micro-scale. In practice, the modeled domain is expected to be equal to the zooming in Fig. 1 area where the experimental data are gathered using scanning electron microscopy (SEM). The spatial whole domain in the RVE is divided into two subdomains (compartments) i.e the fluid compartment  $\Omega_F$  and biofilm compartment  $\Omega_B$ . The interface between

these two  $\Gamma_{FB}$  is the surface where the field variables are coupled. Unknown field variables in  $\Omega_F$  are velocity and nutrient concentration and in  $\Omega_B$  are the geometrical profile due to growth phenomena and nutrient concentration.

An order of magnitude argument has been made related to the different time scales associated with processes occurring in biofilm formation [30,53]. This leads to the assumption that all fast process (smaller time scales) such as fluid flow and nutrient diffusion reach their steady state(temporally homogenized) value when a slower process (large time scale) such as biofilm growth is taking place. In fact it is the main idea of temporal homogenization [54] and consequently different process could be solved efficiently in a staggered nested manner.

### 2.2 SPH discretization

In SPH an arbitrary function  $f$  is expressed as an integral interpolation

$$f(\mathbf{r}) = \int f(\mathbf{r}')W(\mathbf{r} - \mathbf{r}')d\mathbf{r}' \tag{1}$$

The integral reproduces  $f$  exactly if  $W$  is delta function. In SPH,  $W$  is called kernel function mimicking the delta function; it has a maximum value at point  $\mathbf{r}'$  and gradually goes to zero within a compact support. In this work, a cubic spline [55] kernel was chosen. The discrete notation of the above integral leads to the following expression which is the starting point of all SPH based methods:

$$f(\mathbf{r}_a) = \sum_b \frac{m_b}{\rho_b} f(\mathbf{r}_b)W(\mathbf{r}_b - \mathbf{r}_a, h) \tag{2}$$

$m_b$  and  $\rho_b$  represent the mass and density at point  $b$ .  $h$  is the kernel support length which determines the maximum neighborhood radius. Consequently it describes if two particles interact with each other or not. In general  $h$  must be slightly larger but in the order of particle average distance [57] for convergence purposes. In this work it is taken to be 1.5 times the average particle distance ( $h = 1.5\Delta$ ).

It must be noted that in equation (2) the  $\frac{m_b}{\rho_b}$  replaced  $d\mathbf{r}'$  in the integral which is nothing else that volume element. In fact the value of  $f$  at point  $a$  is estimated using the values of its neighborhood. Differentiating the equation (2) with respect to  $r$  provides an estimation for the derivative of  $f$

$$\nabla f(\mathbf{r}_a) = \sum_b \frac{m_b}{\rho_b} f(\mathbf{r}_b)\nabla W(\mathbf{r}_b - \mathbf{r}_a, h) \tag{3}$$

For the second derivative of  $f$ , instead of twice differentiating the integral interpolant a much better approach was proposed by [38]

$$\nabla^2 f(\mathbf{r}_a) = \sum_b 2 \frac{m_b}{\rho_b} (f(\mathbf{r}_b) - f(\mathbf{r}_a)) \frac{(\mathbf{r}_b - \mathbf{r}_a) \cdot \nabla W(\mathbf{r}_b - \mathbf{r}_a, h)}{|\mathbf{r}_b - \mathbf{r}_a|^2 + \epsilon} \quad (4)$$

in which  $\epsilon$  is a small parameter to avoid singularity. Considering that the maximum order of derivative in most physical phenomenon is two, higher order derivatives are not required in practice.

### 2.2.1 Symmetrization of discretized mathematical operators in SPH

In its discretized form, Eq. (3) loses even the zeroth order consistency especially near the boundaries. This situation is worse if the distribution of the particles is irregular. It means that the Eq. (3) can not properly reproduce the derivative of a constant field, which must be equal to zero. Furthermore, the equation is not symmetric. This is important from the physical point of view. The SPH discretized equation are translated finally into inter-particle interactions. If it is intended to model a system of particles, any interaction between two particle must not violate the third law of Newton. otherwise, the total angular or linear momentum is not conserved, see [57]. In order to make the derivative operator symmetrized and exactly zero order consistent, one can use a differentiable test function  $\phi$  in constructing the first derivative of the function  $f$ . Starting with the identity

$$\nabla f = \frac{1}{\phi} (\nabla(\phi f) - f \nabla \phi) \quad (5)$$

If now the Eq. (3) is applied to the both terms of the right hand side of Eq. (5), one can obtain

$$\nabla f(\mathbf{r}_a) = \frac{1}{\phi_a} \sum_b \frac{m_b}{\rho_b} \phi_b (f(\mathbf{r}_b) - f(\mathbf{r}_a)) \nabla_a W(\mathbf{r}_b - \mathbf{r}_a, h) \quad (6)$$

The Eq. (6) vanishes if  $f$  is a constant function. Choosing  $\phi = 1$  gives

$$\nabla f(\mathbf{r}_a) = \sum_b \frac{m_b}{\rho_b} (f(\mathbf{r}_b) - f(\mathbf{r}_a)) \nabla_a W(\mathbf{r}_b - \mathbf{r}_a, h) \quad (7)$$

The Eq. (7) is the practical and final version of the first derivative which is symmetric and exactly zero order consistent. It is obvious that in this equation, the effect of particle  $a$  on  $b$  is the same as that of  $b$  on  $a$  but in opposite direction. Comparing Eqs. (7) and (3) one can notice that they are slightly different. In fact, the Eq. (7) has an extra term ( $\sum_b m_b f(\mathbf{r}_a) \nabla W_{ba}$ ) which is identical to zero in continuum, provided that the support of kernel is complete. Assuming a

single phase material with negligible density fluctuation, the extra term can be approximated as follows

$$f(\mathbf{r}_a) \rho_a \sum_b \frac{m_b}{\rho_a} \nabla W_{ba} \approx f(\mathbf{r}_a) \rho_a \sum_b \frac{m_b}{\rho_b} \nabla W_{ba} \quad (8)$$

where  $W_{ba} := \nabla W(\mathbf{r}_b - \mathbf{r}_a, h)$ . It is obvious that the summation in right hand side of Eq. (8) is zero. It is in fact the discretized form of kernel gradient integral over the kernel support. It is zero if the support is complete (far from the boundaries), see [48]. In the Sects. (2.3.1) and (2.3.4) the Eq. (7) is applied to discretize the continuity equation in which  $f := v$ .

Assuming  $\phi = \frac{1}{\rho}$ , one can find

$$\frac{\nabla f(\mathbf{r}_a)}{\rho_a} = \sum_b m_b \left( \frac{f(\mathbf{r}_b)}{\rho_b^2} + \frac{f(\mathbf{r}_a)}{\rho_a^2} \right) \nabla_a W(\mathbf{r}_b - \mathbf{r}_a, h) \quad (9)$$

This equation is utilized in Sect. (2.3.2) for discretization of momentum equation in which the aim is to discretize the expression  $\frac{\nabla \sigma}{\rho}$ .

## 2.3 Governing equations

### 2.3.1 Mass balance (continuity)

Recalling from continuum mechanics, the local form of the mass balance equation of a regular body not undergoing growth is

$$\frac{\partial \rho}{\partial t} + \nabla \cdot (\rho v) = 0 \quad (10)$$

where  $\rho$  and  $v$  are the density and the velocity field, respectively. When it comes to a biological body which may experience growth, the mass balance equation needs to be modified and indeed the right hand side of equation (10) is replaced by a source term  $\gamma$  accounting for mass generation due to growth [21].  $\gamma$  could be in general a function of other field variables. Here it is assumed that  $\gamma$  is only a function of the nutrient concentration according to Monod kinematic [1].

$$\gamma = Y \frac{K_1 C}{K_2 + C} \quad (11)$$

where  $Y$  is the true yield of bacterial mass per unit of nutrient consumption,  $K_1$  and  $K_2$  are biological constants related to the type of bacteria species and  $C$  is the concentration of nutrient. In general adding a scalar source term into continuity equation is not sufficient to capture inhomogeneous growth which generally results in residual stresses and it is required to start from a multiplicative decomposition of deformation in a tensorial sense. But here, due to the fact,



that the focus is on time periods whose order of magnitude is larger than biological growth time scale, the biofilm behaves like a viscous fluid and all internal stresses are released [21, 22] and hence the scalar source term in the continuity equation is sufficient.

Taking the source term into account and applying the Eq. (7), SPH discretization of mass balance equation follows

$$\frac{\partial \rho_a}{\partial t} = \sum_b m_b (\mathbf{v}_a - \mathbf{v}_b) \cdot \nabla W(\mathbf{r}_a - \mathbf{r}_b, h) + \gamma_a \quad (12)$$

In this study, another version of continuity equation which is equivalent to Eq. (12) has been implemented [48], for the growth process. It will be discussed in Sect. (2.4).

$$\rho_a = \sum_b m_b W(\mathbf{r}_a - \mathbf{r}_b, h) \quad (13)$$

Both Eqs., (12) and (13) are equivalent and theoretically gives identical results except at boundaries. It can be shown that the Eq. (12) is the rate form of Eq. (13). Taking derivative from Eq. (13) with respect to time and using the chain rule ( $\frac{d}{dt} = \frac{d}{dx_i} \cdot \frac{dx_i}{dt}$ ) in the right hand side, the Eq. (13) is achieved. Recalling the Sect. (2.2.1) it should be noted that a zero term needs to be added to the right hand side in order to have zeroth order consistency and symmetric discretized gradient operator. For further, detail the interested readers may refer to [48].

### 2.3.2 Momentum balance

In general, every mass source stemming from growth phenomena is an inherent momentum source as well. This makes both the linear and angular momentum equation complicated. In such cases the Cauchy stress tensor is not symmetric anymore owing to a source term in the angular momentum equation. However, under certain assumptions these effects could be neglected and introducing the growth effect in the continuity equation suffices. The fundamental assumption is that the momentum of the newly deposited material is equal to that of the existing material and this is the case for biological slow growth [56] and hence the linear momentum equation has the regular and well-known structure.

$$\rho \dot{\mathbf{v}} = \nabla \cdot \boldsymbol{\sigma} + \rho \mathbf{b} \quad (14)$$

in which  $\boldsymbol{\sigma}$  and  $\mathbf{b}$  are the Cauchy stress and body force, respectively. The angular momentum leads to symmetricity of Cauchy stress. Using equation (9) SPH approximation of equation (25) is obtained, see [48], as

$$\frac{Dv_a^\alpha}{Dt} = - \sum_b m_j \left( \frac{\sigma_a^{\alpha\beta}}{\rho_a^2} + \frac{\sigma_b^{\alpha\beta}}{\rho_b^2} \right) W_{ab,\beta} \quad (15)$$

where  $W_{ab,\beta}$  is an abbreviation for  $W_{ab,\beta} = \frac{\partial W_{ba}}{\partial x_a^\beta}$ .

### 2.3.3 Diffusion–advection–reaction

In the biofilm domain ( $\Omega_b$  the nutrient concentration  $C$  is an unknown field variable and is computed using diffusion–advection–reaction equation (Eq. 20).

$$\frac{\partial C}{\partial t} + \nabla C v = D \nabla^2 C - \frac{\gamma}{Y} \quad (16)$$

where  $D$  is the diffusivity coefficient and  $\frac{\gamma}{Y}$  is the consumption term expressed in Eq. 11. Since the SPH is based on a Lagrangian description, in the discretized form the advection term ( $\nabla C \cdot v$ ) does not exist explicitly.

$$\frac{DC_a}{Dt} = \sum_b 2D \frac{m_b}{\rho_b} (C_b - C_a) \frac{(\mathbf{r}_b - \mathbf{r}_a) \cdot \nabla W(\mathbf{r}_b - \mathbf{r}_a, h)}{|\mathbf{r}_b - \mathbf{r}_a|^2 + \epsilon} + \frac{\gamma_a}{Y} \quad (17)$$

### 2.3.4 Constitutive equations

*Fluid flow* It is common that the stress tensor can be decomposed into isotropic (pressure)  $P$  and deviatoric  $S$  parts according to the following equation

$$\sigma_{ij} = -P \delta_{ij} + S_{ij} \quad (18)$$

where  $\delta_{ij}$  is the Kronecker tensor. Assuming a Newtonian fluid, the deviatoric stress is proportional to the deviatoric strain rate.

$$S_{ij} = 2\mu_f \epsilon_{ij} \quad (19)$$

where  $\mu_f$  is the fluid dynamic viscosity and

$$\epsilon_{ij} = \frac{1}{2} \left( \frac{\partial v_i}{\partial x_j} + \frac{\partial v_j}{\partial x_i} \right) - \frac{1}{3} \frac{\partial v_k}{\partial x_k} \delta_{ij} \quad (20)$$

in which Einstein’s summation rule has been applied for index  $k$  and  $v$  is the velocity field.

*Elastic solid* As mentioned before, biofilm behaves like a fluid in the growth process, but in short time scales it acts like a solid [34]. In other words, it is necessary to model biofilm as a deformable solid if its interaction with the surrounding fluid is considered. Due to the nature of SPH, it is more convenient to use hypo-elastic approach instead of hyper-elastic one when dealing with deformable solid. In this approach rate constitutive equations are used to reflect the material behavior. Such constitutive laws are similar to Eqs. (18)–(20) with the modification that the stress rate is proportional to the strain rate and  $\mu_f$  is replaced by  $\mu_s$  representing

the shear modulus of the solid. The important point is that the stress rate must be objective to fulfill frame indifference. The Jaumann rate is the most widely adopted [47,48]

$$\dot{S}_{ij} - S_{ik}\omega_{jk} - \omega_{ik}S_{kj} = 2\mu_s\epsilon_{ij} \quad (21)$$

recalling Einstein summation notation and material time derivative ( $\dot{\phantom{x}}$ ), the whole left hand side is indeed the Jaumann stress rate and the tensor  $\omega_{ij}$  is called spin tensor and it is calculated

$$\omega_{ij} = \frac{1}{2} \left( \frac{\partial v_i}{\partial x_j} - \frac{\partial v_j}{\partial x_i} \right) \quad (22)$$

All equations are finally translated into the first derivative of the velocity field and hence can be calculated using an SPH approximation according to Eq. (7).

*Remark* The application of such rate constitutive equations while assuming spatially constant coefficient, is quite questionable and in fact incompatible with elasticity when large deformation and especially severe volume change takes place [49]. Nevertheless, in this paper with the assumption of moderate deformations, this effect has been neglected.

*Equation of state* In the standard SPH which is also called weakly compressible SPH (WCSPH) the pressure is computed from the density using a thermodynamically consistent equation of state. Such approach enjoys the benefit of decoupled pressure and velocity field but suffers from a small time step that is conversely proportional to the sound velocity in the material due to the CFL (Courant, Friedrichs and Levy 1928) stability condition. Here the following equation for the pressure is used

$$P = \frac{c_0^2 \rho_0}{\gamma} \left( \left( \frac{\rho}{\rho_0} \right)^\gamma - 1 \right) \quad (23)$$

where  $c_s$  and  $\rho_0$  are sound velocity and rest density of the bulk material. The parameter  $\gamma$  is set to be “7” for the fluid and “1” the solid. It should be emphasized that the value of  $c_0$  for the fluid is in fact a penalty parameter rather than a true physical sound speed and hence it can be selected in a way that is large enough to insure density fluctuation less than 0.01 and keep the Mach number less than 0.1, and small enough to avoid unnecessary small time steps [57]. In practice, if  $c_0$  is taken at least 10 times the maximum velocity, it is sufficient [60]. Nevertheless, for the solid it is a real material constant related to the bulk modulus( $K$ ) and density( $\rho$ ) according to

$$c_0 = \sqrt{\frac{K}{\rho}} \quad (24)$$

 Springer

Since here SPH is applied to solid deformation using rate-based constitutive equation, this is in the spirit equivalent to the method of explicit dynamic relaxation in finite element (FE) discretizations. In terms of computational cost using SPH for FSI problems is justified if the elastic modulus of the solid is in the order as the assumed fluid bulk modulus. It means that applying SPH to FSI problems is computationally efficient if the characterized time scale of fluid and solid are of the same order, otherwise use of SPH is not recommended because a much smaller time step is associated with the stiff solid and hence rules the whole process. In this paper, fortunately the biofilm is a soft material with elastic modulus in the order of several Pa and Poisson ratio not close to 0.5 [31].

*Remark* In case of fully incompressible solid (for example rubber like materials) whose Poisson ratio approaches the limit 0.5, the bulk modulus tends to infinity and using this approach is unjustifiable. but some authors have shown that an artificial decrease in bulk modulus (or Poisson ratio) would be a remedy for this issue while not affecting the results that much [50]. In this case, the material is allowed to behave nearly incompressible.

#### 2.4 Growth modeling

It was found by the authors that the Eq. (13) is much more suitable for the growth process rather than Eq. (12). In this paper the growth process is handled incrementally. At the beginning of each increment, the new mass is instantaneously generated according to Eq. (11) once the diffusion-reaction equation is solved. It should be clarified that the new mass is added to the existing particles and no new particle is generated. This results in a density increase and consequently a pressure field according to Eqs. (13) and (23). Then the expansion process (growth) starts and the relaxation of accumulated density takes place. As a result, the biofilm expands and this expansion in particle distribution is reflected in more relative distances between the particles and that is exactly the spirit of Eq. (13) which is explicitly a function of particle distribution rather than particle velocity. This is the reason why Eq. (13) has been adopted.

Three important remarks about the growth process need to be clarified. First, the growth process is governed by mass and momentum balance equation in each increment. The only point is that it is driven by internal local density accumulation rather than external forces. Second, the internal energy associated to the initial density accumulation at the beginning of each increment is entirely dissipated by the artificial viscosity at the end of the increment. Third, the relaxation occurring in growth process is not of our primary interest, but rather the final configuration at the end of each increment in which the internal pressure is released is important. It is obvious that the magnitude of dissipative force determines

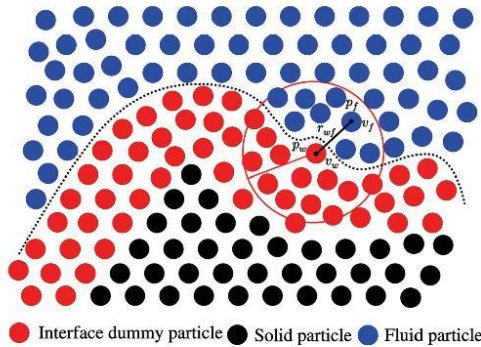


Fig. 2 Pressure and velocity extrapolation through interface particles

how fast the energy is dissipated and the equilibrium state is reached. It should be highlighted that this approach was inspired by a seemingly irrelevant work to this research [51] in which astrophysical gravitational wind accretion has been simulated using SPH method with particles whose masses were varying.

2.5 Boundary conditions and interface modeling

2.5.1 Boundary conditions

The treatment of boundary conditions in SPH is still a controversial issue and not fully solved. The reason stems from the nature of SPH as a collocation method based on the strong form of the governing equations. The completeness condition which means consistency of the method fails at boundaries where the kernel of smoothing function is truncated [58]. Several techniques have been proposed which are based on one of three basic concepts. First using some imaginary particles at the boundary, second using predefined repulsive forces and the third deriving corrective formula for kernel and kernel gradient at free boundaries [57,59]. The aim of this paper is not to discuss these methods in detail, however it should be expressed that the method presented in [60] has been implemented in this paper for fluid-solid interface interaction. This method has been appreciated as a plausible, accurate and stable method by Monaghan, one of the first developer and pioneers of SPH [62].

The main essence of this approach is to consider three layers of solid particle to be dummy (wall) particles through which the pressure and velocity fields of the fluid are extrapolated, see Fig. 2

$$v_w = 2v_s - \frac{\sum_{b \in \Omega_f} v_b^f}{\sum_{b \in \Omega_f} W_{ba}} \tag{25}$$

where  $v_w, v_b^f$  and  $v_s$  are wall (dummy), fluid and solid particle velocities, respectively. It can be said that each interface particle has two identities, the real and dummy one. Although interface particles are solid particles in reality and contribute to the computation of solid phase with the real values such as  $v_s$ , they convey dummy values ( $v_w, p_w$ ) as well. An interface particle with dummy value contributes to the fluid domain computation in order to enforce the interface compatibility conditions. It needs to be stressed that a no-slip condition (velocity compatibility) is implied in Eq. (25) via an approximate mirror projection, see [60]. In addition to the velocity compatibility, an accurate coupling of traction is also required. The novelty of this method is the incorporation of the wall acceleration into the pressure calculation of the dummy particles. It should be noted that it is not an ad hoc formula but it comes from the momentum balance at the interface, see [60]. To do this, we start with the Navier-Stokes equation for the fluid close to the solid boundaries (dummy particles), neglecting the viscous term:

$$a_w = \frac{dv_f}{dt} = -\frac{\nabla P}{\rho} + g \tag{26}$$

in which  $a_w$  is the acceleration of a dummy fluid particle at the interface or boundary. The key assumption is that we have a no-slip boundary condition and it means that the acceleration of a dummy fluid particle is equal to that of solid wall at the boundary ( $a_w = a_s$ ). Rearranging the Eq. (26), one can find an estimation for pressure gradient near the interface. Applying a Taylor series for pressure, yields

$$p_w = p_f + \nabla p \cdot r_{wf} = p_f + \rho_f(g - a_w) \cdot r_{wf} \tag{27}$$

where  $r_{wf} = r_w - r_f$ , see Fig. 2. Taking all the neighbors contribution into account for the Eq. (27) using SPH discretization, one can find the final formula for computing the pressure in dummy particles

$$p_w = \frac{\sum_{b \in \Omega_f} p_b^f W_{ba} + (g - a_w) \cdot \sum_{b \in \Omega_f} \rho_b^f r_{ba} W_{ba}}{\sum_{b \in \Omega_f} W_{ba}} \tag{28}$$

Here  $p_w$  and  $p_b^f$  are wall (dummy) and fluid pressure, respectively.

It is true to say that interface modeling in a FSI problem is crucial. It can affect the output significantly. The more accurate the interface quantities are computed the more correct the fluid-solid coupling is modeled and consequently more realistic and physically sound results are achieved. Finally the exerted force per unit mass on a solid particle  $F_{f \rightarrow s}$  can be evaluated using the extrapolated pressure. It should be clarified that the viscous forces at the interface have been neglected in spite of no-slip boundary condition [60].

$$\mathbf{F}_{f \rightarrow s} = -\frac{\nabla P}{\rho_s} = \frac{1}{\rho_s} \sum_{b \in \Omega_s} \frac{m_b}{\rho_b} P_b \nabla W_{ba} \quad (29)$$

Here one of the most appealing features of SPH shows up. It is its automatically handling of the interface relations which can not be achieved so easily e.g. in FEM. The pressure interface force is always normal to deformed surface of biofilm (it is so-called follower load) and due to updated Lagrangian nature of SPH it is explicitly treated and there is no linearization and computational challenge to encounter [61].

Note that in the solid phase, the above calculated force is added explicitly to the right hand side of momentum equation (15) and the SPH summation is extended only to solid particles, whereas in the fluid phase the SPH summation includes dummy wall particles and no such explicit term is added to momentum equation. In fact, the velocity and pressure of dummy particles which in reality belong to solid phase contribute to the reaction force applied to fluid from solid. It means a two way coupling of fluid and solid in which the kinematic and traction compatibility at the interface is fulfilled in a collocational sense. In other words, the continuity of traction and normal velocity holds true [50]. It should be reminded that the presented boundary treatment has been applied to both deformable solid boundaries (fluid-solid interface) and also rigid fix boundaries (essential boundary conditions). The only difference is that in fixed boundaries the velocity and acceleration are identical to zero ( $v_s = a_w = 0$ ).

### 2.5.2 Erosion (detachment)

The detachment process in biofilm formation has different mechanisms such as erosion, sloughing, abrasion, predator grazing and human intervention [30]. The ones which have a hydrodynamical root are erosion and sloughing. In this work, the focus is on interface erosion in which the bacteria (particles) are gradually washed away because of the shear forces of the flow. To avoid any ambiguity, some important aspects of biofilm detachment need to be clarified.

First, the process is local and taking place at micro-scale and it is almost impossible to have a real-time experimental measurement from which a macroscopic balance of mass could be deduced [30]. In practice, most experiments on biofilm are solely measurement of average height in some points of interests obtained during large time scales of order hours and days. The outcome is indeed a resultant of all processes contributing to biofilm formation and decomposing the real portion of impact for these processes is not possible. In other words, the numerical erosion model of biofilm could not be quantitatively verified through experiments that have been conducted in this research. Nevertheless, it is still a powerful tool to understand qualitatively the physics behind the erosion process in biofilms and to predict detachment.

Second, it has been assumed that the erosion is taking place at the fluid-biofilm interface in the form of a single particle removal when the shear stress induced by the fluid exceeds a failure criteria based on biofilm strength

$$\tau_{interface} > \tau_y \quad (30)$$

Here  $\tau_{interface}$  represents the shear stress induced by the fluid flow and  $\tau_y$  is the shear yield stress in biofilm.

Third, It is well known that the biofilm is a heterogeneous material and its cohesion strength varies from the order of  $10 Pa$  in the base where it is attached to the substratum to the order of  $0.1 Pa$  near the interface [30]. Unfortunately, measuring the mechanical properties of a biofilm which govern its response is a very challenging issue and there is no unique reference value for mechanical properties in the literature. Thus a wide range of values has been reported. On the other hand, it is obvious that the mechanical stress in the biofilm must be higher at the substratum where it is cantilevered [31]. It means it is likely that sloughing as another failure mode in which a bunch of bacteria as a whole are detached, occurs in addition to surface erosion especially in high Reynolds flow. However, in this study the flow conditions are such that the dominant detachment process is surface erosion and the stresses near the substratum are less than the biofilm strength there. Definitely, a continuum damage or crack propagation model is required to be incorporated for capturing bulky failure modes within the biofilm and it could be the matter of further future research.

Fourth, capturing the dynamically changing interface accurately is of great importance because this is the region where biofilm-fluid coupling is taking place. If the interface is not recognized properly several artifacts might appear and finally lead to a crash of the numerical method. Penetration of the fluid into the biofilm, local non-physical tearing of the biofilm due to abrupt change in the interface geometry and forces are two common issues in case that the interface geometry is naively tackled. In this work an algorithm so-called "Alpha shape" has been employed to find the boundary particles in pre-processing stage of the analysis. This has proved to be a robust method especially in case of a general irregular set of particles. This algorithm is based on Delauney triangulation and circumscribed circles. It is available MATLAB software. The input is an arbitrary point cloud and a value corresponding to a rolling circle on the boundary points. The output is the boundary particles. Figure 4 illustrates how the algorithm works. The associated subroutine has been invoked within our FORTRAN code. Furthermore, a dynamic modification of the interface is performed. The procedure of up-dating the interface had been depicted in Fig. 3. Detached (eroded) particle are members of interface (dummy) particles. As soon as a particle is detached, the thickness of interface (about three layers of solid particles) decreases and hence it needs to be updated. New solid par-

Comput Mech

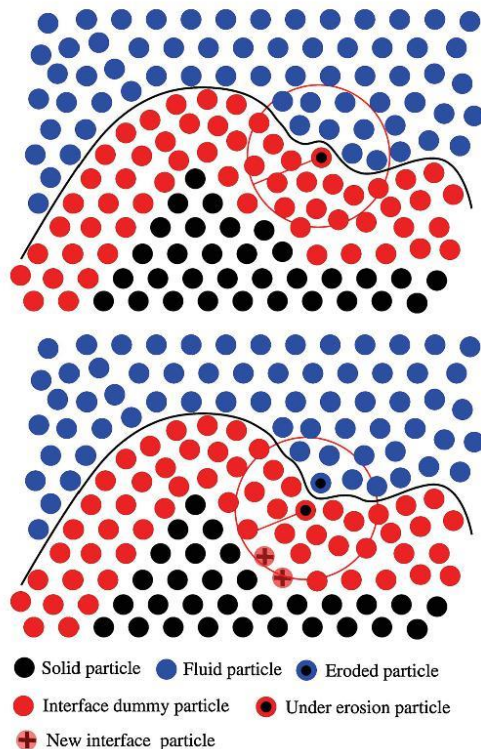


**Fig. 3** Interface modification due to erosion (*top*) before erosion (*bottom*) after erosion

ticles are added to the interface particles set to make up for the detached ones.

Finally, the fact that the minimum size of detached material at the interface is equal to the size of the particle might be physically arguable. This is the case not only in meshless method but also in element based methods when they are applied to model damage and failure phenomena using “death” of elements. Generally such mesh dependency of material behavior, which is undesirable, is a matter of discussion when the equations are transformed from continuum to discretization level. Nonetheless, here it can be argued that the biofilm micro structure in reality is a composite made of bacteria as inclusions being glued together with EPS as a matrix and the damage always happens in the weaker compartment of this composite which is the matrix. It is implied that a single bacteria is not torn apart but removed as a whole. Consequently the minimum size of material removal is confined to the size of a single bacteria. Since here the size of mesh (particles) is the same as a single bacteria, this modeling of material erosion is justifiable.

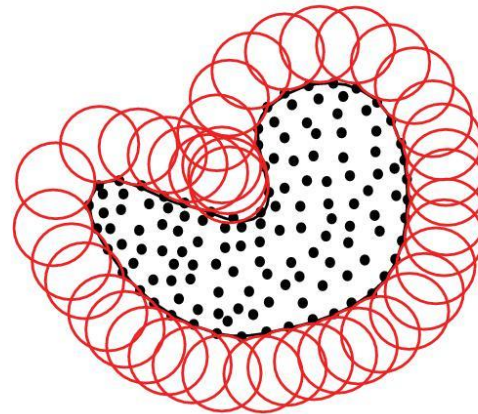


**Fig. 4** Recognizing boundary particles using alpha shape algorithm

## 2.6 Numerical remedies and integration method

### 2.6.1 Tensile instability

In spite of its robustness and simple appearance, SPH like any other computational method has some shortcomings. A great deal of literature has been dedicated to remedy such issues. One of the most cumbersome instabilities in SPH is called tensile instability. It manifests itself in particle clumping when a body is in tension state of stress. Several techniques have been proposed to circumvent this instability. Belytschko [63] was the first who diagnosed this problem in a general framework and found the root and cure of this disorder although it had been already identified by earlier researchers. In [63], it was discovered that the Eulerian nature of the SPH kernel (in current configuration) is the main cause of this instability. So if one uses a Lagrangian kernel (in reference configuration), this instability is cured. Here it is not intended to deeply go through such matters and the reader is referred to a comprehensive review in [58]. In this paper, the method of using artificial stress developed by Monaghan [64] has been employed to deal with tensile instability. The main idea is to introduce a certain amount of artificial stress into the momentum equation in the direction of principal stress whose amount is positive. This kind of stress perturbation removes or at least postpone the emergence of this instability while not changing the physical behavior too much.

### 2.6.2 Artificial viscosity

in SPH an artificial viscosity term must be added to the momentum equation in order to suppress unphysical oscillation and stabilize the numerical scheme [65]. While in the

fluid phase the intrinsic real viscosity of fluid is enough to stabilize the solution, in solid phase an artificial viscosity has to be introduced. This dissipation term could be interpreted as inherent viscous behavior of the solid associated with a certain relaxation time. The final momentum equation including artificial stress and viscosity follows from equation (15)

$$\frac{Dv_a^\alpha}{Dt} = - \sum_b m_b \left( \frac{\sigma_a^{\alpha\beta}}{\rho_a^2} + \frac{\sigma_b^{\alpha\beta}}{\rho_b^2} - \Pi_{ba} \delta_{\alpha\beta} + R_{ba}^{\alpha\beta} \right) W_{ab,\beta} \tag{31}$$

where  $\Pi_{ba} \delta_{\alpha\beta}$  and  $R_{ba}^{\alpha\beta}$  are artificial viscosity and artificial stress terms, respectively. Artificial viscosity can be evaluated, see [65], by

$$\begin{aligned} \Pi_{ba} &= \begin{cases} \frac{-\alpha c_{ba} \mu_{ba}}{\rho_{ba}} & \mathbf{v}_{ba} \cdot \mathbf{r}_{ba} \leq 0 \\ 0 & \mathbf{v}_{ba} \cdot \mathbf{r}_{ba} > 0 \end{cases} \\ \mu_{ba} &= \frac{h \mathbf{v}_{ba} \cdot \mathbf{r}_{ba}}{|\mathbf{r}_{ba}|^2 + 0.01h^2} \end{aligned} \tag{32}$$

where  $\mathbf{r}_{ba} = \mathbf{r}_a - \mathbf{r}_b$ ,  $\mathbf{v}_{ba} = \mathbf{v}_a - \mathbf{v}_b$ ,  $c_{ba} = \frac{1}{2}(c_a + c_b)$ ,  $\rho_{ba} = \frac{1}{2}(\rho_a + \rho_b)$  and  $\alpha$  is a parameter in the order of unity. The artificial stress is calculated using the formula

$$\begin{aligned} R_{ba}^{ij} &= R_a^{ij} + R_b^{ij} \\ R_\xi^{ij} &= \begin{cases} -e \frac{\sigma_\xi^{ij}}{\rho_\xi^2} & \sigma_\xi^{ij} > 0 \\ 0 & \sigma_\xi^{ij} < 0 \end{cases}, \quad \xi := a \text{ or } b \end{aligned} \tag{33}$$

Unlike in equation (31) the superscript  $i, j$  has been used instead of  $\alpha, \beta$  in this equation. The reason is that the artificial stress tensor is computed using the value of principal stresses and directions( $i, j$ ) and afterward it is returned to the regular basis  $\alpha, \beta$  by a transformation matrix  $Q$ .

$$R_{ba}^{\alpha\beta} = Q_{ba}^{\alpha i} R_{ba}^{ij} Q_{ba}^{\beta j} \left( \frac{W(|\mathbf{r}_b - \mathbf{r}_a|, h)}{W(\Delta)} \right)^n \tag{34}$$

The parameter  $e = 0.3$  and  $n = 4$  were taken [64].  $\Delta$  denotes the average particle spacing in the neighborhood of particle  $a$ .

### 2.6.3 Integration method

For the time integration a velocity verlet proposed by [60] was selected and implemented. This integrator is explicit, second order accurate (hence consistent with the SPH nature), symplectic (conserves important quantities like momentum and energy in long term and consequently it is reversible) and efficient due to just one time force calculation per time step.

$$\mathbf{v}_a^{n+\frac{1}{2}} = \mathbf{v}_a^n + \frac{\Delta t}{2} \left( \frac{D\mathbf{v}_a}{Dt} \right)^n \tag{35}$$

$$\mathbf{r}_a^{n+\frac{1}{2}} = \mathbf{r}_a^n + \frac{\Delta t}{2} \mathbf{v}_a^{n+\frac{1}{2}} \tag{36}$$

$$\rho_a^{n+1} = \rho_a^n + \Delta t \left( \frac{D\rho_a}{Dt} \right)^{n+\frac{1}{2}} \tag{37}$$

$$\mathbf{r}_a^{n+1} = \mathbf{r}_a^{n+\frac{1}{2}} + \frac{\Delta t}{2} \mathbf{v}_a^{n+\frac{1}{2}} \tag{38}$$

$$\mathbf{v}_a^{n+1} = \mathbf{v}_a^{n+\frac{1}{2}} + \frac{\Delta t}{2} \left( \frac{D\mathbf{v}_a}{Dt} \right)^{n+1} \tag{39}$$

As mentioned before, to guarantee stability of the computational method the time step is determined by the CFL stability condition in conjunction with extra viscous and force conditions, see [60].

$$\Delta t = \min \left\{ 0.25 \frac{h}{c_{max} + |\mathbf{v}_{max}|}, 0.125 \frac{h^2}{\nu}, 0.25 \left( \frac{h}{|\frac{D\mathbf{v}}{Dt}|_{max}} \right)^{\frac{1}{2}} \right\} \tag{40}$$

Here  $\nu$  is the kinematic viscosity of the fluid. It should be noted that in case of diffusion equation, the time step is similar to viscous term above and is evaluated as follows

$$\Delta t = 0.125 \frac{h^2}{D} \tag{41}$$

in which  $D$  is diffusivity coefficient.

## 3 Numerical examples and discussion

In order to examine the validity of the developed code for the fluid flow and biofilm deformation, first a conceptual example presented in [34] is simulated. In the second example a 2D deformable biofilm undergoing erosion is modeled and in the third example the biological growth process of 3D biofilm is computed and the results are compared with those measured in experiments.

### 3.1 Fluid-biofilm interaction

In this example an artificially shaped 2D biofilm in the form of a rectangular block is deformed as a result of its interaction with the surrounding fluid. The fluid condition, material constants and geometric dimensions can be found in Table 1. The upper plate velocity was set to  $V$  and its motion moves the bulk fluid around the biofilm. It exerts forces on the biofilm structure and finally causes it to deform until a final steady state is reached. Figure 5 depicts the normalized hydrostatic pressure profile prior to applying the horizontal velocity.

Comput Mech

**Table 1** Model parameters and constants [34]

Parameter	Symbol	Value	Unit
Biofilm height	H	150	mm
Biofilm width	W	50	mm
Biofilm Poisson ratio	E	0.5	-
Biofilm shear modulus	$\mu$	1	Pa
Fluid density	$\rho$	1000	Kg/m <sup>3</sup>
Fluid viscosity	$\mu$	1.002E-3	Pa.s
Top plate velocity	V	1.00	$\frac{mm}{s}$
Particle size	$\Delta$	3.0	mm

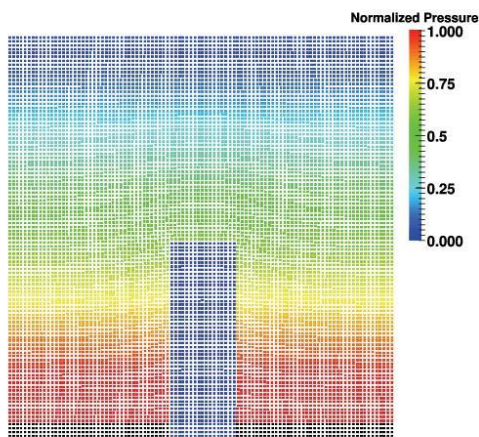


**Fig. 5** The initial configuration of a rectangular biofilm in fluid flow under hydrostatic condition

The reference pressure for normalization is the one computed analytically at the bottom of the domain, namely  $P_{ref} = \rho_f g H$ .

The results which are based on a fully continuum approach show good agreement with those achieved in [34] in which discrete mass-spring elements have been used to model the biofilm deformation. Figure 6 illustrates the final (steady state) configuration of the deformable biofilm in the fluid flow as well as the flow streamlines. It should be noted that the real time having been simulated is much less than characteristic growth time of biofilm and in fact no growth occurs in this test case.

### 3.2 Biofilm erosion and streamer formation

Two dimensional simulation has been performed in the second example to show the process of biofilm erosion due to induced shear forces at the biofilm surface. Table 2 contains

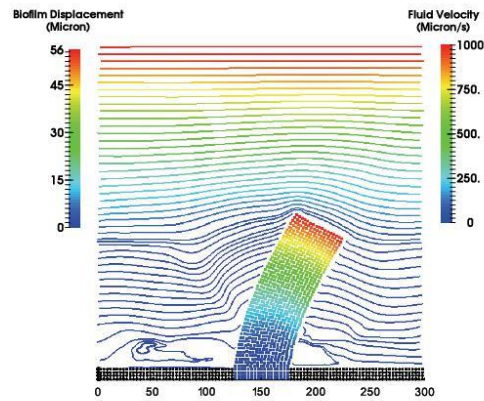


**Fig. 6** The steady state configuration of a rectangular biofilm in fluid flow

**Table 2** Model parameters and constants (Material property from [31])

Parameter	Symbol	Value	Unit
Biofilm initial height	H	30.0	Micron
Biofilm initial maximum width	W	20.0	Micron
Biofilm Young modulus	E	10	Pa
Biofilm Poisson ratio	$\nu$	0.3	-
Biofilm interface strength	$\tau_y$	0.1	Pa
Biofilm density	$\rho_b$	30.0	Kg/m <sup>3</sup>
Fluid density	$\rho_f$	1000	Kg/m <sup>3</sup>
Fluid viscosity	$\mu$	1.002E-3	Pa.s
Particle (bacteria) size	$\Delta$	1.0	Micron

material properties, constants and parameters required for this case.

In this case an initial single biofilm hump is considered which is located at the center of flow chamber. It is exposed to the fluid flow. For the sake of simplicity in visualization, the 2D results (plane stress assumption) are presented. It is observed that the biofilm colony loses gradually some bacteria at the interface where the interfacial shear stress exceeds the biofilm cohesion strength. The detached bacteria are washed away by the fluid forces and form a filamentous streamer-like tail floating in the fluid flow downstream. In some cases, especially when the biofilm is too soft, this streamer formation may happen even prior to detachment and in fact the biofilm is highly deformed and elongated. Such phenomena have been repeatedly reported in the literature, see [32,36,66,67]. An animation of this process can be viewed in the supplementary online materials.

It should be noted that the time has been non-dimensionalized using  $t_{ref} = \frac{100h}{C_0}$ . Two important points can be

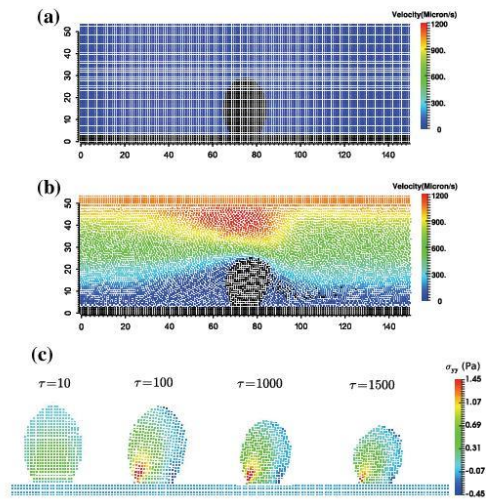


**Fig. 7** Biofilm erosion **a** initial velocity profile **b** velocity profile and eroded bacteria after  $\tau = 1500$  **c** mechanical stress development in not eroded biofilm during time

extracted from Fig. 7. First, before the horizontal fluid velocity is applied and consequently the erosion starts (at time  $\tau = \frac{t}{\tau_{ref}} = 10$ ), the biofilm is in a tension state of stress. The reason is that in a hydrostatic equilibrium an effective upward buoyancy force, originating from density difference between fluid and biofilm, tends to lift up the biofilm. Once the fluid moves, the effective drag force on the biofilm bends it and changes the stress state. As it is expected the mechanical stress has the maximum value at the lower part of the biofilm where it is anchored to the substratum. However the value of stress is less than biofilm strength in this region and no sloughing happens. In Fig. 8 it can be seen that the biofilm experiences a vibrational micro-motion in the fluid flow direction. This is due to continuous erosion which results in sequential impulses on the biofilm structure and triggering the first vibration mode of biofilm structure. It means that the biofilm response to the fluid flow is dynamic during erosion process. It is expected that such movements are gradually suppressed when the erosion process stops due to the reduction of shear forces once enough material is washed out and the fluid velocity decreases in the vicinity of biofilm.

### 3.3 Biofilm growth

The material properties and parameters are listed in Table 3 for this example. The biological growth process of a 3D biofilm was simulated in this case study. It is assumed that an initial semi spherical colony of bacteria exists on the sur-

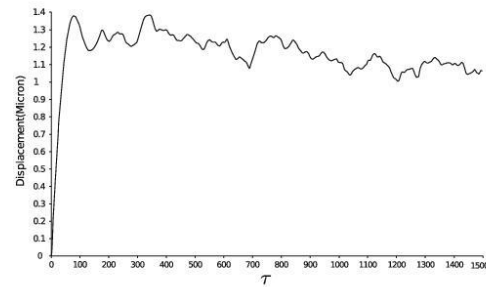


**Fig. 8** Displacement of the biofilm center in time during the erosion process

**Table 3** Model parameters and constants (material property from [31])

Parameter	Symbol	Value	Unit
Biofilm initial height	H	30.0	Micron
Biofilm initial			
Maximum width	W	20.0	Micron
Biofilm density	$\rho_b$	30.0	Kg/m <sup>3</sup>
Reaction Constant			
in Monod law	$K_1$	0.12	1/h
Reaction Constant			
in Monod law	$K_2$	4.0E-18	gr/Micron <sup>3</sup>
Nutrient Concentration			
in Bulk fluid	$C_f$	3.0E-18	gr/Micron <sup>3</sup>
Yield Constant			
in Monod law	Y	1.0	gr/gr
Particle (bacteria) size	$\Delta$	1.0	Micron

face and it starts to grow. In other words, the initial condition is a priori because this is due to the fact that the initial colonization of a surface by the microorganism is a very complex process, taking place in much smaller length scale in the order of molecules size. It is still a not truly understood phenomenon and rare computational modeling could be found in literature, nevertheless some researchers employed theories like DVLO (Derjaguin Landau VerweyOverbeek) incorporating Van der Waals and electrostatic forces to simulate initial adherence of bacteria [68].

Although in reality bacteria need several nutritional substrates, for the sake of simplicity it is assumed that the growth process is limited and affected by the concentration of just one type of nutrient and the other components are unlimitedly supplied. It implies that there is only one diffusion–advection–reaction equation in the computational method corresponding to this substrate [4,35].

Figure 9 illustrates the biofilm growth and the nutrient normalized (non-dimensionelized) concentration during 24h. The reference concentration is that of the bulk fluid ( $C_f$ )



Comput Mech

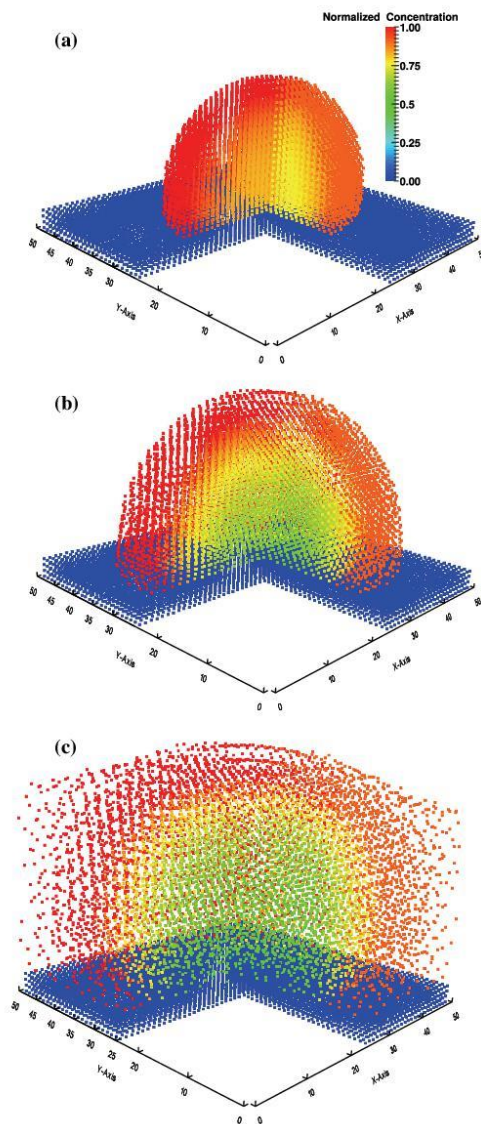


**Fig. 9** Biofilm growth and nutrient concentration **a** after  $T=6$  h **b** after  $T=12$  h **c** after  $T=24$  h

which is in fact the maximum available nutrient concentration. It is a common assumption that the fluid is well mixed due to the dominance of advection transport mechanism and the nutrient concentration is a prescribed variable in bulk fluid but it is computed in the biofilm using the diffusion-

consumption equation. It should be noted that the RVE has a periodic boundary condition at all lateral sides and that is why the biofilm can take the whole spaces around itself as it grows up. Figure 6c reveals that the more the biofilm grows the less nutrient is available inside. Of course there is always a nutrient flux from fluid to biofilm through the interface via the diffusion mechanism. This makes up for the consumed nutrient by the bacteria, however as the biofilm expands spatially the overall nutrient amount in lower region of biofilm decreases. It means that the biofilm has a larger growth rate at the interface and a slower rate in the interior region. In some cases the shortage of nutrient may result in death of bacteria. They form an inactive region in the biofilm which even shrinks because of chemical decay instead of growing. Presence of inactive biomass has been reported in biological observation and was detected by our experimental colleagues as well. In this research the effect of inert biomass shrinkage was neglected because it was found that the portion of inactive biomass is much less than the total active biomass especially in small time period of order 1 day. Some researchers who use individual based methods have introduced this consolidation effect in their model [17]. But it seems that it is much more challenging to incorporate this phenomenon in a continuum based framework. In Fig. 10 the average height of the biofilm has been plotted after 24 h which reflects the biofilm growth. The experiments were repeated 3 times and the data were collected from several point of interest. It can be seen that the relatively large standard deviation implies how nondeterministic the process is. Additionally the portion of inert (dead) biofilm is so small that it could be neglected at least in small time period simulation that was assumed here for the numerical modeling. The computational results are satisfactorily in comparison with those measured in experiments. It is obvious that the parameters of the problem could be calibrated using the experimental results in such a way that the experimental and numerical results fit better. However it does not necessarily mean that such calibrated parameters can be applicable to different environmental conditions other than that of this experiment, because the process has an intrinsic stochasticity.

It should be stressed out that the induced fluid velocity from biofilm growth is so small (of order one micron per hour, Fig. 11) that the fluid flow is not disturbed in practice. It means that it is not required to explicitly resolve the fluid flow field variable as a function of growing. In other words, capturing the interface is sufficient to update the geometrical domain of the fluid flow. That is why some researchers who focus just on the biofilm growth, never deal with the Navier Stokes equation at all [17] and they assume to have a pre-known boundary layer as the fluid-biofilm interface. These are fundamental assumptions in biofilm simulation due to separation of several time-scales corresponding to different phenomena and need to be thoroughly understood.

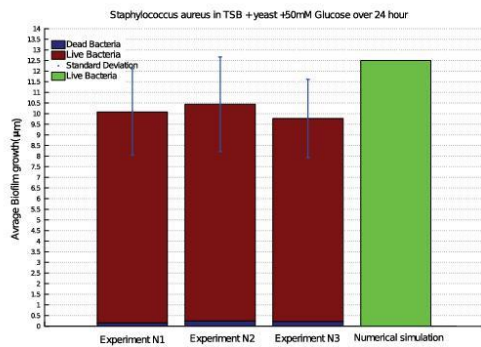


**Fig. 10** Experimental results versus numerical simulation of 3D biofilm growth

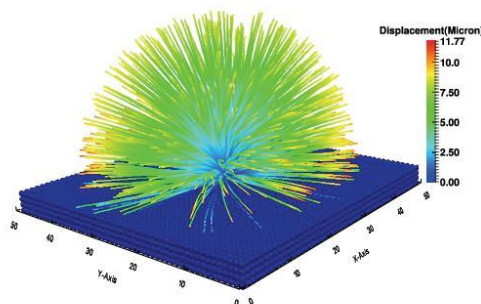


**Fig. 11** Streamline of biofilm growth after  $T=12\text{h}$

#### 4 Conclusion

In this article a fully continuum based numerical scheme for biofilm formation was presented in the SPH framework. The method was motivated by the goal to benefit from the Lagrangian and meshless features of SPH in order to handle several complexities in the problem due to geometrical and physical coupling between the biofilm and the surrounding fluid. The biofilm was modeled in small time scales as a deformable solid submerged in the fluid flow and experienced mechanical deformations and surface erosion due to the forces from the fluid. Furthermore, assuming a viscous fluid, biofilm growth was simulated in large time scales and the results were verified by experiments, conducted by our partners in medical school. It was found that the hydrodynamical conditions of the fluid flow have a significant impact on how biofilm grows and its geometry changes as a result of environmental conditions. The authors believe that the developed computational tool is robust. It can be extended in order to incorporate other aspects and determinant factors of biofilm formation such as a multi species colony of bacteria, shrink-

age of biofilm due to bacteria decay in the long term, other detachment processes, different non-linearity in material behavior, turbulent flow around biofilm, to benefit from GPU implementation and more parallelization concepts like MPI.

**Acknowledgments** The authors sincerely acknowledge the financial support of this research by Ministry of Science and Technology, Niedersachsen, Germany in the context of MARIO graduate program in the Institute Of Continuum Mechanics (IKM) at Leibniz university of Hannover.

#### References

- Rittmann BE, McCarty PL (1980) Model of steady-state-biofilm kinetics. *Biotechnol Bioeng* 22:2343–2357
- Wanner GW (1986) A multispecies biofilm model. *Biotechnol Bioeng* 28(3):314–328
- Picioreanu C, Loosdrecht MCM, Heijnen JJ (1999) Discrete-differential modeling of biofilm structure. *Water Sci Technol* 39:115–122
- Picioreanu C, Loosdrecht MCM, Heijnen JJ (2000) Effect of diffusive and convective substrate transport on biofilm structure formation: a two-dimensional modeling study. *Biotechnol Bioeng* 69:504–515
- Picioreanu C, Loosdrecht MCM, Heijnen JJ (2001) Two-dimensional model of biofilm detachment caused by internal stress from liquid flow. *Biotechnol Bioeng* 72:205–218
- Alpkvist E, Klapper I (2007) A multidimensional multispecies continuum model for heterogeneous biofilm development. *Bull Math Biol* 69:765–789
- Dillon R, Fauci L, Fogelson A, Gaver D (1996) Modeling biofilm processes using the immersed boundary method. *J Comput Phys* 129(1):57–73
- Kreft J-U, Booth G (1998) BacSim, a simulator for individual-based modeling of bacterial colony growth. *Microbiology* 144:3275–3287
- Kreft J-U, Picioreanu C (2001) Individual-based modeling of biofilms. *Microbiology* 147:2897–2912
- Kreft J-U, Picioreanu C, Wimpenny JWT (2004) Particle-based multidimensional multispecies biofilm model. *Appl Environ Microbiol* 70:3024–3040
- Tang Y, Valocchi AJ (2013) An improved cellular automaton method to model multispecies biofilms. *Water Res* 47:5729–5742
- Picioreanu C, van Loosdrecht MCM, Heijnen JJ (1998) A new combined differential-discrete cellular automaton approach for biofilm modeling: application for growth in gel beads. *Biotechnol Bioeng* 57(6):718–731
- Noguera DR, Pizarro G, Stahl DA, Rittmann BE (1999) Simulation of multispecies biofilm development in three dimensions. *Water Sci Technol* 39(7):123–130
- Fujikawa H, Matsushita M (1989) Fractal growth of bacillus subtilis on agar plates. *J Phys Soc Jpn* 58:3875–3878
- Picioreanu C, Kreft J-U, Van Loosdrecht MCM (2004) Particle-based multidimensional multispecies biofilm model. *Appl Environ Microbiol* 70(5):3024–3040
- Eberl HJ, Parker DF, Van Loosdrecht MCM (2001) A new deterministic spatio-temporal continuum model for biofilm development. *J Theor Med* 3:161–175
- Lardon LA, Merkey BV, Martins S, Dötsch A, Kreft JU, Picioreanu C, Wimpenny JWT, Smets BF (2011) iDynoMiCS: next-generation individual-based modeling of biofilms. *Environ Microbiol* 13(9):2416–2434

18. Cumsille P, Asenjo JA, Conca Carlos (2014) A novel model for biofilm growth and its resolution by using the hybrid immersed interface-level set method. *Comput Math Appl* 67:34–51
19. Dockery J, Klapper I (2001) Finger formation in biofilm layers. *SIAM J Appl Math* 62(3):853–869
20. Cogan N (2008) Two-fluid model of biofilm disinfection. *Bull Math Biol* 70:800–819
21. Jones GW, Chapman SJ (2012) Modeling growth in biological materials. *SIAM Rev* 54(1):52–118
22. Kroon W, Delhaas T, Arts T, Bovendeerd P (2009) Computational modeling of volumetric soft tissue growth: application to the cardiac left ventricle. *Biomech Model Mechanobiol* 8:301–309
23. Kuhl E, Holzapfel GA (2007) A continuum model for remodeling in living structures. *J Mater Sci* 42:8811–8823
24. Ambrosi D, Ateshian GA, Aruda EM, Ben M, Amar SC, Cowin J, Dumaïs A, Goriely GA, Holzapfel JD, Humphrey R, Kemkemer E, Kuhl J, Ma JE, Olberding LA, Taber R, Vandeiver, Garikipati K (2011) Perspectives on biological growth and remodeling. *J Mech Phys Solids* 59:863–883
25. Taber LA (1995) Biomechanics of growth, remodeling and morphogenesis. *Appl Mech Rev* 48:487–545
26. Taber LA (1998) A model for aortic growth based on fluid shear and fiber stresses. *Trans ASME J Biomech Eng* 120:348–354
27. Bakke R (1986) Biofilm deattachment, PhD thesis, Montana State University
28. Horn H, Reiff H, Morgenroth E (2003) Simulation of growth and detachment in biofilm systems under defined hydrodynamic conditions. *Biotechnol Bioeng* 81:607–617
29. Picioreanu C, van Loosdrecht MCM, Heijnen JJ (2001) Two-dimensional model of biofilm detachment caused by internal stress from liquid flow. *Biotechnol Bioeng* 72:205–218
30. Duddu R, Chopp DL, Moran B (2009) A two-dimensional continuum model of biofilm growth incorporating fluid flow and shear stress based detachment. *Biotechnol Bioeng* 103(1):92–104
31. Boel M, Moehle RB, Haesner M, Neu TR, Horn H, Krull R (2009) 3D finite element model of biofilm detachment using real biofilm structures from CLSM data. *Biotechnol Bioeng* 103:177–186
32. Stoodley P, Lewandowski Z, Boyle JD, Lappin-Scott HM (1998) Oscillation characteristics of biofilm streamers in turbulent flowing water as related to drag and pressure drop. *Biotechnol Bioeng* 57(5):536–544
33. Stoodley P, Lewandowski Z, Boyle JD, Lappin-Scott HM (1998a) Structural deformation of bacterial biofilms caused by short-term fluctuations in fluid shear: an in situ investigation of biofilm rheology. *Biotechnol Bioeng* 65:83–92
34. Alpkvist E, Klapper I (2007) Description of mechanical response including detachment using a novel particle model of biofilm/flow interaction. *Water Sci Technol* 55(89):265–273
35. Zhijie X, Meakin P, Tartakovsky A, Scheibe TD (2011) Dissipative-particle-dynamics model of biofilm growth. *Phys Rev E* 83:066702
36. Xavier JD, van Picioreanu C (2005a) A general description of detachment for multidimensional modeling of biofilms. *Biotechnol Bioeng* 91(6):651–669
37. Duddu R, Bordas S, Chopp D, Moran B (2008) A combined extended finite element and level set method for biofilm growth. *Int J Numer Methods Eng* 74:848–870
38. Gingold RA, Monaghan JJ (1977) Smoothed particle hydrodynamics: theory and application to non-spherical stars. *Mon Not R Astron Soc* 181:375
39. Lucy LB (1977) Numerical approach to the testing of the fission hypothesis. *Astron J* 82:1013
40. Cleary PW, Monaghan JJ (1999) Conduction modeling using smoothed particle hydrodynamics. *J Comput Phys* 148:227–264
41. Zhu Yi, Fox PJ (2001) Smoothed particle hydrodynamics model for diffusion through porous media. *Transp Porous Media* 43:441–471
42. Aristodemo F, Federico I, Veltri P (2010) Two-phase SPH modeling of advective diffusion processes. *Environ Fluid Mech* 10:451–470
43. Monaghan JJ (1994) Simulating free surface flows with SPH. *J Comput Phys* 110(2):399–406
44. Gomez-Gesteira M, Rogers BD, Dalrymple RA, Crespo AJ (2010) State-of-the-art of classical SPH for free-surface flows. *J Hydraul Res* 48:6–27
45. Kristof P, Benes B, Krivanek J, Stava O (2009) Hydraulic erosion using smoothed particle hydrodynamics. *Comput Gr Forums* 28:219–228
46. Tartakovsky AM, Meakin P, Scheibe TD (2007) Simulations of reactive transport and precipitation with smoothed particle hydrodynamics. *J Comput Phys* 222:654–672
47. Gray JP, Monaghan JJ, Swift RP (2001) SPH elastic dynamics. *Comput Methods Appl Mech Eng* 190:6641–6662
48. Libersky Larry D, Petschek Albert G, Carney Theodore C, Hipp Jim R, Allahdadi Firooz A (1993) High strain lagrangian hydrodynamics: a three-dimensional SPH code for dynamic material response. *J Comput Phys* 109(1):67–75
49. Simo JC, Pister KS (1984) Remarks on rate constitutive equation for finite deformation problems: computational implications. *Comput Methods Appl Mech Eng* 46:201–205
50. Antoci C, Gallati M, Sibilla S (2007) Numerical simulation of fluidstructure interaction by SPH. *Comput Struct* 85:879–890
51. Boffin HMJ, Anzer U (1994) Numerical studies of wind accretion using SPH. *Astron Astrophys* 284:1026–1036
52. Goriely A, Robertson-Tessi M, Tabor M, Vandeiver R (2008) Elastic growth models. In: Mondaini RP, Pardalos PM (eds) *Mathematical modeling of bio-systems*. Springer, Berlin, pp 1–44
53. Hauser M, Vafai K (2013) Analysis of the multidimensional effects in biofilms. *Int J Heat Mass Transf* 56:340–349
54. Qing Y, Fish J (2002) Multiscale asymptotic homogenization for multiphysics problems with multiple spatial and temporal scales. *Int J Solids Struct* 39:6429–6452
55. Monaghan JJ (1992) Smoothed particle hydrodynamics. *Annu Rev Astron Astrophys* 3:543–574
56. Volokh KY (2006) Stresses in growing soft tissues. *Acta Biomater* 2:493–504
57. Monaghan JJ (2005) Smoothed particle hydrodynamics. *Rep Prog Phys* 68:1703–1759
58. Li S, Liu WK (2002) Mesh-free and particle methods and their applications. *Appl Mech* 55(1):1–34
59. Monaghan JJ, Kajtar JB (2009) SPH particle boundary forces for arbitrary boundaries. *Comput Phys Commun* 180:1811–1820
60. Adami S, Hu XY, Adams NA (2012) A generalized wall boundary condition for smoothed particle hydrodynamics. *J Comput Phys* 231:7057–7075
61. Wriggers P (2008) *Non-linear finite element method*. Springer, Heidelberg
62. Valizadeh A, Monaghan JJ (2015) A study of solid wall models for weakly compressible SPH. *J Comput Phys* 300:5–19
63. Belytschko T, Guo Y, Liu WK, Xiao SP (2000) A unified stability analysis of meshless particle methods. *Int J Numer Methods Eng* 48:1359–1400
64. Monaghan JJ (2000) SPH without a tensile instability. *J Comput Phys* 159:290–311
65. Monaghan JJ, Gingold RA (1983) Shock simulation by the particle method SPH. *J Comput Phys* 52(2):374–389
66. Klapper I, Rupp CJ, Cargo R, Purvedorj B, Stoodley P (2002) Viscoelastic fluid description of bacterial biofilm material properties. *Biotechnol Bioeng* 80(3):289–296
67. Stewart PS (2012) Convection around biofilms. *J Bio-adhes Biofilm Res* 28(2):187–198
68. Hermansson Malte (1999) The DLVO theory in microbial adhesion. *Colloids Surf B* 14:105–119

The preceding publication has described the development of the biofilm formation by the means of the numerical investigation in detail. As the biological part is superficial represented as the main focus of the journal is the numerical investigation, an additional biological results and discussion part of the biofilm formation of *S. aureus* under different flow velocities is presented in the following.

### 4.3.1 Results

The influence of flow velocity on the biofilm formation under different flow velocities is shown in Figure 18. The average biofilm height of *S. aureus* under 100-400  $\mu\text{L}/\text{min}$  is represented in section A and the bacterial viability in percentage is shown in section B. The average vital biofilm height reached its maximum of 9.8  $\mu\text{m}$  at a flow rate of 100  $\mu\text{L}/\text{min}$ . The vital biofilm height decreased with increasing flow velocities of 200 and 400  $\mu\text{L}/\text{min}$  down to 3.92  $\mu\text{m}$  and 1.89  $\mu\text{m}$ , respectively. Furthermore, the bacterial viability decreased with the increase of the flow velocity. The dead bacterial population of the biofilm that was formed at a flow rate of 100  $\mu\text{L}/\text{min}$  was less than 5%. With a flow rate of 400  $\mu\text{L}/\text{min}$ , the dead population increased to over 15%.

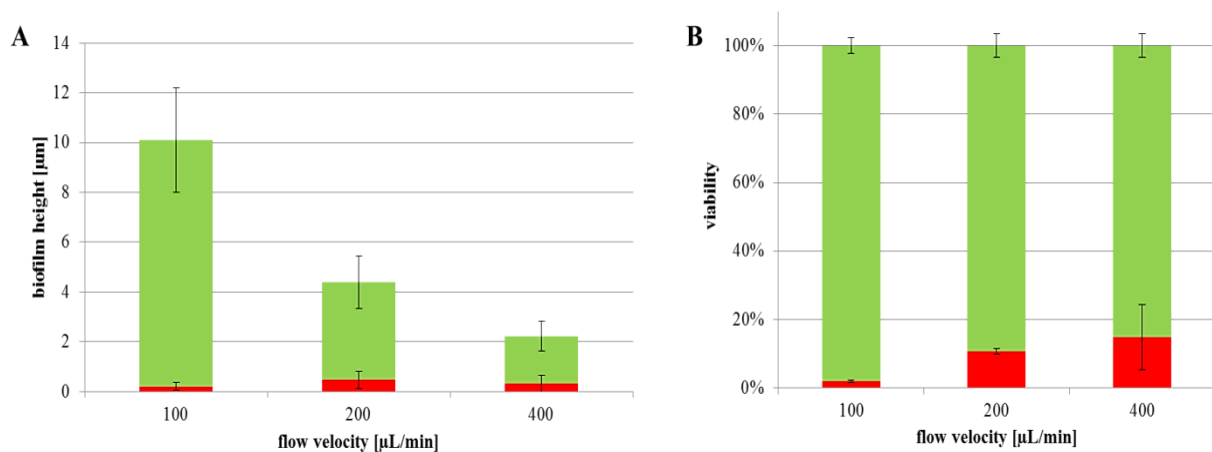


**Figure 18: Biofilm formation of *S. aureus* under different velocities in a flow chamber system.** A) Average biofilm height after 24 h with 100-400  $\mu\text{L}/\text{min}$ , B) Bacterial viability after 24 h with 100-400  $\mu\text{L}/\text{min}$ . Green indicating the vital and red the dead biofilm portion.

### 4.3.2 Discussion

The flow within a biofilm influences many processes *inter alia* the formation of the EPS content, the biofilm morphology and physiology, transport of oxygen, nutrient and signaling molecules for communication.<sup>202-208</sup> As the bacterial cells behave like particles in a fluidic medium, the rate of attachment and colonization on the titanium surface depends mainly on the flow velocity of the medium, the cell size and motility. In general, the attachment process is enforced by van der Waals forces, hydrogen bonds and electrostatic attraction. These mechanisms take place within microseconds. The faster the particles flow over the titanium surface, the faster the adhesion mechanisms had to proceed.<sup>364,432,433</sup> The slower the bacterial cells flow over the titanium discs the more time and chance they have to activate the adhesion processes and to attach to the surface. Consequently, more bacteria are able to adhere on the surface and form biofilm. This phenomenon decreases at higher flow rates.

As a second reason, Islam *et al.* confirmed, that increasing flow velocities lead to a reduced protein expression of *S. aureus*.<sup>359</sup> Specific proteins with metabolic function to regulate the protein synthesis and stress tolerance are significantly decreased and as a consequence, bacterial adhesion is reduced. Furthermore, the phenomenon of a decreased biofilm formation under more violent flow conditions has been described in literature.<sup>390-393</sup>



#### **4.4 Theoretical and experimental evidence of the effects of varying disinfection timing**

Nick Cogan, Henryke Rath, Nadine Kommerein, Nico Sascha Stumpp, Meike Stiesch

FEMS Microbio. Lett., **2016**, 363, fnw264, Epub

DOI 10.1093/femsle/fnw264

The final publication is available at:

<http://femsle.oxfordjournals.org/content/early/2016/12/02/femsle.fnw264>

Reprinted from Federation of European Microbiological Societies Microbiology Letters, **363**, Nick Cogan, Henryke Rath, Nadine Kommerein, Nico Sascha Stumpp, Meike Stiesch, Theoretical and experimental evidence of the effects of varying disinfection timing, Copyright (2016), with permission from the Oxford University Press.

## *Preface*

The aim of this cooperation work was the initial numerical and experimental validation of the theoretical disinfection protocol investigated by Prof. PhD. NICK COGAN. This study has dealt with the time dependent eradication of *S. aureus* persisters by antibiotic ofloxacin treatment. Bacterial persister cells are able to alter their metabolic activity and are not susceptible to antibiotics that mainly interfere with metabolic mechanisms. Prof. NICK COGAN has numerically simulated three different time points of antibiotic treatment and different recultivation time points with medium without antibiotic for the eradication of persistent *S. aureus*. The time point for the complete eradication of *S. aureus* has been the 20 h antibiotic treatment with 4 h recultivation. The predicted outcome has been validated by *in vitro* experiments so that planktonic *S. aureus* persister cells have successfully been eliminated.

To this study HENRYKE RATH, Prof. PhD NICK COGAN and NADINE KOMMEREIN have contributed equally. The simulation has been developed by Prof. PhD NICK COGAN. The experimental set-up of *S. aureus* and the antibiotic ofloxacin have been established by HENRYKE RATH and NADINE KOMMEREIN. The experiments and analysis have been performed 1:1 from both persons. The study has been guided by Dr. SASCHA NICO STUMPP and Prof. Dr. MEIKE STIESCH: The initial manuscript has been written by Prof. PhD. NICK COGAN, HENRYKE RATH, and NADINE KOMMEREIN. It has been refined together with Dr. SASCHA NICO STUMPP and Prof. Dr. MEIKE STIESCH. The study was initiated by Prof. PhD NICK COGAN and Prof. Dr. MEIKE STIESCH. The manuscript of this cooperation project has been accepted by Federation of European Microbiological Societies Microbiology Letters for publication and is depicted in the following.

The supporting information are presented in section 7.2.





FEMS Microbiology Letters, 363, 2016, fnw264

doi: 10.1093/femsle/fnw264

Advance Access Publication Date: 3 December 2016

Research Letter

RESEARCH LETTER – Pathogens &amp; Pathogenicity

## Theoretical and experimental evidence for eliminating persister bacteria by manipulating killing timing

N. G. Cogan\*, H. Rath†, N. Kommerein†, S. N. Stumpp and M. Stiesch

Department of Prosthetic Dentistry and Biomedical Materials Science, Hannover Medical School, Carl-Neuberg-Strasse 1, Hannover, 30625, Germany

\*Corresponding author: Department of Mathematics, Florida State University, 1017 Academic Way, Tallahassee, FL 32306, USA. Tel: +(850)644-2202; Fax: +(850)644-4053; E-mail: [cogan@math.fsu.edu](mailto:cogan@math.fsu.edu)

†These authors contributed equally.

**One sentence summary:** The timing of pulsed antibiotic application that succeeds/fails to eliminate susceptible and persister bacteria is described theoretically and tested experimentally.

Editor: Jan-Ulrich Kneft

### ABSTRACT

Formation of a transient sub-population of bacteria, referred to as persisters, is one of the most important and least understood mechanisms that bacteria employ to evade elimination. Persister cells appear to be slow-growing bacteria that are broadly protected from a wide range of antibiotics. Using both theoretical and experimental methods, we show that alternating the application and withdrawal of antibiotics can be an effective treatment—as long as the timing of the protocol is estimated with precision. More specifically, we demonstrate that timing the alternating treatment based on theoretical predictions is confirmed using experimental observations. These results support a large class of theoretical studies that show that, even without complete understanding of the biological mechanisms, these models can provide insight into properties of the system.

**Keywords:** biofilm; persister; tolerance; *Staphylococcus aureus*; ofloxacin; mathematical modeling

### BACKGROUND

Bacteria are remarkable in their ability to adapt to, respond to, and affect their environment in order to survive. By responding to self-produced chemical signals bacteria can upregulate genes to form biofilms that are becoming recognized as one of the central mechanisms for bacterial survival (Davies *et al.* 1998). The physical protection provided by the biofilm is one layer of defense against killing, but it does not explain all the protective mechanisms. In fact, it has been noted for some time that a small fraction of almost any bacterial population will remain, even after extended exposure to an antibiotic challenge (Bigger, 1944; Lewis, 2007). This was first noticed during the development of penicillin therapy where the majority of the bacteria exposed to penicillin were killed, leaving a tolerant sub-population (Hobby, Meyer and Chaffee, 1942). Note that

persistence is quite different than genotypic drug resistance since the former is not inheritable while the latter is passed on to daughter cells. Additionally, persisters do not only exist in the biofilm stage, they also occur in planktonic phase (Keren *et al.* 2004a).

The persister hypothesis represents a dramatic paradigm shift in our understanding of bacterial eradication. It may not be enough to choose the 'correct' antibiotic and maintain the concentration of antibiotic above a threshold for long enough to eliminate the infection. Instead, persister bacteria provide a compelling story of bacterial tolerance (especially in the context of diseases): a host is infected with a bacterial population; antibiotics are applied, clearing the majority of the bacteria. Once the antibiotic is removed, persister bacteria revert to susceptible types and regrow.

Received: 19 October 2016; Accepted: 15 November 2016

© FEMS 2016. All rights reserved. For permissions, please e-mail: [journals.permissions@oup.com](mailto:journals.permissions@oup.com)

Apparently, the transition from susceptible phenotype into persister phenotype is independent of the antibiotic concentration, while the transition from persister into susceptible phenotype is not. In particular, it appears that the presence of antibiotic may lock in the persister phenotype (Bigger 1944; Keren et al. 2004a,b; Lewis 2007). It has also been shown that persistence is clearly a transient stage—with the removal of the antibiotic, the original growth curve is obtained (Desai et al. 1998; Keren et al. 2004a; Lewis 2007).

This offers a simple method for controlling the population by manipulating the antibiotic. A single dosing cycle eliminates the majority of the bacteria, leaving persisters. By removing the antibiotic challenge, the persisters are allowed to revert to susceptible type. Then a second dosing cycle will eliminate these. This idea was introduced by Bigger (Bigger 1944). Bigger suggested the idea of 'intermittent' or 'fractional' sterilization. He even suggested a course of treatment—although this appears to be a completely empirical proposal, unlike the scheduling proposed here. In fact, we could argue that we are merely quantifying with more precision observations and suggestions that arose seven decades ago.

Guided by this intuitive argument, there have been a number of mathematical modeling studies that indicate that a dose period alternating with a withdrawal period can effectively eliminate the entire bacterial population (Cogan 2006, 2007; Lou, Li and Ouyang 2008; Leenheer and Cogan 2009; Cogan et al. 2012; Szomolay and Cogan 2015). In all of these the main observation, that is quite robust regarding the details of the model kinetics, is that there is a window of timing where the treatment is effective. If the treatment is withdrawn for too long, the population has time to fully recover, but if it is too short the persisters do not have time to revert to susceptibles and even though the treatment may be effective, the timescale can be arbitrarily long. Even though this is a general observation from the mathematics, to our knowledge there has been no experimental confirmation of these theoretical predictions.

In this study, we use a mathematical model to predict the timing of an alternating dose/withdrawal protocol that separates the unsuccessful timing from the successful timing. Specifically, we determine two different regimes: first, where the withdrawal time is long enough that persisters can revert to susceptibles and recolonize the system (i.e. unsuccessful) and the second, where the population of *Staphylococcus aureus* is being reduced between each iteration. Our predictions are confirmed with experiments against *S. aureus* in batch culture. To our knowledge, this is the first confirmation of a class of mathematical predictions regarding the effectiveness of alternating treatment in eradicating bacterial populations.

## MATERIALS AND METHODS

### Bacterial strain and culture conditions

*Staphylococcus aureus* strain DSM 20231 was obtained from the German Collection of Microorganisms and Cell Cultures (DSMZ). Cultures were grown aerobically in tryptic soya broth (TSB; Oxoid, Hampshire, UK) modified with 10% yeast extract (Roth, Karlsruhe, Germany) at 37°C in a SM30 incubator shaker (Edmund Buehler GmbH, Hechingen, Germany) at 200 rpm for 18 h.

### Antibiotic treatment and analysis of microbial growth

Prior to antibiotic treatment, overnight cultures in stationary phase were adjusted to an optical density of  $OD_{600} = 0.2$  (Bio-

Photometer, Eppendorf, Hamburg, Germany). This corresponds to an inoculum of  $\sim 3.33 \times 10^7$  CFU/mL. Bacterial suspensions were treated with 600  $\mu$ g/mL ofloxacin (MP Biomedical; Santa Ana, USA) and the microbial growth was investigated for three different regimes of antibiotic treatment. These were as follows: (R 20/4) 20 h incubation with antibiotic followed by 4 h cultivation in fresh medium without antibiotic selection, (R 15/9) 15 h incubation with antibiotic followed by 9 h cultivation in fresh medium without antibiotic selection and (R 8/16) 8 h incubation with antibiotic and 16 h cultivation in fresh medium without antibiotic selection. The incubation cycles without antibiotics offered the ability to regrow in exponential phase. To prevent antibiotic carry-over effects, cells were harvested by centrifugation (4000 g, 15 min, 4°C; Heraeus Multifuge 15-R, Thermo Scientific, Waltham, USA) and washed twice with Dulbecco's phosphate-buffered saline (PBS; Biochrom GmbH, Berlin, Germany) prior to media change. Each experiment was conducted in quadruplicates over a period of 5–6 days. An untreated *S. aureus* culture was used as control in each experiment. During the 24 h cycles, the OD was measured five times in 300  $\mu$ L bacterial suspension to estimate the antibacterial effect (see Fig. 4). The measurement of OD to estimate the growth rates is a reliable method beside colony forming unit (CFU) counting (Bergan and Carlsen 1980; Yourassowsky et al. 1985; Ulanowska et al. 2006; Biesta-Peters et al. 2010; Sutton 2011). In a first approach, we used OD measurement to determine which of the three different regimes leads to constant or decreasing cell concentrations. In parallel, for bacterial viability testing, 10  $\mu$ L of the treated bacterial cultures and 10  $\mu$ L of the control culture suspension were then plated on TSB/yeast extract plates after each 24 h cycle. For susceptibility testing, further 10  $\mu$ L of each suspension were plated on TSB/yeast extract plates supplemented with 600  $\mu$ g/mL ofloxacin. The plates were incubated for 24 h at 37°C before evaluation. Plates without bacterial growth after 24 h were cultivated for further 48 h to exclude false negative results due to growth impairment. Since we are aware that OD measurement gives limited information about culture viability at low cell concentrations, we additionally used CFU counting to demonstrate disinfection efficiency of the most promising antibiotic regime (R 20/4). Therefore, 100  $\mu$ L of the bacterial suspensions of regime R 20/4 were serially diluted before and after the antibiotic treatment. Subsequently, 10  $\mu$ L of the concentrated and the diluted bacterial cultures were plated in duplicate for CFU counting. For susceptibility testing, further 10  $\mu$ L of each suspension were plated on TSB/yeast extract plates supplemented with 600  $\mu$ g/mL ofloxacin. All plates were incubated for 24 h at 37°C before evaluation. All plates were cultivated for further 48 h to exclude false negative results due to growth impairment.

## MATHEMATICAL MODEL

We divide our bacterial population into three categories based on their response to nutrient (S) and antibiotics (A). Susceptible bacteria, denoted  $B_s$ , consume nutrient, reproduce and are killed by antibiotics. Stationary bacteria, denoted  $B_t$ , are formed from susceptible bacteria as nutrient is depleted and re-emerge if nutrient is introduced. Because stationary bacteria appear when nutrient is scarce, they are not susceptible to antibiotics due to physiological tolerance (Desai et al. 1998; Cogan, Cortez and Fauci 2005). Persister bacteria, denoted  $B_p$ , do not consume nutrient or reproduce. We assume that the populations are dynamic and each compartment may interchange with the others. Figure 1 shows a schematic of the interactions within the

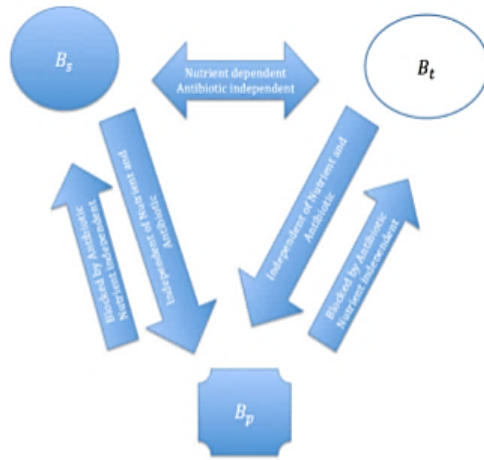


**Figure 1.** Schematic of the model dynamics showing transitions between populations. The transition between susceptible ( $B_s$ ) and stationary ( $B_t$ ) depends on nutrient, while the transition between susceptible and persister ( $B_p$ ) is independent of the nutrient level. The transition from stationary to persister is assumed to be constant, while the reversion from persister to stationary is inhibited by the presence of antibiotic.

bacterial populations indicating whether the rates depend on nutrient and/or antibiotics. All populations are measured in units of OD and depend on time (units of hours). Nutrient and antibiotics are measured in  $\mu\text{g}/\text{mL}$ .

Transition between susceptible and stationary phase bacteria is mediated by the nutrient, but does not depend on the antibiotic concentration. It is known that transitioning into persister phenotype can be both nutrient independent and nutrient dependent—often referred to as Type I and Type II persisters (Balaban et al. 2004). Therefore, we include a small transition from susceptible phenotype directly into persisters (nutrient independent) as well as a transition from stationary state into persisters. While the latter rate is assumed to be constant, the transition from susceptible to stationary is nutrient dependent; therefore, the transition from susceptible into persister depends implicitly on nutrient. This is in contrast with an explicit dependence via the rate. We note that this exchange was not incorporated into previous models—rather the transition into persisters was assumed to be proportional to the growth rate. We also mention that there is some evidence that the transition into persister state may depend on certain antibiotics (Dörr, Vulić and Lewis 2010), and we have shown previously that this provides complimentary, rather than redundant, protection (Szomolay and Cogan 2015).

Transitioning out of persister state is evidently nutrient independent [based on regrowth studies (Keren et al. 2004b; Kussell et al. 2014)] but antibiotic dependent. If antibiotic is present, the likelihood of reversion from persister is negligible. This seems to be a requirement for persister cells to explain the failure of long-term dosing experiments since they can survive long-term exposure. This also differentiates the persister explanation of tolerance from other explanations such as adaptation (Szomolay et al. 2005; Szomolay, Klapper and Dindos 2010) where the cues for the transitions between susceptible and persister are different. In the latter, the transition into the adapted state is antibiotic dependent while the transition out of the adapted state is nutrient dependent.

Guided by the schematic in Fig. 1, we consider the change in susceptible bacteria from growth, death, and transitions into and out of the other states. Stationary and persisters change as the phenotypes are altered, but are assumed to be nongrowing. We also track the (nondimensional) nutrient, explicitly assuming standard Monod kinetics. The main difference between this model and that presented in Cogan (2006) is the presence of a stationary phase. The dynamics of the susceptible bacteria are given by:

$$\frac{dB_s}{dt} = \left( \underbrace{\mu f(S)}_{\text{growth}} - \underbrace{k_{dt}(1-f(S))}_{\text{loss to } B_t \text{ and } B_p} - k_p - \underbrace{k_d(A)f(S)}_{\text{antibiotic}} \right) B_s \quad (1)$$

$$+ \underbrace{k_{st} f(S) B_t + k_{ps}(A) B_p}_{\text{gain from } B_t \text{ and } B_p} \quad (2)$$

where  $f(S)$  denotes the growth kinetics. In our study, we assume a saturating function  $f(S) = \frac{S}{K+S}$ , where  $K$  is the half-saturation coefficient. The rest of the dynamics can be explained similarly:

$$\frac{dB_t}{dt} = k_{dt}(1-f(S)) B_s - k_{st} f(S) B_t - k_p B_t + k_{pt}(A) B_p, \quad (3)$$

$$\frac{dB_p}{dt} = k_p B_s - k_{ps}(A) B_p + k_{pt} B_t - k_{pr}(A) B_p, \quad (4)$$

$$\frac{dS}{dt} = -\frac{\mu}{Y} f(S) B_s, \quad (5)$$

where  $Y$  is the yield coefficient.

We note that we have made several assumptions (that are consistent with our previous studies). Several rates depend explicitly on the antibiotic concentration—namely  $k_d(A)$ ,  $k_{pt}(A)$  and  $k_{ps}(A)$ . These are treated as step functions. Therefore,  $k_d = 0$  if  $A = 0$  and is nonzero constant otherwise (death due to antibiotic application). The other terms are nonzero constants if  $A = 0$ , and zero otherwise to reflect the blocking of the reversion processes in the presence of antibiotic. Additionally, we are assuming that the death rate due to antibiotic is directly proportional to the growth kinetics (i.e.  $f(S)$ ). This represents physiological tolerance—where slowly growing bacteria are more tolerant to antibiotic challenge than rapidly growing bacteria.

In Fig. 2, we show an example simulation of the total bacterial density with a periodic dose/withdrawal cycle. During the first stage, antibiotic is maintained at a constant level and the population decreases. When the antibiotic is withdrawn, the population regrows. Once the antibiotic is fixed at the initial constant level again, the population decreases again. We note that in this example we have not applied a high enough concentration of antibiotic for long enough to remove the majority of the bacteria.

Because we were interested in performing experiments scheduled by the model predictions, we opted to fix the period,  $P$ , of the dose/withdrawal cycle to 24 h and vary the fraction of time spent in dosing,  $\rho$ , where the antibiotic concentration is maintained at a constant level. At the end of each period, the nutrient is refreshed to the original initial condition. This is almost surely not the 'optimal' treatment protocol, but by fixing the period, we reduce the parameter space to explore (and make the experiments less time intensive). We explored the 1D parameter space (e.g. by varying  $\rho$  to determine the model predictions).

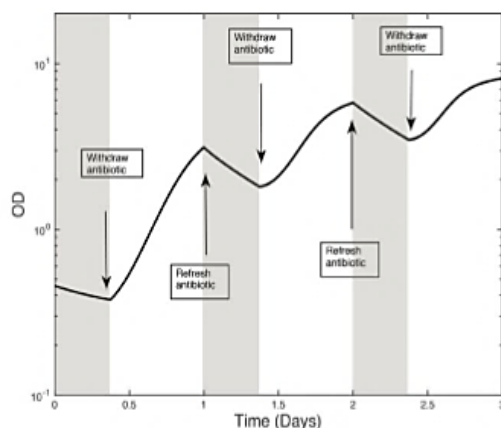


**Figure 2.** We plot the total bacterial population ( $B_s + B_p + B_{st}$ ) for an example of a dosing protocol that alternates between application (marked in gray) and withdrawal cycle with  $\rho = 0.3$ . Here, the protocol is ineffective and the population is not reduced.

**Table 1.** Table of parameters used in the simulations.

Parameter	Notation	Value	Units
Maximal growth rate	$\mu$	1	1/h
Half-saturation constant	$K$	1	Dimensionless
Susceptible to persister	$k_{sp}$	0.015	1/h
Susceptible to stationary	$k_{st}$	1.75	1/h
Stationary to susceptible	$k_{ss}$	0.05	1/h
Persister to susceptible	$k_{ps}$	0.04	1/h
Stationary to persister	$k_{sp}$	0.0125	1/h
Persister to stationary	$k_{pt}$	0.04	1/h
Yield	$Y^{-1}$	0.08	Dimensionless
Period	$P$	24	h
Fraction of $P$ spent dosing	$\rho$	varies	Dimensionless

By varying the dose time/withdrawal time ratio, two different regimes were determined. Most importantly, the analysis indicated the cut-off ratio. If the ratio of dosing to withdrawing was below this threshold, the treatment was effective. Otherwise, the population was not eliminated and the treatment was a failure. Our general observations confirm the qualitative results from previous studies that have shown that for a very large class of transitions and growth functions the timing is both crucial and robust. It is crucial to get the timing correct but, as mentioned earlier, the existence of a cut-off between success and failure is a robust feature of the biology and does not depend on the details of the kinetics of the model.

We solve the equations using MATLAB's ODE45 (variable time-step, Runge-Kutta solver). We first find the numerical solution for the dosing fraction and use the final values as initial conditions for the remaining fraction of the period. This is repeated using the values at the final times as initial conditions. The only differences within the periods is the presence of antibiotic, which is fixed at a constant level (either zero or nonzero) and the subsequent changes in the rates (as noted above). Specific parameters are given in Table 1.

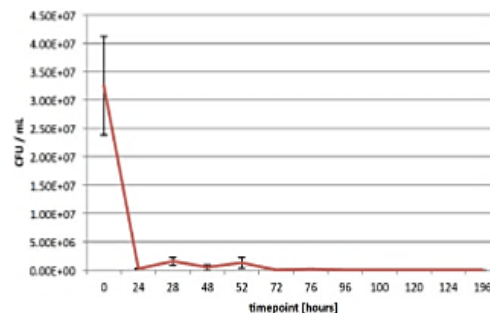


**Figure 3.** Bacterial viability testing via colony forming units (CFUs) determination for R 20/4 in duplicate. After 96 h, no bacterial regrowth could be detected.

## RESULTS AND DISCUSSION

The susceptibility testing on plates showed that the bacteria did not gain any resistance to ofloxacin (data not shown) so that no growth was observed on the appropriate plates. For support, three plates for each of the three different regimes of antibiotic treatment are shown in Fig. S1, Supporting Information: antibiotic regimes R 20/4 and R 15/9 resulted in a reduced number of viable/culturable cells after the first cycle compared to the controls. The 'turn over point', i.e. no observable bacterial growth, was reached after the third cycle of antibiotic treatment. A shorter incubation time of 8 h with antibiotic did not lead to any bacterial reduction compared to the control (R 8/16). For further validation, CFUs were determined for R 20/4 as shown in supplemental material Fig. S2–S4, Supporting Information. The results were summarized in Fig. 3. After 96 h, no bacterial regrowth was detected.

Previous studies focused on determining the optimal protocol—e.g. the one that eliminates the population the fastest. The existence of an optimal solution has been shown in a variety of mathematical settings including batch, chemostat and biofilms. However, all of these results were based on purely theoretical analysis. Here, we have analyzed the model more simply to make a testable prediction: assuming a period of 24 h, what is the dose fraction,  $\rho$ , that separates an unsuccessful (periodically re-emerging population) from a successful (total population tending toward zero) protocol? While this avoids the more difficult, and likely more practical question of optimizing the killing protocol, it gives a simple, testable prediction. If this prediction is correct, there is more support for previous theoretical arguments. It has been shown that a variety of other tolerance mechanisms do not have this separation between treatment success and treatment failure (Cogan, Cortez and Fauci 2005; Szomolay et al. 2005). Therefore, even though this does not prove our assumptions regarding the dynamics of persisters, it strengthens the foundation of the model. In turn, this helps support specific hypotheses regarding persister dynamics over others (such as senescence, or adaptation).

Periodic treatment is applied during a fraction,  $\rho$ , of the total period,  $P$ . The antibiotic is removed and the population is allowed to regrow during the remaining fraction of the period,  $(1 - \rho)P$ . The nutrient is assumed to be refreshed at the beginning of each period. For the purposes of this study, we chose to use a brute-force to determining the cut-off between treatment success and treatment failure. We discretize the interval  $0 \leq \rho \leq 1$  into  $n$  intervals and determine the success and failure for each of the  $n$  values of  $\rho$ . We refined the discretization near the

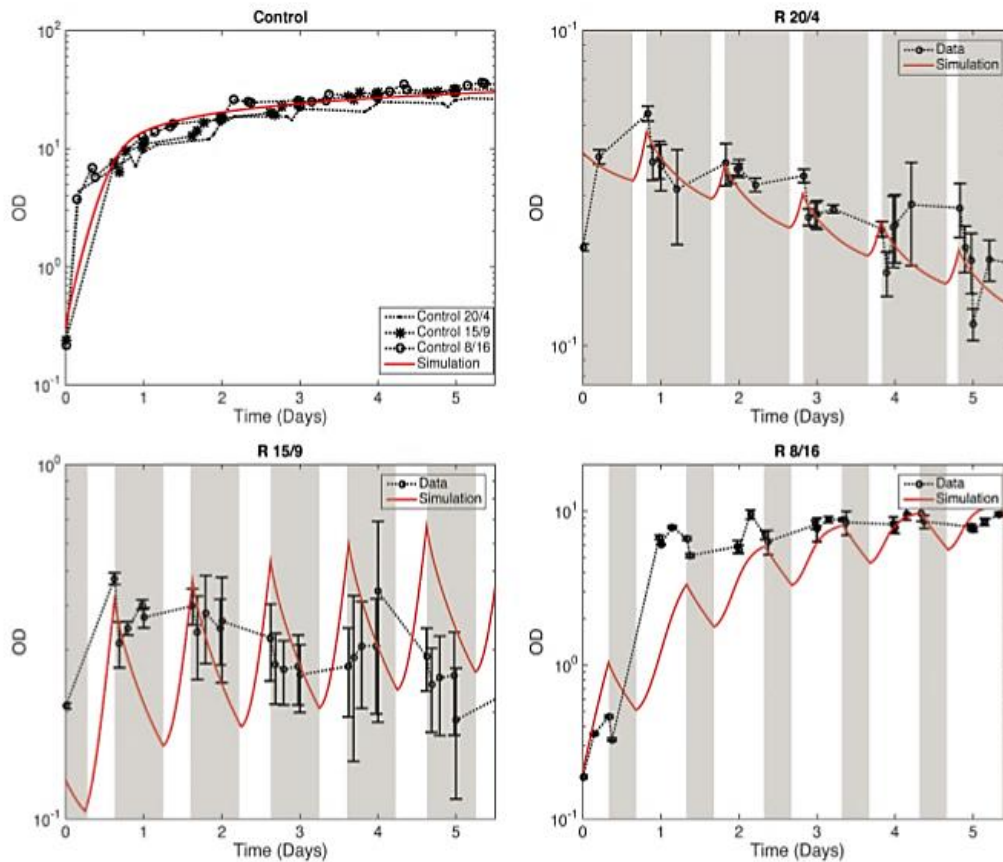


**Figure 4.** Comparison between the model simulations and experimental results. We compare the results of the numerical simulations with the experimental data. Results are presented with the populations in log-scale and the total population ( $B_s + B_i + B_p$ ) shown. The fractions used were  $\rho = 0$  (i.e. control),  $\rho = 5/6$  (R 20/4),  $\rho = 2/3$  (R 15/9) and  $\rho = 1/3$  (R 8/16). Dosing time periods are indicated in gray.

cut-off to obtain a more accurate estimate. We found that below  $\sim 0.67$  the population would regrow. The simplest interpretation is that  $\sim 8$  h is enough time for persisters to revert to susceptibles, which would then begin reproducing and renew the population. We then performed a sequence of experiments to confirm this prediction. We chose ratios of 33% (R 8/16), 67% (R 16/9) and 83% (R 20/4). The first two ratios lead to unsuccessful treatment, while the last ratio leads to elimination of the population.

In Fig. 4, we compared the model predictions (solid curve) to the experimental data (dotted curve). First, we show that when dosing for 8 with 16 h of regrowth, the antibiotic is withdrawn long enough that the persisters have time to revert to susceptible (without the antibiotic signal suppressing the reversion process). Susceptible bacteria reproduce and the population grows. This is an example of an unsuccessful treatment. We also show that for 20 h of dosing, followed by 4 h of regrowth, the antibiotic is applied before the susceptibles have had time to fully repopulate and the entire population eventually declines. Closer to the cut-off period (15 h of dosing, followed by 9 h of regrowth), it is less clear what the outcome will be. The model predicts slow expansion of the population, but the timescale is quite long. This behavior was studied for a similar model in more detail previously

(Leenheer and Cogan 2009). It is worth mentioning again, that it is not clear how well this method will carry over to biofilm-specific treatments as the antibiotic penetration and removal will be delayed by the polymer network. This changes the timing, perhaps a lot, even if the qualitative predictions remain the same (Cogan 2005; Cogan, Szomolay and Dindos 2013).

In fact, the model makes more specific predictions—we expect that using  $\rho = 1/3$  and  $\rho = 2/3$ , the population will regrow and eventually reach a stable periodic solution. This is based on the observations of the specific numerical simulations, but also on analytic results from a similar model (Leenheer and Cogan 2009). Similar results have been obtained for a variety of previous models and the theoretical justifications follow from Leenheer and Cogan (2009), while numerical justifications can be found in Cogan (2006, 2007). The timescale for the emergence of the periodic solution is longer as  $\rho$  increases toward the cut-off value when the population will eventually be eradicated.

The experimental confirmation of this specific prediction opens the door for a host of other experiments aimed at confirming model predictions. The most interesting and useful of these is determining the optimal protocol—that is the scheduling that eliminates the population the fastest. This will require

more data to be able to obtain better quantitative agreement between the model and the experiments, but we feel that the results described here represent an important first step in connecting the theory with the experiment.

### SUPPLEMENTARY DATA

Supplementary data are available at [FEMSLE](#) online.

### ACKNOWLEDGEMENTS

We thank Marly Felicia Dalton for technical assistance.

### FUNDING

Portions of this work were carried out as an integral part of the BIOFABRICATION FOR NIFE Initiative, which is financially supported by the ministry of Lower Saxony and the VolkswagenStiftung (NIFE is the Lower Saxony Center for Biomedical Engineering, Implant Research and Development, a joint translational research center of the Hannover Medical School, the Leibniz University Hannover, the University of Veterinary Medicine Hannover and the Laser Zentrum Hannover e.V.). Financial support of HR was provided by the Ministry of Science and Culture of Lower Saxony within the framework of the Doctoral Program MARIO (Multifunctional Active and Reactive Interfaces and Surfaces) and is gratefully acknowledged. NC was supported by the National Science Foundation DMS #1122378.

### REFERENCES

- Balaban NQ, Merrin J, Chait R et al. Bacterial persistence as a phenotypic switch. *Science* 2004;305:1622–25.
- Bergan T, Carlsen MI. Bacterial kill rates of amoxicillin and ampicillin at exponentially diminishing concentrations simulating in vivo conditions. *Infection* 1980;8:S103–8.
- Biesta-Peters EG, Reij MW, Joosten H et al. Comparison of two optical-density-based methods and a plate count method for estimation of growth parameters of *Bacillus cereus*. *Appl Environ Microb* 2010;76:1399–405.
- Bigger J. Treatment of staphylococcal infections with penicillin by intermittent sterilisation. *Lancet* 1944;244:497–500.
- Cogan NG. Effects of persister formation on bacterial response to dosing. *Journal of theoretical biology* 2006;238:694–703.
- Cogan NG. Incorporating toxin hypothesis into a mathematical model of persister formation and dynamics. *J Theor Biol* 2007;248:340–9.
- Cogan NG. Two-fluid model of biofilm disinfection. *Bull Math Biol* 2008;70:800–19.
- Cogan NG, Brown J, Darres K et al. Optimal control strategies for disinfection of bacterial populations with persister and susceptible dynamics. *Antimicrob Agents Ch* 2012;56:4816–26.
- Cogan NG, Cortez R, Fauci L. Modeling physiological resistance in bacterial biofilms. *Bull Math Biol* 2005;67:831–53.
- Cogan NG, Szomolay B, Dindos M. Effect of periodic disinfection on persisters in a one-dimensional biofilm model. *Bulletin of mathematical biology* 2013;75:94–123.
- Davies DG, Parsek MR, Pearson JP et al. The involvement of cell-to-cell signals in the development of a bacterial biofilm. *Science* 1998;280:295–8.
- Desai M, Bühler T, Weller PH et al. Increasing resistance of planktonic and biofilm cultures of *Burkholderia cepacia* to ciprofloxacin and ceftazidime during exponential growth. *J Antimicrob Chemoth* 1998;42:153–60.
- Dörr T, Vulić M, Lewis K. Ciprofloxacin causes persister formation by inducing the *tisB* toxin in *Escherichia coli*. *PLoS Biol* 2010;8:e1000317.
- Hobby GL, Meyer K, Chaffee E. Observations on the mechanism of action of penicillin. *Exp Biol Med* 1942;50:281–5.
- Keren I, Kaldalu N, Spoering A et al. Persister cells and tolerance to antimicrobials. *FEMS Microbiol Lett* 2004a;230:13–8.
- Keren I, Shah D, Spoering A et al. Specialized persister cells and the mechanism of multidrug tolerance in *Escherichia coli*. *J Bacteriol* 2004b;186:8172–80.
- Kussell E, Kishony R, Balaban NQ et al. Bacterial persistence: a model of survival in changing environments. *Genetics* 2005;169:1807–14.
- Leenheer PD, Cogan NG. Failure of antibiotic treatment in microbial populations. *J Math Biol* 2009;59:563–79.
- Lewis K. Persister cells, dormancy and infectious disease. *Nat Rev Microbiol* 2007;5:48–56.
- Lou C, Li Z, Ouyang Q. A molecular model for persister in *E. coli*. *J Theor Biol* 2008;255:205–9.
- Sutton S. Measurement of microbial cells by optical density. *J Validation Technol* 2011;17:47–9.
- Szomolay B, Cogan NG. Modelling mechanical and chemical treatment of biofilms with two phenotypic resistance mechanisms. *Environmental microbiology*, 2015.
- Szomolay B, Klapper I, Dindos M. Analysis of adaptive response to dosing protocols for biofilm control. *SIAM J Appl Math* 2010;70:3175–202.
- Szomolay B, Klapper I, Dockery J et al. Adaptive responses to antimicrobial agents in biofilms. *Environ Microbiol* 2005;7:1186–91.
- Ulanowska K, Tkaczyk A, Konopa G et al. Differential antibacterial activity of genistein arising from global inhibition of dna, rna and protein synthesis in some bacterial strains. *Arch Microbiol* 2006;184:271–8.
- Yourassowsky E, Van der Linden MP, Lismont MJ et al. Effect on growth curve patterns of brief exposure of bacteria to different concentrations of  $\beta$ -lactam antibiotics. *J Antimicrob Chemoth* 1985;15:27–36.

## 4.5 Definition of electrical stimulation parameters for the inhibition of bacterial growth on PVDF membranes

### *Preface*

The goal of this initial cooperation study was the determination of the electrical stimulation parameters for the inhibition of commensal and periodontopathogenic bacterial growth on implant surfaces and practical implementation by the development of a piezoelectric implant coating material. As PVDF has a good biocompatibility and piezoelectric properties, it was chosen as candidate coating material.

For the initial *in vitro* investigations, two electrical stimulation devices have been designed: an electrical stimulation lid that fits on commercially available six well plates equipped with platinum electrodes and a modified flow chamber device for electrical stimulation under physiological flow conditions. The bacterial candidates for these inhibition studies have been the commensal bacteria *S. gordonii*, *S. salivarius* and the periodontopathogen *P. gingivalis*. All processes regarding the production of PVDF membranes, technical optimization and material characterization have been established by BASTIAN DREYER at the Department of Material Science of the Hannover University of Applied Sciences and Arts and the Institute of Inorganic Chemistry, LUH. Biological experiments and design of the stimulation devices have been developed and conducted by HENRYKE RATH. The project has been guided by Dr. SASCHA NICO STUMPP, Prof. Dr. RALF SINDELAR, Prof. Dr. FRANZ RENZ, and Prof. Dr. MEIKE STIESCH. The initial manuscript has been prepared by HENRYKE RATH and BASTIAN DREYER and refined with Dr. SASCHA NICO STUMPP, Prof. Dr. RALF SINDELAR, Prof. Dr. FRANZ RENZ, and Prof. Dr. MEIKE STIESCH. The study was initiated by Prof. Dr. RALF SINDELAR, Prof. Dr. FRANZ RENZ, and Prof. Dr. MEIKE STIESCH as a collaborative project within the framework of the doctoral program MARIO. The manuscript is in preparation and will be submitted to the *Journal of Biomedical Materials Research Part B: Applied Biomaterials*.

### 4.5.1 Abstract

The present demographical change leads to an aging society. As the health care system has to deal with new demands on the patient's physical conditions, the attention is drawn on the replacement of certain body parts like dental implants. The number of implanted dental prosthetics has drastically increased within in recent years. Unfortunately, the number of implant loss is still immensely. The main cause of implant failure is the colonization of bacterial communities, referred to as biofilms, on the abiotic implant surfaces. Those biofilms are difficult to treat with standard therapeutics as a self-secreted EPS shields the bacteria from external hazard. Therefore, new approaches have to be developed to prevent the bacterial infections.

A promising method for the control of bacterial adhesion is the electrical stimulation that inhibits the bacterial biofilm formation and improves the persistence of the implant. A potential implant coating material is the biocompatible piezoelectric polyvinylidene fluoride (PVDF) as material generates electric voltage due to mechanical deformation.

This study focused on the evaluation of adequate electrical stimulation parameters for the inhibition of the dental relevant biofilm formation of the commensal bacteria *S. gordonii* and *S. salivarius* and periodontopathogenic *P. gingivalis*. Therefore, a static system with a stimulation lid and a dynamic flow chamber system with platinum electrodes have been successfully established. With an alternating electric field, the bacteria were discouraged from the adherence to the PVDF membranes. The bacterial biofilm formation was reduced up to 90% compared to unstimulated controls.

**Keywords:** bacterial biofilm, dental implant-associated infection, electrical stimulation, polyvinylidene fluoride, flow chamber system

### 4.5.2 Introduction

Nowadays, the topic of implantology becomes more relevant due to demographical changes in the human population. To provide patients the best quality for the life, medical investigation on the replacement of certain body parts has increased within the last three decades.<sup>376</sup> Here, especially hip, knee and other orthopedic prosthesis, heart replacements, and dental implants are in the focus. All implants have two main challenges to face: First, the implant has to incorporate in the surrounding tissue to guarantee the best acceptance of the external device, and second the prevention of bacterial inflammation.



The effect of electrical stimulation in biology has been discussed intensively either for the disinfection of surfaces or growth stimulation of biological tissue since years.<sup>65,233,252,434-438</sup> But still, electrical stimulation parameters for implant application have to be developed for the prevention of bacterial infections. In 1994, Costerton *et al.* introduced the term “bioelectric effect”.<sup>65</sup> This phenomenon describes the combination of antibiotic treatment in an electric field that inhibits bacterial growth and was claimed to be one of the most promising mechanisms against bacterial growth.<sup>434,437</sup> But, the antibiotic treatment often results in antibiotic resistance, thus it is vain for the medical application. Therefore, in 2009, del Pozo *et al.* introduced the term of “electricidal effect”.<sup>245</sup> It was shown that the electrical stimulation solely has an inhibiting effect on the bacteria without additional antibiotic treatment.<sup>245,262</sup> This offered the medical research field a new perspective for medical applications on medical devices and implants. In 2006 Hazan *et al.* introduced a successful application of electrical currents in patients by acoustic energies at specific frequencies. This was a piezoelectric ceramic used for the prevention of bacterial attachment on urinary catheters *in vitro*.<sup>263</sup> The so called piezoelectricity describes the development of an electrical polarization of certain solid materials if mechanically deformed, or inversely, the deformation of a material if an electric field is applied.<sup>271,273,439</sup> A promising candidate for the application of the piezoelectricity is PVDF. This material has been proven to be biocompatible and effective in stimulating fibroblast and osteoblasts for the induction of growth processes.<sup>440,441</sup> It is a thermos- and chemical stress stable fluorophore that has anti-ultraviolet radiation resistance, low protein adsorption and a plane surface.<sup>299,300</sup>

Bacterial biofilms are a community of bacteria embedded in a self-produced extra EPS. It shields the bacteria from external threats as antimicrobials and host immune system. This matrix impedes the standard medical treatments tremendously by increasing the bacterial resistance up to 5000 fold.<sup>63,65</sup> A mature bacterial biofilm on an implant leads to the bacterial induced inflammation called “peri-implantitis”.<sup>46,442,443</sup> The initial step of the biofilm formation is the attachment and adhesion of pioneer bacteria as *S. gordonii* and *S. salivarius*.<sup>95,113,119,444</sup> Those bacteria provide the perfect attachment side for secondary and late periodontopathogenic bacteria like *P. gingivalis*.<sup>113,143</sup> To avoid biofilm growth, the implant material has to be unattractive for the bacterial attachment and adhesion processes. The electrical stimulation parameters for the inhibition of oral bacterial are not yet evaluated in detail. Furthermore, the underlying bases of eukaryotic and prokaryotic cell-cell interaction, induced by electrical stimulation, are not clearly understood.

This study focused on the determination of electrical stimulation parameters for the inhibition

of biofilm formation on the potent implant coating material PVDF. Here, the commensal pioneer bacteria *S. gordonii* and *S. salivarius* were investigated. Moreover, the most periodontopathogenic bacterium that affects implant ingrowth and persistence, *P. gingivalis* was studied. Two different electrical stimulation systems were established 1.) a static biofilm experiment and 2.) a dynamic fluid system called flow chamber system. For the static stimulation, a stimulation lid that perfectly fits commercial available six well plates was designed and manufactured. The six wells are independently controllable. For the electric stimulation under physiological conditions, an open flow chamber system that is equipped with platinum electrodes was developed. This system mimics the physiological fluid flow in the oral cavity as the flow influences the cell-cell interaction in a biofilm, the biovolume and cell number, the growth conditions, the biofilm morphology and growth behavior of multispecies biofilms, the bacterial attachment and detachment and the interaction with the eukaryotic cells of the host.<sup>210-219</sup>

The electrical stimulation parameters for all three species were successfully evaluated for both stimulation systems.

### 4.5.3 Materials and methods

#### 4.5.3.1 PVDF film preparation

Polyvinylidene fluoride (20wt%, 275.000 Mw) was dissolved in N,N-Dimethylformamide and stirred at 60°C for 12 h. Thin film preparation was performed via standard doctor blade method. The obtained PVDF films were dried at 60°C overnight. Afterwards, the PVDF film membranes were autoclaved at 121°C for 20 min to guarantee sterile conditions.

#### 4.5.3.2 Bacterial strains

*S. gordonii* DSM 20568, *S. salivarius* DSM 20067 and *P. gingivalis* DSM 20709 were obtained from the DSMZ.

#### 4.5.3.3 Bacterial cultivation

*S. gordonii* and *S. salivarius* were precultured for 18 h in TSB supplemented with 10% yeast extract at 37°C under agitation (200 min<sup>-1</sup>). For static biofilm formation in 6-well plates and dynamic biofilm formation in the flow chamber system, both species were adjusted to an OD<sub>600</sub> of 0.016 with TSB medium modified with 50 mM glucose. This OD corresponds to an inoculum of: 1.94 x 10<sup>6</sup> CFU/mL for *S. gordonii* and 4.19 x 10<sup>6</sup> CFU/mL for *S. salivarius*. Dynamic biofilm cultivation was stirred. Both biofilm settings were performed at 37°C for 24 h with a flow velocity of 100 µL/min. *P. gingivalis* was precultured anaerobically in BHI

supplemented with 10 µg/mL vitamin K (BHIV) for 48 h at 37°C. For static and dynamic biofilm experiments, *P. gingivalis* was adjusted to an OD<sub>600</sub> of 0.0375 (7.88 x 10<sup>6</sup> CFU/mL) in BHIVS. The biofilm formation was performed for 24 h at 37°C. Static experiments were performed microaerophilic in a CO<sub>2</sub> incubator. Dynamic experiments were flushed with anaerobic prior to all the experiment. All experiments modified with vitamin K were protected from light to avoid the destruction of the vitamin by light.

#### 4.5.3.4 *Electrical stimulation set-up and parameters*

For static electrical stimulation, a stimulation lid was designed that fits to commercial six-well plates from Greiner (Figure 19 A). Before the electrical stimulation was performed on PVDF membranes, pre-experiments were performed in six-well plates (polystyrene) to determine the alternating current (AC) electrical stimulation parameters for the growth inhibition of bacteria with biphasic symmetrical compensated wave pulse (*S. gordonii*, *S. salivarius*, and *P. gingivalis*) and biphasic symmetrical compensated sine wave (*S. gordonii*). Culture conditions as described before. Table S1 shows all tested parameter of the pre-experiments. The PVDF membranes were fixed on the polystyrene (static) and titanium discs (dynamic) by Heliobond. For polymerization, the Heliobond was illuminated with a blue light (intensity = 1000 mW/cm<sup>2</sup>) for a total of 30 s. For the experiments on PVDF the parameters tested were: *S. gordonii*: 2 mA, 60 µs, 10 Hz, 340 V; *S. salivarius*: 1.9 mA, 60 µs, 10 Hz, 323 V; and *P. gingivalis*: 3 mA, 500 µs, 10 Hz, 750 V. The stimulation was a biphasic symmetrical compensated wave pulse alternating current. For dynamic simulation, a flow chamber was equipped with platinum electrodes at the inlet and outlet of the chamber. The flow chamber system is adapted from Rath *et al.*<sup>445</sup> The system was used as an open flow system, pumping the bacterial suspension over the PVDF membrane with the planktonic bacteria and ending in a waste bottle (Figure 19 B). The tested parameters for the dynamic system were equal to the static experiments on PVDF. The Stimulus Generator STG 4008 (Multichannels systems Reutlingen, Germany) was used for the electrical stimulation. The stimulation parameters were controlled with an Oscilloscope DSO 1004A.

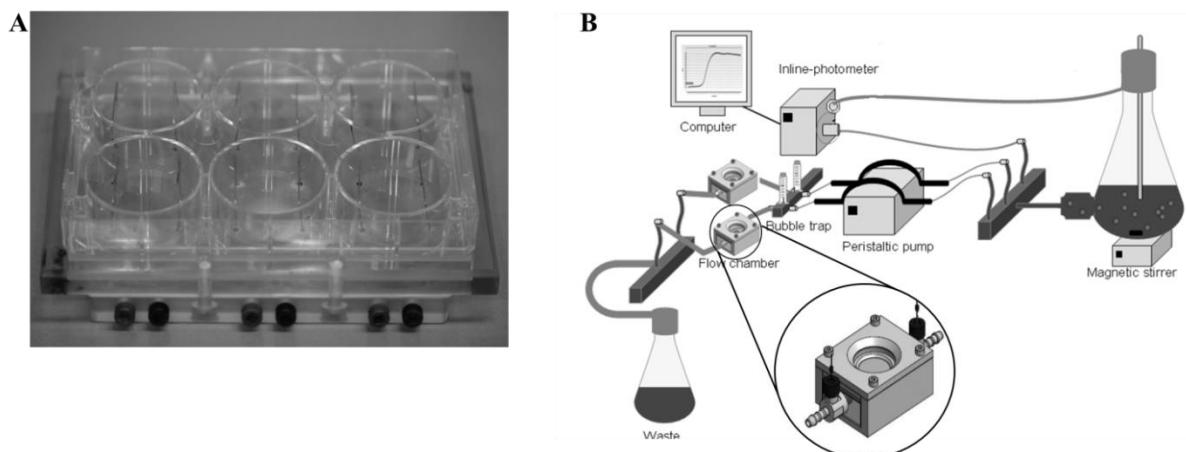


**Figure 19: Stimulation devices.** A) Stimulation lid with commercial available six well plates for static analyses (reversed view). B) Flow chamber system with a stimulation chamber the investigation under dynamic conditions (zoomed view).

#### 4.5.3.5 *pH control and viability testing*

Before the electrical stimulation of the static samples, the pH of the respective medium and the bacterial suspension with the adapted OD was measured with the pH electrode. Additionally, after stimulation of the static samples on PVDF membranes, the supernatant was collected and pH measurement was repeated and compared to the unstimulated values. Additionally, 100  $\mu\text{L}$  of the supernatant were plated on TSB agar plates and incubated for further 24 h at 37°C aerobically for *S. gordonii* and *S. salivarius*. *P. gingivalis* was plated on BHIV agar plates and incubated for 24h at 37°C in a CO<sub>2</sub> incubator microaerophilically. Images of the plates were taken with a sigma E140 DG camera.

#### 4.5.3.6 *Biofilm imaging and analysis*

For static biofilm imaging, the biofilm on polystyrene and PVDF membranes in the 6-well plates were analyzed by CLSM and SEM. For CLSM, the biofilms were washed three times with PBS after the stimulation to remove the planktonic bacteria. Afterwards, the biofilms were stained with a 1:1000 dilution of live/dead staining to distinguish between vital bacteria (Syto9) and dead (propidium) bacteria. Biofilms were stained for 15 min in the dark. Then, the biofilms were fixated by glutaraldehyde for further 15 min. For dynamic stimulated biofilms, the system was flushed with PBS for 20 min to wash away planktonic bacteria. Afterwards, the biofilms were stained with the same live/dead staining as the static biofilm. The dye was flushed in the system for 15 min and then stained for further 15 min in the dark. At last, the biofilms were fixated by glutaraldehyde for 15 min. The velocity of the flushing solution was 100  $\mu\text{L}/\text{min}$ . The biofilms were studied by a CLSM Leica-Upright MP microscope that was connected to a TCS SP2 AOBS can head. Images were recorded with a 40 x objective magnification and 1  $\mu\text{m}$  stacks were taken at five different positions. Afterwards, the images were 3D reconstructed and analyzed by the Imaris 3D image processing software to calculate mean biofilm height.

For SEM imaging of the static biofilms on the PVDF membranes were fixated by glutaraldehyde for 30 min after stimulation. SEM images were performed at a Zeiss Leo 1455VP scanning electron microscope. To prevent electrical charging effects the samples were coated with a layer of Au/Pd (5-10 nm).

#### **4.5.3.7 Determination of chlorine and hydrogen peroxide content**

The determination of the chlorine and hydrogen peroxide in the unstimulated and the stimulated supernatant was performed with MQuant test sticks. for static samples including the respective medium and biofilm control. The tests were performed according to manufactures instruction. The sensitive range was 0.5-1-2-5-10-20 mg/L Cl<sub>2</sub> and 0-0.5-2-5-10-25 mg/L H<sub>2</sub>O<sub>2</sub>.

#### **4.5.3.8 Propidium monoazide assay and DNA isolation**

The PMA assay is a method for the quantification of vital bacteria. The photo-reactive DNA dye binds to double stranded DNA and its reactive acid groups are converted to nitrene radicals by photolysis. The reaction with carbohydrate residuals leads to a stable nitrogen-carbon binding. The molecule is not able to pass the bacterial membrane, because of its size. The PMA molecule is only able to pass damaged cell membranes. The PMA intercalates with the DNA and binds covalently. This prevents the DNA polymerase from reading the PMA-stained DNA in the PCR and does not synthesize new DNA molecules. Consequently, the polymerase chain reaction is blocked and no amplification is performed for the damaged/dead bacteria.

The PMA assay protocol was adapted from Kommerein *et al.*<sup>339</sup> The assay was used for the static stimulated samples. Therefore, after stimulation with defined parameters, the supernatant and the biofilms (BF) were transferred to a 15 mL reaction tube. The biofilm was detached from the PVDF membrane by a cell scraper and was resuspended in 3 mL PBS. Supernatants and biofilms were pelleted (5 min, 4000 x g, RT). The supernatants were discarded and all pellets were resuspended in 1 mL PBS. Afterwards, the bacterial supernatants were divided in vital and dead samples (500 µL). The vital samples were directly supplemented with 4 mM PMA and incubated for 10 min at 4°C in the dark. The subsequent photolysis was triggered with a 470 nm 3 W LED light source for 20 min. Afterwards, samples were directly pelleted (5 min, 4000 x g, RT) and washed once with 1 mL PBS. The pellet was stored at -20°C. The dead samples were supplement with 1:10 with ice cold 70% 2-propanol and vortex for 1 min. Afterwards, the samples were incubated for 15 min at RT. After pelleting (10 min, 5.000 x g, RT), the supernatant was discarded and the pellet was washed twice with 1 mL PBS (10 min, 5.000 x g, RT). The pellets were resuspended in 50 µL PBS and heated for 10 min at 95°C under agitation (350 rpm). Subsequently, the samples were incubated at -80°C for 10 min. Afterwards, samples were treated exactly like the vital samples explained previously.

The DNA of the PMA treated samples were isolated with the Fast DNA SPIN Kit for Soil) according to manufactures instruction. The DNA was eluted in 100  $\mu$ L tridest. water and the concentration was measured a NanoDrop ND-1000 spectrophotometer. At last, the DNA was stored at  $-20^{\circ}\text{C}$  for further processing.

#### 4.5.3.9 Quantitative real-time PCR

The qRT-PCR was performed with the iQ5 real time PCR Multicolor detection system from Bio-Rad. The primer sequences are listed in Table 8. The respective PCR was performed in a total volume of 25  $\mu$ L containing 12.5  $\mu$ L iQ SYBRGreen supermix, 0.2  $\mu$ M forward and reverse primers and 10 ng of the template DNA. The PCR was performed with an initial incubation of 3 min at  $95^{\circ}\text{C}$ , followed by 40 cycles of denaturation for 10 s at  $95^{\circ}\text{C}$ . The annealing was performed for 20 min. The respective annealing temperature ware listed in Table 1. The annealing was followed by the amplification at  $72^{\circ}\text{C}$  for 20 s and a melting curve analysis. The genomic DNA was calculated by a standard curve. The curves were generated with defined concentrations and a dilution series. The corresponding number of bacterial cells was determined by the division of the measured DNA and the total genome weight per cell listed in Table S 4. The experiments were performed in biological and technical triplicates. Here, the respective supernatant and biofilm samples were pooled from six-wells, respectively.

Table 8: Primer for real- time PCR of *S. gordonii*, *S. salivarius*, and *P. gingivalis*.

bacterium	primer name	primer sequence 5' -> 3'	annealing temperature
<i>S. gordonii</i>	S.g. forward	AACGGAATGCACGATGGAGT	56°C
<i>S. gordonii</i>	S.g. reverse	TCGTTCCAATGGAGCCTAGC	
<i>S. salivarius</i>	S.s. forward	GTTGCCACATCTTCACTCGCTT	58°C
<i>S. salivarius</i>	S.s. reverse	CGTTGATGTGCTTGAAA GGCACCATT	
<i>P. gingivalis</i>	P.g. forward	AGGCAGCTTGCCATACTGCG	56°C
<i>P. gingivalis</i>	P.g. reverse	ACTGTTAGCAACTACCGA TGT	

## 4.5.4 Results

### 4.5.4.1 Stimulation parameters

Before the bacteria were stimulated on the PVDF membranes, parameters for electrical stimulation were determined by initial trials on polystyrene. The stimulating parameters are

listed in Table S 3. The results of the trials, i.e. the average biofilm heights and viability, are presented in Figure S 20. After determining the stimulation parameter for all three species, the bacteria were electrically stimulated under static and dynamic conditions on PVDF membranes with the parameters listed in Table 9.

**Table 9: Parameter of the electrical stimulation on PVDF membranes.**

<b>bacterium</b>	<b>stimulation</b>	<b>strength of electric current (<math>\mu\text{A}</math>)</b>	<b>frequency (Hz)</b>	<b>duration (<math>\mu\text{s}</math>)</b>	<b>voltage (V)</b>	<b>resistance of respective medium (kOhm)</b>
<i>S. gordonii</i>	biphasic symmetrically compensated rectangular pulse, AC	2000	10	60	340	170
<i>S. salivarius</i>	biphasic symmetrically compensated rectangular pulse, AC	1900	10	60	323	170
<i>P. gingivalis</i>	biphasic symmetrically compensated rectangular pulse, AC	3000	10	500	750	250

#### **4.5.4.2 pH measurement before and after electrical stimulation**

The pH values of the bacteria in the supernatant simulated (SNS), respective growth medium, and bacteria in the supernatant not simulated (control, SNNS) were measured before and after stimulation. The pH values of the bacterial suspension and the respective medium before stimulation varied between 6.9 and 7.5 and are listed in Table 10.

**Table 10: pH values of the bacterial solution and the respective medium before electrical stimulation in triplicates.**  
A = *S. gordonii*, B = *S. salivarius* and C = *P. gingivalis*.

	<b>pH of bacterial suspension before stimulation</b>	<b>pH of the growth media before stimulation</b>
<b>A1.</b>	7.2	7.3
<b>A2.</b>	7.4	7.4
<b>A3.</b>	7.3	7.3
<b>B1.</b>	6.9	7.3
<b>B2.</b>	7.1	7.2
<b>B3.</b>	7.2	7.3
<b>C1.</b>	7.4	7.5
<b>C2.</b>	7.4	7.3
<b>C3.</b>	7.5	7.3

The Table 11 shows the pH values of the respective medium and the stimulated (SNS) and unstimulated bacterial supernatants (SNNS) after 24 h. Here, every single well was investigated, even though the samples of one experiment are from the same overnight culture. The pH values were reduced to 4.5-3.8 for the growth medium, SNS and SNNS of *S. gordonii* and *S. salivarius* compared to the pH values before stimulation. The pH values varied between 3.5 and 4.5. The pH values of the *P. gingivalis* suspension were decreased and the values varied between 5.0 and 7.1. The pH values of the culture medium of *P. gingivalis* were not decreased compared to the pH values of the medium before stimulation. Table 4 shows the pH values of the respective medium, the stimulated (SNS) and the unstimulated bacterial supernatants (SNNS) after 24 h. Here, every single well was examined, even though the samples of one experiment are from the same overnight culture. For *S. gordonii* and *S. salivarius* the pH values of the growth medium, SNS and SNNS decreased to 3.5-4.5. The pH of the *P. gingivalis* suspension only slightly decreased to 5.0-7.1, while the pH values of the culture medium were not decreased and remained the same for this species.



**Table 11: The pH values of the bacterial supernatant and the respective medium after electrical stimulation in triplicates. A = *S. gordonii*, B = *S. salivarius* and C = *P. gingivalis*.**

conditions	well 1	well 2	well 3	well 4	medium	SNNS
A1. 2mA, 60 $\mu$ s, 10Hz	3.5	3.9	4.1	3.8	4.5	4.0
A2. 2mA, 60 $\mu$ s, 10Hz	4.1	3.9	4.0	3.8	4.2	4.1
A3. 2mA, 60 $\mu$ s, 10Hz	3.9	4.2	4.1	3.8	4.3	3.9
B1. 1.9mA, 60 $\mu$ s, 10Hz	3.9	4.2	4.1	3.8	4.1	4.0
B2. 1.9mA, 60 $\mu$ s, 10Hz	4.1	3.8	4.2	4.1	4.4	3.9
B3. 1.9mA, 60 $\mu$ s, 10Hz	3.9	3.8	4.2	3.8	4.1	3.8
C1. 3mA, 500 $\mu$ s, 10 Hz	5.5	5.3	5.0	5.5	7.4	6.9
C2. 3mA, 500 $\mu$ s, 10 Hz	5.2	5.0	6.1	5.9	7.3	6.8
C3. 3mA, 500 $\mu$ s, 10 Hz	5.0	5.8	5.2	6.1	7.2	7.1

#### 4.5.4.3 *Measurements of the chlorine and hydrogen peroxide content*

The formation of gas bubbles was observed during the application of electric current. However, no chlorine and hydrogen peroxide were detected before and after stimulation.

#### 4.5.4.4 *Average biofilm heights of stimulated bacteria under static and dynamic cultivation on PVDF membranes*

The bacteria were stimulated during the cultivation on PVDF membranes under static (Figure 20 A-C) and dynamic growth conditions (Figure 20D-E). After 24 h, the average biofilm heights of these stimulated species were reduced to 75-90% when compared to the BFNS. All BFNSs showed the expected average biofilm height.

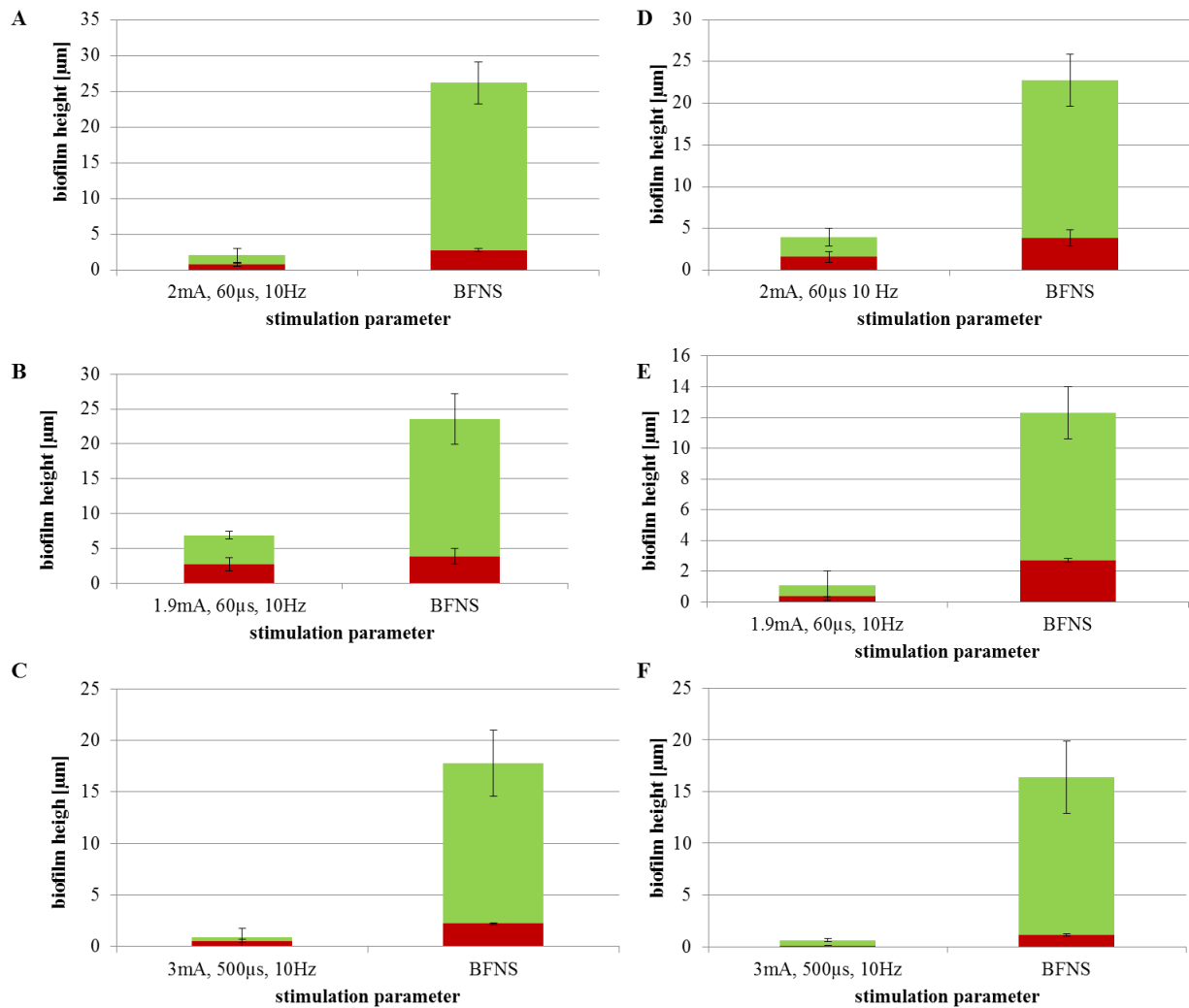


**Figure 20: Biofilm height of stimulated and unstimulated bacteria.** A – C static experiments, D-F dynamic flow chamber experiments. A+D: *S. gordonii*; B+E: *S. salivarius*, C+F: *P. gingivalis*. Green =vital bacteria, red = dead bacteria. BFNS = bacteria

#### 4.5.4.5 Biofilm morphology of stimulated and unstimulated bacteria on PVDF membranes

The morphological differences between electrically stimulated bacteria and unstimulated biofilms were studied by CLSM (Figure 21) and SEM (Figure 22). The 3D-biofilm reconstruction of the CLSM images showed a confluent biofilm growth of the control samples (Figure 21 A, C, E). The PVDF membranes were not confluent colonized by electrically stimulated bacteria (Figure 20 B, D, F). The SEM images showed a decreased bacterial colonization of *S. gordonii* when compared to the BFNS (Figure 22 A and B). The biofilm morphology of *S. salivarius* was altered by electrical stimulation and disordered (Figure 22C and D). The stimulated biofilm of *P. gingivalis* was fused (Figure 22E and F).

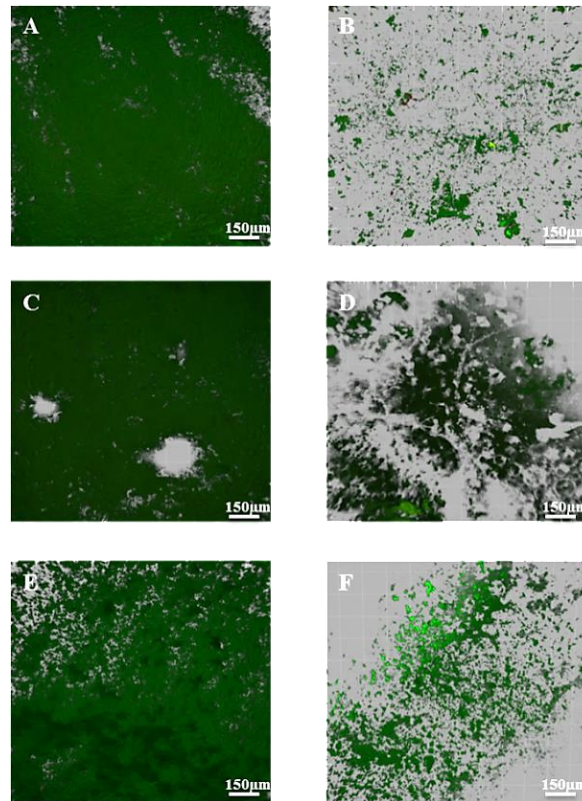


**Figure 21: 3 D-biofilm reconstruction of CLSM stacks.** Static biofilm control (A, C, E) and electrical stimulation (B, D, F) of: A&B = *S. gordonii*, C&D= *S. salivarius*, and E&F = *P. gingivalis*.

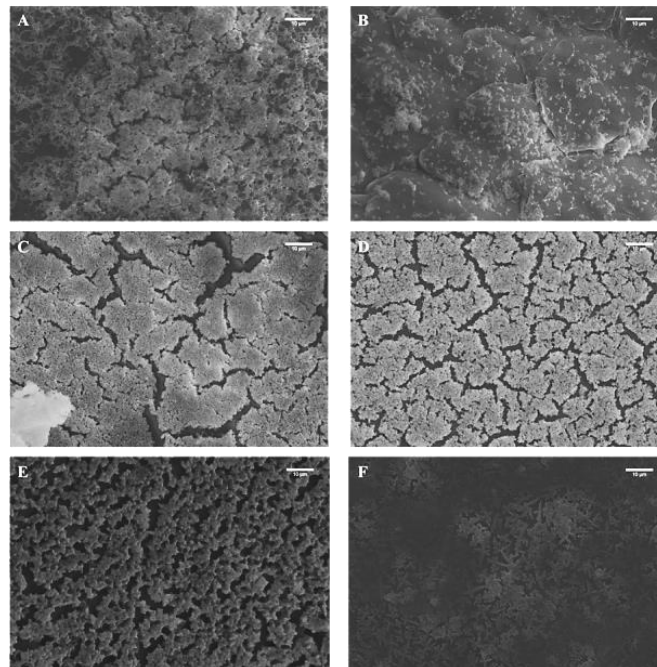


**Figure 22: SEM images of bacterial biofilms.** Control (A, C, E) and electrically stimulated bacteria (B, D, F) after 24 h of incubation. A&B = *S. gordonii*, C&D = *S. salivarius*, and E&F = *P. gingivalis*. The images were recorded and processed by Bastian Dreyer.

#### 4.5.4.6 Viability control of the bacteria in stimulated and unstimulated supernatants

All bacterial suspensions produced viable colonies on the agar plates. The colonization of the SNNS was not as confluent as the stimulated bacterial cultures. The medium controls showed no contamination (Figure 23).

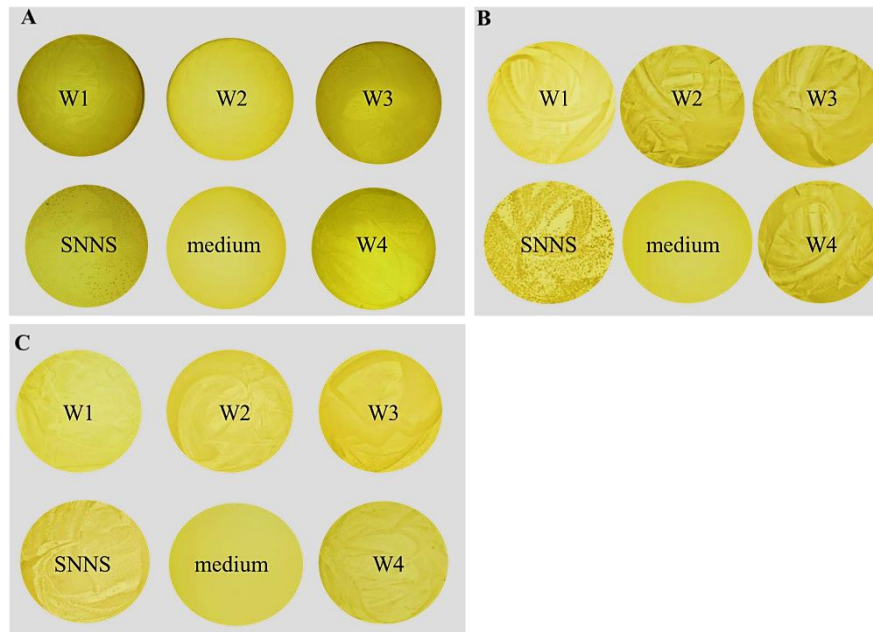


**Figure 23: Representative viability test results of the stimulated bacterial SNS, SNNS and the respective growth medium.** A = *S. gordonii*, B = *S. salivarius* and C = *P. gingivalis*; W = well.

#### 4.5.4.7 PMA treatment and quantitative real-time PCR

To quantify the ratio between vital and dead bacteria in stimulated and control supernatants, a PMA assay and qRT-PCR were performed. The results of the qRT-PCR are summarized in Figure 23. Surprisingly, a higher number of vital bacteria was observed in the SNSs when compared to the SNNSs. In contrast, the stimulated biofilm contained a lower portion of vital cells compared to the non-stimulated biofilm.

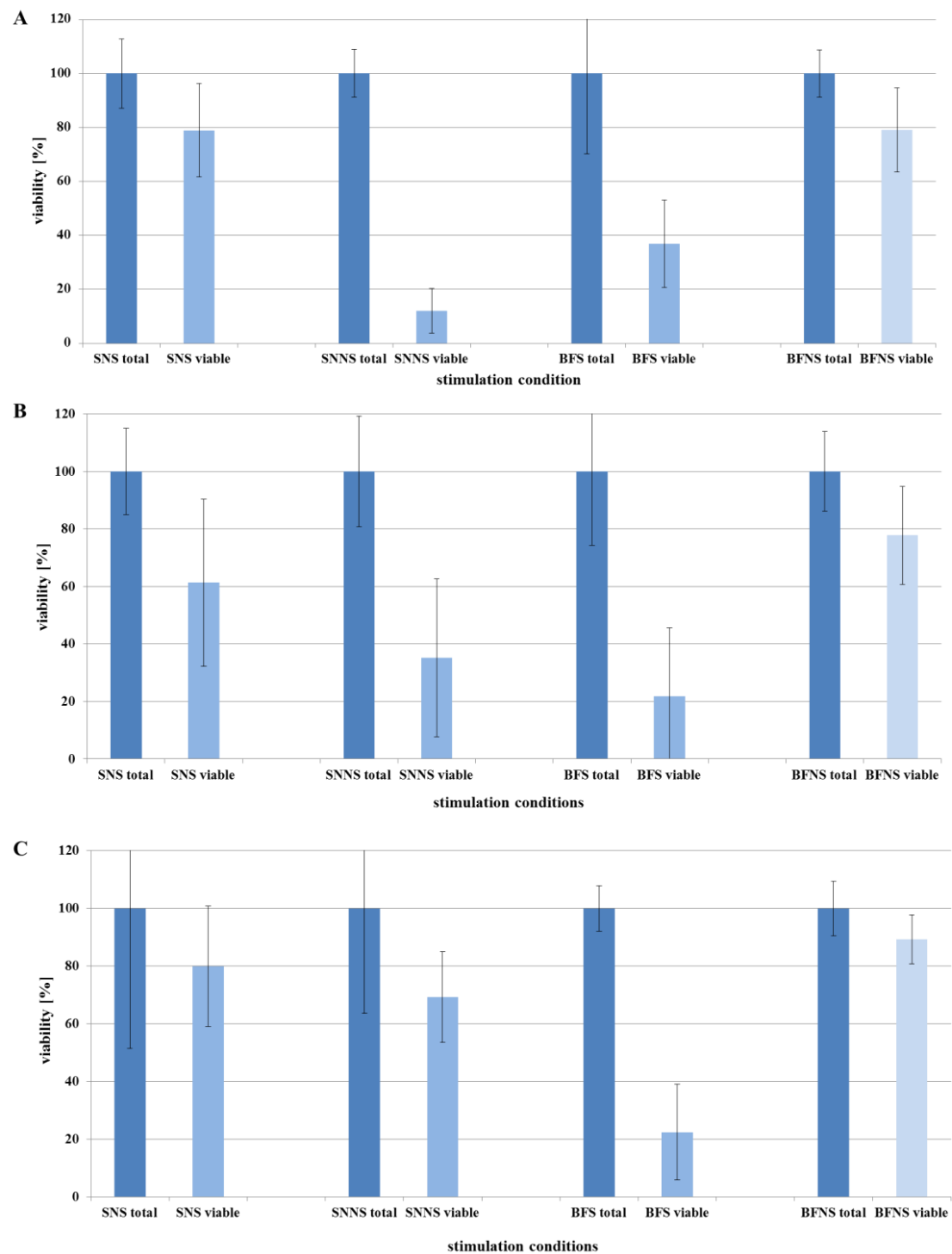


**Figure 24: qRT-PCR results of the total and viable distribution of bacteria under stimulated and unstimulated conditions after 24 h.** A = *S. gordonii*, B = *S. salivarius* and C = *P. gingivalis*. The dark blue represents the total amount of vital and dead bacteria (100%) and the light blue shows the viable portion of the bacteria in percentage. SNS = stimulated supernatant, SNNS = unstimulated supernatant control. BFS = stimulated biofilm, and BFNS = bacteria in biofilm not stimulated (control).

### 4.5.5 Discussion

For the optimized bone integration and infection-resistance of dental implants, new antibacterial strategies and bone ingrowth promoting surfaces are constantly sought. Applying electrical pulses to conductive materials is a promising method to inhibit the bacterial surface attachment. Therefore, electrically active coatings with good biocompatibility are highly promising materials for future implant functionalization. Consequently, the biocompatible PVDF was the coating material of choice for further studies.<sup>440,441</sup> Since the biofilm inhibition of orally relevant bacteria by electrical stimulation is quite unexplored, stimulation parameter for the biofilm inhibition of *S. gordonii*, *S. salivarius*, and *P. gingivalis* were determined under laboratory conditions.

#### 4.5.5.1 Stimulation parameter

The stimulation parameters were chosen according to the results of the static pre-experiments. The inhibition parameters are listed in Before the bacteria were stimulated on the PVDF membranes, parameters for electrical stimulation were determined by initial trials on polystyrene. The stimulating parameters are listed in Table S 3. The results of the trials, i.e. the average biofilm heights and viability, are presented in Figure S 20. After determining the stimulation parameter for all three species, the bacteria were electrically stimulated under static and dynamic conditions on PVDF membranes with the parameters listed in Table 9.

Table 9 The biofilm height was used as a biological parameter to quantify the biofilm-inhibiting effect of the electrical stimulation. The biphasic and symmetrically compensated sine wave stimulation did not affect the bacterial biofilm formation of *S. gordonii*, as shown in Figure S 20. Giladi *et al.* have shown that the biofilm formation of *S. aureus* and *Pseudomonas aeruginosa* can be inhibited by an electric field with a frequency of 10 MHz.<sup>259</sup> They hypothesized that such high frequencies have an effect on the bacterial cell division mechanisms and the enzyme-substrate interactions. The electric field leads to conformational changes within the enzymes and thus interferes with the enzymatic reactions.<sup>259,446</sup> However, a 10°MHz stimulation would also harm living tissue and is therefore not suitable for medical applications *in vivo*. Also, Petrofsky *et al.* found no inhibition with sinusoidal stimulation of *Escherichia coli*, *S. aureus* and *P. aeruginosa* at lower frequencies.<sup>447</sup>

The Figure 20 shows the results of the electrical stimulation under biphasic symmetrically compensated rectangular pulse stimulation. While the control system had normal biofilm heights, the stimulation of *P. gingivalis* under static and dynamic conditions gave decreased

heights down to 10%. These stimulated biofilms consisted of monolayers as depicted in Figure 21 and Figure 22.

A substantially decreased biofilm formation of *S. gordonii* during electrical stimulation was so far only observed in the presence of antibiotics.<sup>448</sup> In our study, the biofilm formation was decreased solely by the electrical stimulation. The difference between the experiments of Wattanakaroon and Stewart and the presented study was the degree of maturity of the biofilm and the stimulation parameters. While they stimulated mature biofilms, the bacteria of the presented study were planktonic at the start of the experiments. The stimulation parameters used in their study were 2 mA, DC, 6-8 V over a period of 24 h with a simultaneous treatment of 2 µg/mL gentamycin. In the present study, 2 mA, AC, 340 V were used for 24 h and the bacterial biofilms were reduced to 85%. With higher electric fields, the biofilm would probably be erased completely, but for the subsequent analysis of the genetic expression patterns, a rest biofilm had to remain. The same results were found for *S. salivarius* and *P. gingivalis*. To the best of our knowledge, this is the first biofilm inhibition of *S. gordonii* that is solely induced by an electrical stimulation. The electrical stimulations of *S. salivarius* and *P. gingivalis* have not yet been described at all.

#### ***4.5.5.2 Vitality test of the stimulated and unstimulated bacteria of the supernatant on agar plates and quantitative real-time PCR***

The bacterial biofilms of the three species were treated by electric stimulation. As the mechanism of the electric stimulation is not yet fully understood, we addressed the following questions: 1.) Are the adherent bacteria killed by electrical stimulation? and 2.) Are planktonic bacteria in the supernatant still viable, as they are unable to attach to the electrified surface? Therefore, the supernatants of the electrically stimulated wells and the BFC were collected after stimulation, plated on solid growth medium and incubated for additional 24<sup>o</sup>h. The agar plates are depicted in Figure 23. As expected, the plated culture medium showed no bacterial colonization. The plates of the stimulated bacteria were confluenty colonized. The plates of the BFNS were also overgrown by bacteria but single colonies were still detectable. This proves that the stimulated bacteria were not dead. However, the biofilm formation was inhibited due to electrical stimulation. Sandvik *et al.* observed the inhibited biofilm formation of *S. epidermidis* after electrical stimulation. The detached cells showed a small viable portion of bacteria, natural detached cells of the control group were fitter.<sup>449</sup> Interestingly, Jass *et al.* detected the impaired attachment of bacteria to surfaces with electrical current in *P. aeruginosa*. To the best of our knowledge, there is no study dealing with the combination of both the planktonic bacteria and the respective biofilm before and after electrical stimulation.

The qRT-PCR was performed to determine the exact portion of vital and dead bacteria in the stimulated biofilm in comparison with the control group as shown in Figure 24. The bacteria in the stimulated supernatant of all three species showed a higher portion of vital cells compared to the control group. Consequently, the stimulated bacteria were not able to adhere on the stimulated surface and stayed planktonic within the supernatant. Moreover, the unstimulated biofilm of all three bacteria controls had a larger portion of vital bacteria compared to the stimulated biofilm control, as expected. This showed that the bacteria within the stimulated biofilms were damaged by the electric field.

#### **4.5.5.3 Influence of the pH on the bacterial growth behavior**

Alteration of the pH value can have a severe effect on bacterial growth, as bacteria have membrane-integrated proton pumps which emit protons from the cytoplasm to generate a transmembrane electrochemical gradient. A change of the external pH can overcome these mechanisms and have a biocidal effect on the cells.<sup>450-452</sup> There are cellular processes which do not adjust to pH volatility such as the secretion of the EPS. The optimum pH for polysaccharide production depends on the specific bacteria species, but in general it is around pH 7.<sup>453</sup> Stoodley *et al.* stated that at least the bioelectric effect was supported by the influence of pH.<sup>255</sup> They claimed that the electric current induces a pH downshift in the aqueous environment and consequently inhibits the growth of the bacteria. Therefore, this phenomenon was investigated in this study. The pH was measured before and after the electrical stimulation (Table 10 and Table 11). The pH values of the medium TSBYG and BHISV were around 7.5. After stimulation, the pH of the TSBYG was lowered to around 4.5 whereas the pH of the BHISV was not influenced. The TSBYG is frequently used for cultivation of streptococcal and staphylococcal bacteria. These are acid producers that can grow at acidic pH. Furthermore, the pH of the biofilm controls of *S. gordonii* and *S. salivarius* were around 4 and resulted from acidic products of the species' polysaccharide metabolism. The pH of the stimulated samples was also reduced to around 4. This showed that the pH drop was mainly induced by acidic metabolic products rather than electrolysis. The BHIVS is the preferred medium for anaerobic bacteria such as *P. gingivalis* that optimally grow at neutral to slightly basic pH.<sup>454</sup> The pH of the stimulated and unstimulated *P. gingivalis* was slightly decreased to around 5.5 to 6.0. This indicates that the reduction of the pH is the result of the naturally occurring metabolic processes that had no major influence on the observed inhibition of the bacteria. Loo *et al.* and Roger *et al.* stated that the optimal growth pH of *S. gordonii* and *S. salivarius* is between pH 4 and 6.5.<sup>355,455</sup> For *P. gingivalis* a pH between 5.5 and 7.5, with a tendency to the neutral pH, was



found to be optimal.<sup>454,456</sup> Summarized, the pH decrease was not responsible for biofilm reduction.

#### **4.5.5.4 Measurements of the chlorine and hydrogen peroxide content**

Electrical stimulation was claimed to produce toxic substances, such as chlorine or hydrogen peroxide that inhibit or kill the bacteria.<sup>236,237</sup> During our stimulation experiments, no chlorine or hydrogen peroxide were detected. Consequently, these substances can be excluded as chemical effectors.

Directly after applying the electric current to the stimulation devices, the evolution of gas bubbles was observed. The electrolysis of an aqueous solutions results in the generation of molecular oxygen, hydroxyl anions, molecular hydrogen, hydrogen cations at 1.23 V. Jass and Lappin-Scott, as well as Stewart *et al.* postulated that oxygen was produced through the application of an electric field that led to the reduction of the viable bacterial cell number.<sup>253,254</sup> This effect is described as a direct consequence of the electrical stimulation. The physical disturbances by the gas bubble formations lead to the detachment and disruption of the bacterial cells. Furthermore, the oxygen was postulated to block the bacterial proliferation and stops the bacterial growth or biofilm formation, even though this phenomenon is not yet significantly verified in literature.<sup>234,236,237</sup> However, we observed that the viability of planktonic bacteria was not negatively influenced by the oxygen formation. We conclude that by applying an electric field, the PVDF surface was rendered unattractive for bacterial attachment so that bacteria remained in the supernatant as free floating cells. Even though the production of gas bubbles decreased the PVDF membrane colonization, gene expression patterns of attached cells were analyzed to evaluate the transcriptional effects of electrical stimulation as described in *section 4.6*.



## 4.6 Gene expression profiles of electrically stimulated and unstimulated dental-relevant bacterium *S. gordonii*

For the initial investigation, genetic pattern of the alteration between stimulated and unstimulated bacteria, a study was performed with *S. gordonii* in stimulated supernatant and biofilms. The gene expression profiles of stimulated bacteria were compared with the unstimulated control. Since several genes were affected, the analyses were restricted to a defined fold change of supernatant (10-fold up- and 5-fold down-regulated) and biofilms ( $\geq 15$ -fold).

### 4.6.1 Results

For detailed investigations of the electrical stimulation effect on bacteria, it was important to study gene expression patterns between stimulated and unstimulated samples. For the gene expression pattern analysis, a total RNA extraction protocol for biofilms was established. The protocol of Szafranski *et al.* was optimized for biofilms of the bacterium *S. gordonii*.<sup>338</sup> A high RNA quality and sufficient RNA yields are crucial to achieve reasonable results by microarray analysis. The concentrations and RNA Integrity Numbers (RINs) are listed in Table 12.

#### 4.6.1.1 RNA and microarray quality

Table 12: RNA concentration and quality of the stimulated and unstimulated *S. gordonii* supernatant and biofilm.

RNA	concentration (ng/ $\mu$ L)	quality (RIN)
Stimulated supernatant	3.4	6.0
Unstimulated supernatant	36.8	6.4
Stimulated biofilm	21.4	8.7
Unstimulated biofilm	52.2	7.3

The RNA was reverse transcribed, and complementary DNAs (cDNA) were competitively hybridized to a microarray chip containing 2195 target genes from *S. gordonii* that was originally developed by Jakubovics *et al.*<sup>341</sup> The microarray analysis revealed differences in the fluorescence intensities between the samples, as SNS and BFNS samples had substantially brighter fluorescence signals (Figure 25).

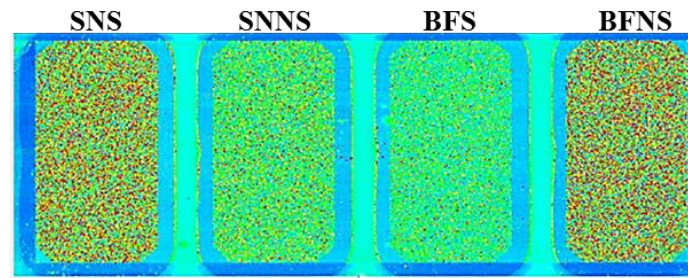


**Figure 25: Fluorescence signal intensities of the microarray assay.** Results of the stimulated supernatant and biofilm compared with the control groups. SNS = supernatant stimulated, SNNS = supernatant not stimulated, BFS = biofilm stimulated, BFNS = biofilm not stimulated.

#### 4.6.1.2 Up- and down-regulated genes in stimulated supernatant

Initially, 224 bacterial genes were up- and 207 genes were down-regulated in the stimulated supernatant. Three genes with a defined function (no hypothetical or potential functions) were up-regulated over 10-fold. Four genes were down-regulated five fold. In Figure 26, the up- and down-regulated genes of the stimulated supernatant are listed. The details of the open reading frames (ORFs), functions, protein domains and fold change in gene expression are listed in Table S 5.

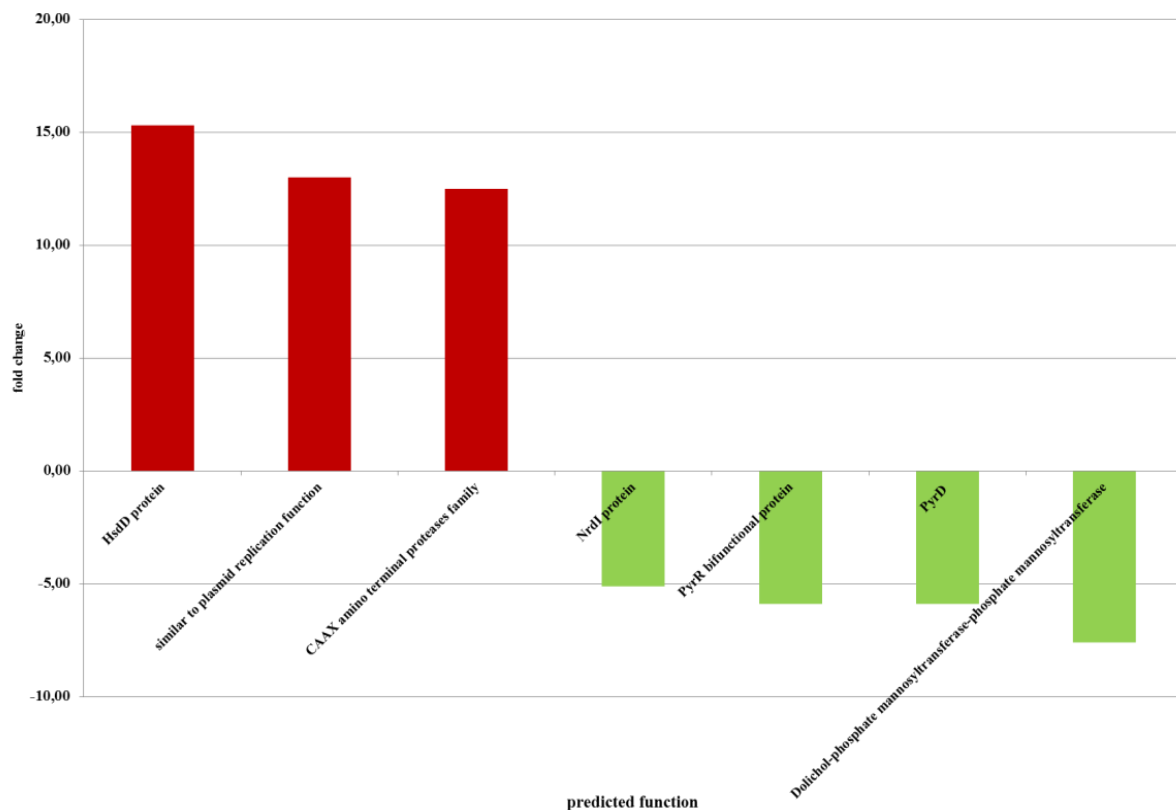


**Figure 26: Up- and down-regulated genes of the stimulated bacteria in the supernatant.** Red = up-regulation and green = down-regulation.

### 4.6.1.3 Up- and down-regulated genes in stimulated biofilm

The gene expressions of the stimulated biofilms differed in 549 genes that were up- and 563 genes that were down-regulated. Among these, some genes had expression alterations of  $\geq 15$ -fold, including 20 up- and 10 down-regulated genes that are described in detail and are listed in Figure 27. The ORFs, protein functions and domains, and fold change of gene expression are listed in Table S 6.

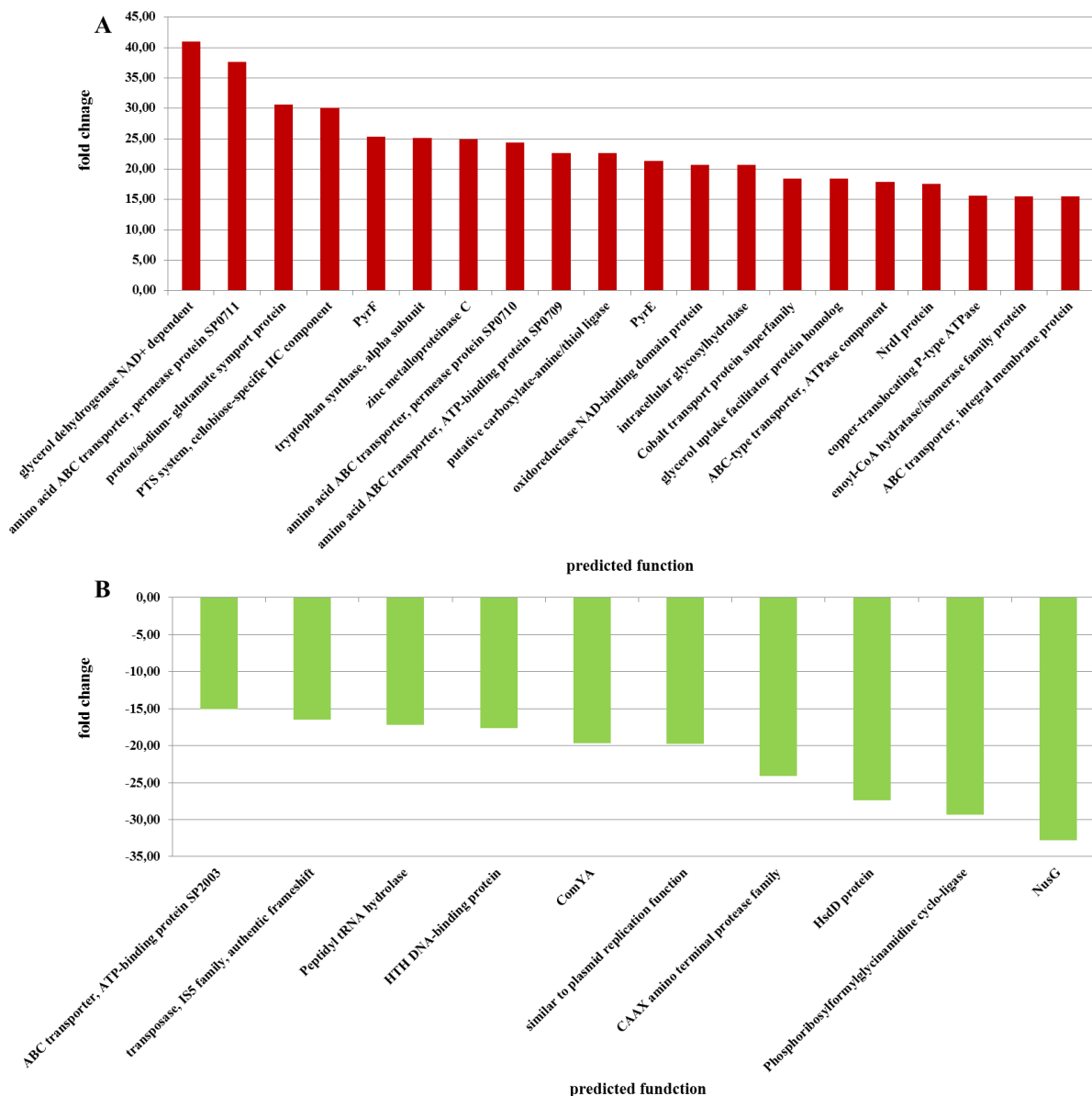


Figure 27: Up- and down-regulated genes of stimulated biofilm bacteria. A) up-regulation, B) down-regulation

## 4.6.2 Discussion

### 4.6.2.1 RNA and microarray quality

The accuracy of gene expression analyses is tremendously influenced by the quantity, purity and integrity of the input RNA.<sup>457</sup> Since RNA is rapidly digested by ribonucleases (RNases), the specimens have to be processed or (cryo)conserved immediately after sampling. However, in the course of RNA processing, a partial degradation can, in some cases, not be completely avoided.<sup>458</sup> As the isolation of RNA by commercially available kits alone can result in low RNA yields, we added three additional steps to the protocol prior to the column purification: 1.) utilization of “RNAprotect Bacteria Reagent” for preservation of the RNA integrity by inactivation of RNases, 2.) addition of mutanolysin, an enzyme derived from *Streptomyces globisporus* for increased cell lysis, and 3.) a final mechanical lysis step for complete cell disruption and RNA release.<sup>338,459-460,461</sup> Accordingly, the different RNAs showed RINs > 6, and were isolated in high yields (Table 12).

Figure 25 shows the microarray chip with hybridized, fluorescence labeled DNA samples. According to the microarray protocol, equal amounts of sample material with comparable RIN values were loaded on the chip. However, the fluorescence signal intensity differed vastly between the samples, especially between cDNA derived from SNS and BFNS and the other two samples. This phenomenon might be explained by different fluorescence labelling efficiencies among the compared samples or by cross hybridization.<sup>462-464</sup> In the latter case, the incorrect transcript hybridization results in combined signals of the correctly and incorrectly hybridized transcripts and the overall fluorescence intensity increases.<sup>465</sup> Even though sample processing failures cannot be completely omitted, the occurrence is very unlikely due to the great practical experience of the experimenters. Furthermore, repetition of the experiments led to almost identical results. In conclusion, the reasons for these findings cannot be clarified.

### 4.6.2.2 Gene expression patterns of the stimulated bacteria in the supernatant

In the stimulated supernatant three genes were up-regulated compared to the unstimulated control by at least 10-fold. The gene functions were assigned to 1) HsdD protein, 2) similar to plasmid replication function and 3) CAAX amino terminal protease family. The HsdD protein catalyzes the endonucleolytic cleavage of double stranded DNA under ATP consumption; similar to plasmid replication function has a role for bacterial competence, i.e. for intra- and interspecies gene transfer.<sup>466-468</sup> Members of the CAAX amino terminal protease family are membrane bound metalloproteases that are expressed in response to cell damage and modulate the cellular repair mechanisms.<sup>469</sup> Furthermore, they catalyze posttranscriptional modifications

and are involved in various transport processes.<sup>106,470</sup> These metalloproteases are believed to be directly involved in the biofilm development of *S. gordonii*.<sup>469</sup> For the HsdD protein and similar to plasmid replication function no direct involvement in biofilm formation has yet been reported, so that we assume that the up-regulation is an unspecific response to electrical stimulation and is not directly linked to the biofilm formation. For the up-regulation of metalloproteases, it can be hypothesized that the bacteria may have unsuccessfully tried to attach to the substrate surface and are therefore in a transition state between sessile and planktonic life cycle.

The following paragraph describes the four down-regulated genes in the stimulated supernatant compared to the unstimulated control in detail:

The transcription of four genes was down-regulated by at least 5-fold. The predicted gene products are the following: 1) Dolichol-phosphate mannosyltransferase, 2) Dihydroorotate dehydrogenase electron transfer subunit encoded by *pyrD*, 3) a bifunctional protein encoded by *pyrR* and 4) the NrdI protein. The Dolichol-phosphate mannosyltransferase participates in biosynthetic processes and the -transport of polysaccharides.<sup>471</sup> The *pyrD* gene encodes a flavoprotein.<sup>472</sup> This is a dehydrogenase that catalyzes processes in the biosynthesis of pyrimidine and its enzymatic function is also fundamental for all respiration processes. The bifunctional protein encoded by *pyrR* regulates transcriptional attenuations of the pyrimidine nucleotide operon and is involved in the conversion of uracil to uridinmonophosphate (UMP). Furthermore, it participates in the regulation of gene expressions and DNA transcriptions. The NrdI protein is a metalloprotease that catalyzes electron transport processes, and has a strong regulative role in the protein translation. All four proteins were not directly involved in the biofilm formation, however it cannot be excluded that there is no effect on the biofilm formation by regulation of cellular and/or metabolic processes.

#### **4.6.2.3 Genetic expression patterns of the stimulated bacteria in the biofilm**

In the bacterial biofilm, 20 genes were up- and ten genes were down-regulated with a fold change  $\geq 15$ . The following paragraph deals with the twenty up-regulated genes.

The gene product glycerol dehydrogenase is an enzyme active in the oxidation processes during the sugar and lipid synthesis.<sup>473,474</sup> Another up-regulated system is the amino acid ABC transporter complex gene cluster. This complex has four main functions: First, as an importer that mediates the uptake of nutrients; second, the export of secreted molecules; third, the translation of mRNA and fourth, the participation in the DNA repair mechanism.<sup>475,476</sup> In detail, the permease protein SP0711, the permeases protein SP0710, the ATP-binding protein

Sp0β709, the ATPase and the integral membrane protein were up-regulated. All these proteins are part of a cluster that is necessary for self-coaggregation of *S. gordonii* and induction of biofilm formation.<sup>477,478</sup> The ABC complex also controls the CAAX amino terminal protease family for the transport of proteins into the cell.<sup>469</sup> Additionally, the amino acid ABC transporter complex is involved in pathogenicity and virulence of the bacteria.<sup>475,478-481</sup> Thus, the up-regulation might have put the cells into a “state of readiness” for an increased cellular fitness.

The proton/sodium glutamate symporter protein is a carrier protein that is involved in the glutamate-aspartate, peptide, lipid and carbohydrate transport system.<sup>482</sup>

The phosphoenolpyruvate-dependent phosphotransferase systems (PTS) cellobiose-specific IIC component is involved in the processes of bacterial viability and pathogenicity as well as the virulence of the bacterium.<sup>475</sup> Moreover, it has a role in the beta-glucoside metabolism that is an adaptive reaction to survival.<sup>483</sup> Especially in *S. gordonii*, PTS participates in the adhesion process and the biofilm formation.<sup>355,483,484</sup>

The orotidine 5'-phosphate decarboxylase encoded by the *pyrF* gene and the PyrR protein are directly involved in the biosynthesis of pyrimidine.<sup>485,486</sup> The decarboxylase is an enzyme that catalyzes the decarboxylation of orotidine monophosphate to form UMP. The PyrR protein mediates the regulation of the *pyr* operon for the pyrimidine synthesis.<sup>486</sup>

The tryptophan synthase alpha subunit catalyzes the final step in the biosynthesis of the amino acid tryptophan. This amino acid is utilized in a broad range of proteins within the bacterial cell and is essential for living organisms.<sup>487</sup>

The zinc metalloproteinase C is a metalloprotease that is stress-induced and protects the cell against oxidative stress.<sup>488,489</sup> The up-regulation might indicate that the electric stimulation activates stress-dependent genes and/or induces bacterial cell reconstruction.<sup>490-492</sup>

The putative carboxylate-amine/thiol ligase is involved in the biosynthesis of amino acids, ribosomes, glutathione peptide glycan, purine, pyrimidine, arginine, lipids, and citric acid.<sup>493</sup>

The oxidoreductase NAD-binding domain protein participates in the metabolism of lipids, amino acids, carbohydrates, cofactors and the xenobiotic mechanisms.<sup>494,495</sup> Furthermore, it catalyzes the transfer of electrons essential for a broad range of cells metabolism processes.<sup>496,497</sup>

The intracellular glycosyl hydrolase catalyzes the hydrolysis of the main biofilm matrix exopolysaccharide PsI (polysaccharide inhibition) as already verified in *P. aeruginosa*. The main function of this enzyme is the inhibition of biofilm formation and the disruption of the biofilm.<sup>498,499</sup>



The cobalt transport protein catalyzes the uptake and efflux of small molecules under ATP consumption.<sup>475</sup>

The glycerol uptake facilitator protein has a role in the regulation of the glycerol quantities within the cell. This is required for the antimicrobial peptide release during biofilm growth for the bacterial defense mechanism against external hazards.<sup>500</sup> Hence, the up-regulation might have put the cells into a cellular “state of readiness”.

The detailed function of the NrdI protein is described in *section 4.6.2.2*. The copper-translocating P-type ATPases facilitates the absorption and assembly of copper in the cell as copper is an important cofactor for a wide a range of enzymes<sup>481</sup>.

The enoyl-CoA hydratase/isomerase family protein is involved in the cell-to-cell communication by synthesizing  $\alpha$ - and  $\beta$ -unsaturated fatty acids.<sup>501</sup> Interestingly, this protein participates in the biofilm disruption. It has a role in the synthesis of autoinducer cis-2-decenoic acid as verified in *P. aeruginosa* and *Xanthomonas campestris*.<sup>501-503</sup> The up-regulation might be explained by the fact that the bacterial biofilm is in threat, starving or the bacteria are not able to stay attached to the surface.<sup>501</sup>

In summary, 17 up-regulated genes are not directly connected to the regulation of the biofilm formation, even though an indirect effect cannot be excluded, e.g. in the metabolic and/or cellular processes as well as bacterial defense mechanisms. The PTS, the intracellular glycosyl hydrolase protein and the enoyl-CoA hydratase/isomerase family protein have a direct effect on the biofilm formation as verified by literature.<sup>355,483,484,498,499,501</sup> The up-regulation of the zinc metalloproteinase C indicates that the bacteria in the biofilm might have been stressed by the electrical stimulation.

The following paragraph deals with the ten down-regulated genes of the bacteria within the stimulated biofilms. These genes have a fold change  $\geq 15$  and are therefore described in detail. The down-regulated genes are: 1) NusG protein, 2) phosphoribosylformylglycinamide cyclo-ligase, 3) HsdD protein 4) CAAX amino terminal protease family, 5) the similar to plasmid replication function, 6) ComYA protein, 7) HTH DNA binding protein, 8) peptidyl tRNA hydrolases 9) transposase IS5 family, 10) ABC transporter, ATP-binding protein SP2003. The NusG protein and HTH DNA are involved in the transcription, elongation, termination and antitermination processes.<sup>504-506</sup> The cyclo-ligase has a catalytical role in the purine synthesis under ATP consumption.<sup>507</sup> The HsdD protein, CAAX amino terminal protease family functions, and similar to plasmid replication function, are described in *section 4.6.2.2*. ComYA protein participate in the bacterial competence processes.<sup>201,466,467,508</sup> Furthermore, the ComYA protein acts as channel protein and transports DNA through the bacterial membranes.<sup>508</sup> The

hydrolases controls the release of peptidyl tRNA and enables the recycling of ribosomes. It cleaves the ester bond between the C-terminal end of the peptide and the tRNA of peptidyl-tRNA molecules.<sup>509-512</sup> Furthermore, it is a key protein for the functionality of several translation factors, such as the prokaryotic initiation factor 1-3, the elongation factor G and the ribosome recycling factor.<sup>509,511,513,514</sup> The down-regulation of the hydrolases might completely prohibit the ribosomal reuse. The transposase IS5 family is a group of enzymes that facilitate the transport of the transposon, mobile DNA sequences of the genome.<sup>515,516</sup> The ABC transporter cluster is described in the previous paragraph.

In conclusion, the ten down-regulated genes are not directly related to the biofilm formation. However, the influence on the biofilm formation processes, e.g. the regulation of cellular replication mechanisms and/or metabolic processes, cannot be excluded completely.

## 5. Conclusion and Outlook

This work deals with the investigation of test systems and new implant surfaces to prevent bacterial infection within the framework of the doctoral program MARIO.

The thesis has two main projects: first, the development of an experimentally reproducible biofilm growth set-up under physiological-like fluid flow conditions for the calibration and validation of numerical biofilm simulations; and second, the determination of electrical stimulation parameter for the inhibition of bacterial biofilm formation on PVDF membranes.

The first part of the thesis was a cooperation project together with two MARIO doctoral students, Dianlei Feng and Meisam Soleimani. A flow chamber system was designed and evaluated, which mimicked the physiological fluid flow within the oral cavity. Initially, biofilm formation was analyzed using flow chambers in a continuous flow circuit for five bacterial species: *S. gordonii*, *S. oralis*, *S. salivarius*, *P. gingivalis*, and *A. actinomycetemcomitans*. The biofilm height, as quantitative parameter for biofilm formation, was significantly reproducible between different experiments for the tested bacteria. For determination of calibrators, i.e. biofilm height and spatial distribution of active (vital) and inactive (dead) bacteria, for numerical simulations, the flow chamber system was further developed to improve the consistency of culture conditions throughout the experiments. An open flow system with continuous feed of nutrients was developed. The Feng simulation was successfully calibrated according to the influence of the flow rates (100-400 $\mu$ L/min). Furthermore, biofilm growth behavior under different nutrient concentrations was numerically described with the Monod kinetics to determine the Monod half-rate constant  $k_s$  (0.05-0.06 x nutrient concentration).

The numerical simulations investigated by Meisam Soleimani focused on the biofilm growth behavior by a SPH model. For this approach, a particle-shaped bacterium *S. aureus* was chosen and the calibrator of the flow velocity influence (100-400  $\mu$ L/min) was successfully determined. The biofilm model was successfully developed for the chosen bacterium on titanium surfaces.

In the future, more complex biofilms models will be developed. Further experimental parameters like, substratum surface characteristics and growth behavior of multi-species biofilms will be implemented. Future applications will be modeling of medical biofilms e.g. for identification of infection-resistant implant materials or for antimicrobial efficacy testing.

These numerical approaches can help reducing cost-intensive and time-consuming *in vitro* testing efforts.

As an affiliated project to the numerical models, a cooperation project, with Prof. Nick Cogan from the Department of Mathematics, University of Florida, was initiated. Prof. Cogan developed a numerical disinfection protocol for persister bacteria. Different antibiotic regimes were experimentally tested on planktonic bacterium of *S. aureus*. As predicted by the simulation, a 20 h/4 h regime, i.e. 20 h with and 4 h without antibiotic over several days resulted in complete eradication of persister cells. In the future, it is planned to apply this treatment on mature biofilms *in vitro* and to evaluate its efficacy in animal models *in vivo*.

The second aim of this thesis was the experimental determination of electrical stimulation parameters for the inhibition and prevention of bacterial adhesion. This project was a cooperation project with Bastian Dreyer who was working on the production and refinement of the materials with defined piezoelectric characteristics. Two different test systems were designed and established to analyze the effect of electrical stimulation. Electrical stimulation parameters were successfully determined for *S. gordonii* (2 mA, 60  $\mu$ s, 10 Hz, 340 V), *S. salivarius* (1.9 mA, 60  $\mu$ s, 10 Hz, 323 V and *P. gingivalis* (3 mA, 500  $\mu$ s, 10 Hz, 750 V) to inhibit attachment over 24 h. Additionally, the effect of electrical treatment on gene expression pattern of *S. gordonii* was analyzed. The expression of different genes that, at least in part, are directly involved in biofilm formation were identified. We assume that the altered gene expression contributed to the observed inhibitory effect. However, physical effects of electrolysis, e.g. gas bubble formation on the substratum surface and interference with further bacterial cellular processes have also contributed to the observed antibacterial effect. In the future, electrically active implant coating materials have to be produced and tested based on these experimental findings. It is planned to fabricate a piezoelectric-active PVDF coating material with electrical properties, as defined in the experimental part of this thesis.

## 6. Literature

1. Darouiche RO. Treatment of infections associated with surgical implants. *N Engl J Med* 2004;350(14):1422-9.
2. Mombelli A, Müller N, Cionca N. The epidemiology of peri-implantitis. *Clin Oral Implants Res* 2012;23 Suppl 6:67-76.
3. Datenreport. Ein Sozialbericht für die Bundesrepublik Deutschland. 2013.
4. Vaupel JW. Biodemography of human ageing. *Nature* 2010;464(7288):536-42.
5. Busscher HJ, van der Mei HC, Subbiahdoss G, Jutte PC, van den Dungen JJ, Zaat SA, Schultz MJ, Grainger DW. Biomaterial-associated infection: locating the finish line in the race for the surface. *Sci Transl Med* 2012;4(153):153rv10.
6. Zimmerli W. Biomaterial associated infection: A perspective from clinic. Springer Verlag; 2012.
7. Costerton JW, Stewart PS, Greenberg EP. Bacterial biofilms: a common cause of persistent infections. *Science* 1999;284(5418):1318-22.
8. Żmudzki J, Chladek G, Kasperski J, Dobrzański LA. One versus two implant-retained dentures: comparing biomechanics under oblique mastication forces. *J Biomech Eng* 2013;135(5):54503.
9. Matsudate Y, Yoda N, Nanba M, Ogawa T, Sasaki K. Load distribution on abutment tooth, implant and residual ridge with distal-extension implant-supported removable partial denture. *J Prosthodont Res* 2016, 60(4):282-88.
10. Zohrabian VM, Abrahams JJ. Inflammatory Diseases of the Teeth and Jaws. *Semin Ultrasound CT MR* 2015;36(5):434-43.
11. Swelem AA, Gurevich KG, Fabrikant EG, Hassan MH, Aqou S. Oral health-related quality of life in partially edentulous patients treated with removable, fixed, fixed-removable, and implant-supported prostheses. *Int J Prosthodont* 2014;27(4):338-47.
12. Derks J, Håkansson J, Wennström JL, Klinge B, Berglundh T. Patient-reported outcomes of dental implant therapy in a large randomly selected sample. *Clin Oral Implants Res* 2015;26(5):586-91.
13. Robitaille N, Reed D, Walters J, Kumar P. Periodontal and peri-implant diseases: identical or fraternal infections? *Mol Oral Microbiol.*; 2015;31(4):285-301.
14. Brånemark PI. Osseointegration and its experimental background. *J Prosthet Dent* 1983;50(3):399-410.

15. Actis LA, Rhodes ER, Tomaras AP. Genetic and molecular characterization of a dental pathogen using genome-wide approaches. *Adv Dent Res* 2003;17:95-9.
16. Meyer DH, Mintz KP, Fives-Taylor PM. Models of invasion of enteric and periodontal pathogens into epithelial cells: a comparative analysis. *Crit Rev Oral Biol Med* 1997;8(4):389-409.
17. Slots J, Genco RJ. Black-pigmented *Bacteroides* species, *Capnocytophaga* species, and *Actinobacillus actinomycetemcomitans* in human periodontal disease: virulence factors in colonization, survival, and tissue destruction. *J Dent Res* 1984;63(3):412-21.
18. Zambon JJ. *Actinobacillus actinomycetemcomitans* in human periodontal disease. *J Clin Periodontol* 1985;12(1):1-20.
19. Petersen PE, Ogawa H. The global burden of periodontal disease: towards integration with chronic disease prevention and control. *Periodontol 2000* 2012;60(1):15-39.
20. Brígido JA, da Silveira VR, Rego RO, Nogueira NA. Serotypes of *Aggregatibacter actinomycetemcomitans* in relation to periodontal status and geographic origin of individuals-a review of the literature. *Med Oral Patol Oral Cir Bucal* 2014;19(2):e184-91.
21. Armitage GC. Periodontal diagnoses and classification of periodontal diseases. *Periodontol 2000* 2004;34:9-21.
22. Armitage GC. Development of a classification system for periodontal diseases and conditions. *Ann Periodontol* 1999;4(1):1-6.
23. Williams RO, Feldmann M, Maini RN. Anti-tumor necrosis factor ameliorates joint disease in murine collagen-induced arthritis. *Proc Natl Acad Sci U S A* 1992;89(20):9784-8.
24. Sakanaka A, Takeuchi H, Kuboniwa M, Amano A. Dual lifestyle of *Porphyromonas gingivalis* in biofilm and gingival cells. *Microb Pathog* 2015;94:42-47.
25. Hajishengallis G. Periodontitis: from microbial immune subversion to systemic inflammation. *Nat Rev Immunol* 2015;15(1):30-44.
26. Darveau RP. Periodontitis: a polymicrobial disruption of host homeostasis. *Nat Rev Microbiol* 2010;8(7):481-90.
27. Raja M, Ummer F, Dhivakar CP. *Aggregatibacter actinomycetemcomitans* - a tooth killer? *J Clin Diagn Res* 2014;8(8):ZE13-6.
28. Könönen E, Müller HP. Microbiology of aggressive periodontitis. *Periodontol 2000* 2014;65(1):46-78.

29. Pérez-Chaparro PJ, Gonçalves C, Figueiredo LC, Faveri M, Lobão E, Tamashiro N, Duarte P, Feres M. Newly identified pathogens associated with periodontitis: a systematic review. *J Dent Res* 2014;93(9):846-58.
30. Charalampakis G, Leonhardt Å, Rabe P, Dahlén G. Clinical and microbiological characteristics of peri-implantitis cases: a retrospective multicentre study. *Clin Oral Implants Res* 2012;23(9):1045-54.
31. Smeets R, Henningsen A, Jung O, Heiland M, Hammächer C, Stein JM. Definition, etiology, prevention and treatment of peri-implantitis--a review. *Head Face Med* 2014;10:34.
32. Lang NP, Berglundh T, Periodontology WGoSEWo. Periimplant diseases: where are we now?--Consensus of the Seventh European Workshop on Periodontology. *J Clin Periodontol* 2011;38 Suppl 11:178-81.
33. Quirynen M, Vogels R, Peeters W, van Steenberghe D, Naert I, Haffajee A. Dynamics of initial subgingival colonization of 'pristine' peri-implant pockets. *Clin Oral Implants Res* 2006;17(1):25-37.
34. Mombelli A, van Oosten MA, Schurch E, Land NP. The microbiota associated with successful or failing osseointegrated titanium implants. *Oral Microbiol Immunol* 1987;2(4):145-51.
35. Sanz M, Newman MG, Nachnani S, Holt R, Stewart R, Flemmig T. Characterization of the subgingival microbial flora around endosteal sapphire dental implants in partially edentulous patients. *Int J Oral Maxillofac Implants* 1990;5(3):247-53.
36. Rams TE, Degener JE, van Winkelhoff AJ. Antibiotic resistance in human peri-implantitis microbiota. *Clin Oral Implants Res* 2014;25(1):82-90.
37. Ata-Ali J, Candel-Martí ME, Flichy-Fernández AJ, Peñarrocha-Oltra D, Balaguer-Martínez JF, Peñarrocha Diago M. Peri-implantitis: associated microbiota and treatment. *Med Oral Patol Oral Cir Bucal* 2011;16(7):e937-43.
38. Salvi GE, Fürst MM, Lang NP, Persson GR. One-year bacterial colonization patterns of *Staphylococcus aureus* and other bacteria at implants and adjacent teeth. *Clin Oral Implants Res* 2008;19(3):242-8.
39. Karoussis IK, Salvi GE, Heitz-Mayfield LJ, Brägger U, Hämmerle CH, Lang NP. Long-term implant prognosis in patients with and without a history of chronic periodontitis: a 10-year prospective cohort study of the ITI Dental Implant System. *Clin Oral Implants Res* 2003;14(3):329-39.

40. Roos-Jansåker AM, Renvert H, Lindahl C, Renvert S. Nine- to fourteen-year follow-up of implant treatment. Part III: factors associated with peri-implant lesions. *J Clin Periodontol* 2006;33(4):296-301.
41. Rosenberg ES, Cho SC, Elian N, Jalbout ZN, Froum S, Evian CI. A comparison of characteristics of implant failure and survival in periodontally compromised and periodontally healthy patients: a clinical report. *Int J Oral Maxillofac Implants* 2004;19(6):873-9.
42. Evian CI, Emling R, Rosenberg ES, Waasdorp JA, Halpern W, Shah S, Garcia M. Retrospective analysis of implant survival and the influence of periodontal disease and immediate placement on long-term results. *Int J Oral Maxillofac Implants* 2004;19(3):393-8.
43. Schou S. Implant treatment in periodontitis-susceptible patients: a systematic review. *J Oral Rehabil* 2008;35 Suppl 1:9-22.
44. Klinge B, Meyle J, 2 WG. Peri-implant tissue destruction. The Third EAO Consensus Conference 2012. *Clin Oral Implants Res* 2012;23 Suppl 6:108-10.
45. Klokkevold PR, Han TJ. How do smoking, diabetes, and periodontitis affect outcomes of implant treatment? *Int J Oral Maxillofac Implants* 2007;22 Suppl:173-202.
46. Mahato N, Wu X, Wang L. Management of peri-implantitis: a systematic review, 2010-2015. *Springerplus* 2016;5:105.
47. Wilson TG. The positive relationship between excess cement and peri-implant disease: a prospective clinical endoscopic study. *J Periodontol* 2009;80(9):1388-92.
48. Agnihotry A, Fedorowicz Z, Nasser M. Adhesively bonded versus non-bonded amalgam restorations for dental caries. *Cochrane Database Syst Rev* 2016;3:CD007517.
49. Burke FJ, Wilson NH, Cheung SW, Mjör IA. Influence of patient factors on age of restorations at failure and reasons for their placement and replacement. *J Dent* 2001;29(5):317-24.
50. Mitchell L, A MD. *Oxford Handbook of clinical Dentistry*. USA: Oxford University Press; 2005.
51. Paes Leme AF, Koo H, Bellato CM, Bedi G, Cury JA. The role of sucrose in cariogenic dental biofilm formation--new insight. *J Dent Res* 2006;85(10):878-87.
52. Bowen WH, Koo H. Biology of *Streptococcus mutans*-derived glucosyltransferases: role in extracellular matrix formation of cariogenic biofilms. *Caries Res* 2011;45(1):69-86.



53. Kuvatanasuchati J, Chamroensaksri N, Tanasupawat S. Phenotypic and genotypic characterization of Thai oral streptococci, lactobacilli and pediococci. *Trop Biomed* 2012;29(2):254-64.
54. Scheinfeld MH, Shifteh K, Avery LL, Dym H, Dym RJ. Teeth: what radiologists should know. *Radiographics* 2012;32(7):1927-44.
55. Hale WG, Saunders VA, Margham JP. *Collins Dictionary of Biology*; 2005.
56. Costerton JW, Geesey GG, Cheng KJ. How bacteria stick. *Sci Am* 1978;238(1):86-95.
57. Costerton JW, Lewandowski Z, Caldwell DE, Korber DR, Lappin-Scott HM. Microbial biofilms. *Annu Rev Microbiol* 1995;49:711-45.
58. Donlan RM, Costerton JW. Biofilms: survival mechanisms of clinically relevant microorganisms. *Clin Microbiol Rev* 2002;15(2):167-93.
59. Flemming HC. Biofouling in water systems--cases, causes and countermeasures. *Appl Microbiol Biotechnol* 2002;59(6):629-40.
60. Flemming HC, Neu TR, Wozniak DJ. The EPS matrix: the "house of biofilm cells". *J Bacteriol* 2007;189(22):7945-7.
61. Sutherland I. Biofilm exopolysaccharides: a strong and sticky framework. *Microbiology* 2001;147(Pt 1):3-9.
62. Pamp SJ, Sternberg C, Tolker-Nielsen T. Insight into the microbial multicellular lifestyle via flow-cell technology and confocal microscopy. *Cytometry A* 2009;75(2):90-103.
63. Costerton JW, Cheng KJ, Geesey GG, Ladd TI, Nickel JC, Dasgupta M, Marrie TJ. Bacterial biofilms in nature and disease. *Annu Rev Microbiol* 1987;41:435-64.
64. Pamp SJ, M. G, Tolker-Nielsen T. The Biofilm Matrix - A Sticky Framework. In: Kjelleberg S, M. G, editors. *The Biofilm Mode of Life*: Northfolk: Horizon Bioscience; 2007:37-69.
65. Costerton JW, Ellis B, Lam K, Johnson F, Khoury AE. Mechanism of electrical enhancement of efficacy of antibiotics in killing biofilm bacteria. *Antimicrob Agents Chemother* 1994;38(12):2803-9.
66. Duguid IG, Evans E, Brown MR, Gilbert P. Effect of biofilm culture upon the susceptibility of *Staphylococcus epidermidis* to tobramycin. *J Antimicrob Chemother* 1992;30(6):803-10.
67. Duguid IG, Evans E, Brown MR, Gilbert P. Growth-rate-independent killing by ciprofloxacin of biofilm-derived *Staphylococcus epidermidis*; evidence for cell-cycle dependency. *J Antimicrob Chemother* 1992;30(6):791-802.

68. Donlan RM. Biofilm formation: a clinically relevant microbiological process. *Clin Infect Dis* 2001;33(8):1387-92.
69. Hoyle BD, Wong CK, Costerton JW. Disparate efficacy of tobramycin on Ca(2+)-, Mg(2+)-, and HEPES-treated *Pseudomonas aeruginosa* biofilms. *Can J Microbiol* 1992;38(11):1214-8.
70. Roilides E, Simitsopoulou M, Katragkou A, Walsh TJ. How Biofilms Evade Host Defenses. *Microbiol Spectr* 2015;3(3):1-10.
71. Salta M, Wharton JA, Blache Y, Stokes KR, Briand JF. Marine biofilms on artificial surfaces: structure and dynamics. *Environ Microbiol* 2013;15(11):2879-93.
72. Abdallah M, Benoliel C, Drider D, Dhulster P, Chihib NE. Biofilm formation and persistence on abiotic surfaces in the context of food and medical environments. *Arch Microbiol* 2014;196(7):453-72.
73. Li YH, Tian X. Quorum sensing and bacterial social interactions in biofilms. *Sensors (Basel)* 2012;12(3):2519-38.
74. De Sordi L, Mühlischlegel FA. Quorum sensing and fungal-bacterial interactions in *Candida albicans*: a communicative network regulating microbial coexistence and virulence. *FEMS Yeast Res* 2009;9(7):990-9.
75. Juhas M, Eberl L, Tümmler B. Quorum sensing: the power of cooperation in the world of *Pseudomonas*. *Environ Microbiol* 2005;7(4):459-71.
76. Parsek MR, Greenberg EP. Sociomicrobiology: the connections between quorum sensing and biofilms. *Trends Microbiol* 2005;13(1):27-33.
77. Shopova I, Bruns S, Thywissen A, Kniemeyer O, Brakhage AA, Hillmann F. Extrinsic extracellular DNA leads to biofilm formation and colocalizes with matrix polysaccharides in the human pathogenic fungus *Aspergillus fumigatus*. *Front Microbiol* 2013;4:141.
78. Jacques M, Marrie TJ, Costerton JW. Review: Microbial colonization of prosthetic devices. *Microb Ecol* 1987;13(3):173-91.
79. Hall-Stoodley L, Costerton JW, Stoodley P. Bacterial biofilms: from the natural environment to infectious diseases. *Nat Rev Microbiol* 2004;2(2):95-108.
80. Wang R, Khan BA, Cheung GY, Bach TH, Jameson-Lee M, Kong KF, Queck SY, Otto M. *Staphylococcus epidermidis* surfactant peptides promote biofilm maturation and dissemination of biofilm-associated infection in mice. *J Clin Invest* 2011;121(1):238-48.

81. Consortium HMP. Structure, function and diversity of the healthy human microbiome. *Nature* 2012;486(7402):207-14.
82. Aas JA, Paster BJ, Stokes LN, Olsen I, Dewhirst FE. Defining the normal bacterial flora of the oral cavity. *J Clin Microbiol* 2005;43(11):5721-32.
83. Pennisi E. A mouthful of microbes. *Science* 2005;307(5717):1899-901.
84. Marcotte H, Lavoie MC. Oral microbial ecology and the role of salivary immunoglobulin A. *Microbiol Mol Biol Rev* 1998;62(1):71-109.
85. Raj L S M, Jude J, I K, Krishna P S, Shankar K A S. Molecular Docking Study for Inhibitors of *Aggregatibacter actinomycetemcomitans* Toxins in Treatment of Aggressive Periodontitis. *J Clin Diagn Res* 2014;8(11):ZC48-51.
86. Kolenbrander PE, Andersen RN, Blehert DS, Eglund PG, Foster JS, Palmer RJ. Communication among oral bacteria. *Microbiol Mol Biol Rev* 2002;66(3):486-505.
87. Brogden KA, Guthmiller JM. *Polymicrobial Diseases*. ASM press; 2002.
88. Hannig M, Hannig C. Der initiale orale Biofilm- pathogen oder protektiv? *Oralprophylaxe & Kinderzahnheilkunde* 2007;29:73-82.
89. Marsh PD. Microbial ecology of dental plaque and its significance in health and disease. *Adv Dent Res* 1994;8(2):263-71.
90. Marsh PD, Percival RS. The oral microflora--friend or foe? Can we decide? *Int Dent J* 2006;56(4 Suppl 1):233-9.
91. Marsh PD. Dental plaque as a biofilm and a microbial community - implications for health and disease. *BMC Oral Health* 2006;6 Suppl 1:S1-14.
92. Hannig M, Kriener L, Hoth-Hannig W, Becker-Willinger C, Schmidt H. Influence of nanocomposite surface coating on biofilm formation in situ. *J Nanosci Nanotechnol* 2007;7(12):4642-8.
93. Whittaker CJ, Klier CM, Kolenbrander PE. Mechanisms of adhesion by oral bacteria. *Annu Rev Microbiol* 1996;50:513-52.
94. Rogers JD, Palmer RJ, Kolenbrander PE, Scannapieco FA. Role of *Streptococcus gordonii* amylase-binding protein A in adhesion to hydroxyapatite, starch metabolism, and biofilm formation. *Infect Immun* 2001;69(11):7046-56.
95. Nyvad B, Kilian M. Microbiology of the early colonization of human enamel and root surfaces in vivo. *Scand J Dent Res* 1987;95(5):369-80.
96. Jenkinson HF. Cell surface protein receptors in oral streptococci. *FEMS Microbiol Lett* 1994;121(2):133-40.

97. Cisar JO, Sandberg AL, Abeygunawardana C, Reddy GP, Bush CA. Lectin recognition of host-like saccharide motifs in streptococcal cell wall polysaccharides. *Glycobiology* 1995;5(7):655-62.
98. Chalmers NI. *Multispecies Oral Biofilms Studied at the Single Community Level as a Model System for Spatiotemporal Development of Biofilms and Interspecies Interaction*: University of Maryland Baltimore; 2008.
99. Bradshaw DJ, Marsh PD, Watson GK, Allison C. Role of *Fusobacterium nucleatum* and coaggregation in anaerobe survival in planktonic and biofilm oral microbial communities during aeration. *Infect Immun* 1998;66(10):4729-32.
100. Kolenbrander PE, Palmer RJ, Rickard AH, Jakubovics NS, Chalmers NI, Diaz PI. Bacterial interactions and successions during plaque development. *Periodontol* 2000 2006;42:47-79.
101. Peyyala R, Kirakodu SS, Ebersole JL, Novak KF. Novel model for multispecies biofilms that uses rigid gas-permeable lenses. *Appl Environ Microbiol* 2011;77(10):3413-21.
102. Lemon KP, Earl AM, Vlamakis HC, Aguilar C, Kolter R. Biofilm development with an emphasis on *Bacillus subtilis*. *Curr Top Microbiol Immunol* 2008;322:1-16.
103. Duran-Pinedo AE, Baker VD, Frias-Lopez J. The periodontal pathogen *Porphyromonas gingivalis* induces expression of transposases and cell death of *Streptococcus mitis* in a biofilm model. *Infect Immun* 2014;82(8):3374-82.
104. Socransky SS, Haffajee AD, Cugini MA, Smith C, Kent RL. Microbial complexes in subgingival plaque. *J Clin Periodontol* 1998;25(2):134-44.
105. Silva N, Abusleme L, Bravo D, Dutzan N, Garcia-Sesnich J, Vernal R, Hernández M, Gamonal J. Host response mechanisms in periodontal diseases. *J Appl Oral Sci* 2015;23(3):329-55.
106. Aruni AW, Dou Y, Mishra A, Fletcher HM. The Biofilm Community-Rebels with a Cause. *Curr Oral Health Rep* 2015;2(1):48-56.
107. Ruby J, Barbeau J. The buccale puzzle: The symbiotic nature of endogenous infections of the oral cavity. *Can J Infect Dis* 2002;13(1):34-41.
108. Zarco MF, Vess TJ, Ginsburg GS. The oral microbiome in health and disease and the potential impact on personalized dental medicine. *Oral Dis* 2012;18(2):109-20.
109. Derks J, Tomasi C. Peri-implant health and disease. A systematic review of current epidemiology. *J Clin Periodontol* 2015;42 Suppl 16:S158-71.

110. Cohen A, Bont L, Engelhard D, Moore E, Fernández D, Kreisberg-Greenblatt R, Oved K, Eden E, Hays JP. A multifaceted 'omics' approach for addressing the challenge of antimicrobial resistance. *Future Microbiol* 2015;10(3):365-76.
111. Karlsson R, Gonzales-Siles L, Boulund F, Svensson-Stadler L, Skovbjerg S, Karlsson A, Davidson M, Hulth S, Kristiansson E, Moore ER. Proteotyping: Proteomic characterization, classification and identification of microorganisms--A prospectus. *Syst Appl Microbiol* 2015;38(4):246-57.
112. Sabharwal A, Liao YC, Lin HH, Haase EM, Scannapieco FA. Draft genome sequences of 18 oral streptococcus strains that encode amylase-binding proteins. *Genome Announc* 2015;3(3):1-2.
113. Cook GS, Costerton JW, Lamont RJ. Biofilm formation by *Porphyromonas gingivalis* and *Streptococcus gordonii*. *J Periodontal Res* 1998;33(6):323-7.
114. Schonfeld ES. Contemporary oral microbiology and immunology. Slots J: Mosby Year. Book, St. Louis; 1992:267-274.
115. Jung CJ, Yeh CY, Shun CT, Hsu RB, Cheng HW, Lin CS, Chia JS. Platelets enhance biofilm formation and resistance of endocarditis-inducing streptococci on the injured heart valve. *J Infect Dis* 2012;205(7):1066-75.
116. Moreillon P, Que YA. Infective endocarditis. *Lancet* 2004;363(9403):139-49.
117. Long SS, Swenson RM. Determinants of the developing oral flora in normal newborns. *Appl Environ Microbiol* 1976;32(4):494-7.
118. Fujiwara T, Hoshino T, Ooshima T, Sobue S, Hamada S. Purification, characterization, and molecular analysis of the gene encoding glucosyltransferase from *Streptococcus oralis*. *Infect Immun* 2000;68(5):2475-83.
119. Willcox MD, Patrikakis M, Knox KW. Degradative enzymes of oral streptococci. *Aust Dent J* 1995;40(2):121-8.
120. Giffard PM, Simpson CL, Milward CP, Jacques NA. Molecular characterization of a cluster of at least two glucosyltransferase genes in *Streptococcus salivarius* ATCC 25975. *J Gen Microbiol* 1991;137(11):2577-93.
121. Alam S, Brailsford SR, Adams S, Allison C, Sheehy E, Zoitopoulos L, Kidd EA, Beighton D. Genotypic heterogeneity of *Streptococcus oralis* and distinct aciduric subpopulations in human dental plaque. *Appl Environ Microbiol* 2000;66(8):3330-6.
122. Byers HL, Tarelli E, Homer KA, Beighton D. Isolation and characterisation of sialidase from a strain of *Streptococcus oralis*. *J Med Microbiol* 2000;49(3):235-44.

123. Kelm S, Schauer R. Sialic acids in molecular and cellular interactions. *Int Rev Cytol* 1997;175:137-240.
124. Rothe B, Roggentin P, Schauer R. The sialidase gene from *Clostridium septicum*: cloning, sequencing, expression in *Escherichia coli* and identification of conserved sequences in sialidases and other proteins. *Mol Gen Genet* 1991;226(1-2):190-7.
125. Beighton D, Carr AD, Oppenheim BA. Identification of viridans streptococci associated with bacteraemia in neutropenic cancer patients. *J Med Microbiol* 1994;40(3):202-4.
126. Douglas CW, Heath J, Hampton KK, Preston FE. Identity of viridans streptococci isolated from cases of infective endocarditis. *J Med Microbiol* 1993;39(3):179-82.
127. Hardie JM. Recent developments in streptococcal taxonomy: their relation to infections. In: RA W, editor. *Rev Med Microbiol*; 1994;5:151-162.
128. West PW, Al-Sawan R, Foster HA, Electricwala Q, Alex A, Panigrahi D. Speciation of presumptive viridans streptococci from early onset neonatal sepsis. *J Med Microbiol* 1998;47(10):923-8.
129. Whalan RH, Funnell SG, Bowler LD, Hudson MJ, Robinson A, Dowson CG. Distribution and genetic diversity of the ABC transporter lipoproteins PiuA and PiaA within *Streptococcus pneumoniae* and related streptococci. *J Bacteriol* 2006;188(3):1031-8.
130. Guédon E, Delorme C, Pons N, Cruaud C, Loux V, Couloux A, Gautier C, Sanchez N, Layec S, Galleron N and others. Complete genome sequence of the commensal *Streptococcus salivarius* strain JIM8777. *J Bacteriol* 2011;193(18):5024-5.
131. Lévesque C, Vadeboncoeur C, Chandad F, Frenette M. *Streptococcus salivarius* fimbriae are composed of a glycoprotein containing a repeated motif assembled into a filamentous nondissociable structure. *J Bacteriol* 2001;183(9):2724-32.
132. Klemm P. *Fimbriae: adhesion, genetics, biogenesis, and vaccines*: CRC Press; 1994.
133. Hamada S, Amano A, Kimura S, Nakagawa I, Kawabata S, Morisaki I. The importance of fimbriae in the virulence and ecology of some oral bacteria. *Oral Microbiol Immunol* 1998;13(3):129-38.
134. Handley PS, Carter PL, Fielding J. *Streptococcus salivarius* strains carry either fibrils or fimbriae on the cell surface. *J Bacteriol* 1984;157(1):64-72.
135. Marsh P. *Oral ecology and its impact on oral microbial diversity*. UK: Horizon Scientific Press; 2000.

136. Becker MR, Paster BJ, Leys EJ, Moeschberger ML, Kenyon SG, Galvin JL, Boches SK, Dewhirst FE, Griffen AL. Molecular analysis of bacterial species associated with childhood caries. *J Clin Microbiol* 2002;40(3):1001-9.
137. Sterer N, Rosenberg M. *Streptococcus salivarius* promotes mucin putrefaction and malodor production by *Porphyromonas gingivalis*. *J Dent Res* 2006;85(10):910-4.
138. Bostanci N, Belibasakis GN. *Porphyromonas gingivalis*: an invasive and evasive opportunistic oral pathogen. *FEMS Microbiol Lett* 2012;333(1):1-9.
139. Duran-Pinedo AE, Chen T, Teles R, Starr JR, Wang X, Krishnan K, Frias-Lopez J. Community-wide transcriptome of the oral microbiome in subjects with and without periodontitis. *Isme j* 2014;8(8):1659-72.
140. Hasegawa Y, Tribble GD, Baker HV, Mans JJ, Handfield M, Lamont RJ. Role of *Porphyromonas gingivalis* SerB in gingival epithelial cell cytoskeletal remodeling and cytokine production. *Infect Immun* 2008;76(6):2420-7.
141. Holt SC, Kesavalu L, Walker S, Genco CA. Virulence factors of *Porphyromonas gingivalis*. *Periodontol 2000* 1999;20:168-238.
142. Potempa J, Pike R, Travis J. Titration and mapping of the active site of cysteine proteinases from *Porphyromonas gingivalis* (gingipains) using peptidyl chloromethanes. *Biol Chem* 1997;378(3-4):223-30.
143. Lamont RJ, Hersey SG, Rosan B. Characterization of the adherence of *Porphyromonas gingivalis* to oral streptococci. *Oral Microbiol Immunol* 1992;7(4):193-7.
144. Lamont RJ, Yilmaz O. In or out: the invasiveness of oral bacteria. *Periodontol 2000* 2002;30:61-9.
145. Holt SC, Ebersole J, Felton J, Brunsvold M, Kornman KS. Implantation of *Bacteroides gingivalis* in nonhuman primates initiates progression of periodontitis. *Science* 1988;239(4835):55-7.
146. Haffajee AD, Socransky SS. Microbial etiological agents of destructive periodontal diseases. *Periodontol 2000* 1994;5:78-111.
147. Del Prete S, Vullo D, De Luca V, Carginale V, Scozzafava A, Supuran CT, Capasso C. A highly catalytically active  $\gamma$ -carbonic anhydrase from the pathogenic anaerobe *Porphyromonas gingivalis* and its inhibition profile with anions and small molecules. *Bioorg Med Chem Lett* 2013;23(14):4067-71.
148. Del Prete S, De Luca V, Vullo D, Scozzafava A, Carginale V, Supuran CT, Capasso C. Biochemical characterization of the  $\gamma$ -carbonic anhydrase from the oral pathogen *Porphyromonas gingivalis*, PgiCA. *J Enzyme Inhib Med Chem* 2014;29(4):532-7.

149. Amano A, Nakagawa I, Okahashi N, Hamada N. Variations of *Porphyromonas gingivalis* fimbriae in relation to microbial pathogenesis. *J Periodontol Res* 2004;39(2):136-42.
150. Kishi M, Hasegawa Y, Nagano K, Nakamura H, Murakami Y, Yoshimura F. Identification and characterization of novel glycoproteins involved in growth and biofilm formation by *Porphyromonas gingivalis*. *Mol Oral Microbiol* 2012;27(6):458-70.
151. Park Y, Simionato MR, Sekiya K, Murakami Y, James D, Chen W, Hackett M, Yoshimura F, Demuth DR, Lamont RJ. Short fimbriae of *Porphyromonas gingivalis* and their role in coadhesion with *Streptococcus gordonii*. *Infect Immun* 2005;73(7):3983-9.
152. Stathopoulou PG, Benakanakere MR, Galicia JC, Kinane DF. Epithelial cell pro-inflammatory cytokine response differs across dental plaque bacterial species. *J Clin Periodontol* 2010;37(1):24-9.
153. Murakami J, Kato T, Kawai S, Akiyama S, Amano A, Morisaki I. Cellular motility of Down syndrome gingival fibroblasts is susceptible to impairment by *Porphyromonas gingivalis* invasion. *J Periodontol* 2008;79(4):721-7.
154. Kaplan JB, Perry MB, MacLean LL, Furgang D, Wilson ME, Fine DH. Structural and genetic analyses of O polysaccharide from *Actinobacillus actinomycetemcomitans* serotype f. *Infect Immun* 2001;69(9):5375-84.
155. Kim TS, Frank P, Eickholz P, Eick S, Kim CK. Serotypes of *Aggregatibacter actinomycetemcomitans* in patients with different ethnic backgrounds. *J Periodontol* 2009;80(12):2020-7.
156. Van Dyke TE, Bartholomew E, Genco RJ, Slots J, Levine MJ. Inhibition of neutrophil chemotaxis by soluble bacterial products. *J Periodontol* 1982;53(8):502-8.
157. Reddi K, Meghji S, Nair SP, Arnett TR, Miller AD, Preuss M, Wilson M, Henderson B, Hill P. The *Escherichia coli* chaperonin 60 (groEL) is a potent stimulator of osteoclast formation. *J Bone Miner Res* 1998;13(8):1260-6.
158. Henderson B, Nair SP, Ward JM, Wilson M. Molecular pathogenicity of the oral opportunistic pathogen *Actinobacillus actinomycetemcomitans*. *Annu Rev Microbiol* 2003;57:29-55.
159. Holt SC, Tanner AC, Socransky SS. Morphology and ultrastructure of oral strains of *Actinobacillus actinomycetemcomitans* and *Haemophilus aphrophilus*. *Infect Immun* 1980;30(2):588-600.



160. Lally ET, Kieba IR, Sato A, Green CL, Rosenbloom J, Korostoff J, Wang JF, Shenker BJ, Ortlepp S, Robinson MK and others. RTX toxins recognize a beta2 integrin on the surface of human target cells. *J Biol Chem* 1997;272(48):30463-9.
161. Sharma A. Virulence mechanisms of *Tannerella forsythia*. *Periodontol* 2000 2010;54(1):106-16.
162. Simpson DL, Berthold P, Taichman NS. Killing of human myelomonocytic leukemia and lymphocytic cell lines by *Actinobacillus actinomycetemcomitans* leukotoxin. *Infect Immun* 1988;56(5):1162-6.
163. Rahamat-Langendoen JC, van Vonderen MG, Engström LJ, Manson WL, van Winkelhoff AJ, Mooi-Kokenberg EA. Brain abscess associated with *Aggregatibacter actinomycetemcomitans*: case report and review of literature. *J Clin Periodontol* 2011;38(8):702-6.
164. Baba T, Bae T, Schneewind O, Takeuchi F, Hiramatsu K. Genome sequence of *Staphylococcus aureus* strain Newman and comparative analysis of staphylococcal genomes: polymorphism and evolution of two major pathogenicity islands. *J Bacteriol* 2008;190(1):300-10.
165. Muenks CE, Hogan PG, Wang JW, Eisenstein KA, Burnham CD, Fritz SA. Diversity of *Staphylococcus aureus* strains colonizing various niches of the human body. *J Infect* 2016;72(6):698-705.
166. Fitzpatrick F, Humphreys H, O'Gara JP. The genetics of staphylococcal biofilm formation--will a greater understanding of pathogenesis lead to better management of device-related infection? *Clin Microbiol Infect* 2005;11(12):967-73.
167. Arciola CR, Campoccia D, Speziale P, Montanaro L, Costerton JW. Biofilm formation in *Staphylococcus* implant infections. A review of molecular mechanisms and implications for biofilm-resistant materials. *Biomaterials* 2012;33(26):5967-82.
168. Scherr TD, Heim CE, Morrison JM, Kielian T. Hiding in Plain Sight: Interplay between Staphylococcal Biofilms and Host Immunity. *Front Immunol* 2014;5:37.
169. Watkins RR, David MZ, Salata RA. Current concepts on the virulence mechanisms of methicillin-resistant *Staphylococcus aureus*. *J Med Microbiol* 2012;61(Pt 9):1179-93.
170. Montanaro L, Speziale P, Campoccia D, Ravaioli S, Cangini I, Pietrocola G, Giannini S, Arciola CR. Scenery of *Staphylococcus* implant infections in orthopedics. *Future Microbiol* 2011;6(11):1329-49.
171. Otto M. Staphylococcal infections: mechanisms of biofilm maturation and detachment as critical determinants of pathogenicity. *Annu Rev Med* 2013;64:175-88.

172. Lina G, Piémont Y, Godail-Gamot F, Bes M, Peter MO, Gauduchon V, Vandenesch F, Etienne J. Involvement of Panton-Valentine leukocidin-producing *Staphylococcus aureus* in primary skin infections and pneumonia. *Clin Infect Dis* 1999;29(5):1128-32.
173. Pannaraj PS, Hulten KG, Gonzalez BE, Mason EO, Kaplan SL. Infective pyomyositis and myositis in children in the era of community-acquired, methicillin-resistant *Staphylococcus aureus* infection. *Clin Infect Dis* 2006;43(8):953-60.
174. Herald MC. General model of inflammation. *Bull Math Biol* 2010;72(4):765-79.
175. Abbas AK, Lichtman AH, Pober JS. *Cellular and Molecular Immunology*: Saunders; 2000.
176. Janeway CA, Travers P, Walport M, Shlomchik MJ. *Immunobiology - the Immune System in Health and Disease*; 2005.
177. Goldsby RA, Kindt TJ, Kuby J, Osborne BA. *Immunology*; 2002.
178. Akira S, Takeda K, Kaisho T. Toll-like receptors: critical proteins linking innate and acquired immunity. *Nat Immunol* 2001;2(8):675-80.
179. Arancibia SA, Beltrán CJ, Aguirre IM, Silva P, Peralta AL, Malinarich F, Hermoso MA. Toll-like receptors are key participants in innate immune responses. *Biol Res* 2007;40(2):97-112.
180. Mori Y, Yoshimura A, Ukai T, Lien E, Espevik T, Hara Y. Immunohistochemical localization of Toll-like receptors 2 and 4 in gingival tissue from patients with periodontitis. *Oral Microbiol Immunol* 2003;18(1):54-8.
181. Sugawara Y, Uehara A, Fujimoto Y, Kusumoto S, Fukase K, Shibata K, Sugawara S, Sasano T, Takada H. Toll-like receptors, NOD1, and NOD2 in oral epithelial cells. *J Dent Res* 2006;85(6):524-9.
182. Kikkert R, Laine ML, Aarden LA, van Winkelhoff AJ. Activation of toll-like receptors 2 and 4 by gram-negative periodontal bacteria. *Oral Microbiol Immunol* 2007;22(3):145-51.
183. Franchi L, Warner N, Viani K, Nuñez G. Function of Nod-like receptors in microbial recognition and host defense. *Immunol Rev* 2009;227(1):106-28.
184. Dennison DK, Van Dyke TE. The acute inflammatory response and the role of phagocytic cells in periodontal health and disease. *Periodontol* 2000 1997;14:54-78.
185. Dixon DR, Darveau RP. Lipopolysaccharide heterogeneity: innate host responses to bacterial modification of lipid a structure. *J Dent Res* 2005;84(7):584-95.

186. Martinon F, Burns K, Tschopp J. The inflammasome: a molecular platform triggering activation of inflammatory caspases and processing of proIL-beta. *Mol Cell* 2002;10(2):417-26.
187. Dagenais M, Skeldon A, Saleh M. The inflammasome: in memory of Dr. Jurg Tschopp. *Cell Death Differ* 2012;19(1):5-12.
188. von Moltke J, Ayres JS, Kofoed EM, Chavarría-Smith J, Vance RE. Recognition of bacteria by inflammasomes. *Annu Rev Immunol* 2013;31:73-106.
189. Olsen I, Yilmaz Ö. Modulation of inflammasome activity by *Porphyromonas gingivalis* in periodontitis and associated systemic diseases. *J Oral Microbiol* 2016;8:30385.
190. Botero JE, Contreras A, Lafaurie G, Jaramillo A, Betancourt M, Arce RM. Occurrence of periodontopathic and superinfecting bacteria in chronic and aggressive periodontitis subjects in a Colombian population. *J Periodontol* 2007;78(4):696-704.
191. Graves DT, Oates T, Garlet GP. Review of osteoimmunology and the host response in endodontic and periodontal lesions. *J Oral Microbiol* 2011;3.
192. Jäger A, Kuchroo VK. Effector and regulatory T-cell subsets in autoimmunity and tissue inflammation. *Scand J Immunol* 2010;72(3):173-84.
193. da Silva Domingues JF, van der Mei HC, Busscher HJ, van Kooten TG. Phagocytosis of bacteria adhering to a biomaterial surface in a surface thermodynamic perspective. *PLoS One* 2013;8(7):e70046.
194. Ford PJ, Gamonal J, Seymour GJ. Immunological differences and similarities between chronic periodontitis and aggressive periodontitis. *Periodontol 2000* 2010;53:111-23.
195. Pihlstrom BL, Michalowicz BS, Johnson NW. Periodontal diseases. *Lancet* 2005;366(9499):1809-20.
196. Lima HR, Gelani V, Fernandes AP, Gasparoto TH, Torres SA, Santos CF, Garlet GP, da Silva JS, Campanelli AP. The essential role of toll like receptor-4 in the control of *Aggregatibacter actinomycetemcomitans* infection in mice. *J Clin Periodontol* 2010;37(3):248-54.
197. Farquharson SI, Germaine GR, Gray GR. Isolation and characterization of the cell-surface polysaccharides of *Porphyromonas gingivalis* ATCC 53978. *Oral Microbiol Immunol* 2000;15(3):151-7.
198. Schifferle RE, Reddy MS, Zambon JJ, Genco RJ, Levine MJ. Characterization of a polysaccharide antigen from *Bacteroides gingivalis*. *J Immunol* 1989;143(9):3035-42.

199. Koziel J, Karim AY, Przybyszewska K, Ksiazek M, Rapala-Kozik M, Nguyen KA, Potempa J. Proteolytic inactivation of LL-37 by karilysin, a novel virulence mechanism of *Tannerella forsythia*. *J Innate Immun* 2010;2(3):288-93.
200. Hamlet SM, Ganashan N, Cullinan MP, Westerman B, Palmer JE, Seymour GJ. A 5-year longitudinal study of *Tannerella forsythia* prtH genotype: association with loss of attachment. *J Periodontol* 2008;79(1):144-9.
201. Gilmore KS, Srinivas P, Akins DR, Hatter KL, Gilmore MS. Growth, development, and gene expression in a persistent *Streptococcus gordonii* biofilm. *Infect Immun* 2003;71(8):4759-66.
202. de Beer D, Stoodley P, Lewandowski Z. Liquid flow in heterogeneous biofilms. *Biotechnol Bioeng* 1994;44(5):636-41.
203. Stoodley P, Dodds I, Boyle JD, Lappin-Scott HM. Influence of hydrodynamics and nutrients on biofilm structure. *J Appl Microbiol* 1998;85 Suppl 1:19S-28S.
204. Park, Joeong, Lee, Kim, Lee. Effect of shear stress on the formation of bacterial biofilm in a microfluidic channel. *BioChip J.*; 2011;5:236-241.
205. Purevdorj B, Costerton JW, Stoodley P. Influence of hydrodynamics and cell signaling on the structure and behavior of *Pseudomonas aeruginosa* biofilms. *Appl Environ Microbiol* 2002;68(9):4457-64.
206. de Kievit TR, Iglewski BH. Bacterial quorum sensing in pathogenic relationships. *Infect Immun* 2000;68(9):4839-49.
207. Miller MB, Bassler BL. Quorum sensing in bacteria. *Annu Rev Microbiol* 2001;55:165-99.
208. Kim J, Park HD, Chung S. Microfluidic approaches to bacterial biofilm formation. *Molecules* 2012;17(8):9818-34.
209. Wolfaardt GM, Lawrence JR, Robarts RD, Caldwell SJ, Caldwell DE. Multicellular organization in a degradative biofilm community. *Appl Environ Microbiol* 1994;60(2):434-46.
210. Klausen M, Heydorn A, Ragas P, Lambertsen L, Aaes-Jørgensen A, Molin S, Tolker-Nielsen T. Biofilm formation by *Pseudomonas aeruginosa* wild type, flagella and type IV pili mutants. *Mol Microbiol* 2003;48(6):1511-24.
211. Klausen M, Aaes-Jørgensen A, Molin S, Tolker-Nielsen T. Involvement of bacterial migration in the development of complex multicellular structures in *Pseudomonas aeruginosa* biofilms. *Mol Microbiol* 2003;50(1):61-8.

212. Pamp SJ, Tolker-Nielsen T. Multiple roles of biosurfactants in structural biofilm development by *Pseudomonas aeruginosa*. *J Bacteriol* 2007;189(6):2531-9.
213. Hansen SK, Rainey PB, Haagensen JA, Molin S. Evolution of species interactions in a biofilm community. *Nature* 2007;445(7127):533-6.
214. Christensen BB, Haagensen JA, Heydorn A, Molin S. Metabolic commensalism and competition in a two-species microbial consortium. *Appl Environ Microbiol* 2002;68(5):2495-502.
215. Nielsen AT, Tolker-Nielsen T, Barken KB, Molin S. Role of commensal relationships on the spatial structure of a surface-attached microbial consortium. *Environ Microbiol* 2000;2(1):59-68.
216. Breugelmans P, Barken KB, Tolker-Nielsen T, Hofkens J, Dejonghe W, Springael D. Architecture and spatial organization in a triple-species bacterial biofilm synergistically degrading the phenylurea herbicide linuron. *FEMS Microbiol Ecol* 2008;64(2):271-82.
217. Bjarnsholt T, Jensen P, Burmølle M, Hentzer M, Haagensen JA, Hougen HP, Calum H, Madsen KG, Moser C, Molin S and others. *Pseudomonas aeruginosa* tolerance to tobramycin, hydrogen peroxide and polymorphonuclear leukocytes is quorum-sensing dependent. *Microbiology* 2005;151(Pt 2):373-83.
218. Hansen SK, Haagensen JA, Gjermansen M, Jørgensen TM, Tolker-Nielsen T, Molin S. Characterization of a *Pseudomonas putida* rough variant evolved in a mixed-species biofilm with *Acinetobacter* sp. strain C6. *J Bacteriol* 2007;189(13):4932-43.
219. Kühl M, Rickelt LF, Thar R. Combined imaging of bacteria and oxygen in biofilms. *Appl Environ Microbiol* 2007;73(19):6289-95.
220. Landry RM, An D, Hupp JT, Singh PK, Parsek MR. Mucin-*Pseudomonas aeruginosa* interactions promote biofilm formation and antibiotic resistance. *Mol Microbiol* 2006;59(1):142-51.
221. Christensen BB, Sternberg C, Andersen JB, Palmer RJ, Nielsen AT, Givskov M, Molin S. Molecular tools for study of biofilm physiology. *Methods Enzymol* 1999;310:20-42.
222. Sternberg C, Tolker-Nielsen T. Growing and analyzing biofilms in flow cells. *Curr Protoc Microbiol* 2006;Chapter 1:Unit 1B.2.
223. Lewis K. Persister cells, dormancy and infectious disease. *Nat Rev Microbiol* 2007;5(1):48-56.
224. Bigger JW. Treatment of streptococcal infections with penicillin by intermittent sterilisation. *The Lancet: Elsevier*; 1944;244:497-500.

225. Keren I, Kaldalu N, Spoering A, Wang Y, Lewis K. Persister cells and tolerance to antimicrobials. *FEMS Microbiol Lett* 2004;230(1):13-8.
226. Lewis K. Riddle of biofilm resistance. *Antimicrob Agents Chemother* 2001;45(4):999-1007.
227. Balaban NQ, Merrin J, Chait R, Kowalik L, Leibler S. Bacterial persistence as a phenotypic switch. *Science* 2004;305(5690):1622-5.
228. Desai M, Bühler T, Weller PH, Brown MR. Increasing resistance of planktonic and biofilm cultures of *Burkholderia cepacia* to ciprofloxacin and ceftazidime during exponential growth. *J Antimicrob Chemother* 1998;42(2):153-60.
229. Christensen SK, Pedersen K, Hansen FG, Gerdes K. Toxin–antitoxin loci as stress-response elements: ChpAK/MazF and ChpBK cleave translated RNAs and are counteracted by tmRNA. *J. Mol. Biol.*; 2003;332:809–819.
230. Hayes F. Toxins-antitoxins: plasmid maintenance, programmed cell death, and cell cycle arrest. *Science*; 2003;301:1496–1499.
231. Anderson AK, Finkelstein R. A study of the electropure process of treating milk. *J. Dairy. Sci.* 1919;2.
232. Rowley BA. Electrical current effects on *E. coli* growth rates. *Proc Soc Exp Biol Med* 1972;139(3):929-34.
233. Freebairn D, Linton D, Harkin-Jones E, Jones DS, Gilmore BF, Gorman SP. Electrical methods of controlling bacterial adhesion and biofilm on device surfaces. *Expert Rev Med Devices* 2013;10(1):85-103.
234. Karba R, M. G, L. V. Growth inhibition in *Candida albicans* due to low intensity constant direct current. *J. Bioelectricity*; 1991;10.
235. Karba R, Gubina M, Vodovnik L. Growth inhibition in *Candida albicans* due to low intensity constant direct current. *J. Bioelectricity*; 1991;10.
236. Liu WK, Brown MR, Elliott TS. Mechanisms of the bactericidal activity of low amperage electric current (DC). *J Antimicrob Chemother* 1997;39(6):687-95.
237. Pareilleux A, Sicard N. Lethal effects of electric current on *Escherichia coli*. *Appl Microbiol* 1970;19(3):421-4.
238. Cevc G. Membrane electrostatics. *Biochim Biophys Acta* 1990;1031(3):311-82.
239. Boda SK, Bajpai I, Basu B. Inhibitory effect of direct electric field and HA-ZnO composites on *S. aureus* biofilm formation. *J Biomed Mater Res B Appl Biomater* 2016;104(6):1064-75.

240. Harold FM, Baarda JR. Gramicidin, valinomycin, and cation permeability of *Streptococcus faecalis*. *J Bacteriol* 1967;94(1):53-60.
241. Del Pozo JL, Rouse MS, Patel R. Bioelectric effect and bacterial biofilms. A systematic review. *Int J Artif Organs* 2008;31(9):786-95.
242. Sabelnikov AG, Cymbalyuk ES, Gongadze G, Borovyagin VL. *Escherichia coli* membranes during electrotransformation: an electron microscopy study. *Biochim Biophys Acta* 1991;1066(1):21-8.
243. Szuminsky NJ, Albers AC, Unger P, Eddy JG. Effect of narrow, pulsed high voltages on bacterial viability. *Phys Ther* 1994;74(7):660-7.
244. Asadi MR, Torkaman G. Bacterial Inhibition by Electrical Stimulation. *Adv Wound Care (New Rochelle)* 2014;3(2):91-97.
245. del Pozo JL, Rouse MS, Mandrekar JN, Steckelberg JM, Patel R. The electricidal effect: reduction of *Staphylococcus* and *pseudomonas* biofilms by prolonged exposure to low-intensity electrical current. *Antimicrob Agents Chemother* 2009;53(1):41-5.
246. Guffey JS, Asmussen MD. In vitro bactericidal effects of high voltage pulsed current versus direct current against *Staphylococcus aureus*. *J. Electrophysiol.*; 1989;1:5.
247. Hofbauer R, Moser D, Kaye AD, Knapp S, Gmeiner B, Kapiotis S, Wagner O, Frass M. Prostaglandin E(1) is able to increase migration of leukocytes through endothelial cell monolayers. *Microvasc Res* 2000;59(3):354-60.
248. McLoughlin TJ, Mylona E, Hornberger TA, Esser KA, Pizza FX. Inflammatory cells in rat skeletal muscle are elevated after electrically stimulated contractions. *J Appl Physiol (1985)* 2003;94(3):876-82.
249. Böhmer M. *In situ* observation of 2-dimensional clustering during electrophoretic deposition. *Langmuir* 1996;13:5747-50.
250. Poortinga AT, Bos R, Busscher HJ. Controlled electrophoretic deposition of bacteria to surfaces for the design of biofilms. *Biotechnol Bioeng* 2000;67(1):117-20.
251. Blenkinsopp SA, Khoury AE, Costerton JW. Electrical enhancement of biocide efficacy against *Pseudomonas aeruginosa* biofilms. *Appl Environ Microbiol* 1992;58(11):3770-3.
252. Jass J, Costerton JW, Lappin-Scott HM. The effect of electrical currents and tobramycin on *Pseudomonas aeruginosa* biofilms. *J Ind Microbiol* 1995;15(3):234-42.
253. Stewart PS, Wattanakaroon W, Goodrum L, Fortun SM, McLeod BR. Electrolytic generation of oxygen partially explains electrical enhancement of tobramycin efficacy

- against *Pseudomonas aeruginosa* biofilm. *Antimicrob Agents Chemother* 1999;43(2):292-6.
254. Jass J, Lappin-Scott HM. The efficacy of antibiotics enhanced by electrical currents against *Pseudomonas aeruginosa* biofilms. *J Antimicrob Chemother* 1996;38(6):987-1000.
255. Stoodley P, deBeer D, Lappin-Scott HM. Influence of electric fields and pH on biofilm structure as related to the bioelectric effect. *Antimicrob Agents Chemother* 1997;41(9):1876-9.
256. Poortinga AT, Smit J, van der Mei HC, Busscher HJ. Electric field induced desorption of bacteria from a conditioning film covered substratum. *Biotechnol Bioeng* 2001;76(4):395-9.
257. Verwey EJ. Theory of the stability of lyophobic colloids. *J Phys Colloid Chem* 1947;51(3):631-6.
258. Rosenberg B, Vancamp L, Krigas T. Inhibition of cell division in *Escherichia coli* by electrolysis products from a platinum electrode. *Nature* 1965;205:698-9.
259. Giladi M, Porat Y, Blatt A, Wasserman Y, Kirson ED, Dekel E, Palti Y. Microbial growth inhibition by alternating electric fields. *Antimicrob Agents Chemother* 2008;52(10):3517-22.
260. Caubet R, Pendarros-Caubet F, Chu M, Freye E, de Belém Rodrigues M, Moreau JM, Ellison WJ. A radio frequency electric current enhances antibiotic efficacy against bacterial biofilms. *Antimicrob Agents Chemother* 2004;48(12):4662-4.
261. del Pozo JL, Rouse MS, Mandrekar JN, Sampedro MF, Steckelberg JM, Patel R. Effect of electrical current on the activities of antimicrobial agents against *Pseudomonas aeruginosa*, *Staphylococcus aureus*, and *Staphylococcus epidermidis* biofilms. *Antimicrob Agents Chemother* 2009;53(1):35-40.
262. Del Pozo JL, Rouse MS, Euba G, Kang CI, Mandrekar JN, Steckelberg JM, Patel R. The electricidal effect is active in an experimental model of *Staphylococcus epidermidis* chronic foreign body osteomyelitis. *Antimicrob Agents Chemother* 2009;53(10):4064-8.
263. Hazan Z, Zumeris J, Jacob H, Raskin H, Kratysh G, Vishnia M, Dror N, Barliya T, Mandel M, Lavie G. Effective prevention of microbial biofilm formation on medical devices by low-energy surface acoustic waves. *Antimicrob Agents Chemother* 2006;50(12):4144-52.



264. Dror N, Mandel M, Hazan Z, Lavie G. Advances in microbial biofilm prevention on indwelling medical devices with emphasis on usage of acoustic energy. *Sensors (Basel)* 2009;9(4):2538-54.
265. Oulahal-Lagsir N, Martial-Gros A, Bonneau M, Blum LJ. "Escherichia coli-milk" biofilm removal from stainless steel surfaces: synergism between ultrasonic waves and enzymes. *Biofouling* 2003;19(3):159-68.
266. Pitt WG, Ross SA. Ultrasound increases the rate of bacterial cell growth. *Biotechnol Prog* 2003;19(3):1038-44.
267. Harper D. Piezoelectric. [http://www.etymonline.com/index.php?term=piezoelectric&allowed\\_in\\_frame=0](http://www.etymonline.com/index.php?term=piezoelectric&allowed_in_frame=0); last checked 12<sup>th</sup> of August 2016.
268. Manbachi A, Cobbold RSC. Development and application of piezoelectric materials for ultrasound generation and detection. *Ultrasound* 2001;19:187-96.
269. Cady WG. *Piezoelectricity*. McGraw-Hill; 1946:699.
270. Ballato A. Piezoelectricity: history and new thrusts. *IEEE Proceeding of Ultrasonic Symposium* 1996;13:575-83.
271. Curie J, Curie P. Development par compression de l'electricite polaire dans les cristaux hemiedres a faces inclinees. *Compt. Rend* 1880;91: 383-86.
272. Lippmann G. Sur le principe de la conversation de l'electricite. *Compt. Rend.* 1881;92: 1149-52.
273. Curie J, Curie P. Contractions et dilations produites par des tensions electriques dans les cristaux hemiedres a faces inclinees. *Compt. Rend.* 1881;93:1137-40.
274. Vatansever D, Siores E, Shah T. Alternative Resources of renewable energy: Piezoelectric and Photovoltaic Smart Structures. *Global Warming - Impacts and Future Perspectives* 2012:263-90.
275. Minazara E, Vasic D, Costa F, Poulin G. Piezoelectric diaphragm for vibration energy harvesting. *Ultrasonics* 2006;44 Suppl 1:e699-703.
276. Valasek J. Note on the piezo.electric effect in rochelle salt crystals. *Science* 1927;65(1679):235-6.
277. Duchesne J, Depireux J, Bertinchamps A, cornet N, Van der Kaa JM. Thermal and electrical properties of nucleic acids and proteins. *Nature* 1960;188:405-6.
278. Wang T, Feng Z, Song Y, Chen X. Piezoelectric properties of human dentin and some influencing factors. *Dent Mater* 2007;23(4):450-3.

279. Yucel T, Cebe P, Kaplan DL. Structural Origins of Silk Piezoelectricity. *Adv Funct Mater* 2011;21(4):779-785.
280. Fukada E. Piezoelectricity of Wood. *JPSJ* 1955;108:149.
281. Bazhenov VA. Piezoelectric properties of wood. Consultant Bureau Enterprises; 1961.
282. Fukada E, Yasuda I. On the Piezoelectric Effect of Bone. *JPSJ* 1957;12:1158.
283. Fukada E, Yasuda I. Piezoelectric Effects in Collagen. *Jpn. J. Appl. Phys.* 1964;3:117.
284. Ueda H, Fukada E. Piezoelectricity in Myosin and Actin. *Jpn. J. Appl. Phys.* 1971;10:1650-51.
285. Fukada E. Piezoelectricity in Oriented DNA Films. *J. Polym. Sci. A Polym.* 1972;10:565-67.
286. Robert S. Dielectric and Piezoelectric properties of Barium Titanate. *Phys. Rev.* 1947;71:890-95.
287. Shirane G, Suzuki K. Crystal Structure of  $\text{Pb}(\text{Zr-Ti})\text{O}_3$ . *J. Phys. Soc. Jpn.* 1952;7:333-36.
288. Shirane G, Hoshino S, Suzuki K. X-ray study of the phase transition in lead titanate. *Phys. Rev.* 1950;71:890-95.
289. Sawaguchi E. Ferroelectricity versus antiferroelectricity in the solid solutions of  $\text{PbZrO}_3$  and  $\text{PbTiO}_3$ . *JPSJ* 1953;8:615-29.
290. Jaffe B, Roth RS, Marzullo S. Piezoelectric Properties of lead zirconate-lead titanate solid-solution ceramic ware. *J. Appl. Phys.* 1954;25:809-10.
291. Egerton L, Dillon DM. Piezoelectric and Dielectric Properties of Ceramics in the System Potassium-Sodium Niobate. *J. Am. Ceram. Soc.* 1959;42:438-42.
292. Weis RS, Gaylord TK. Lithium niobate: Summary of physical properties and crystal structure. *Appl. Phys. A-Mater.* 1985;37:191-203.
293. Smith RT, Welsh F. Temperature Dependence of the Elastic, Piezoelectric, and Dielectric Constants of Lithium Tantanate and Lithium Niobate. *J. Appl. Phys* 1971;42:2219-30.
294. Kawai H. The piezoelectricity of poly(vinylidene fluoride). *Jpn. J. Appl. Phys* 1969;8: 975-76.
295. Labanca M, Azzola F, Vinci R, Rodella LF. Piezoelectric surgery: twenty years of use. *Br J Oral Maxillofac Surg* 2008;46(4):265-9.
296. Kholkin A, Amdursky N, Bdikin I, Gazit E, Rosenman G. Strong piezoelectricity in bioinspired peptide nanotubes. *ACS Nano* 2010;4(2):610-4.

297. Minary-Jolandan M, Yu MF. Nanoscale characterization of isolated individual type I collagen fibrils: polarization and piezoelectricity. *Nanotechnology* 2009;20(8):085706.
298. Platt SR, Farritor S, Garvin K, Haider H. The use of piezoelectric ceramics for electric power generation within orthopedic implants. *IEEE/ASME Trans. Mechatronics* 2005:10.
299. Laroche G, Marois Y, Guidoin R, King MW, Martin L, How T, Douville Y. Polyvinylidene fluoride (PVDF) as a biomaterial: from polymeric raw material to monofilament vascular suture. *J Biomed Mater Res* 1995;29(12):1525-36.
300. Zhang Q, Lu X, Zhao L. Preparation of Polyvinylidene Fluoride (PVDF) Hollow Fiber Hemodialysis Membranes. *Membranes (Basel)* 2014;4(1):81-95.
301. Jian K, Pintauro PN. Asymmetric PVDF hollow-fiber membranes for organic/water pervaporation separations. *J. Membr. Sci.* 1997;135:41-53.
302. Damjanovic D. Ferroelectric, dielectric and piezoelectric properties of ferroelectric thin films and ceramics. *Rep. Prog. Phys.* 1998;61:1267-1324.
303. Duk. commons.wikimedia.org. Wikipedia; 2004. p Version 1.2.
304. Ji GL, Zhu BK, Cui ZY, Zhang CF, Xu YY. PVDF porous matrix with controlled microstructure prepared by TIPS process as polymer electrolyte for lithium ion battery. *Polymers* 2007;48:6415-25.
305. Reis J, Frias C, Canto e Castro C, Botelho ML, Marques AT, Simões JA, Capela e Silva F, Potes J. A new piezoelectric actuator induces bone formation in vivo: a preliminary study. *J Biomed Biotechnol* 2012;2012:613403.
306. Kadow-Romacker A, Hoffmann JE, Duda G, Wildemann B, Schmidmaier G. Effect of mechanical stimulation on osteoblast- and osteoclast-like cells in vitro. *Cells Tissues Organs* 2009;190(2):61-8.
307. Lewandowska-Szumieł M, Sikorski K, Szummer A, Lewandowski Z, Marczyński W. Osteoblast response to the elastic strain of metallic support. *J Biomech* 2007;40(3):554-60.
308. Bourrin S, Palle S, Pupier R, Vico L, Alexandre C. Effect of physical training on bone adaptation in three zones of the rat tibia. *J Bone Miner Res* 1995;10(11):1745-52.
309. Hsieh YF, Turner CH. Effects of loading frequency on mechanically induced bone formation. *J Bone Miner Res* 2001;16(5):918-24.
310. Rubin CT, Lanyon LE. Regulation of bone formation by applied dynamic loads. *J Bone Joint Surg Am* 1984;66(3):397-402.

311. Campbell M, Bureau MN, Yahia L. Performance of CF/PA12 composite femoral stems. *J Mater Sci Mater Med* 2008;19(2):683-93.
312. Lamotta EJ. Internal diffusion and reaction in biological films. *Environ Sci Technol* 1976;10(8):765-9.
313. Williamson K, McCarty PL. A model of substrate utilization by bacterial films. *J Water Pollut Control Fed* 1976;48(1):9-24.
314. Harremoes P. The significance of pore diffusion to filter denitrification. *J. Water Pollut Control* 1976;48:377-88.
315. Harris NP, Hansford GS. A study of substrate removal in a microbial film reactor. *Water Res.* 1976;10:935-43.
316. Eberl H, Parker D, van Loosdrecht M. A new deterministic spatio-temporal continuum model for biofilm development. *J. Theor. Med* 2001;3:161-75.
317. Eberl HJ, Sudarsan R. Exposure of biofilms to slow flow fields: the convective contribution to growth and disinfection. *J Theor Biol* 2008;253(4):788-807.
318. Eberl HJ, van Loosdrecht MC, Morgenroth E, Noguera DR, Perez J, Picioreanu C, Rittmann BE, Schwarz AO, Wanner O. Modelling a spatially heterogeneous biofilm and the bulk fluid: selected results from benchmark problem 2 (BM2). *Water Sci Technol* 2004;49(11-12):155-62.
319. Wanner O, Reichert P. Mathematical modeling of mixed-culture biofilms. *Biotechnol Bioeng* 1996;49(2):172-84.
320. Wanner O, Gujer W. A multispecies biofilm model. *Biotech. and Bioeng.* 1986;28:314-28.
321. Dockery J, Klapper I. Finger formation in biofilm layers. *Siam. J. Appl. Math.* 2001;62:853-69.
322. Alpkvist E, Klapper I. A multidimensional multispecies continuum model for heterogeneous biofilm development. *Bull Math Biol* 2007;69(2):765-89.
323. Cogan NG, Keener JP. The role of the biofilm matrix in structural development. *Math Med Biol* 2004;21(2):147-66.
324. Clarelli F, Di Russo C, Natalini R, Ribot M. A fluid dynamics multidimensional model of biofilm growth: stability, influence of environment and sensitivity. *Math Med Biol* 2015;33(4):371-95.
325. Zhang T, Cogan N, Wang Q. Phase field models of biofilms. ii. 2-d numerical simulation of biofilm-flow interaction. *Commun. Comput. Phys.* 2008;4:72-101.

326. Albero AB, Ehret AE, Böl M. A new approach to the simulation of microbial biofilms by a theory of fluid-like pressure-restricted finite growth. *Comput. Method Appl. M.* 2014;272:271-289.
327. Kreft JU, Picioreanu C, Wimpenny JW, van Loosdrecht MC. Individual-based modelling of biofilms. *Microbiology* 2001;147(Pt 11):2897-912.
328. Wimpenny JW, Colasant R. A unifying hypothesis for the structure of microbial biofilms based on cellular automaton models. *FEMS Microbiology Ecology* 1997;22:1-16.
329. Mabrouk N, Deffuant G, Tolker-Nielsen T, Lobry C. Bacteria can form interconnected microcolonies when a self-excreted product reduces their surface motility: evidence from individual-based model simulations. *Theory in Biosciences* 2012;129:1-13.
330. Horn H, Lackner S. Modeling of biofilm systems: a review. *Adv Biochem Eng Biotechnol* 2014;146:53-76.
331. Xavier JB, Picioreanu C, van Loosdrecht MC. A framework for multidimensional modelling of activity and structure of multispecies biofilms. *Environ Microbiol* 2005;7(8):1085-103.
332. Xavier JB, Picioreanu C, van Loosdrecht MC. A general description of detachment for multidimensional modelling of biofilms. *Biotechnol Bioeng* 2005;91(6):651-69.
333. Monod J. The growth of bacterial cultures. *Annu. Rev. Microbiol.* 1949;3:371-94.
334. Elberling B, Damgaard LR. Microscale measurements of oxygen diffusion and consumption in subaqueous sulfide tailing. *Geochim. Cosmochim. Acta* 2001;65:1897-1905.
335. Lorke A, Müller B, Maerki M, Wüst A. Breathing sediments: the control of diffusive transport across the sediment-water interface by periodic boundary-layer turbulence. *Limnol. Oceanogr.* 2003;48:2077-85.
336. Duddu R, Chopp DL, Moran B. A two-dimensional continuum model of biofilm growth incorporating fluid flow and shear stress based detachment. *Biotechnol Bioeng* 2009;103(1):92-104.
337. Limbert G, Bryan R, Cotton R, Young P, Hall-Stoodley L, Kathju S, Stoodley P. On the mechanics of bacterial biofilms on non-dissolvable surgical sutures: a laser scanning confocal microscopy-based finite element study. *Acta Biomater* 2013;9(5):6641-52.
338. Szafranski SP, Deng ZL, Tomasch J, Jarek M, Bhujju S, Meisinger C, Kühnisch J, Sztajer H, Döbler IW. Functional biomarkers for the chronic periodontitis and insights

- into the roles of *Prevotella nigrescens* and *Fusobacterium nucleatum*; a metatranscriptome analysis. *Npj Biofilms and Microbiomes* 2015;1:1-12.
339. Kommerein N, Stumpp SN, Müsken M, Winkel A, Häussler S, Büttner FF, Stiesch M. Oral multispecies-biofilm model for high content screening applications. Clinic of Prosthetic Dentistry and Biomedical Materials Science, Hannover Medical School, Hannover, Germany. *PLoS One* 2017. Unpublished.
340. NCBI. <http://www.ncbi.nlm.nih.gov/geo/query/acc.cgi?acc=GPL5736>. National center for Biotechnology Information; 2007.
341. Jakubovics NS, Gill SR, Iobst SE, Vickerman MM, Kolenbrander PE. Regulation of gene expression in a mixed-genus community: stabilized arginine biosynthesis in *Streptococcus gordonii* by coaggregation with *Actinomyces naeslundii*. *J Bacteriol* 2008;190(10):3646-57.
342. NCBI. <http://www.ncbi.nlm.nih.gov/nuccore/CP000725>. National Center for Biotechnology Information; 2016.
343. Feng D, Neuweiler I, Nackenhorst U. A spatially stabilized TDG based finite element framework for modeling biofilm growth with A-K model and numerical analysis. Unpublished; 2017.
344. Gingold RA, Monaghan JJ. Smoothed particle hydrodynamics - Theory and application to non-spherical stars. *Mon. Not. R. Astron. Soc.* 1977;181:375-89.
345. Lucy LB. A numerical approach to the testing of the fission hypothesis. *Astron. J.* 1977;82:1013-24.
346. Costerton JW, Montanaro L, Arciola CR. Biofilm in implant infections: its production and regulation. *Int J Artif Organs* 2005;28(11):1062-8.
347. Stewart PS, Costerton JW. Antibiotic resistance of bacteria in biofilms. *Lancet* 2001;358(9276):135-8.
348. Stewart PS. Mechanisms of antibiotic resistance in bacterial biofilms. *Int J Med Microbiol* 2002;292(2):107-13.
349. Stewart PS. Antimicrobial Tolerance in Biofilms. *Microbiol Spectr* 2015;3(3).
350. Roberts AP, Pratten J, Wilson M, Mullany P. Transfer of a conjugative transposon, Tn5397 in a model oral biofilm. *FEMS Microbiol Lett* 1999;177(1):63-6.
351. Paquette DW, Brodala N, Williams RC. Risk factors for endosseous dental implant failure. *Dent Clin North Am* 2006;50(3):361-74, vi.

352. Kroukamp O, Dumitrache RG, Wolfaardt GM. Pronounced effect of the nature of the inoculum on biofilm development in flow systems. *Appl Environ Microbiol* 2010;76(18):6025-31.
353. Shemesh J, Jalilian I, Shi A, Heng Yeoh G, Knothe Tate ML, Ebrahimi Warkiani M. Flow-induced stress on adherent cells in microfluidic devices. *Lab Chip* 2015;15(21):4114-27.
354. Fux CA, Costerton JW, Stewart PS, Stoodley P. Survival strategies of infectious biofilms. *Trends Microbiol* 2005;13(1):34-40.
355. Loo CY, Corliss DA, Ganeshkumar N. *Streptococcus gordonii* biofilm formation: identification of genes that code for biofilm phenotypes. *J Bacteriol* 2000;182(5):1374-82.
356. Besemer K, Singer G, Limberger R, Chlup AK, Hochedlinger G, Hödl I, Baranyi C, Battin TJ. Biophysical controls on community succession in stream biofilms. *Appl Environ Microbiol* 2007;73(15):4966-74.
357. Sternberg C, Christensen BB, Johansen T, Toftgaard Nielsen A, Andersen JB, Givskov M, Molin S. Distribution of bacterial growth activity in flow-chamber biofilms. *Appl Environ Microbiol* 1999;65(9):4108-17.
358. Zhang W, Sileika TS, Chen C, Liu Y, Lee J, Packman AI. A novel planar flow cell for studies of biofilm heterogeneity and flow-biofilm interactions. *Biotechnol Bioeng* 2011;108(11):2571-82.
359. Islam N, Kim Y, Ross JM, Marten MR. Proteomic analysis of *Staphylococcus aureus* biofilm cells grown under physiologically relevant fluid shear stress conditions. *Proteome Sci* 2014;12:21.
360. Zhao B, van der Mei HC, Subbiahdoss G, de Vries J, Rustema-Abbing M, Kuijter R, Busscher HJ, Ren Y. Soft tissue integration versus early biofilm formation on different dental implant materials. *Dent Mater* 2014;30(7):716-27.
361. Chin MY, Busscher HJ, Evans R, Noar J, Pratten J. Early biofilm formation and the effects of antimicrobial agents on orthodontic bonding materials in a parallel plate flow chamber. *Eur J Orthod* 2006;28(1):1-7.
362. Merritt JH, Kadouri DE, O'Toole GA. Growing and analyzing static biofilms. *Curr Protoc Microbiol* 2005;Chapter 1:Unit 1B.1.
363. Waters EM, McCarthy H, Hogan S, Zapotoczna M, O'Neill E, O'Gara JP. Rapid quantitative and qualitative analysis of biofilm production by *Staphylococcus epidermidis* under static growth conditions. *Methods Mol Biol* 2014;1106:157-66.

364. Rijnaarts HH, Norde W, Bouwer EJ, Lyklema J, Zehnder AJ. Bacterial Adhesion under Static and Dynamic Conditions. *Appl Environ Microbiol* 1993;59(10):3255-65.
365. Dawes C, Watanabe S, Biglow-Lecomte P, Dibdin GH. Estimation of the velocity of the salivary film at some different locations in the mouth. *J Dent Res* 1989;68(11):1479-82.
366. Weiger R, Decker EM, Krastl G, Brex M. Deposition and retention of vital and dead *Streptococcus sanguinis* cells on glass surfaces in a flow-chamber system. *Arch Oral Biol* 1999;44(8):621-8.
367. Hauser-Gerspach I, Kulik EM, Weiger R, Decker EM, Von Ohle C, Meyer J. Adhesion of *Streptococcus sanguinis* to dental implant and restorative materials in vitro. *Dent Mater J* 2007;26(3):361-6.
368. Meier R, Hauser-Gerspach I, Luthy H, Meyer J. Adhesion of oral streptococci to all-ceramics dental restorative materials in vitro. *J Mater Sci Mater Med* 2008;19(10):3249-53.
369. Diaz PI, Xie Z, Sobue T, Thompson A, Biyikoglu B, Ricker A, Ikonomidou L, Dongari-Bagtzoglou A. Synergistic interaction between *Candida albicans* and commensal oral streptococci in a novel in vitro mucosal model. *Infect Immun* 2012;80(2):620-32.
370. Paramonova E, Kalmykova OJ, van der Mei HC, Busscher HJ, Sharma PK. Impact of hydrodynamics on oral biofilm strength. *J Dent Res* 2009;88(10):922-6.
371. Gowrishankar, Kamaladevi, Ayyanar, Balamurugan, Pandian. *Bacillus amyloliquefaciens*-secreted cyclic dipeptide – cyclo(L-leucyl-L-prolyl) inhibits biofilm and virulence production in methicillin-resistant *Staphylococcus aureus*. *RSC Adv.* 2015;5:95788-804.
372. Sliopen I, Hofkens J, Van Essche M, Quirynen M, Teughels W. *Aggregatibacter actinomycetemcomitans* adhesion inhibited in a flow cell. *Oral Microbiol Immunol* 2008;23(6):520-4.
373. Davey ME. Techniques for the growth of *Porphyromonas gingivalis* biofilms. *Periodontol* 2000 2006;42:27-35.
374. Gashti MP, Asselin J, Barbeau J, Boudreau D, Greener J. A microfluidic platform with pH imaging for chemical and hydrodynamic stimulation of intact oral biofilms. *Lab Chip* 2016;16(8):1412-9.
375. Christensen BB, Sternberg C, Andersen JB, Eberl L, Moller S, Givskov M, Molin S. Establishment of new genetic traits in a microbial biofilm community. *Appl Environ Microbiol* 1998;64(6):2247-55.



376. Laupacis A, Bourne R, Rorabeck C, Feeny D, Wong C, Tugwell P, Leslie K, Bullas R. The effect of elective total hip replacement on health-related quality of life. *J Bone Joint Surg Am* 1993;75(11):1619-26.
377. Featherstone JD. The caries balance: the basis for caries management by risk assessment. *Oral Health Prev Dent* 2004;2 Suppl 1:259-64.
378. Flemmig TF, Beikler T. Control of oral biofilms. *Periodontol* 2000 2011;55(1):9-15.
379. Decker EM. The ability of direct fluorescence-based, two-colour assays to detect different physiological states of oral streptococci. *Lett Appl Microbiol* 2001;33(3):188-92.
380. Diaz PI, Chalmers NI, Rickard AH, Kong C, Milburn CL, Palmer RJ, Kolenbrander PE. Molecular characterization of subject-specific oral microflora during initial colonization of enamel. *Appl Environ Microbiol* 2006;72(4):2837-48.
381. Kilian O, Balser G, Heiss C, Pavlidis T, Schnettler R. [Subjective and clinical outcome after rotator cuff repair in elderly patients]. *Z Orthop Unfall* 2008;146(4):471-7.
382. Kilian M, Mikkelsen I, Henrichsen J. Taxonomic Study of Viridans Streptococci: Descriptopn of *Streptococcus gordonii* sp. nov. and Emended Desriptopns of *Streptococcus sanguis* (White and Niven 1946), *Streptococcus oralis* (Bridge and Sneath 1982), and *Streptococcus mitis* ( Andrewes and Horder 1906). *Int. J. Syst. Evol. Microbiol* 1989;39:471-84.
383. Periasamy S, Kolenbrander PE. Mutualistic biofilm communities develop with *Porphyromonas gingivalis* and initial, early, and late colonizers of enamel. *J Bacteriol* 2009;191(22):6804-11.
384. Horn H, Hempel DC. Substrate utilization and mass transfer in an autotrophic biofilm system: Experimental results and numerical simulation. *Biotechnol Bioeng* 1997;53(4):363-71.
385. Rittmann BE, Manem JA. Development and experimental evaluation of a steady-state, multispecies biofilm model. *Biotechnol Bioeng* 1992;39(9):914-22.
386. Clement TP, Peyton BM, Skeen RS, Jennings DA, Petersen JN. Microbial growth and transport in porous media under denitrification conditions. Experiments and simulations. *J Contam Hydrol* 1997;24:269-85.
387. Peszynska M, Tzrykozko A, Iltis G, Schlueter S, Wildenschild D. Biofilm growth on porous media. Experiments, computational modeling at the porescale, and upscaling. *Adv. Water Resour.* 2015;91:1-6.

388. Rath H, Feng D, Neuweiler I, Stumpp SN, Nackenhorst U, Stiesch M. Biofilm formation by the oral pioneer colonizer *Streptococcus gordonii* an experimental and numerical study. unpublished; 2017.
389. Eberl H. Mathematical modeling of biofilms. International Water Association; 2006.
390. Bakker DP, van der Plaats A, Verkerke GJ, Busscher HJ, van der Mei HC. Comparison of velocity profiles for different flow chamber designs used in studies of microbial adhesion to surfaces. *Appl Environ Microbiol* 2003;69(10):6280-7.
391. Busscher HJ, van der Mei HC. Microbial adhesion in flow displacement systems. *Clin Microbiol Rev* 2006;19(1):127-41.
392. Lewandowski, Beyenal. Fundamentals of biofilm research. Boca Raton: CRC Press Taylor & Francis Group; 2014.
393. Tsai YP. Impact of flow velocity on the dynamic behaviour of biofilm bacteria. *Biofouling* 2005;21(5-6):267-77.
394. León Ohl A, Horn H, Hempel DC. Behaviour of biofilm systems under varying hydrodynamic conditions. *Water Sci Technol* 2004;49(11-12):345-51.
395. Liu Y, Tay JH. Metabolic response of biofilm to shear stress in fixed-film culture. *J Appl Microbiol* 2001;90(3):337-42.
396. Hughes TJ, Hulbert GM. Space-time finite element methods for elasto-dynamics: formulations and error estimates. *Computer Methods in Applied Mechanics and Engineering* 1988;66:339-63.
397. Onate E, Vallas A, Garcia J. Computation of turbulent flows using finite calculus-finite element formulation. *Computers & Fluids* 2007;54:609-37.
398. Sapotnick A, Nackenhorst U. A combined FIC-TDG finite element approach for the numerical solution of coupled advection-diffusion-reaction equations with application to a bioregulatory model for bone fracture healing. *Int. J. Numer. Meth. Eng.* 2012;92:301-17.
399. Attin T, Becker K, Wiegand A, Tauböck TT, Wegehaupt FJ. Impact of laminar flow velocity of different acids on enamel calcium loss. *Clin Oral Investig* 2013;17(2):595-600.
400. Foster JS, Kolenbrander PE. Development of a multispecies oral bacterial community in a saliva-conditioned flow cell. *Appl Environ Microbiol* 2004;70(7):4340-8.
401. Gu F, Lux R, Anderson MH, del Aguila MA, Wolinsky L, Hume WR, Shi W. Analyses of *Streptococcus mutans* in saliva with species-specific monoclonal antibodies. *Hybrid Hybridomics* 2002;21(4):225-32.

402. Nielsen SP, Petersen OH. Excretion of magnesium, calcium, and inorganic phosphate by the cat submandibular gland. *Pflugers Arch* 1970;318(1):63-77.
403. Dworkin, Falkow, Rosenberg, Schleifer, Stackebrandt. *The Prokaryotes A Handbook on the Biology of Bacteria: Bacteria: Firmicutes, Cyanobacteria*. Berlin Heidelberg: Springer-Verlag New York Inc.; 2006. 78 pp.
404. Arweiler NB, Hellwig E, Sculean A, Hein N, Auschill TM. Individual vitality pattern of in situ dental biofilms at different locations in the oral cavity. *Caries Res* 2004;38(5):442-7.
405. Bowden GH, Li YH. Nutritional influences on biofilm development. *Adv Dent Res* 1997;11(1):81-99.
406. Hope CK, Wilson M. Measuring the thickness of an outer layer of viable bacteria in an oral biofilm by viability mapping. *J Microbiol Methods* 2003;54(3):403-10.
407. Netuschil L, Auschill TM, Sculean A, Arweiler NB. Confusion over live/dead stainings for the detection of vital microorganisms in oral biofilms--which stain is suitable? *BMC Oral Health* 2014;14:2.
408. Corbin A, Pitts B, Parker A, Stewart PS. Antimicrobial penetration and efficacy in an in vitro oral biofilm model. *Antimicrob Agents Chemother* 2011;55(7):3338-44.
409. Asally M, Kittisopikul M, Rué P, Du Y, Hu Z, Çağatay T, Robinson AB, Lu H, Garcia-Ojalvo J, Süel GM. Localized cell death focuses mechanical forces during 3D patterning in a biofilm. *Proc Natl Acad Sci U S A* 2012;109(46):18891-6.
410. Bernimoulin JP. Recent concepts in plaque formation. *J Clin Periodontol* 2003;30 Suppl 5:7-9.
411. Busscher HJ, Bos R, van der Mei HC. Initial microbial adhesion is a determinant for the strength of biofilm adhesion. *FEMS Microbiol Lett* 1995;128(3):229-34.
412. Garrett TR, Bhakoo M, Zhang Z. Characterisation of bacterial adhesion and removal in a flow chamber by micromanipulation measurements. *Biotechnol Lett* 2008;30(3):427-33.
413. Mueller RF, Characklis WG, Jones WL, Sears JT. Characterization of initial events in bacterial surface colonization by two *Pseudomonas* species using image analysis. *Biotechnol Bioeng* 1992;39(11):1161-70.
414. Webb JS, Thompson LS, James S, Charlton T, Tolker-Nielsen T, Koch B, Givskov M, Kjelleberg S. Cell death in *Pseudomonas aeruginosa* biofilm development. *J Bacteriol* 2003;185(15):4585-92.

415. Ellis RE, Yuan JY, Horvitz HR. Mechanisms and functions of cell death. *Annu Rev Cell Biol* 1991;7:663-98.
416. Engelberg-Kulka H, Glaser G. Addiction modules and programmed cell death and antideath in bacterial cultures. *Annu Rev Microbiol* 1999;53:43-70.
417. Lewis K. Programmed death in bacteria. *Microbiol Mol Biol Rev* 2000;64(3):503-14.
418. Meier P, Finch A, Evan G. Apoptosis in development. *Nature* 2000;407(6805):796-801.
419. Lawrence JR, Korber DR, Hoyle BD, Costerton JW, Caldwell DE. Optical sectioning of microbial biofilms. *J Bacteriol* 1991;173(20):6558-67.
420. Raff MC. Social controls on cell survival and cell death. *Nature* 1992;356(6368):397-400.
421. Steinmoen H, Knutsen E, Håvarstein LS. Induction of natural competence in *Streptococcus pneumoniae* triggers lysis and DNA release from a subfraction of the cell population. *Proc Natl Acad Sci U S A* 2002;99(11):7681-6.
422. Steller H. Mechanisms and genes of cellular suicide. *Science* 1995;267(5203):1445-9.
423. Vaux DL, Haecker G, Strasser A. An evolutionary perspective on apoptosis. *Cell* 1994;76(5):777-9.
424. Jakubovics NS, Shields RC, Rajarajan N, Burgess JG. Life after death: the critical role of extracellular DNA in microbial biofilms. *Lett Appl Microbiol* 2013;57(6):467-75.
425. Thomas VC, Thurlow LR, Boyle D, Hancock LE. Regulation of autolysis-dependent extracellular DNA release by *Enterococcus faecalis* extracellular proteases influences biofilm development. *J Bacteriol* 2008;190(16):5690-8.
426. Thomas VC, Hiromasa Y, Harms N, Thurlow L, Tomich J, Hancock LE. A fratricidal mechanism is responsible for eDNA release and contributes to biofilm development of *Enterococcus faecalis*. *Mol Microbiol* 2009;72(4):1022-36.
427. Cvitkovitch DG, Li YH, Ellen RP. Quorum sensing and biofilm formation in Streptococcal infections. *J Clin Invest* 2003;112(11):1626-32.
428. Dufour D, Cordova M, Cvitkovitch DG, Lévesque CM. Regulation of the competence pathway as a novel role associated with a streptococcal bacteriocin. *J Bacteriol* 2011;193(23):6552-9.
429. Kreft JU. Biofilms promote altruism. *Microbiology* 2004;150(Pt 8):2751-60.
430. Kuramitsu HK, He X, Lux R, Anderson MH, Shi W. Interspecies interactions within oral microbial communities. *Microbiol Mol Biol Rev* 2007;71(4):653-70.
431. Nadell CD, Xavier JB, Foster KR. The sociobiology of biofilms. *FEMS Microbiol Rev* 2009;33(1):206-24.

432. Donlan RM. Biofilms: microbial life on surfaces. *Emerg Infect Dis* 2002;8(9):881-90.
433. Rupp CJ, Fux CA, Stoodley P. Viscoelasticity of *Staphylococcus aureus* biofilms in response to fluid shear allows resistance to detachment and facilitates rolling migration. *Appl Environ Microbiol* 2005;71(4):2175-8.
434. Wellman N, Fortun SM, McLeod BR. Bacterial biofilms and the bioelectric effect. *Antimicrob Agents Chemother* 1996;40(9):2012-4.
435. Spadaro JA, Berger TJ, Barranco SD, Chapin SE, Becker RO. Antibacterial effects of silver electrodes with weak direct current. *Antimicrob Agents Chemother* 1974;6(5):637-42.
436. Beattie JM, Lewis FC. The Electric Current (apart from the Heat Generated): A Bacteriological Agent in the Sterilization of Milk and other Fluids. *J Hyg (Lond)* 1925;24(2):123-37.
437. Steiner M, Ramp WK. Electrical stimulation of bone and its implications for endosseous dental implantation. *J Oral Implantol* 1990;16(1):20-7.
438. Ehrensberger MT, Tobias ME, Nodzo SR, Hansen LA, Luke-Marshall NR, Cole RF, Wild LM, Campagnari AA. Cathodic voltage-controlled electrical stimulation of titanium implants as treatment for methicillin-resistant *Staphylococcus aureus* periprosthetic infections. *Biomaterials* 2015;41:97-105.
439. Martin RM. Piezoelectricity. *Physical Review B* 1972;4:1607-13.
440. Weber N, Lee YS, Shanmugasundaram S, Jaffe M, Arinze TL. Characterization and in vitro cytocompatibility of piezoelectric electrospun scaffolds. *Acta Biomater* 2010;6(9):3550-6.
441. Costa R, Ribeiro C, Lopes AC, Martins P, Sencadas V, Soares R, Lanceros-Mendez S. Osteoblast, fibroblast and in vivo biological response to poly(vinylidene fluoride) based composite materials. *J Mater Sci Mater Med* 2013;24(2):395-403.
442. Heitz-Mayfield LJ, Lang NP. Comparative biology of chronic and aggressive periodontitis vs. peri-implantitis. *Periodontol* 2000 2010;53:167-81.
443. Dhir S. Biofilm and dental implant: The microbial link. *J Indian Soc Periodontol* 2013;17(1):5-11.
444. Murray PA, Prakobphol A, Lee T, Hoover CI, Fisher SJ. Adherence of oral streptococci to salivary glycoproteins. *Infect Immun* 1992;60(1):31-8.
445. Rath H, Stumpp NS, Stiesch M. Development of a flow chamber system for the reproducible *in vitro* analysis of biofilm formation on implant material. *Clinic of*

- Prosthetic Dentistry and Biomedical Materials Science, Hannover Medical School, Hannover, Germany. PLoS One; unpublished 2017.
446. Robertson B, Astumian RD. Michaelis-Menten equation for an enzyme in an oscillating electric field. *Biophys J* 1990;58(4):969-74.
  447. Petrofsky J, Schwab E, Lo T, Cúneo M, George J, Kim J, Al-Malty A. Effects of electrical stimulation on skin blood flow in controls and in and around stage III and IV wounds in hairy and non hairy skin. *Med Sci Monit* 2005;11(7):CR309-16.
  448. Wattanakaroon W, Stewart PS. Electrical enhancement of *Streptococcus gordonii* biofilm killing by gentamicin. *Arch Oral Biol* 2000;45(2):167-71.
  449. Sandvik EL, McLeod BR, Parker AE, Stewart PS. Direct electric current treatment under physiologic saline conditions kills *Staphylococcus epidermidis* biofilms via electrolytic generation of hypochlorous acid. *PLoS One* 2013;8(2):e55118.
  450. Garrett TR, Bhakoo M, Zhang Z. Bacterial adhesion and and biofilms on surfaces. *Prog. Nat. Sci* 2008;18:1049-56.
  451. Rowland BM. Bacterial contamination of dental unit waterlines: what is your dentist spraying into your mouth? *Clin Microbiol Newslett* 2003;25:73-7.
  452. Booth IR. Regulation of cytoplasmic pH in bacteria. *Microbiol. Rev.* 1985;49:359-78.
  453. Oliveira R, Melo L, Oliveira A, Salgueiro R. Polysaccharide production and biofilm formation by *Pseudomonas fluorescens*: effects of pH and surface material. *Colloids Surf. B: Biointerf.* 1994;241-6.
  454. Takahashi N, Schachtele CF. Effect of pH on the growth and proteolytic activity of *Porphyromonas gingivalis* and *Bacteroides intermedius*. *J Dent Res* 1990;69(6):1266-9.
  455. Roger P, Delettre J, Bouix M, Béal C. Characterization of *Streptococcus salivarius* growth and maintenance in artificial saliva. *J Appl Microbiol* 2011;111(3):631-41.
  456. Pöllänen MT, Paino A, Ihalin R. Environmental stimuli shape biofilm formation and the virulence of periodontal pathogens. *Int J Mol Sci* 2013;14(8):17221-37.
  457. Fleige S, Pfaffl MW. RNA integrity and the effect on the real-time qRT-PCR performance. *Mol Aspects Med* 2006;27(2-3):126-39.
  458. Auer H, Lyianarachchi S, Newsom D, Klisovic MI, Marcucci G, Marcucci U, Kornacker K. Chipping away at the chip bias: RNA degradation in microarray analysis. *Nat Genet* 2003;35(4):292-3.
  459. Jahn CE, Charkowski AO, Willis DK. Evaluation of isolation methods and RNA integrity for bacterial RNA quantitation. *J Microbiol Methods* 2008;75(2):318-24.

460. Frazão C, McVey CE, Amblar M, Barbas A, Vonnrhein C, Arraiano CM, Carrondo MA. Unravelling the dynamics of RNA degradation by ribonuclease II and its RNA-bound complex. *Nature* 2006;443(7107):110-4.
461. Vandeventer PE, Weigel KM, Salazar J, Erwin B, Irvine B, Doeblner R, Nadim A, Cangelosi GA, Niemz A. Mechanical disruption of lysis-resistant bacterial cells by use of a miniature, low-power, disposable device. *J Clin Microbiol* 2011;49(7):2533-9.
462. Newton MA, Kendzierski CM, Richmond CS, Blattner FR, Tsui KW. On differential variability of expression ratios: improving statistical inference about gene expression changes from microarray data. *J Comput Biol* 2001;8(1):37-52.
463. Tran PH, Peiffer DA, Shin Y, Meek LM, Brody JP, Cho KW. Microarray optimizations: increasing spot accuracy and automated identification of true microarray signals. *Nucleic Acids Res* 2002;30(12):e54.
464. Lee ML, Kuo FC, Whitmore GA, Sklar J. Importance of replication in microarray gene expression studies: statistical methods and evidence from repetitive cDNA hybridizations. *Proc Natl Acad Sci U S A* 2000;97(18):9834-9.
465. Casneuf T, Van de Peer Y, Huber W. In situ analysis of cross-hybridisation on microarrays and the inference of expression correlation. *BMC Bioinformatics* 2007;8:461.
466. del Solar G, Giraldo R, Ruiz-Echevarría MJ, Espinosa M, Díaz-Orejas R. Replication and control of circular bacterial plasmids. *Microbiol Mol Biol Rev* 1998;62(2):434-64.
467. Wegrzyn G, Wegrzyn A. Stress responses and replication of plasmids in bacterial cells. *Microb Cell Fact* 2002;1(1):2.
468. Roberts RJ. Restriction enzymes and their isoschizomers. *Nucleic Acids Res* 1990;18 Suppl:2331-65.
469. Zhang Y, Whiteley M, Kreth J, Lei Y, Khammanivong A, Evavold JN, Fan J, Herzberg MC. The two-component system BfrAB regulates expression of ABC transporters in *Streptococcus gordonii* and *Streptococcus sanguinis*. *Microbiology* 2009;155(Pt 1):165-73.
470. Choy E, Chiu VK, Silletti J, Feoktistov M, Morimoto T, Michaelson D, Ivanov IE, Philips MR. Endomembrane trafficking of ras: the CAAX motif targets proteins to the ER and Golgi. *Cell* 1999;98(1):69-80.
471. Maeda Y, Kinoshita T. Dolichol-phosphate mannose synthase: structure, function and regulation. *Biochim Biophys Acta* 2008;1780(6):861-8.

472. Rowland P, Nørager S, Jensen KF, Larsen S. Structure of dihydroorotate dehydrogenase B: electron transfer between two flavin groups bridged by an iron-sulphur cluster. *Structure* 2000;8(12):1227-38.
473. Yamada H, Nagao A, Nishise H, Tani Y. Formation of glycerol dehydrogenase by microorganism. In: Chem AB, editor. *Agric. Biol. Chem.: Agric. Biol. Chem.* 1982;46: 2325-31.
474. Ruzheinikov SN, Burke J, Sedelnikova S, Baker PJ, Taylor R, Bullough PA, Muir NM, Gore MG, Rice DW. Glycerol dehydrogenase. structure, specificity, and mechanism of a family III polyol dehydrogenase. *Structure* 2001;9(9):789-802.
475. Davidson AL, Dassa E, Orelle C, Chen J. Structure, function, and evolution of bacterial ATP-binding cassette systems. *Microbiol Mol Biol Rev* 2008;72(2):317-64, table of contents.
476. Saier MH. A functional-phylogenetic classification system for transmembrane solute transporters. *Microbiol Mol Biol Rev* 2000;64(2):354-411.
477. Kolenbrander PE, Andersen RN, Ganeshkumar N. Nucleotide sequence of the *Streptococcus gordonii* PK488 coaggregation adhesin gene, scaA, and ATP-binding cassette. *Infect Immun* 1994;62(10):4469-80.
478. Hinsa SM, Espinosa-Urgel M, Ramos JL, O'Toole GA. Transition from reversible to irreversible attachment during biofilm formation by *Pseudomonas fluorescens* WCS365 requires an ABC transporter and a large secreted protein. *Mol Microbiol* 2003;49(4):905-18.
479. Sauer K, Camper AK. Characterization of phenotypic changes in *Pseudomonas putida* in response to surface-associated growth. *J Bacteriol* 2001;183(22):6579-89.
480. Sauer K. The genomics and proteomics of biofilm formation. *Genome Biol* 2003;4(6):219.
481. Chakraborty K. Translational regulation by ABC systems. *Res Microbiol* 2001;152(3-4):391-9.
482. Tolner B, Ubbink-Kok T, Poolman B, Konings WN. Characterization of the proton/glutamate symport protein of *Bacillus subtilis* and its functional expression in *Escherichia coli*. *J Bacteriol* 1995;177(10):2863-9.
483. Kiliç AO, Tao L, Zhang Y, Lei Y, Khammanivong A, Herzberg MC. Involvement of *Streptococcus gordonii* beta-glucoside metabolism systems in adhesion, biofilm formation, and in vivo gene expression. *J Bacteriol* 2004;186(13):4246-53.



484. Loo CY, Mitrakul K, Voss IB, Hughes CV, Ganeshkumar N. Involvement of an inducible fructose phosphotransferase operon in *Streptococcus gordonii* biofilm formation. *J Bacteriol* 2003;185(21):6241-54.
485. Iiams V, Desai BJ, Fedorov AA, Fedorov EV, Almo SC, Gerlt JA. Mechanism of the orotidine 5'-monophosphate decarboxylase-catalyzed reaction: importance of residues in the orotate binding site. *Biochemistry* 2011;50(39):8497-507.
486. Martinussen J, Schallert J, Andersen B, Hammer K. The pyrimidine operon *pyrRPB-carA* from *Lactococcus lactis*. *J Bacteriol* 2001;183(9):2785-94.
487. Dunn MF, Niks D, Ngo H, Barends TR, Schlichting I. Tryptophan synthase: the workings of a channeling nanomachine. *Trends Biochem Sci* 2008;33(6):254-64.
488. Gaballa A, Helmann JD. A peroxide-induced zinc uptake system plays an important role in protection against oxidative stress in *Bacillus subtilis*. *Mol Microbiol* 2002;45(4):997-1005.
489. Faulkner MJ, Helmann JD. Peroxide stress elicits adaptive changes in bacterial metal ion homeostasis. *Antioxid Redox Signal* 2011;15(1):175-89.
490. Shafeeq S, Kuipers OP, Kloosterman TG. The role of zinc in the interplay between pathogenic streptococci and their hosts. *Mol Microbiol* 2013;88(6):1047-57.
491. Lagartera L, González A, Hermoso JA, Saíz JL, García P, García JL, Menéndez M. Pneumococcal phosphorylcholine esterase, *Pce*, contains a metal binuclear center that is essential for substrate binding and catalysis. *Protein Sci* 2005;14(12):3013-24.
492. Hammerschmidt S. Surface-exposed adherence molecules of *Streptococcus pneumoniae*. *Methods Mol Biol* 2009;470:29-45.
493. Galperin MY, Koonin EV. A diverse superfamily of enzymes with ATP-dependent carboxylate-amine/thiol ligase activity. *Protein Sci* 1997;6(12):2639-43.
494. Bijtenhoorn P, Mayerhofer H, Müller-Dieckmann J, Utpatel C, Schipper C, Hornung C, Szesny M, Grond S, Thürmer A, Brzuszkiewicz E and others. A novel metagenomic short-chain dehydrogenase/reductase attenuates *Pseudomonas aeruginosa* biofilm formation and virulence on *Caenorhabditis elegans*. *PLoS One* 2011;6(10):e26278.
495. Oppermann U, Filling C, Hult M, Shafqat N, Wu X, Lindh M, Shafqat J, Nordling E, Kallberg Y, Persson B and others. Short-chain dehydrogenases/reductases (SDR): the 2002 update. *Chem Biol Interact* 2003;143-144:247-53.
496. Hyde GE, Crawford NM, Campbell WH. The sequence of squash NADH:nitrate reductase and its relationship to the sequences of other flavoprotein oxidoreductases. A

- family of flavoprotein pyridine nucleotide cytochrome reductases. *J Biol Chem* 1991;266(35):23542-7.
497. Niraula NP, Shrestha P, Oh TJ, Sohng JK. Identification and characterization of a NADH oxidoreductase involved in phenylacetic acid degradation pathway from *Streptomyces peucetius*. *Microbiol Res* 2010;165(8):649-56.
498. Yu S, Su T, Wu H, Liu S, Wang D, Zhao T, Jin Z, Du W, Zhu MJ, Chua SL and others. PslG, a self-produced glycosyl hydrolase, triggers biofilm disassembly by disrupting exopolysaccharide matrix. *Cell Res* 2015;25(12):1352-67.
499. Latchford JW, Borthakur D, Johnston AW. The products of *Rhizobium* genes, *psi* and *pss*, which affect exopolysaccharide production, are associated with the bacterial cell surface. *Mol Microbiol* 1991;5(9):2107-14.
500. Yan L, Boyd KG, Adams DR, Burgess JG. Biofilm-specific cross-species induction of antimicrobial compounds in bacilli. *Appl Environ Microbiol* 2003;69(7):3719-27.
501. Amari DT, Marques CN, Davies DG. The putative enoyl-coenzyme A hydratase DspI is required for production of the *Pseudomonas aeruginosa* biofilm dispersion autoinducer *cis*-2-decenoic acid. *J Bacteriol* 2013;195(20):4600-10.
502. Barber CE, Tang JL, Feng JX, Pan MQ, Wilson TJ, Slater H, Dow JM, Williams P, Daniels MJ. A novel regulatory system required for pathogenicity of *Xanthomonas campestris* is mediated by a small diffusible signal molecule. *Mol Microbiol* 1997;24(3):555-66.
503. Slater H, Alvarez-Morales A, Barber CE, Daniels MJ, Dow JM. A two-component system involving an HD-GYP domain protein links cell-cell signalling to pathogenicity gene expression in *Xanthomonas campestris*. *Mol Microbiol* 2000;38(5):986-1003.
504. Pasmán Z, von Hippel PH. Regulation of rho-dependent transcription termination by NusG is specific to the *Escherichia coli* elongation complex. *Biochemistry* 2000;39(18):5573-85.
505. Zhou Y, Filter JJ, Court DL, Gottesman ME, Friedman DI. Requirement for NusG for transcription antitermination in vivo by the lambda N protein. *J Bacteriol* 2002;184(12):3416-8.
506. Ni L, Xu W, Kumaraswami M, Schumacher MA. Plasmid protein TubR uses a distinct mode of HTH-DNA binding and recruits the prokaryotic tubulin homolog TubZ to effect DNA partition. *Proc Natl Acad Sci U S A* 2010;107(26):11763-8.

507. Ueda A, Attila C, Whiteley M, Wood TK. Uracil influences quorum sensing and biofilm formation in *Pseudomonas aeruginosa* and fluorouracil is an antagonist. *Microb Biotechnol* 2009;2(1):62-74.
508. Lunsford RD, Roble AG. comYA, a gene similar to comGA of *Bacillus subtilis*, is essential for competence-factor-dependent DNA transformation in *Streptococcus gordonii*. *J Bacteriol* 1997;179(10):3122-6.
509. Kössel H, RajBhandary UL. Studies on polynucleotides. LXXXVI. Enzymic hydrolysis of N-acylaminoacyl-transfer RNA. *J Mol Biol* 1968;35(3):539-60.
510. Cuzin F, Kretchmer N, Greenberg RE, Hurwitz R, Chapeville F. Enzymatic hydrolysis of N-substituted aminoacyl-tRNA. *Proc Natl Acad Sci U S A* 1967;58(5):2079-86.
511. Das G, Varshney U. Peptidyl-tRNA hydrolase and its critical role in protein biosynthesis. *Microbiology* 2006;152(Pt 8):2191-5.
512. Ito K, Murakami R, Mochizuki M, Qi H, Shimizu Y, Miura K, Ueda T, Uchiumi T. Structural basis for the substrate recognition and catalysis of peptidyl-tRNA hydrolase. *Nucleic Acids Res* 2012;40(20):10521-31.
513. Karimi R, Pavlov MY, Heurgué-Hamard V, Buckingham RH, Ehrenberg M. Initiation factors IF1 and IF2 synergistically remove peptidyl-tRNAs with short polypeptides from the P-site of translating *Escherichia coli* ribosomes. *J Mol Biol* 1998;281(2):241-52.
514. Rao AR, Varshney U. Specific interaction between the ribosome recycling factor and the elongation factor G from *Mycobacterium tuberculosis* mediates peptidyl-tRNA release and ribosome recycling in *Escherichia coli*. *EMBO J* 2001;20(11):2977-86.
515. Schnetz K, Rak B. IS5: a mobile enhancer of transcription in *Escherichia coli*. *Proc Natl Acad Sci U S A* 1992;89(4):1244-8.
516. Aziz RK, Breitbart M, Edwards RA. Transposases are the most abundant, most ubiquitous genes in nature. *Nucleic Acids Res* 2010;38(13):4207-17.
517. Nelson KE, Fleischmann RD, DeBoy RT, Paulsen IT, Fouts DE, Eisen JA, Daugherty SC, Dodson RJ, Durkin AS, Gwinn M and others. Complete genome sequence of the oral pathogenic *Bacterium porphyromonas gingivalis* strain W83. *J Bacteriol* 2003;185(18):5591-601.



## 7. Supplementary Information

The following book chapter manuscript is the additional detailed numerical investigation of the biofilm formation of *S. gordonii* under physiological-like flow conditions (*section 4.2*). For the model, the experimental data from *section 4.2* were implemented into the simulation. The manuscript of the book chapter manuscript was submitted to *Lecture Notes in Applied and Computational Mechanics*, Springer Verlag, **2016**. The initial manuscript was written by DIANLEI FENG and HENRYKE RATH and refined by Dr. SASCHA NICO STUMPP, Prof. Dr. INSA NEUWEILER, Prof. Dr. UDO NACKENHORST, and Prof. Dr. MEIKE STIESCH.

### 7.1 A deeper insight of a multi-dimensional continuous biofilm growth model: experimental observation and parameter studies

**Abstract:** *S. gordonii* is one of the first colonizing bacteria on tooth or dental implant materials forming so called biofilms together with other bacterial species. These biofilms cause severe inflammation that, as a consequence, lead to tooth or implant failure. A promising way to study the *S. gordonii* biofilm formation is by combining experimental investigations and numerical simulation. Our previous research has shown the potential to model the growth process of the *S. gordonii* biofilm in a mimic human oral environment by using a mathematical model developed by the A-K model. The parameters used for the simulation were calibrated by the experimental results. However, what are the crucial parameters having a strong influence on the biofilm growth behavior and thus need to be determined accurately is an open question. In this paper, parameter studies on four independent parameters are carried out.

#### 7.1.1 Introduction

Due to the demographical change in the world, the human population grows older nowadays. This gives clinicians the major challenge to provide good and appropriate healthcare that ensures a high quality of life in every stage of age. Special attention was drawn on dental implants within the last decades. In Germany about one million dental implants are inserted each year. They are among the most widely used medical implant systems. Despite the striking advantages of this treatment, about 20% of patients develop device-related infections which are termed “peri-implantitis”.<sup>1</sup> The human oral cavity is inhabited by over more than 700 bacterial species.<sup>2</sup> The oral microbiota contains harmless as well as (opportunistic) pathogens. The latter is directly involved in the development of oral infectious diseases like periodontitis, peri-implantitis and tooth decay.<sup>2,3</sup> Surfaces within the oral cavity are covered with bacterial

agglomerates, referred to as biofilms. These are complex structured microbial communities in which bacteria are embedded in a self-secreted EPS.<sup>4</sup> This matrix shields the bacteria from external threats. It acts as a potent diffusion barrier so that the antibiotic resistance is up to 5000 fold higher in biofilms compared to planktonic bacteria.<sup>5,6</sup> As a consequence, conventional treatments fail. If the adhesion of so called first colonizers is controlled, also further stages of biofilm development are influenced. The periodontopathogenic late colonizing species will decrease as they cannot attach to the biofilm in a stable way. One of these first colonizers is *S. gordonii*.<sup>7,8,9</sup> This is an opportunistic pathogen, gram positive bacterium that adheres to tooth or implant substratum.<sup>10,11,12</sup> The biofilm formation is influenced by environmental conditions: a) the transport of nutrients, oxygen or signaling molecules b) contribution to gene expression, c) biotransformation reactions.<sup>14,15,16,17,18</sup> For this specific study, we have designed an open flow chamber system with continuous fed of nutrients and a strategy to study the *S. gordonii* biofilm formation by combining the experimental studies together with numerical simulation.<sup>18</sup> Numerical simulations help to identify situations that lead to fast biofilm growth. A mathematical model developed by Alpkvist and Klapper (A-K model) is used to simulate the *S. gordonii* biofilm formation.<sup>20</sup> Our previous study shows that the A-K model has a good potential to describe the *S. gordonii* biofilm formation under the experimental condition for physiologic fluid oral environment. A comparison of the simulation results and experimental observations, which has been reported (as shown in section 4) is presented again in this paper.<sup>18</sup> However, quite a few parameters are required for the numerical modeling and only few of them are quantitatively measured from experiments. Therefore, parameter studies are useful in order to identify the crucial parameters that need to be well determined to make prediction with the model.<sup>19</sup> In this study, we introduce the A-K model briefly in section 2 and the numerical strategy developed by Feng *et al.* to solve the model is shortly presented in section 3.<sup>21</sup> Both the experimental and numerical set-ups are described in section 4. In section 5 an analysis of the independence of the parameters is carried out and four independent parameters are found. Then parameter studies are presented on those four crucial parameters.

## 7.1.2 Mathematical model

### 7.1.2.1 Governing equations

Based on our previous study the mathematical model (A-K model) developed by Alpkvist and Klapper has been founded to be suitable to model the *S. gordonii* biofilm growth in human oral environment.<sup>18</sup> We briefly describe the mathematical model in this section which is originally presented in Alpkvist and Klapper.<sup>20</sup> The numerical study in this paper limits to a two-

dimensional (2-d) model. The 2-d A-K model is considered within a computational domain of  $\Omega \rightarrow$  as illustrated in Figure S 1.

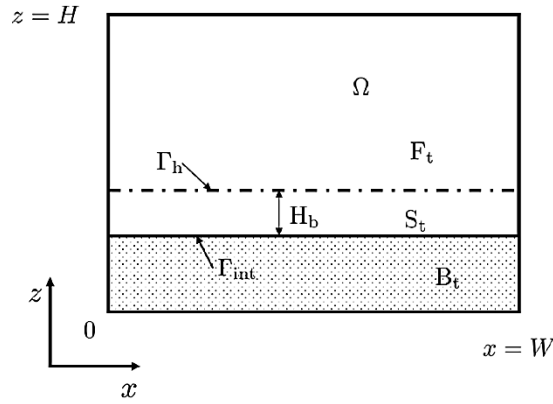


Figure S 1: Two-dimensional illustration of the computational domain.

The computational domain  $\Omega$  is composed of the time changing biofilm domain  $B_t$  and the fluid domain  $F_t$ . The biofilm-fluid interface is denoted as  $\Gamma_{\text{int}} = F_t \cap B_t$ . Even though the input medium is fully mixed with a concentration of  $\bar{s}$ , there still exists a very thin boundary layer above the biofilm-fluid interface within which is dominated by molecular diffusion. Therefore, a diffusive boundary layer of a constant thickness  $H_b$  is assumed above the biofilm-fluid interface. The domain below the top of the boundary layer  $\Gamma_h$  is a substrate transport domain  $S_t$  in which the governing transport equation of the substrate is solved. The nutrient is the TSB medium is considered as the only biofilm growth limiting substrate in this paper. Therefore, the biofilm growth rate is limited by the concentration of TSB medium  $s$  [ $\text{kg}/\text{m}^3$ ].

$$\begin{aligned}
 -D\nabla^2 s &= r(\mathbf{v}, s), & \mathbf{x} \in S_t, \\
 s &= \bar{s}, & \mathbf{x} \in \Gamma_h, \\
 \frac{\partial s}{\partial n_s} &= 0 & \mathbf{x} \in \Gamma_s.
 \end{aligned} \tag{S1}$$

Due to the time scale of the medium transport process is much smaller than the time scale of biofilm growth, it is usually considered as quasi-steady and the mass balance for the medium reads where  $D$  is the diffusion coefficient of the medium and  $r(\mathbf{v}, s)$ , describes the consumption rate of the medium by the active biomass.  $\mathbf{v} = (v_1, v_2, v_3, \dots)^T$  refers to the volume fractions of different biomass components. No-flux boundary is applied at  $\Gamma_s \rightarrow \partial S_t \cap \partial \Omega$  and  $\mathbf{n}_s$  here refers to the normal vector of  $\Gamma_s$ . We consider two components of biomass, namely the active biomass and inactive biomass that are distinguished by indexes 1 and 2 respectively. The mass balance for each component of biomass reads

$$\begin{aligned}
 \frac{\partial \mathbf{v}}{\partial t} + \nabla \cdot (\mathbf{u} \mathbf{v}) &= \mathbf{g}(\mathbf{v}, s), & \mathbf{x} \in \Omega \\
 \frac{\partial \mathbf{v}}{\partial n_b} &= 0, & \mathbf{x} \in \partial \Omega
 \end{aligned} \tag{S2}$$

where the right hand side term  $\mathbf{g}(\mathbf{v}, s) = (g_1(\mathbf{v}, s), g_2(\mathbf{v}, s))^T$  describe the transformation process of each component of biomass.  $\mathbf{v} = (v_1, v_2)^T$  refers to the volume fractions of the active biomass and inactive biomass respectively and they grow with the same velocity  $\mathbf{u}$ . The biofilm growth velocity  $\mathbf{u}$  is assumed to be irrotational. Therefore, there exists a potential  $\Phi$  that satisfies

$$\nabla * \mathbf{u} = \nabla^2 \Phi = g_1 + g_2 \quad \mathbf{x} \in B_t \quad (\text{S3})$$

Equations (S1), (S2) and (S3) compose the full A-K model used in this paper.

### 7.1.2.2 Transformation Processes

It is assumed that the medium is consumed as a consequence of self-reproduction of the active biomass. The reaction term  $r(\mathbf{v}, s)$  reads

$$r(\mathbf{v}, s) = -v_1 \rho \frac{1}{Y} \frac{\mu s}{k_s + s}, \quad (\text{S4})$$

where  $\rho$  is the density of biofilm and  $Y$  is the biofilm yield,  $\mu$  and  $k_s$  are constant parameters required in the Monod kinetic. The inactive biomass is generated by the transformation of the active biomass and the transformation process here is noted as inactivation which is described by introducing an inactivation rate  $k_i$  in the mathematical model. With all these arguments above, the terms  $g_1$  and  $g_2$  can be eventually defined as

$$\begin{aligned} g_1(\mathbf{v}, s) &= v \left( \frac{\mu s}{k_s + s} - k_i \right), \\ g_2(\mathbf{v}, s) &= v_1 k_i. \end{aligned} \quad (\text{S5})$$

### 7.1.3 Numerical strategy

To solve the governing equations (S1), (S2) and (S3) numerically is challenging. Equations (S1) and (S3) are second order elliptic partial differential equations (PDEs) which can be solved easily by using the standard finite element method. However, the boundaries  $\Gamma_{\text{int}}$  and  $\Gamma_{\text{h}}$  change over time due to the growth of biofilm. Therefore, one needs special treatment for the moving boundaries. We use the iso-line of the total biomass concentration of a threshold value as the biofilm-fluid interface and  $\Gamma_{\text{h}}$  is determined by using a rolling ball algorithm. More challenges arise when solving equation (S2) which is a set of hyperbolic PDEs with nonlinear reaction terms. To solve such PDEs accurately, higher order stable numerical schemes in both time and space are required. However, it is well known that higher order schemes suffer from instability problems. For this reason, the combined TDG-FIC (time discontinuous Galerkin - finite



incremental calculus) method is applied for solving equation (S2).<sup>22,23</sup> We refer to Feng *et al.* and Sapotnick and Nackenhorst for more detailed information of the numerical aspects.<sup>21,24</sup>

## 7.1.4 Biofilm height after 24 h: experimental observation and simulation

### 7.1.4.1. Experiment set-up

*S. gordonii* DSM 20568 was acquired from the DSMZ. The bacterium was pre-cultivated in TSBY. The bacterial solution was incubated at 37°C for 18 h under agitation. For biofilm cultivation in the flow chamber, the overnight culture was adjusted to an OD<sub>600</sub> of 0.016 with TSBYG. The starting OD<sub>600</sub> equaled 1.94 x 10<sup>6</sup> CFU/mL. The flow chamber system is a device for the *in vitro* analysis of biofilm formation under flow conditions. The flow chamber itself is 7.0 cm x 5.5 cm x 3.5 cm in size. For macroscopic and microscopic analysis, the system is provided with a 28 mm glass cover slip. The 12 mm titanium (grade 4) was used as test specimen. The system was applied and analyzed as described in Rath *et al.*<sup>388</sup> Within this study we focused on the influence of different flow velocities. Therefore, the bacterial suspension was pumped through the system with 100-400 µL/min over at 37°C. The influence of nutrient supply on biofilm formation was tested with TSBYG media concentrations between 0.1 x - 1.0 x (0.01, 0.03, 0.05, 0.06, 0.07, 0.1, 0.3, 0.5, 0.7, 1.0). The biofilm formation was performed at 37°C for 24 h with a flow velocity of constant 100 µL/min. Both experiments were performed in triplicates of independent experiments.

### 7.1.4.2 Numerical simulation and results

The study in Rath *et al.* shows that there is no significant change of biofilm height after 24 h growth under the flow discharges of 100 µL/min and 200 µL/min.<sup>18</sup> This means the detachment effect can be omitted in the case of a flow discharge of 100 µL/min. The initial thickness of biofilm is set to 1 µm which is of the length scale of single bacterium. Therefore, the initial biofilm-fluid interface is defined as

$$\Gamma_{int}^0 \rightarrow z = 1(\mu\text{m}) \quad (\text{S6})$$

Parameters used for the simulation are listed in Table S 1. Experimental observations as well as numerical simulation results are presented in Figure S 2. Error bars of the experimental results are the standard deviation calculated from different repeating measurements. The active biofilm height  $h_1$  and inactive biofilm height  $h_2$  used in the figure are defined as

$$h_i = \mathfrak{S}_i h_{\text{biofilm}} \quad (i = 1, 2) \quad (\text{S7})$$

where  $\vartheta_1$  refers to the mass fraction of the corresponding biomass in the system and  $h_{\text{biofilm}}$  is the total biofilm height. Specially, we define the inactivation fraction  $f$  of the biofilm as

$$f = \frac{\vartheta_2}{\vartheta_1 + \vartheta_2} \quad (\text{S8})$$

The mathematical model used in this paper was calibrated using the data shown in Figure S 2 and it was validated with a time series of the biofilm height. However, it would have been beneficial to have some of the parameters pre-determined. Also, the parameters need to be determined, if the model should be used to predict biofilm growth under different conditions. On the other hand, it is very difficult to measure all parameters of a biology system experimentally. For this reason, it is useful to study how the change of parameters' values influence the simulation results by carrying out parameter studies. This allows to identify those parameters that are crucial and are really needed to be measured accurately. Meanwhile, the studies can also uncover (not in a comprehensive way) the abilities of the mathematical model for predicting the biofilm growth process.

### 7.1.5 Parameter study of the mathematical method

As shown in section 4, the simulation results have good agreement with the experimental measurements if the parameters listed in Table S 1 are used. To investigate the sensitivity of the biofilm growth on the different parameters, parameter studies are carried out in the following sections. Here, we focus explicitly on the *S. gordonii* biofilm and consider the parameters that were calibrated with experiments as reference values.

**Table S 1: Parameters used for the simulation.**

Quantity name	Symbol	Value	Unit
Length of the computational domain	$W$	100	$\mu\text{m}$
Height of the computational domain	$H$	100	$\mu\text{m}$
Thickness of the boundary layer	$H_b$	15	$\mu\text{m}$
Maximum input medium concentration (1x TSB medium)	$s_{\text{max}}$	43.9	$\text{kg}/\text{m}^3$
Diffusion coefficient of TSB medium	$D$	$5 \times 10^{-10}$	$\text{m}^2/\text{s}$
Biofilm density	$\rho$	1100	$\text{kg}/\text{m}^3$
Biofilm yield	$Y$	$10^{-1}$	$[-]$
Maximum growth rate of biofilm	$\mu$	$3.0 \times 10^{-5}$	$\text{s}^{-1}$
Monod half-rate constant	$k_s$	$0.025 \times s_{\text{max}}$	$\text{kg}/\text{m}^3$
Inactivation rate	$\kappa_i$	$4.0 \times 10^{-6}$	$\text{s}^{-1}$

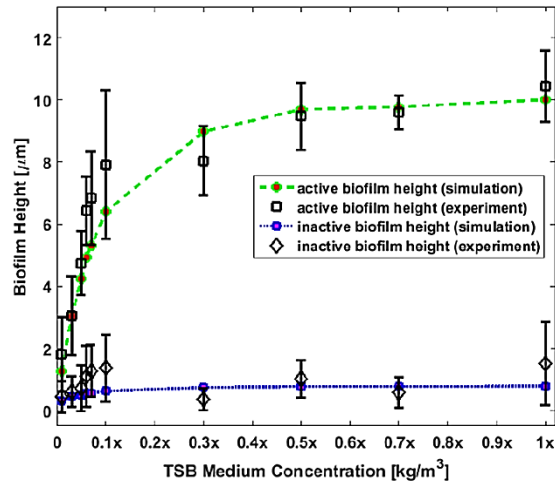


**Figure S 2: Comparison of experimental results and numerical simulation results of the biofilm height at different concentrations of medium after 24 h growth.**

Different sets of parameters are applied for numerical simulation and the influences of the parameters on active biofilm height  $h_1$ , inactive biofilm height  $h_2$  and inactivation fraction  $f$  are studied by changing these values. The results also give an illustration of what kind of bio-dynamics behaviors of biofilm can be simulated by using the A-K model. Of course, one may argue that the cases (different sets of parameters) studied in this paper cannot represent all possible results gained from the A-K model and the bio-dynamic behaviors of biofilm obtained from the parameter studies are not comprehensive. The system here is restricted to *S. gordonii* systems that close to the reference system presented in section 4. Therefore, only one parameter (the being studied one) is changed while the others are the same as the ones listed in Table S 1: Parameters used for the simulation. Moreover, the results also show the sensitivities of the biofilm heights (active and inactive) and inactivation fraction to each parameter. There are 10 parameters listed in Table S 1. Several of those parameters are fixed due to the set-up of the experiments and simulations. Those include the size of the computational domain  $W$  and  $H$  and the maximum input TSB medium concentration  $s_{max}$ . The remaining 7 parameters are not all independent as can be seen in the dimensionless governing equations. For instance, one can expect with a thicker boundary layer, less TSB medium will access the biofilm-fluid surface and same effect can be achieved by using a smaller diffusion coefficient of the TSB medium  $D$  in the diffusive boundary layer. Actually, the penetration properties of the TSB medium in the biofilm are mainly controlled by a dimensionless variable  $\theta^2 = \frac{H^2 \mu p^2}{Y D s}$  which is called the Thiele modulus. Changing of the Thiele modulus  $\theta^2$  can be achieved by changing either biofilm density  $p$ , maximum growth rate  $\mu$ , biofilm yield  $Y$  or TSB medium diffusion coefficient  $D$ . For this reason, we carry out the parameter study of the biofilm yield  $Y$  and the results can be also viewed as parameter studies results of  $\theta^2$ ,  $p$ ,  $D$  or  $H_b$ . What should be noted is that the maximum biofilm growth rate  $\mu$  appears in more than one dimensionless variable (not only in

the Thiele modulus  $\theta^2$ ) in the governing equations which means that we need to do the parameter study of  $\mu$  separately. By the end, only four parameters, namely the biofilm yield  $Y$  (can be viewed as the inverse of the Thiele modulus  $\theta^2$ ), maximum biofilm growth rate  $\mu$ , Monod half-rate constant  $k_s$  and the inactivation rate  $k_i$ , are left for parameter studies.

#### ***7.1.5.1 Influence of maximum growth rate $\mu$***

Studies on the influence of the maximum biofilm growth rate  $\mu$  are carried out with three different values of  $m$  as  $1.0 \times 10^{-5} \text{ [s}^{-1}\text{]}$ ,  $3.0 \times 10^{-5} \text{ [s}^{-1}\text{]}$  and  $5.0 \times 10^{-5} \text{ [s}^{-1}\text{]}$ . The simulation results of the active biofilm height, inactive biofilm height and inactivation fraction over the input TSB medium concentrations are shown in Figure S 3. Each point in the figure represents a 24 h simulation result. It is not surprising that generally larger biofilm heights are obtained if a larger maximum growth rate  $\mu$  is used and the growth process is limited when the supplement of the TSB medium concentration reaches a certain value (around 0.3 x standard TSB medium concentration). The results can be roughly divided into two sub-planes, namely the Plane I and Plane II as shown in Figure S 3. The solution depends on the medium concentration significantly in Plane I but is not influenced much in Plane II on the other hand. The dependency of the biofilm heights on the maximum growth rate  $\mu$  is, however, not linear. Also, for a very small value of  $\mu = 1.0 \times 10^{-5} \text{ [s}^{-1}\text{]}$ , the inactive biofilm height decreases with increasing nutrient concentrations. As we expected, the results demonstrate that the biofilm heights (active and inactive) as well as the inactivation fraction are very sensitive to the maximum biofilm growth rate  $\mu$  due to the proportional behavior, which means a properly determined (by experimental study or numerical calibration)  $\mu$  is important for modeling the biofilm growth numerically. As a remark, the real role of the maximum growth rate  $\mu$  in the mathematical model is not limited to the results of this study. For instance, one can imagine that if the TSB medium cannot fully penetrate the biofilm, the biofilm heights could be less sensitive. However, as mentioned previously, we only look into biofilm systems that are close to the reference one.

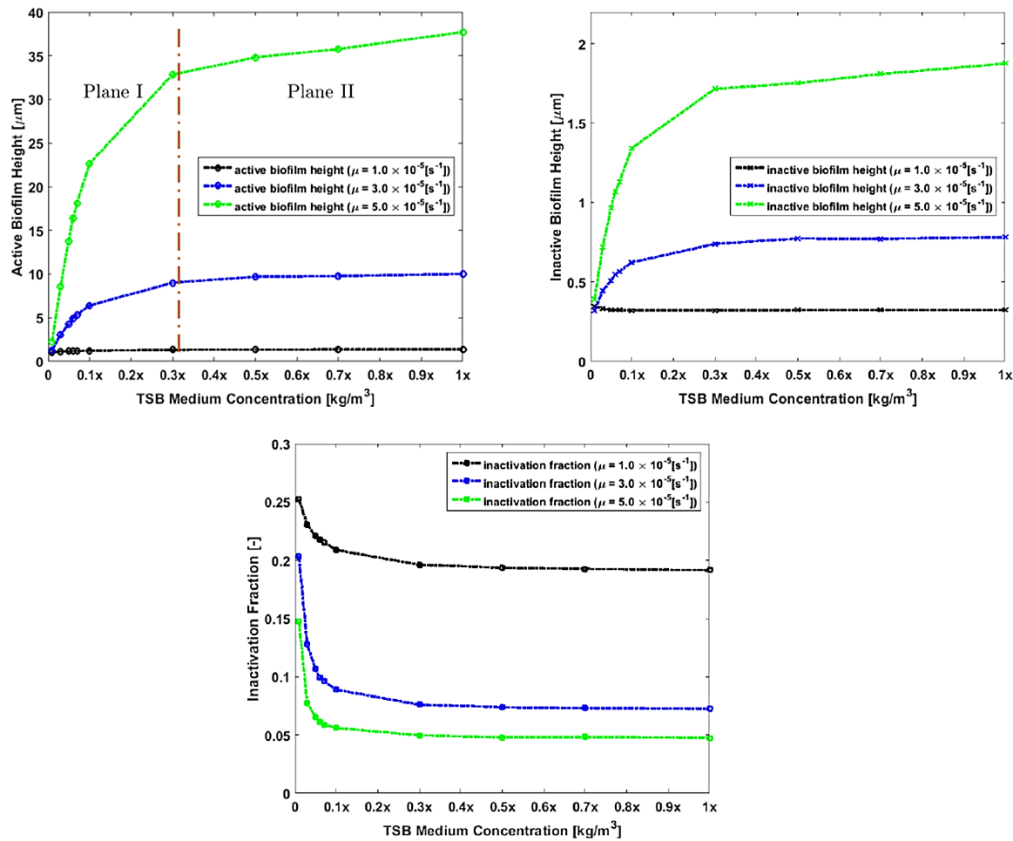


Figure S 3: Influence of the maximum biofilm growth rate  $\mu$  on the active biofilm height, inactive biofilm height and inactivation fraction over different input TSB medium concentrations.

### 7.1.5.2 Influence of monod half-rate constant $k_s$

The influence of the Monod half-rate constant  $k_s$  are studied using four different values of  $k_s$  as shown in Figure S 4 where again the results after 24 h are plotted depending on the TSB medium concentrations. It is shown that the TSB medium concentration does not influence the biofilm heights much in Plane I and the results even show a trend of converging in the cases of  $k_s = 0.025 \times s_{\max}$ ,  $k_s = 0.035 \times s_{\max}$  and  $k_s = 0.045 \times s_{\max}$  in Plane II. An interesting observation from the results is that non-monotonic behaviors (as the results plotted in the circle) of the inactive biofilm height as well as the inactivation fraction are observed in the case of  $k_s = 0.015 \times s_{\max}$ . After checking the simulation results corresponding to the plots presented in the circle, we found both the active biomass and the inactive biomass increase over an increment of the TSB medium concentrations. However, the inactivation fraction could increase or decrease (see equation S8) over the TSB medium concentration as a result of competition of the active biomass production and inactivation processes. This leads to the non-monotonic behavior of the inactivation fraction and naturally leads to a similar behavior of the inactive biofilm height as shown in the circle.

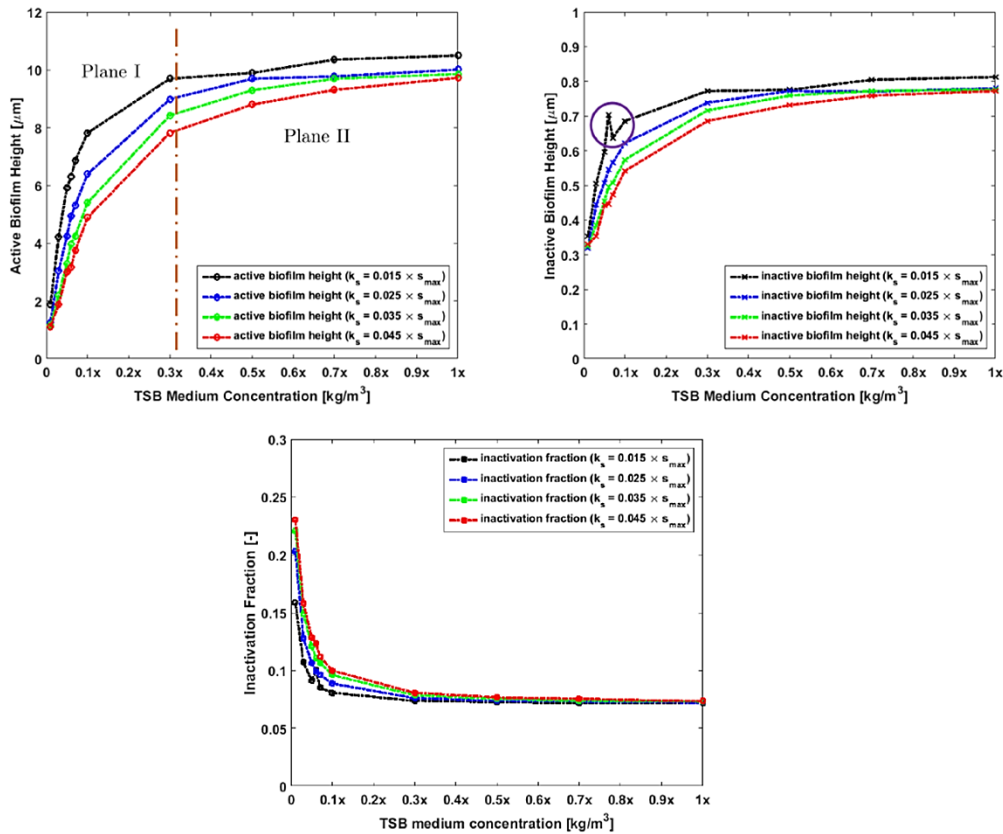


Figure S 4: Influence of the Monod half-rate constant  $k_s$  on the active biofilm height, inactive biofilm height and inactivation fraction over different input TSB medium concentrations.

### 7.1.5.3 Influence of inactivation rate $k_i$

Another important parameter used in the model is the inactivation rate  $k_i$ , which is introduced to describe the inactivation process. However, the mechanism of the inactivation is still not clear from a biologist's point of view. Our experimental results (as shown in Figure S 2: Comparison of experimental results and numerical simulation results of the biofilm height at different concentrations of medium after 24 h growth.) demonstrate that the inactivation process happens anyway no matter how large the input concentration of the TSB medium is in the system. For this reason, the inactivation process is modeled as a reaction transforming the active biomass into inactive biomass with a constant rate. Obviously, one expects that with a larger value of the inactivation rate  $k_i$ , more inactive biomass is produced and the simulation results are as expected sensitive to the inactivation rate  $k_i$  as a result of that. The results of three cases with inactivation rates of  $k_i = 4.0 \times 10^{-7}$  [s<sup>-1</sup>],  $k_i = 4.0 \times 10^{-6}$  [s<sup>-1</sup>] and  $k_i = 4.0 \times 10^{-5}$  [s<sup>-1</sup>] are illustrated in Figure S 5. It is shown that the simulation results agree with our expectation. Specially, in the case of  $k_i = 4.0 \times 10^{-7}$  [s<sup>-1</sup>], the inactivation fraction is larger than 0.6 even in the Plane II. This indicates that the amount of

inactive biomass is always more than the active biomass in this case regardless of how much medium is in the system.

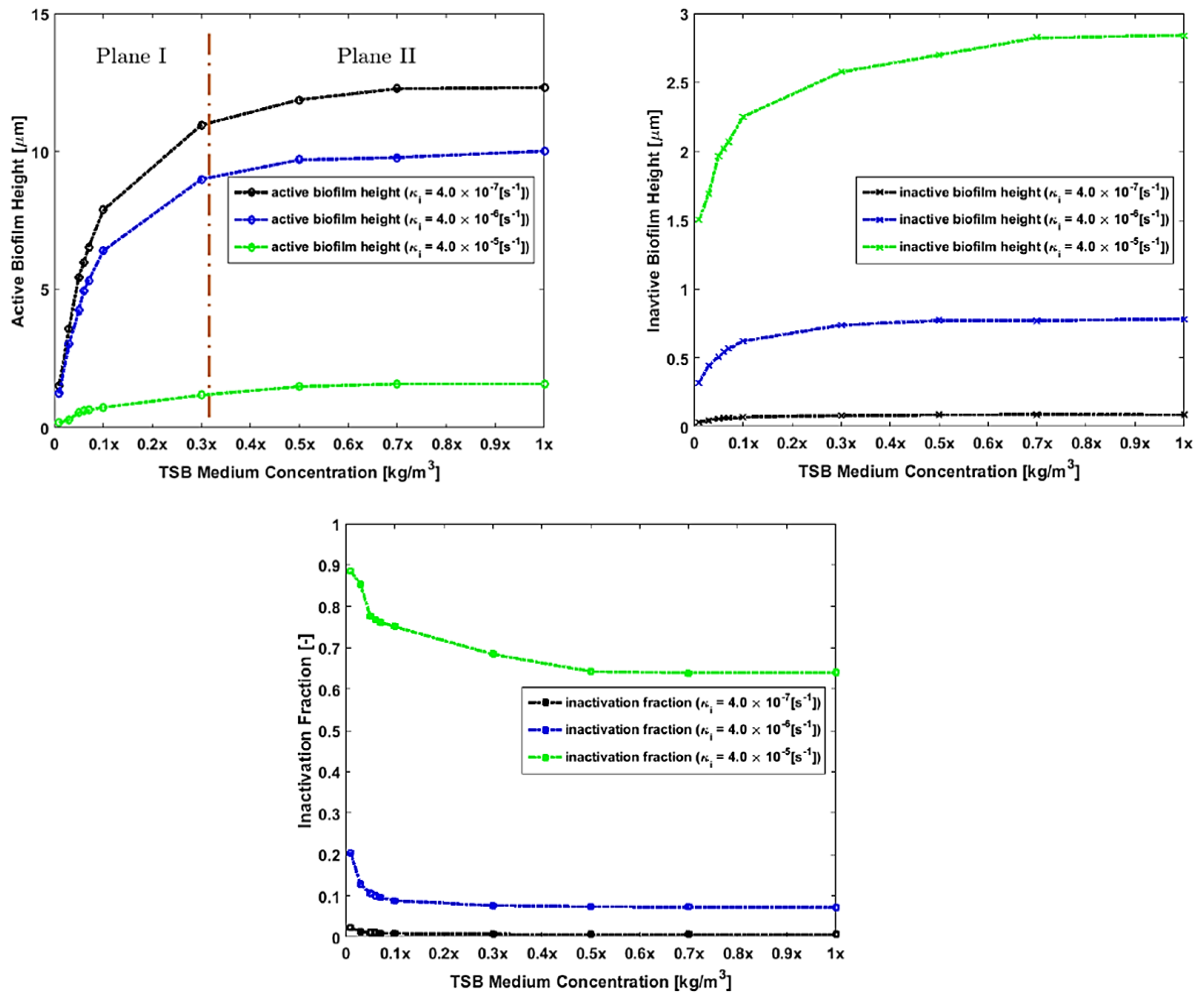


Figure S 5: Influence of the inactivation rate  $k_i$  on the active biofilm height, inactive biofilm height and inactivation fraction over different input TSB medium concentrations.

#### 7.1.5.4 Influence of biofilm yield $Y$

The influence of biofilm yield  $Y$  on the biofilm heights and the inactivation fraction is discussed in the following. The biofilm yield is widely used and can be interpreted as with one unit growth limiting substrate consumed,  $Y$  unit mass of active biomass is produced. The value of the biofilm yield depends on the species of bacteria as well as the growth limiting substrate. Simulation results of the influence of the biofilm yield  $Y$  (or Thiele modulus  $\theta^2$ ) on active biofilm height, inactive biofilm height and inactivation fraction are presented in Figure S 6. It is shown that the curves corresponding to  $Y = 1.0 \times 10^{-1}$  and  $Y = 1.0 \times 10^{-2}$  are almost coincident. This is because in both of these two cases, the biofilm yield  $Y$  is large enough to guarantee that the TSB medium fully penetrates the biofilm and all bacteria have enough medium to reproduce themselves. The result also demonstrates that changing the diffusion

coefficient of the medium a little bit in biofilm or in water will not change the final result significantly if the parameters listed in Table S 1 are used. What should be noted is that in the case of  $Y = 1.0 \times 10^{-3}$ , the TSB medium also fully penetrates the biofilm. However, the concentration is not large enough to ensure the bacteria at the bottom of the biofilm have enough TSB medium supply and the growth of the biofilm is partly limited by the medium concentration (especially in Plane I). Therefore, smaller active biofilm heights and inactive biofilm heights compared to the cases of  $Y = 1.0 \times 10^{-1}$  and  $Y = 1.0 \times 10^{-2}$  are observed in Plane I. With increase of the medium concentration, this partly limiting phenomenon is less pronounced and the results converge to the same value again. This can be verified by the time behavior of the active biofilm height shown in Figure S 7. The results of the development of the active biofilm height over time with an input TSB medium concentration of  $0.05 \times [\text{kg}/\text{m}^3]$  are shown in the left figure of Figure S 7 and the right figure illustrates the results with an input TSB medium concentration of  $1.0 \times [\text{kg}/\text{m}^3]$ . The time dependent results demonstrate that the biofilm growth velocity is not influenced much by different biofilm yield values if the values are large (e.g.  $Y = 1.0 \times 10^{-1}$  and  $Y = 1.0 \times 10^{-2}$ ). However, the biofilm grows slower in the case of  $Y = 1.0 \times 10^{-3}$  when a small input TSB medium concentration ( $0.05 \times [\text{kg}/\text{m}^3]$ ) is applied. But almost no difference is observed on the biofilm growth speed if large enough TSB medium concentration ( $1.0 \times [\text{kg}/\text{m}^3]$ ) is supplied. This explains why the curves corresponding to  $Y = 1.0 \times 10^{-1}$ ,  $Y = 1.0 \times 10^{-2}$  and  $Y = 1.0 \times 10^{-3}$  in Figure S 6 converge to the same value when the TSB medium concentration is  $1.0 \times [\text{kg}/\text{m}^3]$ . The results of an extreme case of  $Y = 1.0 \times 10^{-4}$  are presented as the red curves in Figure S 6. The TSB medium concentration is almost zero at the bottom of the biofilm which limits the biofilm growth significantly. The results shown in Figure S 7 also indicate that the biofilm growth is limited all the time in the case of  $Y = 1.0 \times 10^{-4}$  even with an input TSB medium concentration of  $1 \times$ . Overall, one can draw the conclusion that the biofilm heights and inactivation fraction are sensitive to the biofilm yield (or Thiele modulus  $\theta^2$ ) only when the biofilm yield is small enough ( $\theta^2$  is large enough). Another interesting observation is that the inactivation fraction of the case  $Y = 1.0 \times 10^{-4}$  also shows non-monotonic behavior. This is also due the competition between the active biomass production and the inactive biomass transformation as explained in *section 7.1.3.2*.



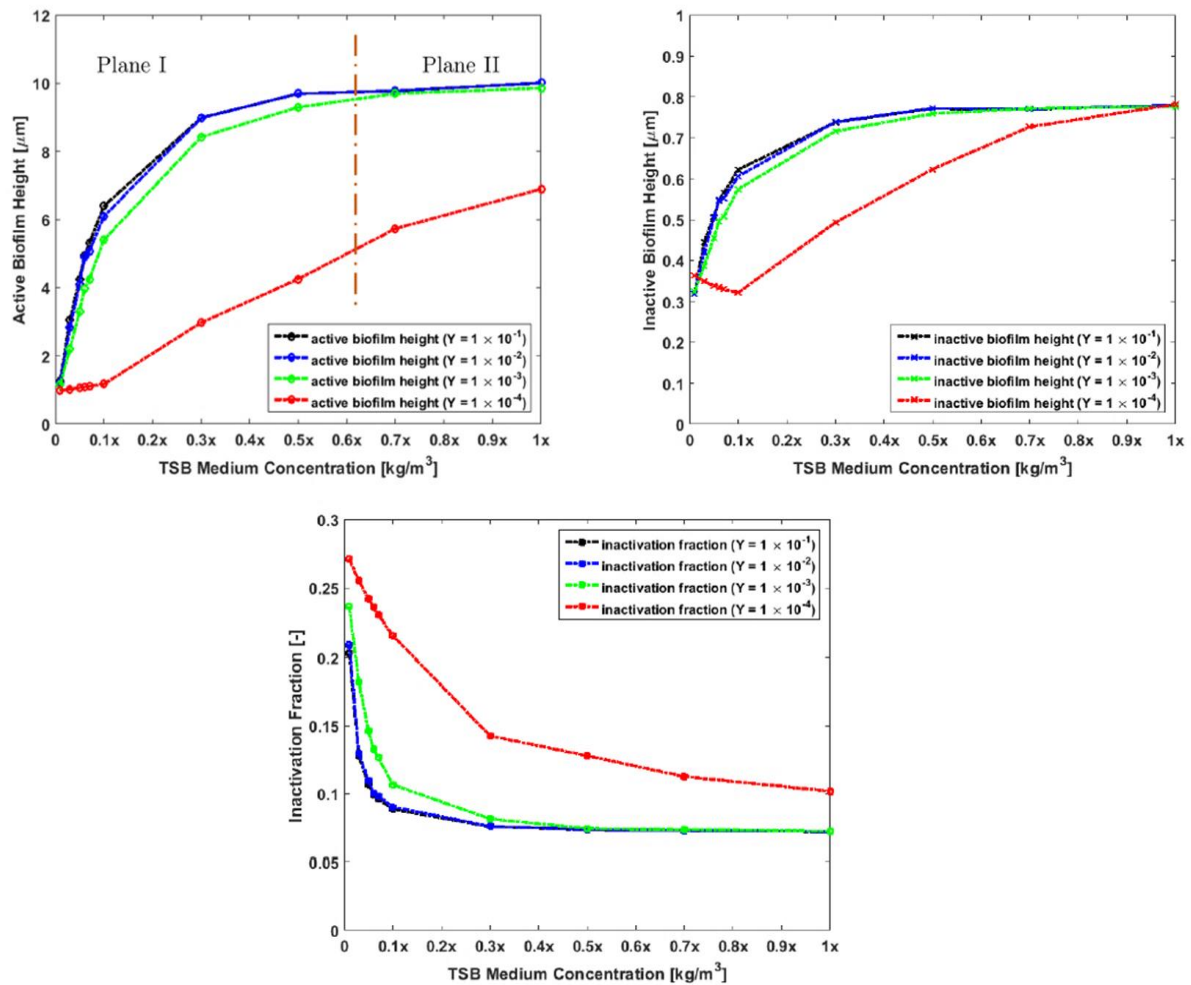


Figure S 6: Influence of the biofilm yield  $Y$  on the active biofilm height, inactive biofilm height and inactivation fraction (from top to bottom) over different input TSB medium concentrations.

### 7.1.6 Summary and conclusion

The *S. gordonii* biofilm formation within 24 h is studied by combining experimental investigations and numerical simulations. Here, the biofilm behavior was studied in a flow chamber system mimicking the physiological flow within the oral cavity. A multi-species continuum biofilm growth model (the A-K model) is applied for numerical simulation. Our previous research demonstrated that the mathematical model as well as the numerical strategy used for solving the model is capable to present the biology behavior of the *S. gordonii* biofilm formation in such an environment. In this study, parameter studies are carried out for better understanding of the model as well as the biological processes and to identify the requirements for accurately measured parameters.

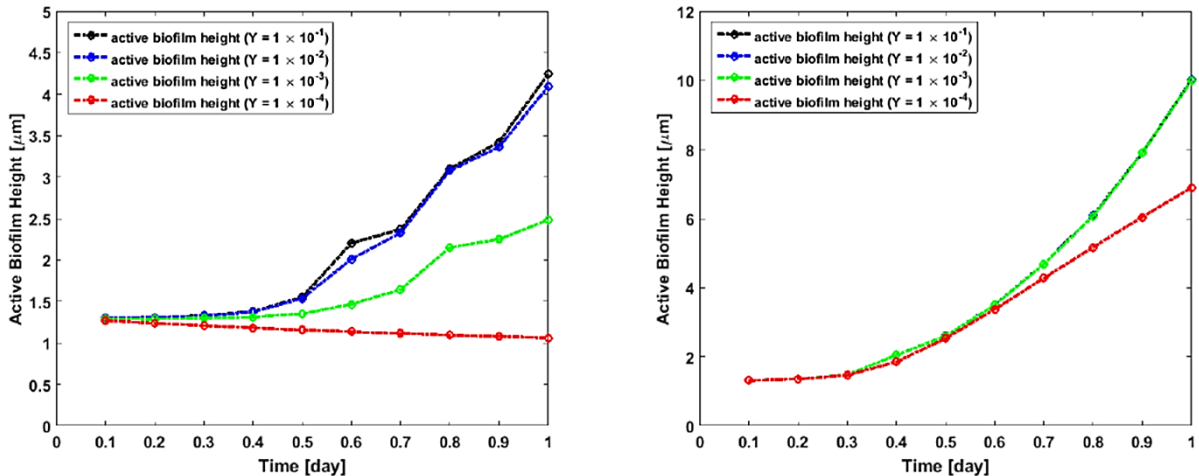


Figure S 7: Influence of the biofilm yield  $Y$  on the active biofilm height over time with input TSB medium concentrations of 0.05 x (left) and 1 x (right).

Influence of the maximum biofilm growth rate  $\mu$ , Monod half-rate constant  $k_s$ , inactivation rate  $k_i$  and biofilm yield  $Y$  (or the Thiele modulus  $\theta^2$ ) on biofilm heights (active and inactive) as well as the inactivation fraction are studied. The parameters corresponding to the realistic *S. gordonii* biofilm system are taken as the references parameter and all the parameter studies are carried out based on the reference set. As expected that the solutions are rather sensitive to the TSB medium concentrations in most of the cases when the concentration is under a certain value (in Plane I) while the results are not depending on the TSB medium concentration much with larger concentrations (in Plane II). The simulation results demonstrate that biofilm heights and inactivation fraction are sensitive to the maximum growth rate  $\mu$  and inactivation rate  $k_i$ . This is also not surprising, because the biological definitions of these two parameters relate to the biofilm heights directly. One can expect that by using a larger maximum growth rate shall lead to a thicker biofilm. However, even though our simulation results agree with our expectation, this is not always the golden rule. For instance, the biofilm growth process could also be limited as a result of too thick of a biofilm and the TSB medium can hardly fully penetrate the biofilm. This did not happen in our simulations that are close to the reference *S. gordonii* biofilm system described in section 4. We also found that the influences of the Monod half-rate constant  $k_s$  on the simulation results differ for small and large TSB medium concentrations. The simulation results demonstrate that the biofilm heights as well as the inactivation fraction are sensitive to  $k_s$  if the nutrient concentration is low while are not very sensitive to the  $k_s$  if the nutrient is sufficient. Parameter studies on the biofilm yield  $Y$  (or could also be viewed as studies on  $p$ ,  $H_b$  or  $D$  in the Thiele modulus  $\theta^2$ ) showed that the solutions are significantly influenced by the parameter only when  $Y$  is below a threshold value  $Y_{\text{crit}}$  ( $Y < Y_{\text{crit}} = 1.0 \times 10^{-3}$ ). This is due to the TSB medium, which cannot fully penetrate the

biofilm and the biofilm growth is limited by the lack of the nutrient supply. As a summary, the sensitivities of the results to these parameters are presented in Table S 2.

**Table S 2: Sensitivity of the biofilm heights  $h_1$ ,  $h_2$  and inactivation fraction  $f$  to the parameters  $\mu$ ,  $k_s$ ,  $k_i$  and  $Y$ .**

	small TSB medium concentrations			large TSB medium concentrations		
	$h_1$	$h_2$	$f$	$h_1$	$h_2$	$f$
$\mu$	high	high	high	high	high	high
$k_s$	fair	fair	small to fair	small	small	none
$k_i$	high	high	high	high	high	high
$Y \geq Y_{crit}$	small	small	small	none	none	none
$Y < Y_{crit}$	high	high	high	high	small to none	high

### 7.1.7 References

1. Mombelli A, Müller N, Cionca N. The epidemiology of peri-implantitis. *Clin Oral Implants Res* 2012;23(s6):67-76.
2. Aas JA, Paster BJ, Stokes LN, Olsen I, Dewhirst FE. Defining the normal bacterial flora of the oral cavity. *J Clin Microbiol* 2005;43(11):5721-32.
3. Raj LM, Jude J, Kannan I, Krishna PS, Shankar K. Molecular Docking Study for Inhibitors of *Aggregatibacter actinomycetemcomitans* Toxins in Treatment of Aggressive Periodontitis. *J Clin Diagn Res* 2014;8(11):ZC48-51.
4. Flemming HC, Neu TR, Wozniak DJ. The EPS matrix: the "house of biofilm cells". *J Bacteriol* 2007;189(22):7945-7.
5. Anwar H, Costerton JW. Enhanced activity of combination of tobramycin and piperacillin for eradication of sessile biofilm cells of *Pseudomonas aeruginosa*. *Antimicrob Agents Chemother* 1990;34(9):1666-71
6. Costerton JW, Ellis B, Lam K, Johnson F, Khoury AE. Mechanism of electrical enhancement of efficacy of antibiotics in killing biofilm bacteria *Antimicrob Agents Chemother* 1994;38(12):2803-9.
7. Hall-Stoodley L, Costerton JW, Stoodley P. Bacterial biofilms: from the natural environment to infectious diseases. *Nature Rev Microbiol* 2004;2(2):95-108.
8. Jung CJ, Yeh CY, Shun CT, Hsu RB, Cheng HW, Lin CS, Chia JS. Platelets enhance biofilm formation and resistance of endocarditis-inducing streptococci on the injured heart valve. *J Infect Dis* 2012;205(7):1066-75.
9. Moreillon P, Que YA. Infective endocarditis. *Lancet* 2004;363(9403):139-49.

10. Diaz PI, Chalmers NI, Rickard AH, Kong C, Milburn CL, Palmer RJ, Kolenbrander PE. Molecular characterization of subject-specific oral microflora during initial colonization of enamel. *Appl Environ Microbiol* 2006;72(4):2837-48.
11. Kilian M, Mikkelsen L., Henrichsen J. Taxonomic study of viridans streptococci: Description of *Streptococcus gordonii* sp. nov. and emended descriptions of *Streptococcus sanguis* (White and Niven 1946), *Streptococcus oralis* (Bridge and Sneath 1982), and *Streptococcus mitis* (Andrewes and Horder 1906). *Int J Syst Evol Microbiol* 1989;39(4):471-84.
12. Nyvad B, Kilian M. Microbiology of the early colonization of human enamel and root surfaces in vivo. *Eur J Oral Sci* 1987;95(5):369-80.
13. Wolfaardt GM, Lawrence RJ, Robarts RD, Caldwell SJ, Caldwell DE. Multicellular organization in a degradative biofilm community. *Appl Environ Microbiol* 1994;60(2):434-46.
14. de Beer D, Stoodley P, Lewandowski Z. Liquid flow in heterogeneous biofilms. *Biotechnol Bioeng* 1994, 44(5):636-41.
15. De Kievit TR, Iglewski BH. Bacterial quorum sensing in pathogenic relationships. *Infect Immun* 2000;68(9):4839-49.
16. Miller MB, Bassler BL. Quorum Sensing in Bacteria. *Ann Rev Microbiol* 2001;55(1):165-199.
17. Park A, Jeong HH, Lee J, Kim KP, Lee CS. Effect of shear stress on the formation of bacterial biofilm in a microfluidic channel. *BioChip J* 2011;5:236–241.
18. Rath H, Feng D, Stumpp NS, Neuweiler I, Nackenhorst U, Stiesch M. Formation of bacterial biofilms of the oral pioneer colonizer *Streptococcus gordonii*: a combined experimental and numerical study 2016. Unpublished paper.
19. Dawes C, Watanabe S, Biglow-Lecomte P, Dibdin GH. Estimation of the velocity of the salivary film at some different locations in the mouth. *J Dent Res* 1989;68(11):1479-82.
20. Alpkvist E, Klapper I. A multidimensional multispecies continuum model for heterogeneous biofilm development. *Bull Math Biol* 2007;69(2):765-89.
21. Feng D, Neuweiler I, Nackenhorst U. A spatially stabilized TDG based finite element framework for modeling biofilm growth with A-K model and numerical analysis 2016. Unpublished paper.
22. Hughes TJ, Hulbert GM. Space-time finite element methods for elastodynamics: Formulations and error estimates. *Comput Method Appl M* 1988;66(3):339-63.

23. Oñate E, Miquel J, F. Zárata. Stabilized solution of the multidimensional advection–diffusion–absorption equation using 1 linear finite elements. *Comput Fluids* 2007;36(1):92-112.
24. Sapotnick A, Nackenhorst U. On the Numerical Solution of Advection-Diffusion-Reaction Equations: Time-Discontinuous Galerkin and Finite Calculus Methods. *Int J Numer Meth Eng* 2012;92(3):301-17.



## 7.2 Theoretical and experimental evidence of the effects of varying disinfection timing

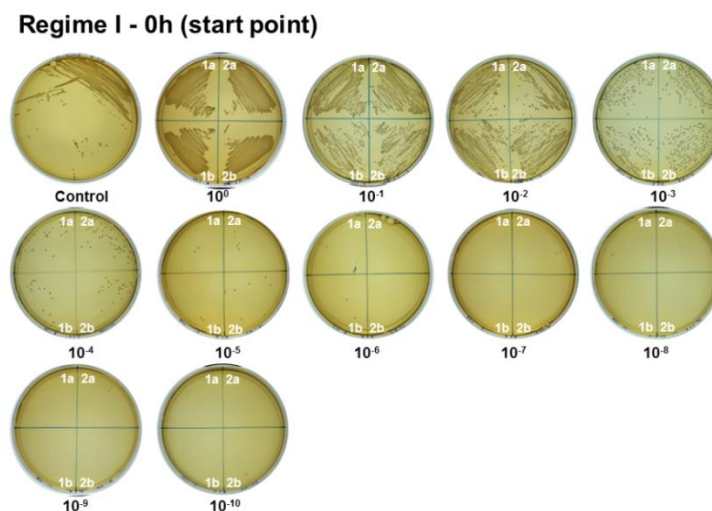
For the investigation of a numerically developed disinfection protocol for persister cells, experimental analyses have been performed with planktonic *S. aureus* cultures (section 4.4). In the following, the ofloxacin susceptibility agar plates for the detection of ofloxacin resistance are shown. Furthermore, the agar plates for the viability detection (CFU/mL) of the regime I over a period of 124 h are presented.

### 7.2.1 Susceptibility tests

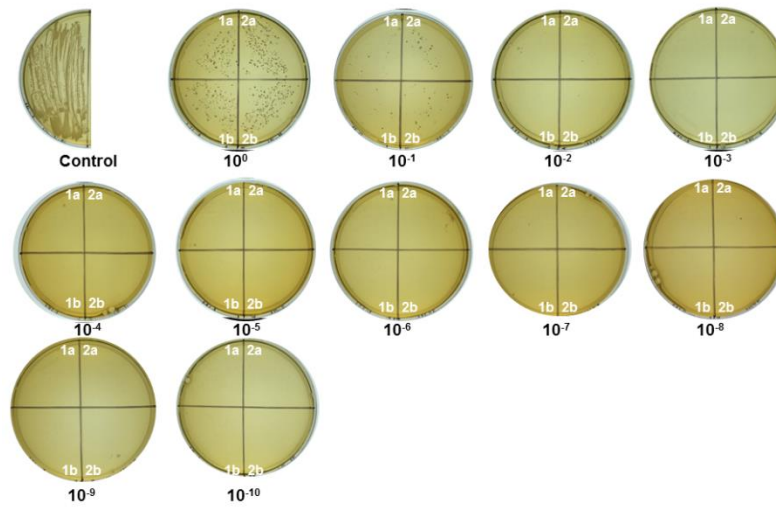


**Figure S 8: Ofloxacin susceptibility test for the identification of antibiotic resistance of *S. aureus*.** The test was performed daily with 100  $\mu$ L bacterial culture. *S. aureus* control was also investigated. Over the period of 6 d no resistance against ofloxacin was determined.

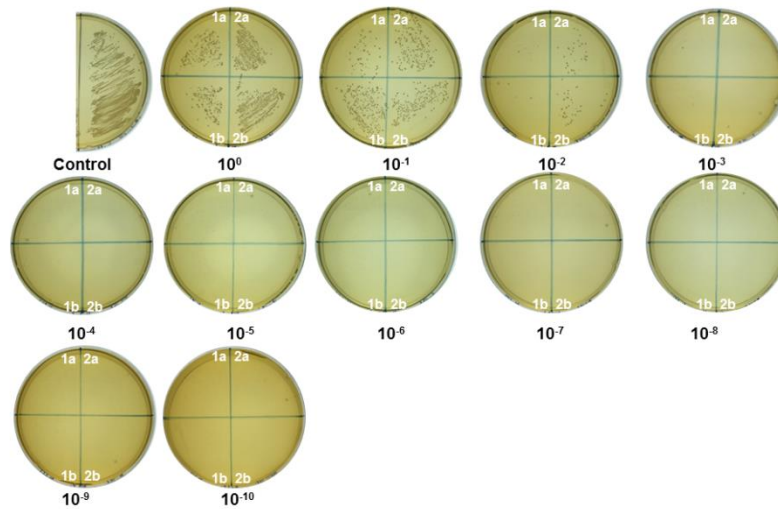
### 7.2.2 Viability test



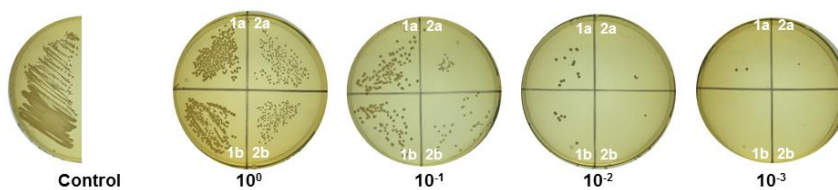
**Figure S 9: Bacterial viability testing via CFUs determination for regime I at time point 0 (start point).** After serial decimal dilutions (1:10), 10  $\mu$ L of the concentrated and the diluted bacterial cultures were then plated on TSBY agar and incubated for 24 h at 37°C. All plates were cultivated for further 48 h to exclude false negative results due to growth impairment.

**Regime I - 24h**

**Figure S 10: Bacterial viability testing via CFUs determination for regime I after 24 h.** After serial decimal dilutions (1:10), 10  $\mu$ L of the concentrated and the diluted bacterial cultures were then plated on TSBY agar and incubated for 24 h at 37°C. All plates were cultivated for further 48 h to exclude false negative results due to growth impairment.

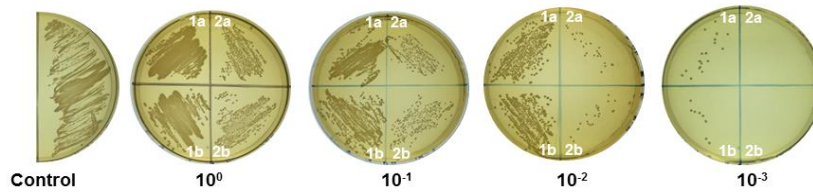
**Regime I - 28h**

**Figure S 11: Bacterial viability testing via CFUs determination for regime I after 28 h.** After serial decimal dilutions (1:10), 10  $\mu$ L of the concentrated and the diluted bacterial cultures were then plated on TSBY agar and incubated for 24 h at 37°C. All plates were cultivated for further 48 h to exclude false negative results due to growth impairment.

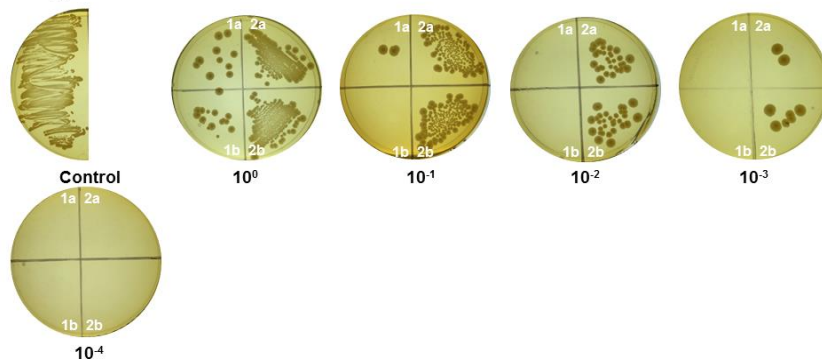
**Regime I - 48h**

**Figure S 12: Bacterial viability testing via CFUs determination for regime I after 48 h.** After serial decimal dilutions (1:10), 10  $\mu$ L of the concentrated and the diluted bacterial cultures were then plated on TSBY agar and incubated for 24 h at 37°C. All plates were cultivated for further 48 h to exclude false negative results due to growth impairment.

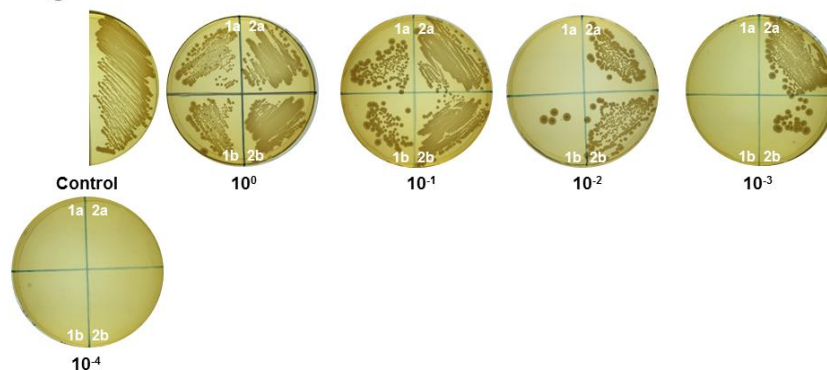


**Regime I - 52h**

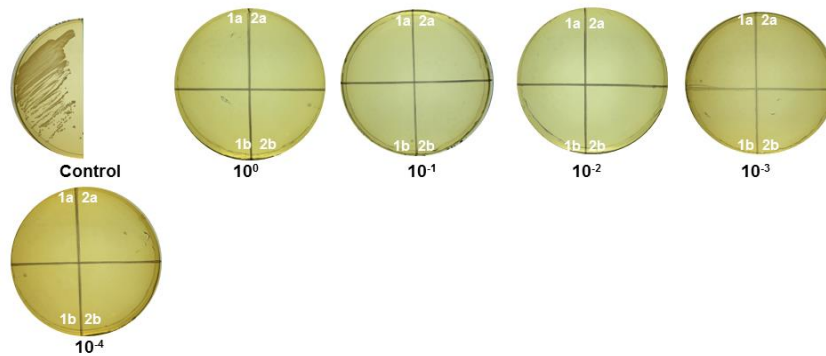
**Figure S 13: Bacterial viability testing via CFUs determination for regime I after 52 h.** After serial decimal dilutions (1:10), 10  $\mu$ L of the concentrated and the diluted bacterial cultures were then plated on TSBY agar and incubated for 24 h at 37°C. All plates were cultivated for further 48 h to exclude false negative results due to growth impairment.

**Regime I - 72h**

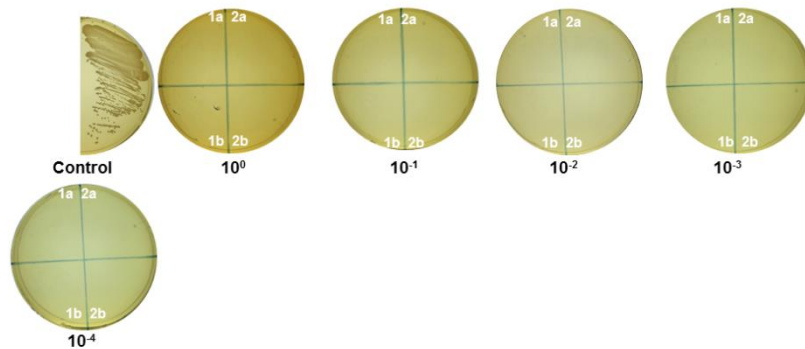
**Figure S 14: Bacterial viability testing via CFUs determination for regime I after 72 h.** After serial decimal dilutions (1:10), 10  $\mu$ L of the concentrated and the diluted bacterial cultures were then plated on TSBY agar and incubated for 24 h at 37°C. All plates were cultivated for further 48 h to exclude false negative results due to growth impairment.

**Regime I - 76h**

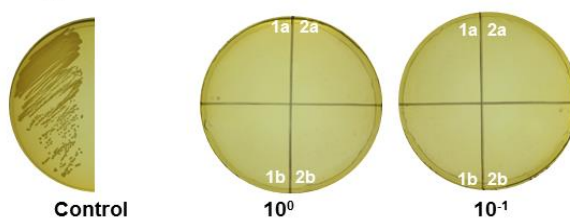
**Figure S 15: Bacterial viability testing via CFUs determination for regime I after 76 h.** After serial decimal dilutions (1:10), 10  $\mu$ L of the concentrated and the diluted bacterial cultures were then plated on TSBY agar and incubated for 24 h at 37°C. All plates were cultivated for further 48 h to exclude false negative results due to growth impairment.

**Regime I - 96h**

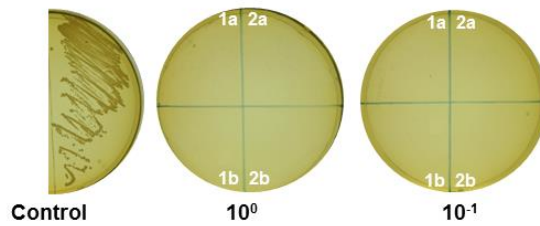
**Figure S 16: Bacterial viability testing via CFUs determination for regime I after 96 h.** After serial decimal dilutions (1:10), 10  $\mu$ L of the concentrated and the diluted bacterial cultures were then plated on TSBY agar and incubated for 24 h at 37°C. All plates were cultivated for further 48 h to exclude false negative results due to growth impairment.

**Regime I - 100h**

**Figure S 17: Bacterial viability testing via CFUs determination for regime I after 100 h.** After serial decimal dilutions (1:10), 10  $\mu$ L of the concentrated and the diluted bacterial cultures were then plated on TSBY agar and incubated for 24 h at 37°C. All plates were cultivated for further 48 h to exclude false negative results due to growth impairment.

**Regime I - 120h**

**Figure S 18: Bacterial viability testing via CFUs determination for regime I after 120 h.** After serial decimal dilutions (1:10), 10  $\mu$ L of the concentrated and the diluted bacterial cultures were then plated on TSBY agar and incubated for 24 h at 37°C. All plates were cultivated for further 48 h to exclude false negative results due to growth impairment.

**Regime I - 124h**

**Figure S 19: Bacterial viability testing via CFUs determination for regime I after 124 h.** After serial decimal dilutions (1:10), 10  $\mu$ L of the concentrated and the diluted bacterial cultures were then plated on TSBY agar and incubated for 24 h at 37°C. All plates were cultivated for further 48 h to exclude false negative results due to growth impairment.



### 7.3 Definition of electrical stimulation parameters for the inhibition of bacterial growth under static and dynamic culture conditions on PVDF membranes

In an initial study, the electrical stimulation parameter for the inhibition of the biofilm formation of three dental relevant bacteria on biocompatible PVDF membranes were determined (*section 4.5*). Beforehand, the initial parameters were defined on polystyrene for the three species. All test parameters are summarized in Table S 3. The results are presented in Figure S 20. For the determination of the viability distribution of stimulated bacteria and control, the genome sizes and weights are listed in Table S 4.

**Table S 3: Determination of electrical effective parameter on polystyrene for the static stimulation.**

organism	stimulation	strength of electric current ( $\mu\text{A}$ )	frequency (Hz)	duration ( $\mu\text{s}$ )	
<i>S. gordonii</i>	biphasic symmetrically compensated sine stimulation	20	10	60	
		100	10	60	
		1000	10	60	
		14000	1	60	
		14000	2.5	60	
		14000	5	60	
		14000	10	60	
		14000	10	60	
		biphasic symmetrically compensated rectangular pulse	20	10	60
			100	10	60
			100	100	60
			500	10	60
			800	10	60
	900		10	60	
	1000		10	60	
	1000		1	60	
	1000		50	60	
	1000		100	60	
	1000	100	10		
	1000	10	500		
	1200	10	100		
	1200	10	500		
	1400	10	100		
1400	10	500			
1600	10	100			
1600	10	500			
2000	10	60			

<b>organism</b>	<b>stimulation</b>	<b>strength of current (<math>\mu\text{A}</math>)</b>	<b>electric frequency (Hz)</b>	<b>duration (<math>\mu\text{s}</math>)</b>
		2000	10	100
		2000	10	500
		2000	10	800
<i>S. gordonii</i>	biphasic symmetrically compensated rectangular pulse	2200	10	60
		2400	10	60
		2600	10	60
<i>S. salivarius</i>	biphasic symmetrically compensated rectangular pulse	500	10	60
		1000	10	60
		1800	5	60
		1800	7.5	60
		1800	5	500
		1800	10	60
		1900	10	60
		2000	10	60
		2000	2.5	60
		2000	5	60
		3000	10	60
		4000	10	60
<i>P. gingivalis</i>	biphasic symmetrically compensated rectangular pulse	500	10	60
		1000	10	60
		1000	10	500
		1300	10	200
		2000	10	60
		2000	10	500
		3000	10	60
		3000	10	400
		3000	10	100
		3000	10	400
		3000	10	500
		3500	10	60
		3800	10	60
		4000	10	60

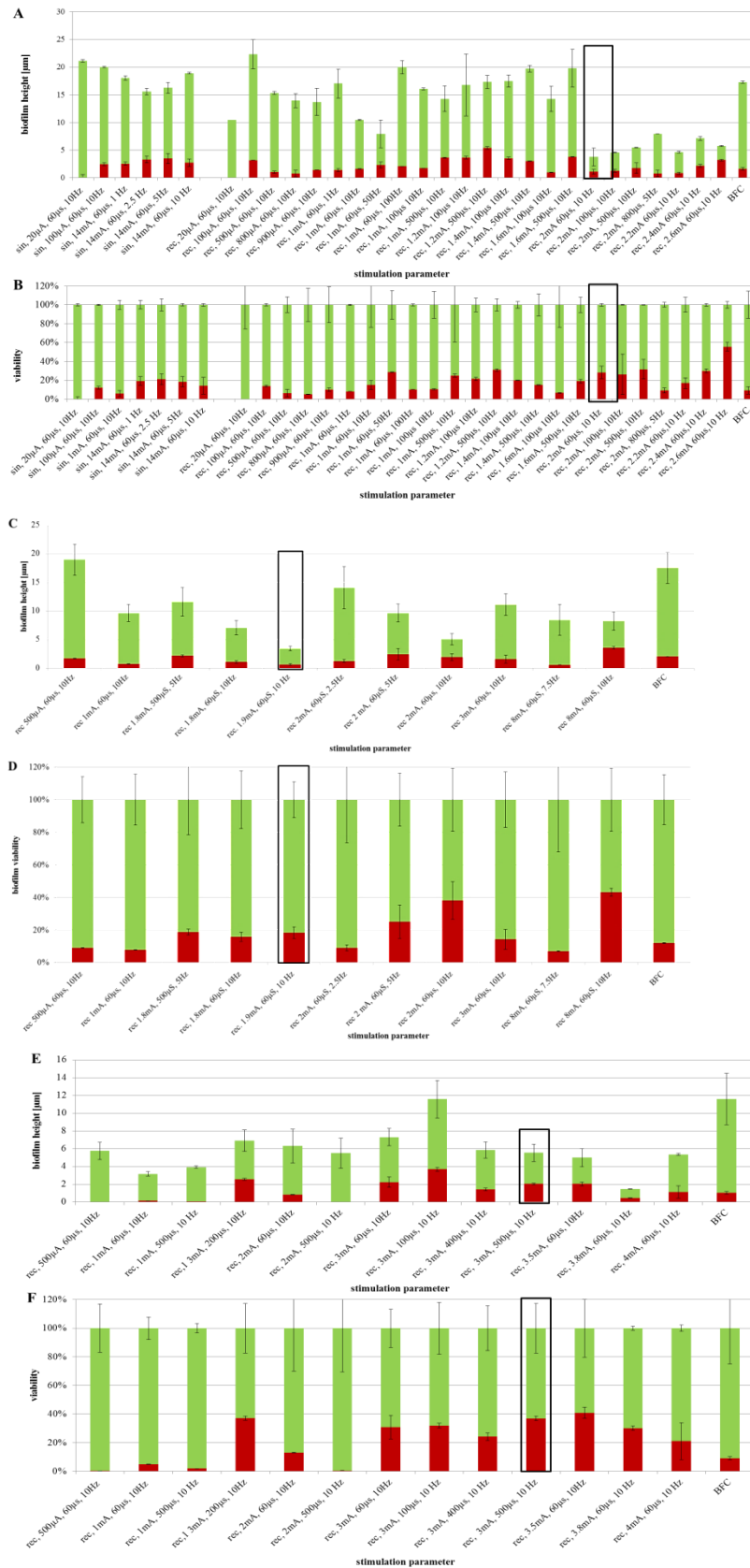


**Figure S 20: Electrical stimulation initial trials on polyester for the evaluation of the growth inhibiting parameter. A+B= *S. gordonii*, C+D= *S. salivarius* and E+F= *P. gingivalis*; BFC = biofilm control (unstimulated). The parameter marked by the black boxes are the parameters used for the electrical stimulation on PVDF membranes. Green = vital bacteria, red= dead bacteria.**

**Table S 4: The organisms, the genome size, calculated genome weight and the corresponding reference for the qRT-PCR.**

<b>organism</b>	<b>genome size</b>	<b>genome weight (ng)</b>	<b>reference</b>
<i>S. gordonii</i> (Challis substr. CH1)	2.19 E+06	2.41 E-6	Cohen <i>et al.</i> Karlsson <i>et al.</i> Sabharwal <i>et al.</i> <sup>110-112</sup>
<i>S. salivarius</i> (JIM8777)	2.21 E+07	2.24 E-5	Guédon <i>et al.</i> (2011) <sup>130</sup>
<i>P. gingivalis</i> (W83)	2.34 E+06	2.57 E-6	Nelson <i>et al.</i> (2003) <sup>517</sup>



## 7.4 Gene expression profiles of electrically stimulated and unstimulated dental-relevant bacterium *S. gordonii*

The microarray analysis for the alteration in gene expression of the electrically stimulated *S. gordonii* in supernatants and biofilm were investigated in section 4.6. In the following, the ORF, the predicted functions, the fold changes and protein domains of the genes analyzed in section 4.6 are summarized in Table S 5 for the bacteria in the supernatants and Table S 6 for the bacteria in the biofilms.

**Table S 5: Up- and downregulated genes and their function of stimulated supernatant samples of *S. gordonii*.** Orange indicates the up-regulated and dark grey the down-regulated genes. The genes are enumerated fold change descending. ORF = open reading frame.

ORF	predicted function	fold change	protein domains
ORF02147	HsdD protein	+ 15.3 x	<ul style="list-style-type: none"> <li>Hydroxysteroid dehydrogenase</li> <li>Type I site-specific deoxyribonuclease activity: Absolut requirement for ATP.</li> </ul>
ORF02146	similar to plasmid replication function	+ 13.0 x	<ul style="list-style-type: none"> <li>Competence</li> <li>For inter- and intraspecies gene transfer</li> </ul>
ORF00658	CAAX amino terminal protease family	+12.5 x	<ul style="list-style-type: none"> <li>Membrane-bound metalloprotease</li> <li>Involved in transport of proteins, peptides, oligopeptides, for the development of biofilm</li> </ul>
ORF00582	Dolichol-phosphate mannosyltransferase	- 7.6 x	<ul style="list-style-type: none"> <li>participates in polysaccharide biosynthetic process and transport</li> </ul>
ORF01797	Dihydroorotate dehydrogenase electron transfer subunit (PyrD)	- 5.9 x	<ul style="list-style-type: none"> <li>FMN flavoprotein: fundamental for all cell respiration processes</li> <li>catalyzes the fourth step in the <i>de novo</i> biosynthesis of pyrimidine, the conversion of dihydroorotate into orotate</li> </ul>

<b>ORF</b>	<b>predicted function</b>	<b>fold change</b>	<b>protein domains</b>
ORF01949	PyrR bifunctional protein	- 5.9 x	<ul style="list-style-type: none"> <li>• regulates transcriptional attenuation of the pyrimidine nucleotide operon</li> <li>• leading to a reduced expression of downstream genes</li> <li>• participates in DNA-templated transcription, termination and nucleoside metabolic process</li> <li>• uracil phosphoribosyltransferase activity: catalyzes the conversion of uracil and 5-phospho-alpha-D-ribose 1-diphosphate (PRPP) to uridinmonophosphat (UMP) and diphosphate.</li> </ul>
ORF01552	NrdI protein	- 5.1 x	<ul style="list-style-type: none"> <li>• metalloproteases</li> <li>• participates in translation initiation factor activity</li> <li>• catalyzes the transfer of electrons from one molecule to another</li> </ul>

**Table S 6: Up- and down-regulated genes and their function of stimulated bacteria in the biofilm of *S. gordonii*.** Orange indicates the up-regulated and dark grey the down regulated genes.

ORF	predicted function	fold change	protein domains
ORF01253	glycerol dehydrogenase NAD+ dependent	+ 41.0 x	<ul style="list-style-type: none"> <li>• Participates in sugar and lipid synthesis</li> <li>• energy supplementation</li> <li>• metal-dependent</li> </ul>
ORF02080	amino acid ABC transporter, permease protein SP0711	+ 37.7 x	<ul style="list-style-type: none"> <li>• for self-coaggregation process</li> <li>• controls CAAX amino terminal protease family</li> <li>• participates in cell viability, biosynthesis, pathogenicity, virulence</li> <li>• attachment function</li> </ul>
ORF00513	proton/sodium-symport protein	glutamate + 30.6 x	<ul style="list-style-type: none"> <li>• participates in transportation of metals, peptides, lipids and carbohydrates</li> </ul>
ORF01393	PTS system, cellobiose-specific IIC component	+ 30.1 x	<ul style="list-style-type: none"> <li>• biofilm-associated beta-glucoside metabolism</li> <li>• participates in phosphotransferase system</li> <li>• phosphoenolpyruvate-dependent</li> </ul>
ORF01799	orotidine 5'-phosphate decarboxylase (PyrF)	+ 25.4 x	<ul style="list-style-type: none"> <li>• codes for pyrimidine biosynthesis</li> </ul>
ORF00469	tryptophan synthase, alpha subunit	+ 25.1 x	<ul style="list-style-type: none"> <li>• amino acid</li> <li>• for protein synthesis</li> </ul>
ORF02130	zinc metalloproteinase C	+ 24.9 x	<ul style="list-style-type: none"> <li>• cleaves proteins</li> <li>• stress-induced</li> </ul>

<b>ORF</b>	<b>predicted function</b>	<b>fold change</b>	<b>protein domains</b>
ORF02081	amino acid ABC transporter, permease protein SP0710	+ 24.4 x	<ul style="list-style-type: none"> <li>• for self-coaggregation process</li> <li>• controls CAAX amino terminal protease family</li> <li>• participates in cell viability, biosynthesis, pathogenicity, virulence</li> <li>• attachment function</li> </ul>
ORF02082	amino acid ABC transporter, ATP-binding protein SP0709	+ 22.7 x	<ul style="list-style-type: none"> <li>• for self-coaggregation process</li> <li>• controls CAAX amino terminal protease family</li> <li>• participates in cell viability, biosynthesis, pathogenicity, virulence</li> <li>• attachment function</li> <li>• biofilm formation</li> </ul>
ORF00512	putative carboxylate-amine/thiol ligase	+ 22.7 x	<ul style="list-style-type: none"> <li>• participates in the function of ribosomes, glutathione, peptide glycan, purine, fatty acid, amino acids, urea, arginine, pyrimidine, lipids, and citric acid biosynthesis</li> </ul>
ORF01800	PyrE	+ 21.4 x	<ul style="list-style-type: none"> <li>• involved in pyrimidine biosynthesis</li> </ul>

<b>ORF</b>	<b>predicted function</b>	<b>fold change</b>	<b>protein domains</b>
ORF01533	oxidoreductase domain protein	NAD-binding + 20.7 x	<ul style="list-style-type: none"> <li>• play essential roles in cellular activities including lipid, amino acid, carbohydrate, cofactor, and xenobiotic metabolisms; but also in redox sensor mechanisms</li> <li>• oxidoreductase catalyzes the transfer of electrons from one molecule to another</li> </ul>
ORF01384	intracellular glycosylhydrolase	+ 20.7 x	<ul style="list-style-type: none"> <li>• involved in biofilm disruption</li> </ul>
ORF02154	Cobalt transport superfamily	protein + 18.4 x	<ul style="list-style-type: none"> <li>• comprises two groups, one catalyzes the uptake of small molecules, including ions from the external environment and the other which is involved in the efflux of small molecular weight compounds and ions from within the cell. ATP hydrolysis derived energy processes of uptake and efflux.</li> </ul>

<b>ORF</b>	<b>predicted function</b>	<b>fold change</b>	<b>protein domains</b>
ORF00674	glycerol uptake facilitator protein homolog	+ 18.4 x	<ul style="list-style-type: none"> <li>• provides the uptake of glycerol into the cell</li> <li>• glycerol is required for antimicrobial peptide release during biofilm growth</li> </ul>
ORF01545	ABC-type transporter, ATPase component	+ 17.9 x	<ul style="list-style-type: none"> <li>• for self-coaggregation process</li> <li>• controls CAAX amino terminal protease family</li> <li>• participates in cell viability, biosynthesis, pathogenicity, virulence</li> <li>• attachment function</li> </ul>
ORF01552	NrdI protein	+ 17.6 x	<ul style="list-style-type: none"> <li>• metalloproteases</li> <li>• participates in translation initiation factor activity</li> <li>• catalyzes the transfer of electrons from one molecule to another</li> </ul>
ORF00615	copper-translocating ATPase	P-type + 15.6 x	<ul style="list-style-type: none"> <li>• copper is competent of many enzymes</li> <li>• participates in transport that facilitates copper absorption and assembly</li> </ul>

<b>ORF</b>	<b>predicted function</b>	<b>fold change</b>	<b>protein domains</b>
ORF01335	enoyl-CoA hydratase/isomerase family protein	+ 15.5 x	<ul style="list-style-type: none"> <li>• cell to cell communication molecule</li> <li>• participates in metabolism of unsaturated fatty acids</li> <li>• involved in biofilm disruption</li> </ul>
ORF01546	ABC transporter, integral membrane protein	+ 15.5 x	<ul style="list-style-type: none"> <li>• for self-coaggregation process</li> <li>• controls CAAX amino terminal protease family</li> <li>• participates in cell viability, biosynthesis, pathogenicity, virulence</li> <li>• attachment function</li> </ul>
ORF01045	transcription termination/antitermination factor NusG	- 32.8 x	<ul style="list-style-type: none"> <li>• participates in transcription elongation, termination and antitermination</li> </ul>
ORF00887	Phosphoribosylformylglycinamide cyclo-ligase	- 29.3 x	<ul style="list-style-type: none"> <li>• part of purine synthesis</li> </ul>
ORF02148	HsdD protein	- 27.4 x	<ul style="list-style-type: none"> <li>• Hydroxysteroid dehydrogenase</li> <li>• Type I site-specific deoxyribonuclease activity: Absolut requirement for ATP.</li> </ul>
ORF00658	CAAX amino terminal protease family	- 24.1 x	<ul style="list-style-type: none"> <li>• Involved inn transport of proteins</li> </ul>
ORF02146	similar to plasmid replication function	- 19.8 x	<ul style="list-style-type: none"> <li>• Competence</li> <li>• For inter- and intraspecies gene transfer</li> </ul>

<b>ORF</b>	<b>predicted function</b>	<b>fold change</b>	<b>protein domains</b>
ORF01113	ComYA	- 19.7 x	<ul style="list-style-type: none"> <li>• competence factor</li> <li>• ABC transporter subunit</li> <li>• for the external DNA transport over the membrane within the early or middle stage of growth phase</li> </ul>
ORF01131	HTH DNA-binding protein	- 17.6 x	<ul style="list-style-type: none"> <li>• helix-turn-helix motive</li> <li>• Transcription/replication regulation</li> </ul>
ORF00931	Peptidyl tRNA hydrolase	- 17.2 x	<ul style="list-style-type: none"> <li>• for protein synthesis</li> </ul>
ORF00693	transposase, IS5 family, authentic frameshift	- 16.5 x	<ul style="list-style-type: none"> <li>• transports transposons to another part within the genome</li> </ul>
ORF01305	ABC transporter, ATP-binding protein SP2003	- 15.1 x	<ul style="list-style-type: none"> <li>• for self-coaggregation process</li> <li>• controls CAAX amino terminal protease family</li> <li>• participates in cell viability, biosynthesis, pathogenicity, virulence</li> <li>• attachment function</li> <li>• biofilm formation</li> </ul>



## 8. Curriculum Vitae

### Henryke Rath

<b>Date of Birth:</b>	07. June 1987
<b>Place of Birth:</b>	Hannover
<b>Nationality:</b>	German
<b>Qualification:</b>	M. Sc. Bioscience

### Education

**May 2013 – December 2016**      **Dissertation** at the Institute of Inorganic Chemistry, Gottfried Leibniz University Hannover in the group of Prof. Dr. Behrens in cooperation with the Hannover Medical School, Clinic for Prosthetic Dentistry and Biomedical Materials Science in the group of Prof. Dr. Stiesch.

**Title of Dissertation:** “Experimental and numerical investigations of implant infection-associated bacterial biofilms in dynamic bioreactor systems”.

**April 2008 – December 2012**      **Study** of Bioscience at the Technical University of Kaiserslautern.

Title of **Master thesis:** “Production, purification, and biophysical characterization of Mystic mutants”.

Title of **Bachelor thesis:** “Site-directed mutagenesis of the membrane protein Mystic: from strategy development to experimental realization”.

### Awards

**May 2013 – April 2016**      **Georg Christoph Lichtenberg Scholarship** within the doctoral program MARIO (Multifunktionale active und reaktive Interfaces and Surfaces).

**September 2015**      **Poster award** by the Scientific Committee of the "11. Theme day of surface and interface engineering and 10. Thuringian biomaterial Colloquium" for the poster: “Flow-chamber systems for the evaluation of biofilm formation on titanium discs”.



## 9. Publications

### 9.1 Publikation

**BIOFABRICATION for NIFE – Development of Innovative Strategies for the Prevention and Control of Biofilm-Associated Implant Infections;** S. N. Stumpp, **H. Rath**, K. Doll, N. Kommerein, P. Behrens, B. Chichkov, M. Stiesch, *Biomedical Engineering / Biomedizinische Technik SI* **2014**, 59, 95-96. (published)

**Numerical Simulation and experimental validation of Biofilm in a Multi-physics framework using an SPH based Method;** M. Soleimani, P. Wriggers, H. Rath, M. Stiesch, *Journal of Computational Mechanics* **2016**, 58, 1-15. (published)

**Theoretical and Experimental Evidence of the Effects of Varying Disinfection Timing;** N. Cogan, **H. Rath**, A. Kommerein, S. N. Stumpp, M. Stiesch, *FEMS Microbiology Letters*, **2016**, 363, fnw264, Epub. (published)

**Development of a flow chamber system for the reproducible *in vitro* analysis of biofilm formation on implant materials;** **H. Rath**, N. Stumpp, M. Stiesch, *Public Library of Science (PLoS) One*, **2017**. (submitted)

**Biofilm formation by the oral pioneer colonizer *Streptococcus gordonii* an experimental and numerical study;** **H. Rath**, D. Feng, S. N. Stumpp, I. Neuweiler, U. Nackenhorst, M. Stiesch, *FEMS Microbiology Ecology* **2017**. (submitted)

**Definition of electrical stimulation parameters for the inhibition of bacterial growth under static and dynamic culture conditions on polyvinylidene fluoride membranes;** **H. Rath**, B. Dreyer, S. N. Stumpp, R. Sindelar, F. Renz, M. Stiesch. (manuscript in preparation)

### 9.2 Book Chapter

**A deeper insight of a multi-dimensional continuous biofilm growth model: experimental observation and parameter studies;** D. Feng, **H. Rath**, I. Neuweiler, S. N. Stumpp, U. Nackenhorst, M. Stiesch, *Lecture Notes in Applied and Computational Mechanics* **2017**, Springer Verlag. (accepted for publication)

### 9.3 Presentations

**A study on oral-disease relevant *Streptococcus gordonii* bacterial biofilm formation with a combination of experimental methods and numerical modelling;** H. Rath, D. Feng, S. N. Stumpp, I. Neuweiler, U. Nackenhorst, M. Stiesch, *International conference of biomedical technology 2015*, Hannover.

### 9.4 Poster

**Evaluation of a flow-chamber system for the investigation of biofilm formation *in vitro*;** H. Rath, S. N. Stumpp, A. Winkel, S. Grade, M. Dalton, P. Behrens, M. Stiesch, *Models for bacterial biofilms formation: mathematical, physical and biological perspectives Summer school 2014*, Nizza.

**Interactions of human cells and oral bacterial biofilms in a bacteria-cell-implant co-culture model;** A. Ingendoh, A. Winkel, C. Blume, S. Grade, H. Rath, H. Hartwig, M. Dalton, T. Scheper, J. Eberhard, M. Stiesch, *1<sup>st</sup> Biofabrication for Nife Retreat 2014*, Hannover.

**The influence of electrical stimulation on the initial attachment and biofilm formation of *Streptococcus gordonii*;** H. Rath, S. N. Stumpp, A. Winkel, S. Grade, M. Dalton, M. Stiesch, *Deutsche Gesellschaft für Biomedizinische Technik 2014*, Hannover.

**Establishment of a flow-chamber system for the investigation of biofilm formation on implant surfaces;** H. Rath, S. N. Stumpp, M. Stiesch, *10<sup>th</sup> Pacific Symposium on Flow Visualization and Image Processing 2015*, Neapel.

**Piezoelectric-active polymer coatings and their influence on bacterial cell-cell interaction;** B. Dreyer, H. Rath, M.A. Nowak, S. N. Stumpp, M. Stiesch, R. Sindelar, F. Renz, *International society of chemical ecology 2015*, Stockholm.

**Flow-chamber systems for the evaluation of biofilm formation on titanium discs;** H. Rath, S. N. Stumpp, M. Stiesch, *11. Thementage Grenz- und Oberflächentechnik und 10. Thüringer Biomaterial-Kolloquium 2015*, Zeulenroda.